

**Canterbury Earthquakes 2010/11 Port Hills Slope
Stability: Debris avalanche risk assessment for
Richmond Hill**

C. I. Massey
B. Lukovic

T. Taig
W. Ries

F. Della Pasqua
G. Archibald

**GNS Science Consultancy Report 2014/34
August 2014 FINAL**



DISCLAIMER

This report has been prepared by the Institute of Geological and Nuclear Sciences Limited (GNS Science) exclusively for and under contract to Christchurch City Council. The report considers the risk associated with geological hazards. As there is always uncertainty inherent within the nature of natural events GNS Science gives no warranties of any kind concerning its assessment and estimates, including accuracy, completeness, timelines or fitness for purpose and accepts no responsibility for any actions taken based on, or reliance placed on them by any person or organisation other than Christchurch City Council. GNS Science excludes to the full extent permitted by law any liability to any person or organisation other than Christchurch City Council for any loss, damage or expense, direct or indirect, and however caused, whether through negligence or otherwise, resulting from any person or organisation's use of, or reliance on this report.

The data presented in this Report are available to GNS Science for other use after the public release of this document.

BIBLIOGRAPHIC REFERENCE

Massey, C. I.; Taig, T.; Della Pasqua, F.; Lukovic, B.; Ries, W.; Archibald, G. 2014. Canterbury Earthquakes 2010/11 Port Hills Slope Stability: Debris avalanche risk assessment for Richmond Hill, *GNS Science Consultancy Report 2014/34*. 132 p. + Appendices

REVIEW DETAILS

This report in draft form was independently reviewed, Dr L. Richards and Dr J. Wartman. Internal GNS Science reviews of drafts were provided by N. Litchfield, M. McSaveney and D. Mieler, and risk calculations were checked by R. Buxton.

Risk calculations were independently checked by TTAC Limited.

CONTENTS

EXECUTIVE SUMMARY	IX
ES 1 INTRODUCTION	IX
ES2 INVESTIGATION PROCESS AND FINDINGS	IX
ES2.1 Cliff-collapse hazards	x
ES2.2 Failure volumes and triggering frequencies	xi
ES3 REPORT CONCLUSIONS	XII
ES3.1 Hazard	xii
ES3.2 Risk.....	xii
ES4 RECOMMENDATIONS	XIII
ES4.1 Policy and planning	xiii
ES4.2 Short-term actions	xiii
ES4.3 Long-term actions.....	xiv
1.0 INTRODUCTION	1
1.1 BACKGROUND.....	1
1.1 THE RICHMOND HILL MASS MOVEMENTS.....	5
1.1.1 Context and terminology	5
1.1.2 Local and random cliff collapse source areas	6
1.2 PREVIOUS WORK AT THE RICHMOND HILL SITE	9
1.3 SCOPE OF THIS REPORT	11
1.4 REPORT STRUCTURE.....	12
1.5 METHODS OF ASSESSMENT	12
1.5.1 Engineering geology assessment	12
1.5.2 Hazard assessment.....	13
1.5.3 Risk assessment	15
2.0 DATA USED	19
3.0 SITE ASSESSMENT (RESULTS)	23
3.1 SITE HISTORY.....	23
3.1.1 Aerial photograph interpretation	23
3.1.2 Before the 2010/11 Canterbury earthquakes	24
3.1.3 During the 2010/11 Canterbury earthquakes	25
3.1.4 After the 2010/11 Canterbury earthquakes	26
3.2 SITE INVESTIGATIONS	27
3.2.1 Geomorphological mapping	27
3.2.2 Subsurface trenching and drilling	27
3.2.3 Surface movement	39
3.2.4 Sub-surface movement	44
3.2.5 Groundwater	44

3.3	ENGINEERING GEOLOGICAL MODEL	44
3.3.1	Slope materials.....	45
3.3.2	Geotechnical material properties.....	48
3.3.3	Rainfall and groundwater response.....	51
3.4	SLOPE FAILURE MECHANISMS	56
3.4.1	Landslide types affecting the site	56
3.4.2	Cliff collapse failure mechanisms	60
4.0	HAZARD ASSESSMENT RESULTS	63
4.1	SLOPE STABILITY (SOURCE AREAS 1–10).....	63
4.1.1	Slope stability – Static conditions (deep-seated failures).....	63
4.1.2	Slope stability – Dynamic conditions	71
4.1.3	Slope stability – Summary of results	81
4.2	RUNOUT DISTANCE.....	82
4.2.1	Potential future source volume estimation	82
4.2.2	Runout modelling	87
4.2.3	Forecast runout modelling.....	91
5.0	RISK ASSESSMENT RESULTS	95
5.1	TRIGGERING EVENT FREQUENCIES	95
5.1.1	Frequency of earthquake triggers	95
5.1.2	Frequency of rainfall triggers.....	99
5.1.3	Dwelling occupant risk.....	100
5.1.4	Variables adopted for the risk assessment	100
5.1.5	Debris avalanche.....	101
5.1.6	Cliff-top recession.....	108
5.2	ROAD USER RISK.....	109
5.2.1	Risk per Journey.....	110
5.2.2	Alternative risk parameters for road users	117
6.0	DISCUSSION.....	121
6.1	DWELLING OCCUPANT RISK	121
6.2	ROAD USER RISK.....	121
6.3	RISK ASSESSMENT SENSITIVITY TO UNCERTAINTIES.....	122
6.3.1	Debris volumes.....	122
6.3.2	Area of cliff-top lost.....	122
6.3.3	Debris runout	122
6.3.4	Other sensitivities and uncertainties.....	123
6.3.5	How reliable are the results?.....	123
7.0	REPORT CONCLUSIONS.....	125
7.1	HAZARD	125
7.2	RISK.....	125

7.2.1	Dwelling occupant	125
7.2.2	Road user	125
8.0	RECOMMENDATIONS.....	127
8.1	POLICY AND PLANNING	127
8.2	SHORT-TERM ACTIONS	127
8.2.1	Hazard monitoring strategy	127
8.2.2	Risk monitoring strategy.....	127
8.2.3	Surface/subsurface water control.....	128
8.2.4	Pavement closure.....	128
8.3	LONG-TERM ACTIONS	128
8.3.1	Engineering measures	128
8.3.2	Reassessment.....	128
9.0	ACKNOWLEDGEMENTS.....	129
10.0	REFERENCES	129

EQUATIONS

Equation 1	16
Equation 2	51

FIGURES

Figure 1	Location map.....	3
Figure 2	The Richmond Hill mass movement location map showing the assessed source areas 1 and 2.	7
Figure 3	A) Debris avalanche triggered by the 2010/11 Canterbury earthquakes (location of one fatality) at the northern end of the site.....	10
Figure 4	Main features identified at the site from field mapping and the interpretation of historical aerial photographs.....	25
Figure 5	Engineering geological map.....	29
Figure 6	Site investigation map.	30
Figure 7	Engineering geological cross-sections 1–7.	31
Figure 8	Cracks observed below the Richmond Hill cliff top near the interface between rock and loess.....	40
Figure 9	View to the west onto the northern cliff at Wakefield Avenue. The homes are accessed from Richmond Hill Road.....	48
Figure 10	Geological strength index plot for basalt and trachy-basalt lavas and basalt and trachy-basalt lava breccias exposed on the cliffs at Wakefield Avenue (Modified after Hoek, 1999).....	49
Figure 11	Daily rainfalls at Christchurch Gardens and landslides in the Port Hills.	52
Figure 12	Rainfall depth-duration-return period relations estimated for Christchurch Gardens by Griffiths et al. (2009) using recorded rainfall data.....	55

Figure 13	Engineering geological model.	57
Figure 14	Schematic cross-section (cross-section 2, Figure 7) of the cliff showing the inferred failure mechanisms and differences in rock mass strength derived from the downhole shear wave surveys.....	59
Figure 15	View to the south along Richmond Hill after the 13 June 2011 earthquake.	60
Figure 16	Schematic diagram showing the increasing frequency of defects in the slope in response to the successive 2010/11 Canterbury earthquakes.....	63
Figure 17	Cross-section 2 limit equilibrium stability assessment, soil (loess) failure.	67
Figure 18	Cross-section 2 limit equilibrium stability assessment.	68
Figure 19	Cross-section 2 finite element stability assessment.	69
Figure 20	Modelled Slope/W decoupled displacements for cross-section 2 Richmond Hill Road, adopting the model 2 and 3 estimates of the material strengths.	72
Figure 21	Modelled Slope/W decoupled displacements for cross-section 2 Richmond Hill Road, adopting loess shear strength of friction (ϕ) of 30° and cohesion (c) of 10 kPa, where the slide surfaces are constrained to the loess only.	73
Figure 22	Estimated displacements of the Richmond Hill slope (cross-section 2) during the 22 February 2011, earthquake.	74
Figure 23	Estimated displacements of the Richmond Hill slope (cross-section 2) during the 13 June 2011 earthquake.	75
Figure 24	Cross-section 2 seismic slope stability assessment for the 22 February 2011 earthquake.....	75
Figure 25	Cross-section 2 seismic slope stability assessment for the 13 June 2011 earthquake.	76
Figure 26	Decoupled Slope/W displacements calculated for different ratios of yield acceleration to maximum average acceleration of the mass (K_y/K_{MAX}), and maximum acceleration of the mass (K_y/A_{FF}), for selected slide-surface geometries, for cross-section 2. A_{FF} is the peak acceleration of the input earthquake time acceleration history.....	78
Figure 27	Relationship between free field peak ground accelerations at Richmond Hill and the volume of debris leaving the Richmond Hill slope.	82
Figure 28	Proportion and cumulative proportion of volume from cliff collapses in the Port Hills greater than or equal to a given volume.	84
Figure 29	Estimation of landslide volume assuming a quarter-ellipsoid shape.....	86
Figure 30	Proportion of debris volume passing a given fahrboeschung angle line, from debris avalanches triggered during the 22 February and 13 June 2011 earthquakes at Richmond Hill/Wakefield Avenue, Shag Rock Reserve and Redcliffs.	87
Figure 31	The empirical fahrboeschung relationships, expressed as the ratio of height (H) to length (L) for debris avalanche talus and boulder roll (rockfalls), recorded in the Port Hills. N = 45 sections.	88
Figure 32	Range of parameters used to back-analyse the runout of debris avalanches in the Port Hills triggered by the recent earthquakes using the RAMMS software (RAMMS, 2011).	89
Figure 33	Range of parameters for different mass movement processes: a) debris flows, b) snow avalanches, c) snow avalanches, d) ice avalanches, e) debris floods.....	89
Figure 34	Mean volume difference between the RAMMS modelled volumes and the actual recorded volumes per 1 m ² grid cell. N = 23 debris avalanches triggered by 22 February and 13 June 2011 earthquakes.	90
Figure 35	Comparison between the RAMMS modelled and the empirical-modelled debris runout (Figure 32, and the actual recorded runout for debris avalanches triggered by the 22 February and 13 June 2011 earthquakes. N = 23 debris avalanches.	90
Figure 36	Cliff collapse hazard map.	93

Figure 37	Cliff collapse annual individual fatality risk (scenarios A–C).....	103
Figure 38	Cliff collapse annual individual fatality risk (scenario B 100% distributed).....	106
Figure 39	Results from the debris avalanche risk assessment per scenarios A, B and C (dwelling occupant).....	107
Figure 40	Results from the cliff top recession risk assessment, per scenarios A, B and C (dwelling occupant). Refer to Table 25 for details of the each scenario.	109
Figure 41	Risk per journey under rockfall scenarios A, B and C.	111
Figure 42a	Road user risk contributions (per 100 million journeys) from individual cells – Scenario A.	112
Figure 42b	Road user risk contributions (per 100 million journeys) from individual cells – Scenario B.	113
Figure 42c	Road user risk contributions (per 100 million journeys) from individual cells – Scenario C.	114
Figure 43	Risk contributions from hazards 1 and 2 and seismic versus other triggers.....	115
Figure 44	Effect of treating all rockfall as uniformly distributed along the cliff – Scenario B.	116
Figure 45	Annual individual fatality risk for heavy users of Wakefield Avenue, scenarios A, B and C.....	118

TABLES

Table 1	Mass movement relative hazard exposure matrix (from the Stage 1 report; Massey et al., 2013).	5
Table 2	Risk scenarios used in the modelling of cliff collapses.	18
Table 3	Summary of the main data used in the analysis. LiDAR is Light Detecting and Ranging.	19
Table 4	Summary of observations from aerial photographs used to assess the site history at Richmond Hill Road.	23
Table 5	Summary of the ground investigations carried out at the site by Aurecon NZ Ltd. (Revell and Pletz, 2013) and Tonkin and Taylor Ltd. (Tonkin and Taylor, 2012a).	28
Table 6	Estimated cliff top displacements across crack apertures in response to the 22 February and 13 June 2011 earthquakes (mainly the 13 June earthquake).	40
Table 7	Estimated cliff top displacements as per Table 7a, but only for those cracks with both vertical and horizontal displacements across the apertures recorded for cross-sections 1–3 at the cliff top.	41
Table 8	Estimated volumes lost from the cliffs calculated from the terrestrial laser scan (TLS) and LiDAR surveys.....	43
Table 9	Summary of inclinometer details.	44
Table 10	Engineering geological descriptions of the main geological units forming the cliffs.....	46
Table 11	Geotechnical material parameters derived from testing and used for the modelling.	50
Table 12	Shear wave velocity profiles (measured in the Aurecon NZ Ltd. drillholes).	51
Table 13	Annual frequencies of given rainfall in the Christchurch for four main events following the 2010/11 Canterbury earthquakes (rainfalls are calculated daily from 09:00 to 09:00 NZST).	54
Table 14	Example results from the static slope stability assessment adopting model 2 material strength estimates.	64
Table 15	Calculated factors of safety and yield accelerations for cross-sections 1–7, adopting model 2 and 3 material strength parameters (Table 11).	79
Table 16	Forecast modelling results from the dynamic slope stability assessment for cross-sections 2, 4 and 6, adopting model 3 material parameters, and no water in tension cracks.	80

Table 17	The volumes of debris leaving the slope during each of the 2010/11 earthquakes and the earthquake's estimated peak ground acceleration, at the Richmond Hill site – horizontal (PGA H) and vertical (PGA V) components are listed separately.....	82
Table 18	The estimated volumes of debris leaving the slope for different bands of peak ground acceleration (PGA).....	83
Table 19	The mean and mean-minus-one-standard-deviation (-1 STD) fahrboeschungs (F-angles) for each source area (1–10) and each volume (lower, middle and upper estimates).....	85
Table 20	Information used to estimate event volumes contributing to the total risk from non-seismic rockfall triggering events, all sites.....	86
Table 21	The annual frequency of a given peak ground acceleration (PGA) band occurring on rock (Site Class B) for different years from the 2012 seismic hazard model for Christchurch (G. McVerry, personal communication 2014).....	95
Table 22	Proportion of the total debris volume per peak ground acceleration band allocated to distributed and local failures, for upper, central and lower estimates of volume.....	96
Table 23	Forecast modelling results from the dynamic slope stability assessment for cross-sections 2, 4 and 6, adopting model 3 material parameters, and no water in tension cracks. Estimated displacements are rounded to the nearest 0.1 m.	98
Table 24	Representative annual event frequency of debris avalanches occurring, and the representative volume of the avalanche, for each time-period band.	99
Table 25	Area of cliff top lost per peak ground acceleration (PGA) band for upper, middle and lower volume estimates.....	108
Table 26	Volume of debris and area of cliff top lost per non-seismic band (based on historical rockfall rates in Massey et al., 2012a).....	108
Table 27	Number of trips per day for high road users.....	117
Table 28	Total trips per day for all road users.....	119
Table 29	Average total expected deaths per year.....	120
Table 30	Uncertainties and their implications for risk.....	123

APPENDICES

A1	APPENDIX 1: METHODS OF ASSESSMENT.....	A1-1
A1.1	HAZARD ASSESSMENT METHOD.....	A1-1
	A1.1.1 Slope stability modelling.....	A1-1
	A1.1.2 Static slope stability.....	A1-1
	A1.1.3 Dynamic stability assessment (decoupled method).....	A1-2
	A1.1.4 Estimation of slope failure volumes.....	A1-5
	A1.1.5 Debris runout modelling.....	A1-5
A1.2	RISK ASSESSMENT.....	A1-6
	A1.2.1 Fatality risk to dwelling occupants.....	A1-6
A1.3	ROAD-USER RISK ASSESSMENT.....	A1-14
A1.4	ROAD USER RISK ASSESSMENT ILLUSTRATION.....	A1-21
A1.5	ROAD USER RISK – ADDITIONAL DISCUSSION ON MAIN ASSUMPTIONS.....	A1-25
A2	APPENDIX 2: RESULTS FROM AIRBORNE LIDAR SURVEYS.....	A2-1

A3	APPENDIX 3: RESULTS FROM THE TERRESTRIAL LASER SCAN SURVEYS.....	A3-1
A4	APPENDIX 4: RESULTS FROM THE SURVEY OF CADASTRAL SURVEY MARKS.....	A4-1
A5	APPENDIX 5: STEREONET KINEMATIC ANALYSIS OF RICHMOND HILL DISCONTINUITY DATA	A5-1
A6	APPENDIX 6: RESULTS FROM THE TWO-DIMENSIONAL SITE RESPONSE ASSESSMENT FOR CROSS-SECTION 2	A6-1
	A6.1 DYNAMIC CONDITIONS –GROUND RESPONSE.....	A6-1
A7	APPENDIX 7: RAMMS MODELLING RESULTS FOR SOURCE AREAS 1–10 ADOPTING THE MIDDLE ESTIMATES OF SOURCE VOLUME; DEBRIS HEIGHT	A7-1
A8	APPENDIX 8: RAMMS MODELLING RESULTS FOR SOURCE AREAS 1–10 ADOPTING THE MIDDLE ESTIMATES OF SOURCE VOLUME; DEBRIS VELOCITY.....	A8-1
A9	APPENDIX 9: ROCKFALL MODELLING RESULTS FOR CROSS-SECTIONS 1 AND 7.....	A9-1

APPENDIX EQUATIONS

Equation 2A	A1-10
Equation 3B	A1-10
Equation 3C	A1-10
Equation 3A	A1-11
Equation 4B	A1-11
Equation 4	A1-12
Equation 5	A1-21
Equation 6	A1-26
Equation 7	A1-26
Equation 8	A1-26
Equation 9	A1-27

APPENDIX FIGURES

Figure A1.1	Expanded calculation of the probability of each local source area “scoop” occurring.....	A1-10
Figure A1.2	Debris avalanche at the northern end of Richmond Hill site triggered by the 22 February 2011 earthquakes.....	A1-14
Figure A1.3	Event tree model for road user risk assessment – Wakefield Avenue.....	A1-15
Figure A1.4	Overview of vulnerability factors for road users in path of rockfall.....	A1-33
Figure A6.1	Amplification relationship between the synthetic free field rock outcrop input motions (A_{FF}) and the modelled cliff edge maximum accelerations (A_{MAX}) for cross-section 2.	A6-1
Figure A6.2	Modelled peak horizontal ground acceleration contours for the 22 February 2011 earthquake at Richmond Hill, cross-section 2, adopting the 2003 airborne LiDAR slope surface geometry.....	A6-2
Figure A6.3	Modelled peak horizontal ground acceleration contours for the 13 June 2011 earthquake at Richmond Hill, cross-section 2, adopting the 2003 airborne LiDAR slope surface geometry.	A6-2
Figure A6.4	Relationship between the modelled horizontal and vertical maximum accelerations modelled at the cliff edge (A_{MAX}) for cross-section 2, using the synthetic free field rock outcrop motions for the Richmond Hill site by Holden et al. (2014) as inputs to the assessment.	A6-3

APPENDIX TABLES

Table A1.1	Derivation of key event tree parameters.....	A1-17
Table A1.2	Assumptions used in quantifying road user risk event tree.....	A1-19
Table A1.3	Calculation process for risk from hazard 1 (single cell, per journey).	A1-22
Table A1.4	Calculation process for risk from hazard 2 (single cell, per journey).	A1-23
Table A1.5	Calculation of risk parameters of interest from single cell risk per journey	A1-24
Table A1.6	Average journey speeds and resulting values of P_1 (= 2m/speed converted to metres/year).	A1-25
Table A1.7	Stopping times and values of P3 (when rockfall debris present on road).	A1-28
Table A1.8A	Derivation of stopping times for cars (+ general points).	A1-29
Table A1.8B	Derivation of stopping times, motorcycles and pedal cycles.....	A1-30
Table A1.9	Some recent incidents of rockfall contacting road (and track) users.	A1-32
Table A1.10	Vulnerabilities adopted for road users in path of rockfall.	A1-34
Table A1.11	Proportion of motor vehicle crashes involving injury.....	A1-36
Table A1.11	Lethality of injury collisions with NZ MOT categories of target object.	A1-37
Table A1.12	Motorcycle accident lethality on New Zealand roads.....	A1-38
Table A6.1	Results from the two-dimensional site response assessment for cross-section 2 using the synthetic free field rock outcrop motions for the Richmond Hill site by Holden et al.....	A6-3

EXECUTIVE SUMMARY

ES 1 INTRODUCTION

This report brings together recent field information on the Richmond Hill site and uses numerical models of slope stability to assess the risk to people in dwellings and users of Wakefield Avenue from cliff-collapse hazards (debris avalanches and cliff-top recession) at the site, over and above those assessed in an earlier cliff collapse study (Massey et al., 2012a).

Following the 22 February 2011 earthquakes, extensive cracking of the ground occurred in some areas of the Port Hills. In many areas, the cracks were thought to represent only localised relatively shallow ground deformation in response to shaking. In other areas, however, the density and pattern of cracking and the amounts of displacement across cracks clearly indicated large mass movements.

Christchurch City Council contracted GNS Science to carry out further detailed investigations of these areas of systematic cracking, in order to assess the nature of the hazard, the frequency of the hazard occurring, and whether the hazard could pose a risk to life, a risk to existing dwellings and/or a risk to critical infrastructure. This work on what are termed mass movements is being undertaken in stages. Stage 1 is now complete (Massey et al., 2013) and stages 2 and 3 are detailed investigations of mass movements from highest to lowest priority.

The Stage 1 report identified 36 mass movements of concern in the Port Hills project area. Four of these were further subdivided based on failure type, giving a total of 46 mass movements including their sub areas. Fifteen of these were assessed as being in the Class I (highest) relative hazard-exposure category. Mass movements in the Class I category could cause loss of life, if the hazard were to occur, as well as severe damage to dwellings and/or critical infrastructure, which may lead to the loss of services for many people.

The Richmond Hill mass movement was assessed in the Stage 1 report (Massey et al., 2013) as being in the highest relative hazard exposure category (Class I, involving potential risk to life). Following the 22 February 2011 earthquakes significant localised cracking was noted in the loess (soil) mantling the steep rock slope and in the cliff face at the Richmond Hill site.

This report, as part of the Stage 2 investigations, presents the revised risk assessment results for the Richmond Hill Class I mass movement.

ES2 INVESTIGATION PROCESS AND FINDINGS

Detailed investigations of the site and its history were carried out by GNS Science. These investigations have identified several relict landslides (up to 1,000–13,000 m³ in volume) at the site that appear to date from before the time of European settlement (about 1840 AD). Rockfalls are also apparent from the steep rock slope in aerial photographs covering the period 1946–1984. The areas of past failures from the slope coincide with the same areas that failed during the 2010/11 Canterbury earthquakes.

The slopes at Richmond Hill were significantly cracked during the 22 February, 16 April, 13 June and 23 December 2011 earthquakes. Over 5,000 m³ of debris fell from the slope during the 22 February 2011 earthquakes and over 10,000 m³ during the 13 June 2011 earthquakes. The cliff top recessed by up to 5 m during the 13 June 2011 earthquake.

The relative ground displacements at this site through the 2010/11 Canterbury earthquakes are constrained by the mapping of crack apertures, measured before and after the main earthquakes. The bulk strength of the rock mass forming the slope was weakened by cracking, and in particular, the presence of open surface cracks have made the slope more susceptible to the ingress of run-off water.

The main types of landslide hazard identified at the site are debris avalanches and cliff-top recession, which are a relatively rapid type of landslide involving many hundreds to thousands of boulders. The risk to life of people in dwellings from debris avalanches and cliff top recession hazards associated with the steep rock slope has already been estimated by Massey et al. (2012a).

Further investigation of the site has involved field mapping, ground investigation (comprising subsurface drilling and trenching), laboratory testing, numerical modelling and monitoring (of the features in the field and how they have responded to earthquakes and rain).

The further investigation has identified an additional 10 potential source areas, where local larger volumes of rock may fall from the cliff, during a triggering event, as single or multiple failures, with the resultant debris travelling further on the valley floor than occurred in the 2010/11 Canterbury earthquakes. This is the reason for the Richmond Hill mass movement being included in the Class I (high priority for further investigation) mass movements.

This assessment improves on the original work by Massey et al. (2012a) by taking into account:

1. Large localised failures from 10 assessed source areas; and
2. Other failures, randomly distributed across the slope.

These 10 assessed source areas are in addition to the randomly distributed source areas, from which debris could fall from anywhere along the cliff. Numerical models have been used to assess the stability of the Richmond Hill slopes, in particular the 10 potential landslide sources. Analyses have considered both:

- static (without earthquake shaking); and
- dynamic (with earthquake shaking) conditions.

ES2.1 Cliff-collapse hazards

Cliff-top recession and associated debris avalanches pose the greatest landslide hazards and landslide risk to people on the cliff top and cliff toe. These slope-instability processes form the basis of the hazard and risk assessments contained in this report.

Under current conditions, it is possible for failure of the slope to occur under either static or dynamic conditions. However, it should be noted that material strengths – and therefore the slope factors of safety – may reduce with time (weathering), water content, and further movement of the slope under either static or dynamic conditions.

For non-earthquake triggers, given the relatively low static factors of safety, an increase in pore water pressures in open tension cracks within the overlying loess and joints within the underlying rock mass could lead to instability of the slope under static conditions (i.e., short duration, high intensity rain).

For earthquake triggers, given the relatively low yield acceleration of the slope, it is likely that future earthquakes could generate permanent displacements that could be quite large, and potentially lead to large volumes of debris falling from the slope. Earthquake-induced failures are likely to be larger in volume and the debris travel further, due to the larger volume, than rainfall-induced failures.

Parts of the slope crest have already undergone more than one metre of permanent slope displacement during the 2010/11 Canterbury earthquakes and this displacement may have reduced the shear strength of critical materials in the slope, making the slope more susceptible to future earthquakes.

ES2.2 Failure volumes and triggering frequencies

The volumes of rock that could fall from the cliff under dynamic (earthquake) and static (non-earthquake, e.g., rain) conditions have been assessed.

The original cliff-collapse risk assessment by Massey et al. (2012a) was based on future failures that were all randomly distributed across the slope face. The results of the engineering geological assessments identified that although many failures were randomly distributed across the slopes, these failures only accounted for a relatively small proportion of the total volume of rock leaving the slopes. Much of the debris leaving the Richmond hill slope (and other similar slopes in the Port Hills), derived from a few non-random (local) failures that involved larger volumes of rock, particularly in areas where the rock mass strength had been weakened as a result of earthquake-induced cracking.

The volumes of material involved in, and the frequency of, cliff collapse from the slopes are assessed. Three source-volume ranges (upper, middle and lower volumes), and seven earthquake event annual frequencies (representing different ranges of peak ground acceleration), and four non-earthquake event band annual frequencies (representing mainly rainfall triggers) have been modelled. All are uncertain and the frequency of the triggering events is particularly uncertain.

Three scenarios have been adopted for modelling the risk to dwelling occupants and users of Main Road to provide an indication of the range of uncertainty associated with the risk estimates. The three scenarios span reasonable ranges of: 1) the assessed total volume that could be generated in a representative event; and 2) the volume of debris that passes a given distance down the slope.

ES3 REPORT CONCLUSIONS

ES3.1 Hazard

1. The strength of the rock mass forming the slope at Richmond Hill has been reduced by earthquake-induced fractures and movement and it will continue to weaken over time due to factors such as physical and chemical weathering, wetting and drying and further ground movement. Failures, of volumes of rock greater than those that failed during the 2010/11 Canterbury earthquakes, from the cliff are now more likely to be triggered by future earthquakes or by non-earthquake triggers such as rain. Failure volumes triggered by earthquakes may now be larger than any that fell during the 2010/11 Canterbury earthquakes; they could be more similar in size to past failures (from the same slope) identified from pre-1940 aerial photographs and pre-2010/11 earthquakes slope geometry.

ES3.2 Risk

ES3.2.1 Dwelling occupant

1. There are very few additional dwellings in the debris avalanche or cliff recession zones that do not already have “red zone” offers made by the Canterbury Earthquake Recovery Authority.
2. Earthquake-triggered cliff collapses contribute most to the risk.
3. The results show that the most critical uncertainty in the risk assessment is the volumes of material that could be generated at different bands of peak ground acceleration. There are approximately two orders of magnitude difference (a factor of 100 times) in the risk estimates between the upper and lower failure volume estimates (scenarios A and C respectively) in the distal ends of the risk zone.
4. The inclusion of the assessed local source areas 1–10 in the risk assessment increases the runout and hence the risk farther out from the toe of the slope.
5. The revised cliff-top recession risk maps show that the inclusion of local source areas 1–10 has also extended the cliff-top-recession risk zone further from the cliff edge.

ES3.2.2 Road user

1. The section of Richmond Hill Road at the cliff top in the assessment area is unlikely to be lost through cliff-top recession. However, further cracking and deformation of the road, retaining-wall failures and local small landslides (in loess/fill materials) could occur again in future earthquakes and affect the operation of the road.
2. For users of Wakefield Avenue, the rockfall risk increases directly with their time spent on the road and is greatest for the slowest road users (pedestrians, then cyclists), because slower travel exposes them to risk for longer on each journey.
3. The rockfall risk to road users has been compared with risk from road accidents for a journey of the same length on average New Zealand urban roads. The relativity between rockfall risk and road traffic accident risk is different for the different road user groups, in particular:

- a. For car drivers and pedal cyclists the rockfall risk is similar to the road accident risk;
 - b. For car passengers the rockfall risk (assumed the same as for the driver) is higher than the road-accident risk (which is much smaller for car passengers than for drivers);
 - c. For motorcyclists, the road-accident risk is greater than rockfall risk (because the former is so high); and
 - d. For pedestrians, the rockfall risk on the side of the road closer to the slope (west) is comparable with or greater than road-accident risk, for scenarios A (upper failure volume estimates) and B (middle failure volume estimates), but is comparable with or less than road-accident risk for scenario C (lower failure volume estimates).
4. The risks to the pedestrian (the user exposed to the highest level of risk) are substantially lower (typically by a factor of two or more) on the eastern side of Wakefield Avenue road compared to the western side.

ES4 RECOMMENDATIONS

GNS Science recommends that based on the results of this study, Christchurch City Council:

ES4.1 Policy and planning

1. Decide what levels of life risk to dwelling occupants and road users will be regarded as tolerable.
2. Decide how Council will manage risk on land where life risk is assessed to be at the defined threshold of intolerable risk and where the level of risk is greater than the threshold.
3. Prepare policies and other planning provisions to address risk lesser than the intolerable threshold in the higher risk range of tolerable risk.

ES4.2 Short-term actions

ES4.2.1 Hazard monitoring strategy

1. Include the report findings in a slope stability monitoring strategy with clearly stated aims and objectives, and list how these would be achieved, aligning with the procedures described by McSaveney et al. (2014). In the meantime, extend the current survey network (by increasing the number of slope monitoring marks) further up the slope (particularly into source area 1), so as to maintain awareness of changes in the behaviour of the slope.
2. Ensure that the emergency management response plan for the area identifies the dwellings that could be affected by movement and runout, and outlines a process to manage a response.
3. Although not assessed as part of this study, the slump (in loess – mass movement 3B), should also be routinely inspected to assess any potentially dangerous trends in its movement.

ES4.2.2 Risk monitoring strategy

Monitoring the slope for early warning of potentially dangerous trends in groundwater or slope movement as part of a hazard warning system is not recommended. Monitoring alerts for slope deformation and groundwater changes cannot be relied upon to provide adequate early warning as experience from Port Hills and elsewhere shows that deformation and groundwater changes can occur rapidly, with little warning.

ES4.2.3 Surface/subsurface water control

1. Reduce water ingress into the slopes, where safe and practicable to do so, by:
 - a. Identifying and either relocating or upgrading (to withstand further ground movement) all water-reticulation services (water mains, sewer pipes and storm water) inside the identified mass-movement boundaries (at the slope crest) to locations outside the boundary, in order to control water infiltration into the slope. In particular, the broken household storm water pipes at the crest of the slope; and
 - b. Filling the accessible cracks on the slope and providing an impermeable surface cover to minimise water ingress, and control all surface water/drainage where possible.
2. These measures alone are not thought sufficient to address the risk and longer-term solutions should be explored.

ES4.2.4 Pavement closure

1. Maintain the closure of the pavement on the slope-side of the road, and continue to divert pedestrians onto the footpath on the other side of the road.
2. It is not known how effective the current temporary containers would be if impacted by a sizable debris avalanche (as per those discussed in this report). The effectiveness of such temporary risk management measures should be reassessed to ensure they are “fit-for-purpose”.

ES4.3 Long-term actions

ES4.3.1 Engineering measures

1. Explore the technical cost and effectiveness of engineering solutions, for example (but not limited to) earth bunds (check dams) at the northern and southern ends of the site (along the western side of Wakefield Avenue) to prevent any debris from impacting the dwellings on the eastern side of Wakefield Avenue. Such works would require a detailed assessment and design and to be carried out by a certified person.
2. For the sections of Main Road within the risk zone, liaise with whoever is responsible for roading in this area to ensure that the debris avalanche risk is taken into account in any road design (or in the design of modifications to the road).

ES4.3.2 Reassessment

Reassess the risk and revise and update the findings of this report in a timely fashion, for example:

- a. in the event of any changes in ground conditions (e.g., a large landslide occurs, movement at slope crest is noticed; or
- b. in anticipation of further development or land use decisions.

1.0 INTRODUCTION

This report uses results from recent field investigation and numerical models of slope stability for the Richmond Hill site to assess the risks to people in dwellings and users of Wakefield Avenue from cliff-collapse hazards (debris avalanches and cliff-top recession). This report provides an update from the original risk assessment for Wakefield Avenue presented by Massey et al. (2012a) and Taig and Massey (2013).

1.1 BACKGROUND

Following the 22 February 2011 earthquakes, members of the Port Hills Geotechnical Group (a consortium of geotechnical engineers contracted to Christchurch City Council to assess slope instability in the Port Hills) identified some areas in the Port Hills where extensive cracking of the ground had occurred. In many areas, cracks were thought to represent only localised relatively shallow ground deformation in response to shaking. In other areas however, the density and pattern of cracking and the amounts of displacement across cracks clearly indicated that larger areas had moved systematically *en masse* as a mass movement.

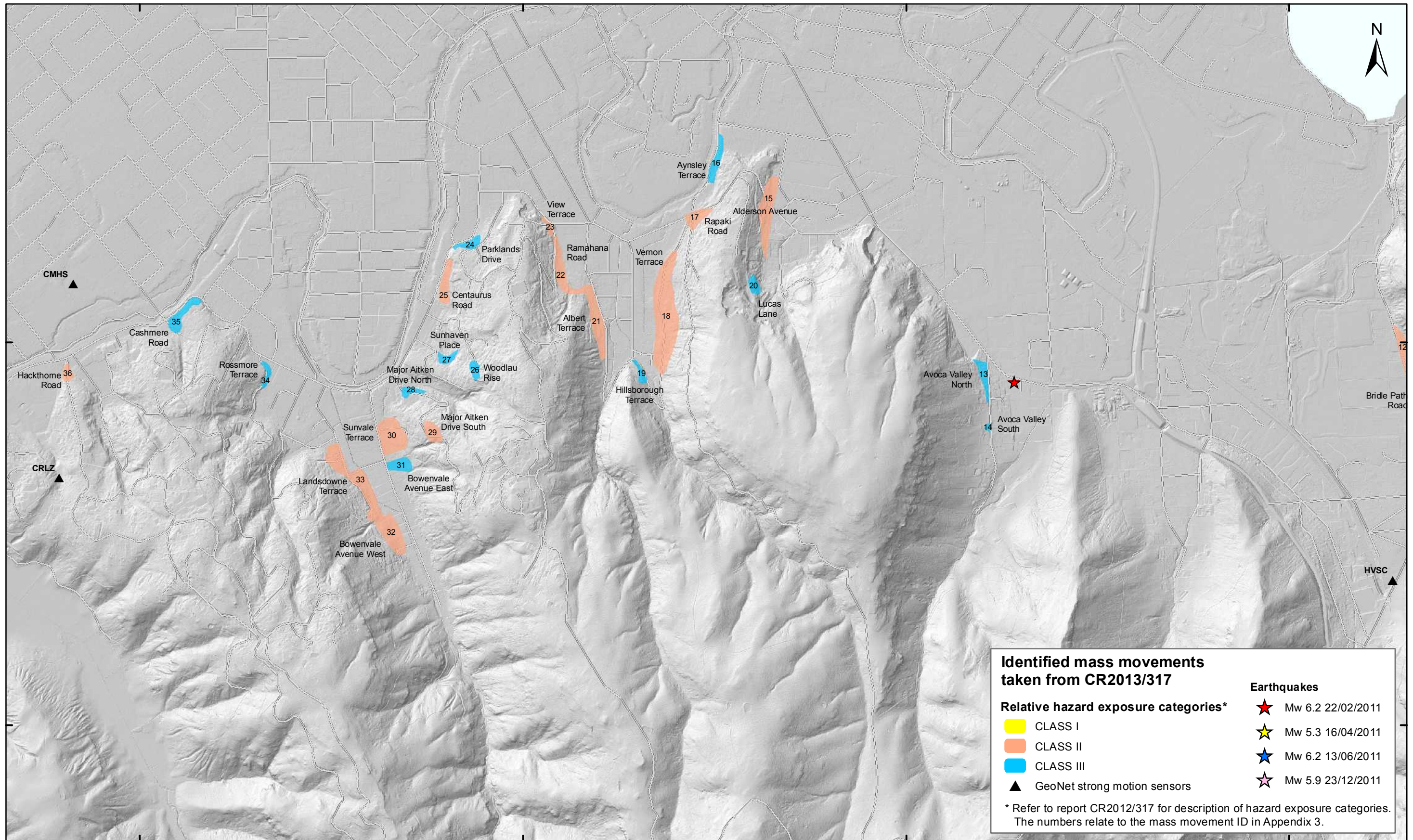
Christchurch City Council contracted GNS Science to carry out detailed investigations of the identified areas of mass movement, in order to assess the nature of the hazard, the frequency of the hazard occurring, and whether the hazard could pose a risk to life, a risk to existing dwellings and/or a risk to critical infrastructure (defined as water mains, sewer mains, pump stations, electrical substations and transport routes). This work is carried out under Task 4 of contract No. 4600000886 (December 2011).

The main purpose of the Task 4 work is to provide information on slope-stability hazards in the Port Hills. This is to assist Christchurch City Council land-use and infrastructure planning and management in the area, as well as to establish procedures to manage on-going monitoring and investigation of the hazards.

The Task 4 work is being undertaken in stages. Stage 1 is now complete (Massey et al., 2013; hereafter referred to as the Stage 1 report) and comprised: 1) a list of the areas susceptible to significant mass movement; 2) the inferred boundaries of these areas (as understood at the time of reporting); and 3) an initial “hazard-exposure” assessment (Table 1) intended only to prioritise the areas with regards to future investigations.

The Stage 1 report identified 36 mass movements of concern in the Port Hills project area. Four of these were further subdivided based on failure type, giving a total of 46 mass movements including their sub areas (Figure 1). Fifteen of these were assessed as being in the Class I (highest) relative hazard-exposure category, and the results of their detailed investigation and assessment are presented in Stage 2, which includes this (Stage 2) report on the Richmond Hill Class 1 mass movement areas. Mass movements assessed as being in the Class I category could cause loss of life, if the hazard were to occur, as well as severe damage to dwellings and/or critical infrastructure, which may lead to the loss of services for many people.

The Stage 1 report recommended that mass movements in the Class I relative hazard-exposure category should be given a high priority by Christchurch City Council for detailed investigations and assessment.



1570000

1572000

1574000

1576000

SCALE BAR: 0 0.5 1 km

EXPLANATION:
 Refer to Appendices 2 and 3 of report CR2012/317 for maps and more details of each mass movement.
 Background shade model derived from NZAM post earthquake 2011c (July 2011) LiDAR survey resampled to a 1 m ground resolution.
 Roads provided by Christchurch City Council (20/02/2012).
 PROJECTION: New Zealand Transverse Mercator 2000

DRW:
BL
 CHK:
CM



LOCATION MAP

**Port Hills
Christchurch**

FIGURE 1

Map 2

FINAL

REPORT:
CR2014/34

DATE:
June 2014

Table 1 Mass movement relative hazard exposure matrix (from the Stage 1 report; Massey et al., 2013).

		Hazard Class		
		1. Displacement* greater than 0.3 m and debris runout	2. Displacement* greater than 0.3 m; no runout	3. Displacement* less than 0.3 m; no runout
Consequence Class	1. Life – potential to cause loss of life if the hazard occurs	CLASS I	CLASS III	CLASS III
	2. Critical infrastructure ¹ – potential to disrupt critical infrastructure if the hazard occurs	CLASS I	CLASS II ²	CLASS II
	3. Dwellings – potential to destroy dwellings if the hazard occurs	CLASS I	CLASS II	CLASS III

*Note: Displacements for each assessed mass movements are inferred by adding together the mapped crack apertures (openings) along cross-sections through the assessed mass movements. They are a lower bound estimate of the total displacement, as no account is given for plastic deformation of the mass and not every crack has been mapped.

¹ Critical infrastructure is defined, for the purpose of this report, as infrastructure vital to public health and safety. It includes transport routes (where there is only one route to a particular destination), telecommunication networks, all water related mains and power networks (where there is no redundancy in the network), and key medical and emergency service facilities. Networks include both linear features such as power lines or pipes and point features such as transformers and pump stations.

² This relative hazard exposure category is based largely on an assumption that ‘critical infrastructure’ exists within these areas. Until further assessments are made on the nature of toe slumps and the existence of critical infrastructure in these areas, the relative hazard exposure category of these assessed mass movements has been appropriately assessed as “Class II”. It is likely that many of the assessed mass movements in the Class II relative hazard exposure category (where the hazard class is 2 and the consequence class is 2) would be more appropriately classified as “Class III” following further assessments.

1.1 THE RICHMOND HILL MASS MOVEMENTS

The Richmond Hill mass movement areas (numbers 2 and 3A), is shown in Figure 1 and Figure 2. These mass movements were assessed in the Stage 1 report (Massey et al., 2013) as being in the highest relative hazard exposure category (Class I). During the 22 February 2011 earthquake, a person was killed from falling rock whilst outside at Wakefield Avenue (Figure 2 and Figure 3). The risk to life of people in dwellings at the slope crest and toe, and road users along Wakefield Avenue from debris avalanches and cliff top recession hazards (collectively termed cliff collapse) presented in this report, provides an update from the original risk assessments presented by Massey et al. (2012a) and Taig and Massey, (2014).

1.1.1 Context and terminology

This report uses the terms: “cliff-top recession” to describe the result of landslides from the top and face of cliffs, and “debris avalanche” to describe the landslide process that inundates land at the cliff foot (referred to as “toe”) with countless boulders. The two are collectively referred to as cliff collapse.

Debris avalanche refers to a type of landslide comprising many boulders falling simultaneously from a slope. The avalanching mass starts by sliding, toppling or falling before descending the slope rapidly (>5 m/sec) (following Cruden and Varnes, 1996) by any combination of falling, bouncing and rolling.

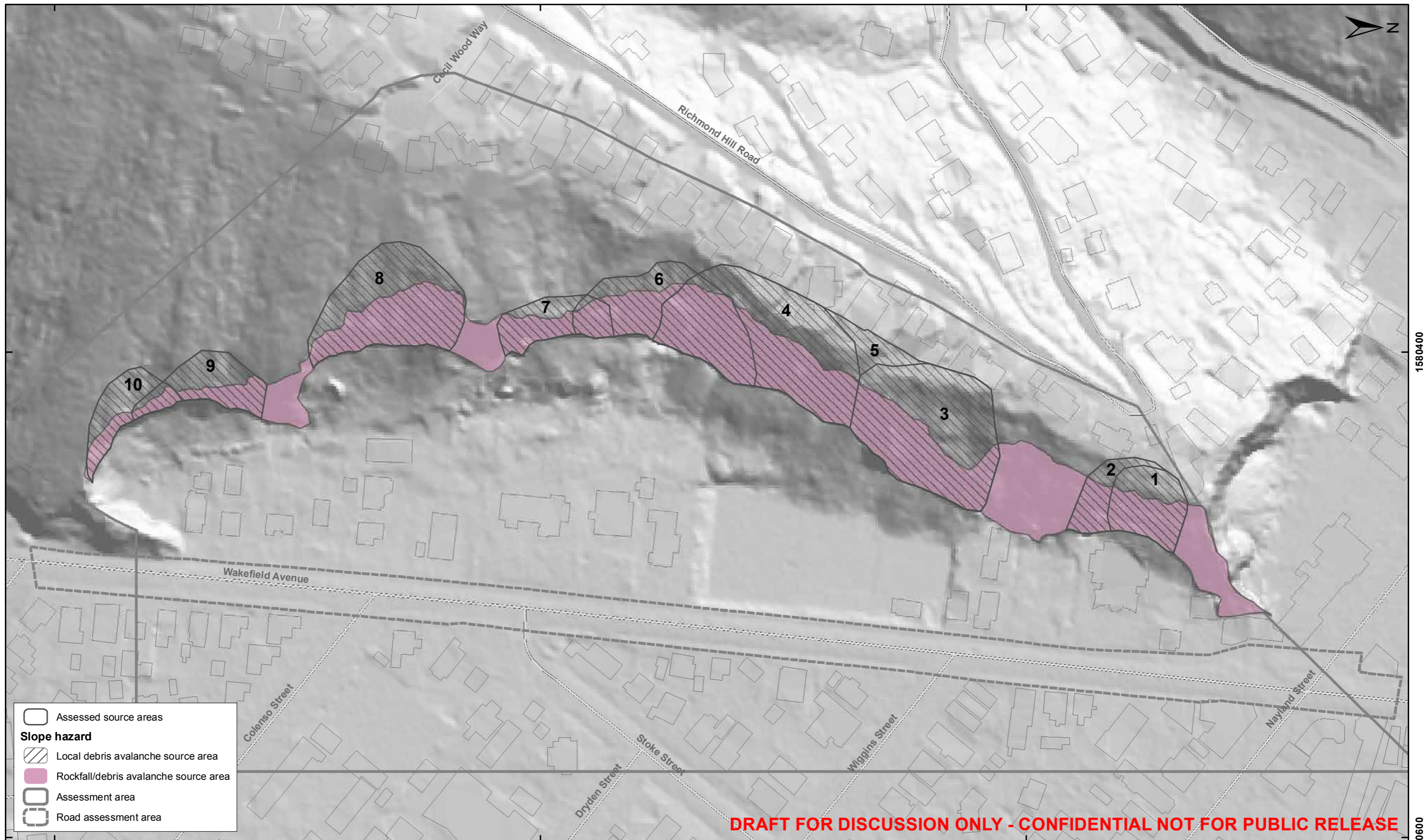
Cliff collapses have been considered separately from the failure and runout of individual boulders, referred to as “boulder rolls”. Although cliff collapses and boulder rolls both can be classified as rockfalls (Cruden and Varnes, 1996), the risk analysis for boulder rolls uses information on the location of each fallen boulder. Mapping individual boulder locations in a cliff collapse is impractical because of the large number of boulders involved. The main reason for the difference is that in a debris avalanche the boulders interact with one another, for rockfalls, involving individual boulders, the boulders behave more or less independently.

1.1.2 Local and random cliff collapse source areas

Further investigation of the site has involved field mapping, ground investigation (comprising subsurface drilling and trenching), laboratory testing, numerical modelling and monitoring (of the features in the field and how they have responded to earthquakes and rain). During the 2010/11 Canterbury earthquakes many rocks fell from these slopes, forming debris avalanches. The majority of failures involved relatively small volumes of debris, which fell from locations distributed randomly over the cliff face. The larger proportion of the total volume of debris that fell from the slopes however, came from a few much larger volume debris avalanches that were localised “discrete” failures of weaker parts of the rock mass.

The original assessment by Massey et al. (2012a) treated all of the debris avalanches as occurring from random locations anywhere on the slope. The original assessment is now superseded by this assessment, which identifies 10 specific areas on the slope where local cracking and rock-mass deformation has been focused. These areas are potentially more susceptible to failure during a future triggering event, and could result in local larger volumes of debris leaving the cliff, as single or multiple failures, with the resultant debris travelling further on the valley floor than occurred in the 2010/11 Canterbury earthquakes. These 10 assessed cliff-collapse source areas are additional to the randomly distributed cliff collapse sources, from which debris could fall from anywhere along the cliff during a future event.

This is the reason for the Richmond Hill mass movement being included in the Class I (high priority for further investigation) mass movements. The Richmond Hill assessment area is shown on Figure 2 and this report presents: 1) annual individual fatality risks for given users of Wakefield Avenue; and 2) revised annual individual fatality risks for dwelling occupants, within the given assessment area. Recommendations are provided to assist Christchurch City Council in considering potential options to mitigate the risk.



5175400 5175600 5175800 1580400 1580600

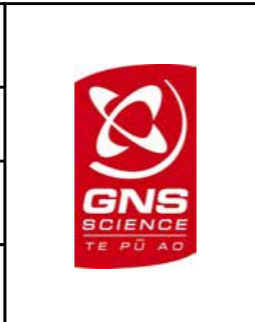


EXPLANATION:

Background shade model derived from NZAM post earthquake 2011c (July 2011) LiDAR survey resampled to a 1 m ground resolution.
 Roads and building footprints provided by Christchurch City Council (20/02/2012).
 PROJECTION: New Zealand Transverse Mercator 2000

DRW:
BL

CHK:
CM



MASS MOVEMENT LOCATION MAP

**Richmond Hill Road
Christchurch**

FIGURE 2

DRAFT

REPORT: CR2014/34 DATE: March 2014

1.2 PREVIOUS WORK AT THE RICHMOND HILL SITE

During the 22 February 2011 earthquakes, within the Richmond Hill assessment area, significant volumes of debris fell from the steep rock slope (debris avalanches), inundating dwellings at the cliff bottom, along with localised recession and cracking of the cliff top. These have been collectively termed cliff-collapse hazards (Figure 3). Previous investigations of the site comprised:

1. The risk to life of people in dwellings at the cliff top and bottom from cliff top recession and debris avalanche hazards has already been estimated by Massey et al. (2012a);
2. Field mapping of the crack distributions at the cliff top was carried out by GNS Science and Geotech Ltd., and the results are contained in the Stage 1 report (Massey et al., 2013); and
3. Engineering geological and geomorphological mapping of the site – including the cliff face (presented by Massey et al., 2012a).



Figure 3 A) Debris avalanche triggered by the 2010/11 Canterbury earthquakes (location of one fatality) at the northern end of the site. Wakefield Avenue is in the foreground. Photograph by G. Hancox GNS Science. B) Debris avalanches triggered by the 2010/11 Canterbury earthquakes have fallen onto properties at the foot of the former sea cliff along the western side of Wakefield Avenue (right foreground). Photograph by G. Hancox, GNS Science.

1.3 SCOPE OF THIS REPORT

The scope of this report as per Appendix A of contract No. 4600000886 (December 2011) is to:

1. Estimate the annual individual fatality risk for affected dwelling occupants from cliff collapse hazards (debris avalanche and cliff-top recession) in the assessment area in Figure 2;
2. Estimate the fatality risk for users of Wakefield Avenue from cliff collapse hazards for the section of road shown in Figure 2; and
3. Provide recommendations to assist Christchurch City Council with considering options to mitigate life risks, associated with the assessed cliff collapse hazards.

For the purpose of this risk assessment, dwellings are defined as timber framed single-storey dwellings, of building importance category 2a (AS/NZS 1170.0.2002). The consequences of the hazards discussed in this report on other building types have not been assessed.

The risk results contained in this report supersede the preliminary results contained in Working Note CR2013/04 (Massey and Della Pasqua, 2013).

An area of slumping, in loess, has also been identified at the southern end of the site, located about 100 m upslope from the cliff edge (mass movement 3B, Figure 1). This mass movement was assessed as being in the Class II relative hazard exposure category (Stage 1 report; Massey et al., 2013). This mass movement has not been assessed as part of this study.

The stability of the retaining walls along Richmond Hill Road at the slope crest has not been assessed as part of this work. Site specific investigations would be required to assess the stability of the retaining walls.

1.4 REPORT STRUCTURE

- Section 1.6 of the report details the methodology.
- Section 2 details the data used in the assessments.
- Sections 3–5 contain the results from the engineering geological, hazard and risk assessments respectively.
- Section 6 discusses the results of the risk assessment and explores the uncertainties associated with the estimated risks.
- Section 7 summarises the assessment findings.
- Section 8 presents recommendations for Christchurch City Council to consider.

1.5 METHODS OF ASSESSMENT

The site assessment comprised three stages:

1. Engineering geology assessment;
2. Hazard assessment; and
3. Risk assessment.

The methodology adopted for each stage is described in detail in Appendix 1, and is summarised in the following sections.

1.5.1 Engineering geology assessment

The findings presented in this report are based on engineering geological models of the site developed by GNS Science. The engineering geological assessment comprised:

1. Interpretation of aerial photographs covering the period 1940–2011, to determine the history of the site.
2. Geological and geomorphological field mapping to identify the materials and processes that have been active within the study area.
3. Surveying of cadastral survey marks within and around the study area, to determine the magnitudes of displacement of the slope during the 2010/11 Canterbury earthquakes.
4. Assessment of the results from the surveying of monitoring marks installed on the site by Aurecon NZ Ltd. (under contract to Christchurch City Council), following the 22 February 2011 earthquake. This was undertaken to assess the amount of slope displacement relating to the 22 February, 16 April, 13 June and 23 December 2011 earthquakes.
5. Assessment of airborne LiDAR (Light Detecting and Ranging) surveys collected by AAM Hatch Ltd. in 2003 and New Zealand Aerial Mapping Ltd. in March 2011 and July–August 2011.
6. Assessment of results from terrestrial laser scan survey monitoring of the slope face carried out by GNS Science between 1 March 2011 and 1 October 2013.
7. Assessment of the results of exploratory work carried out by: Aurecon New Zealand Ltd. for Christchurch City Council; and Tonkin and Taylor Ltd. for the Earthquake Commission. The work comprised:

- Aurecon NZ Ltd.: 1) diamond core drilling of three holes (vertical), totalling 232 m; 2) installation of 1 piezometer (in 1 drillhole); and 3) installation of two inclinometers (in two drillholes, a total length of about 160 m). Refer to Revell and Pletz (2013) for details.
 - Tonkin and Taylor Ltd.: 1) diamond core drilling of four holes (two vertical and two inclined), totalling about 115 m; 2) installation of one piezometer in one drillhole; 3) cone penetration tests (CPT), two tests, to depths of 5.9 and 6.3 m below ground level respectively and installation of two piezometers, one in each CPT; 4) excavation of four test pits, to depths of 1.8–4.1 m; and 5) mapping of cracks at the cliff top. Refer to Tonkin and Taylor (2012a) for details.
8. Laboratory strength testing – carried out in-house by GNS Science – of selected samples retrieved from drillholes and from field exposures in the Port Hills. Refer to Carey et al. (2014) for details.
 9. Assessment of results from borehole (downhole) shear-wave seismic surveys carried out by Southern Geophysical Ltd. for GNS Science. These works comprised the surveying of a surface-generated shear wave signal at 2 m intervals between the surface and the maximum reachable depth inside the drillholes. Two of the drillholes carried out by Aurecon New Zealand Ltd were surveyed. Refer to Southern Geophysical Ltd. (2013) for details.
 10. Construction of an engineering geological map and seven engineering geological cross-sections, based on the results from the aerial photograph interpretation, surveying, field mapping, and the ground investigations carried out by Aurecon NZ Ltd. (Revell and Pletz, 2013), and Tonkin and Taylor Ltd. (Tonkin and Taylor, 2012a). These were used as the basis for the hazard and risk assessments.

1.5.2 Hazard assessment

The hazard assessment method followed three main steps:

Step 1 comprises assessment of the static stability of the slope under non-earthquake (static) conditions, and an assessment of the dynamic (earthquake) stability of the slope, adopting selected slope cross-sections, to determine the likelihood of large-scale cliff collapse, and whether these can/cannot be triggered under static and/or dynamic conditions.

Step 2 uses the results from step 1 to define the likely failure geometries (source areas) of potential failures, which are combined with the crack patterns and slope morphology and engineering geology mapping to estimate their likely volume. Three volumes are defined for each source area (upper, middle and lower volumes), which represent the probable range of potential source areas that could occur within the assessment area.

Step 3 models: 1) the distance the debris travels down the slope (runout); and 2) the volume of debris passing a given location, should the failure occur. Modelling is done for each representative source area, and for the upper, middle and lower volume estimates.

The results from this characterisation are then used in the risk assessment.

1.5.2.1 Estimation of Slope Failure volumes

The original cliff-collapse risk assessment by Massey et al. (2012a) was based on the simulation of potential future cliff collapses that were all randomly distributed across the slope face. The results of the engineering geological assessments identified that during the 2010/11 Canterbury earthquakes many cliff collapses were randomly distributed across the slopes. However, these only accounted for a relatively small proportion of the total volume of debris leaving the cliff. Much of the debris leaving the Richmond Hill cliff (and other similar cliffs in the Port Hills), derived from a few discrete (local) failures that involved larger volumes of rock, particularly in areas where the rock mass strength had been weakened as a result of earthquake-induced cracking.

This assessment improves on the original work by Massey et al. (2012a), by:

1. Taking into account the potential for large local cliff collapses from 10 assessed source areas;
2. Revising the risk estimates from other cliff collapses that are randomly distributed across the cliff; and
3. Including an assessment of the risk from cliff collapses on users of Wakefield Avenue.

The volumes of debris that could fall from the cliff under dynamic (earthquake) and static (non-earthquake, e.g., rain) conditions have been assessed.

Earthquake generated failure volumes:

- The volumes of material lost from cliffs during the 2010/11 Canterbury earthquakes were estimated using change models generated from airborne LiDAR and terrestrial laser scan surveys. The volumes lost in each earthquake were graphed against the corresponding synthetic free-field rock-outcrop peak horizontal ground accelerations relating to the earthquake (calculated specifically for Richmond Hill; Holden et al., 2014). The synthetic free-field rock-outcrop motions were used because there are no instrumental records at the site, and the existing instrumental records from nearby sites each contain site effects that relate to the instrument site.
- Assessment of the many failures that occurred from the steep rock slopes in the Port Hills during the 2010/11 earthquakes indicates that about 60% of the total volume of debris leaving the cliffs during the 13 June 2011 earthquakes is attributable to a small number of specific local failures of greater than 2,500 m³ in volume.
- The most likely locations and volumes of 10 potential large local failures were estimated based on the assessment of crack distributions, inferred displacements, slope morphology and geology and numerical analyses. The purpose of this exercise was to constrain the likely depth, width and length of the three assessed source areas.
- Three possible failure volumes were estimated for each assessed source area; a low, middle and upper estimate. This variation in failure volume is intended to reflect the range of uncertainty from the results of the modelling and mapping, e.g., the depth, width and length dimensions.
- The credibility of these potential failure volumes was evaluated by comparing them against: 1) the volumes of relict failures recognised in the geomorphology near the site and elsewhere in the Port Hills; and 2) the volume frequency distribution of debris that fell from this site and other similar sites in the Port Hills during the 2010/11 earthquakes.

Non-earthquake generated failure volumes:

- There are four main sources of information on historical non-earthquake failures for the Port Hills: 1) archived newspaper reports from 1870–1945; 2) the GNS Science landslide database, which is “complete” only since 1996; 3) insurance claims made to the Earthquake Commission for landslips which are “complete” only since 1996; and 4) information from local consultants (M. Yetton, Geotechnical Consulting Ltd.) which incompletely covers the period 1987–present. These have been used to estimate the likely process rate of non-seismic rockfalls from the slope. These data are detailed in Massey et al. (2012a).
- These failure volumes were assumed to be randomly distributed across the slope as per those recorded from sequential terrestrial laser scan surveys of the slope carried out after the 2010/11 earthquakes, during a period when no strong earthquakes occurred.

1.5.2.2 Estimation of debris runout

The distance that debris from debris avalanches travels down a slope is called the runout. The runout distance of debris falling from Richmond Hill has been assessed both empirically and numerically. The methods adopted are described in Appendix 1.

For large local failures from the three assessed source areas, the volume of debris passing a given distance down the slope was assessed numerically, using the RAMMS software. These calculated runout distances were calibrated using data from debris avalanches that occurred from Richmond Hill and other similar slopes in the Port Hills, during the 2010/11 Canterbury earthquakes.

For the randomly distributed failures, empirical models were used to estimate the debris runout down the slope. These models were based on the volumes of debris that fell and travelled given distances downslope at Richmond Hill during the 2010/11 earthquakes.

1.5.3 Risk assessment

The risk metric assessed in this report is the annual individual fatality risk. The risk is assessed for dwelling occupants and regular road users from the cliff-collapse hazards assessed in this report. The cliff collapse hazards are:

1. Debris avalanches – a type of landside comprising many boulders falling simultaneously from a slope. The rocks start by sliding, toppling or falling before descending the slope rapidly (typically at greater than five metres a second) by any combination of falling, bouncing and rolling; and
2. Cliff-top recession – the result of parts of the cliff top collapsing, causing the cliff edge to move back up the slope.

The quantitative risk assessment uses risk-estimation methods that follow appropriate parts of the Australian Geomechanics Society framework for landslide risk management (Australian Geomechanics Society, 2007). It provides risk estimates suitable for use under SA/SNZ ISO1000: 2009.

Using the Australian Geomechanics Society (2007) guidelines for landslide risk management, the annual fatality risk to an individual is calculated from:

$$R_{(LOL)} = P_{(H)} \times P_{(S:H)} \times P_{(T:S)} \times V_{(D:T)} \quad \text{Equation 1}$$

where:

$R_{(LOL)}$ is the risk (annual probability of loss of life (death) of a person) from debris/earth flows/avalanches;

$P_{(H)}$ is the annual probability of the initiating event;

$P_{(S:H)}$ is the probability that a person, if present, is in the path of the debris at a given location;

$P_{(T:S)}$ is the probability that a person is present at that location; and

$V_{(D:T)}$ is the vulnerability, or probability that a person is killed if present and hit by debris.

The details relating to each of the above input parameters used in the risk assessments are discussed in Appendix 1.

1.5.3.1 Event annual frequencies

The frequency of occurrence of the events that could trigger the assessed cliff collapse failure volumes is unknown. In place of this lack of information, the ranges of frequencies are defined, and the magnitudes of representative triggering events with these frequencies of occurrence are used to estimate the likely volumes of collapses that are triggered when the triggering event occurs.

- For non-earthquake triggers such as rainfall, rates of debris avalanches, rockfalls and cliff top recession triggered without earthquakes were taken from Massey et al. (2012a). These rates were used to estimate the contribution to total risk from non-earthquake triggering events. Four representative event-trigger frequencies were used and the volumes of the debris triggered by events with these frequencies were estimated.
- For earthquake events, rates of debris avalanches and rockfalls and cliff top recession were estimated using the empirical relationship between the volumes of debris leaving the cliffs, and amounts of cliff top recession recorded during the 2010/11 Canterbury earthquakes, and the synthetic free field peak ground acceleration of the event that triggered them. Seven representative event-trigger frequencies were used and the volumes of debris triggered by events with these frequencies were estimated.
- For earthquake triggers, the frequency of a given free-field peak ground acceleration occurring is obtained from the New Zealand National Seismic Hazard Model (Stirling et al., 2012), using a modified form of the 2010 version of the National Seismic Hazard Model (Gerstenberger et al., 2011), which takes into account the increased level of seismicity in the Christchurch region.
- For the 10 assessed source areas – where larger volumes of rock could potentially fall, leading to larger areas of cliff top to be lost – the probability of failure was estimated based on the amount of permanent slope displacement that could occur in response to each of the seven representative events. This was done, adopting the decoupled method (Makdisi and Seed, 1978), by using:

- a. The relationship between the yield acceleration (K_y) and the maximum average acceleration of the mass (K_{MAX}), derived from back-analysing the permanent displacement of the slope during the 2010/11 earthquakes; and
- b. The New Zealand National Seismic Hazard Model to provide the annual frequencies (return periods) of free-field rock outcrop peak horizontal ground accelerations (A_{MAX}) and therefore the annual frequencies of the equivalent maximum average acceleration of the mass (K_{MAX}).

The methods adopted are discussed in detail in Appendix 1.

1.5.3.2 Scenarios adopted for modelling

Three cliff collapse risk scenarios have been adopted for modelling (Table 2). The three scenarios are chosen to examine the effect on risk of uncertainties in: 1) the assessed total volume that could be generated in a representative event; and 2) the volume of debris that passes a given distance down the slope.

Table 2 Risk scenarios used in the modelling of cliff collapses.

Volume	Source-volume scenario	Runout volume scenario
Earthquake-induced volumes		
Total volume generated in a representative earthquake event. Based on the empirical relationship between peak ground acceleration and volume leaving the slope, estimated from slope failures at Richmond Hill during the 2010/11 earthquakes.	<ul style="list-style-type: none"> A) The relationship adopted is the mean plus one standard deviation B) The relationship adopted is the mean C) The relationship adopted is the mean minus one standard deviation 	
Local earthquake failures. Representing 60% of the total earthquake volume	<ul style="list-style-type: none"> A) Adopting upper estimates of the source volumes (of assessed source areas 1–3) B) Adopting middle estimates of the source volumes (of assessed source areas 1–3) C) Adopting lower estimates of the source volumes (of assessed source areas 1–3) 	<ul style="list-style-type: none"> A) RAMMS model adopting upper source volume estimates B) RAMMS model adopting mean source volume estimates C) RAMMS model adopting the lower source volume estimates
Randomly distributed earthquake failures. Representing 40% of the total earthquake volume.	<ul style="list-style-type: none"> A) Adopting 40% of the total volume derived from the mean plus one standard deviation relationship B) Adopting 40% of the total volume derived from the mean relationship C) Adopting 40% of the total volume derived from the mean minus one standard deviation relationship 	<ul style="list-style-type: none"> A) Empirical model adopting the mean plus 1 standard deviation relationship B) Empirical model adopting the mean relationship C) Empirical model adopting the mean minus 1 standard deviation relationship
Non-earthquake induced volumes		
Randomly distributed non-earthquake failures. Volume estimated from historical non-earthquake rockfall production rates	<ul style="list-style-type: none"> A) Historical rates multiplied by a factor of two to take into account the increased production rates as the rock mass (post-2010/11 earthquakes) is now broken. B) Historical rates C) Historical rates divided by two to take into account any potential overestimate of the historical rockfall rates 	<ul style="list-style-type: none"> A) RAMMS model adopting upper source volume estimates B) RAMMS model adopting mean source volume estimates C) RAMMS model adopting the lower source volume estimates

2.0 DATA USED

The data and the sources of the data used in this report are listed in Table 2.

Table 3 Summary of the main data used in the analysis. LiDAR is Light Detecting and Ranging.

Data	Description	Data source	Date	Use in this report
Post-22 February 2011 earthquake digital aerial photographs	Aerial photographs were taken on 24 February 2011 by NZ Aerial Mapping and were orthorectified by GNS Science (10 cm ground resolution).	NZ Aerial Mapping	Last updated 24 February 2011	Used for base maps and to map extents of cliff collapses triggered by the 22 February 2011 earthquakes.
Post-13 June 2011 earthquake digital aerial photographs	Aerial photographs were taken between 18 July–26 August 2011 and orthorectified by NZ Aerial Mapping (0.5 m ground resolution).	NZ Aerial Mapping	18 July–26 August 2011	Used to map extents of cliff collapses triggered by the 13 June 2011 earthquakes.
Historical aerial photographs	Photographs taken in 1940, 1946, 1975, 1975 and 1984 by multiple sources and orthorectified by NZ Aerial Mapping and GNS Science (at variable ground resolutions).	NZ Aerial mapping and GNS Science	1940, 1946, 1975, 1975 and 1984	Used to assess the site history before the 2010/11 Canterbury earthquakes.
LiDAR digital elevation model (2003)	Digital Elevation Model derived from LiDAR survey carried out in 2003; resampled to a 1 m ground resolution.	AAM Hatch	2003	Used as the pre-22 February 2011 ground model.
LiDAR digital elevation model (2011a)	Digital Elevation Model derived from post-22 February 2011 earthquake LiDAR survey; re-sampled to 1 m ground resolution.	NZ Aerial Mapping	8–10 March 2011	To generate change models (between the 2003 and 2011a surveys) to determine the locations, extents and volumes of material leaving the cliffs and where it was deposited.
LiDAR digital elevation model (2011b)	Digital Elevation Model derived from LiDAR survey; resampled to a 1 m ground resolution.	AAM Hatch	May 2011	To generate a model of changes (between the 2011a and 2011b surveys) to determine the locations, extents and volumes of the material leaving the cliffs and where it was deposited.

Data	Description	Data source	Date	Use in this report
LiDAR digital elevation model (2011c)	Digital Elevation Model derived from post-13 June 2011 earthquake LiDAR survey; re-sampled to 1 m ground resolution.	NZ Aerial Mapping	18 July– 26 August 2011	To generate a model of changes (between the 2011b and 2011c, and the 2011a and 2011c surveys) to determine the locations, extents and volumes of the material leaving the cliffs and where it was deposited.
Terrestrial laser scan (TLS) surveys	Multiple Digital Elevation Model's derived from surveys following the 22 February, 16 April and 13 June 2011 earthquakes.	GNS Science	Last survey carried out October 2013	To generate models of changes (between surveys) to determine the distribution and volume of material leaving the cliffs at selected areas where surveys were made.
Christchurch building footprints	Footprints are derived from aerial photographs. The data originate from 2006 but have been updated in the cliff collapse zones by CCC using the post-earthquake aerial photos.	Christchurch City Council (CCC)	Unknown	Used to identify the locations of residential buildings in the cliff collapse zones and to distribute the population (from the 2006 census data).
Christchurch City Council (CCC) cliff collapse database	The location, date and size of debris associated with cliff collapses mapped in the field from 22 February and 13 June 2011 earthquakes	Engineering consultants working for CCC. Data compiled by CCC.	Last updated 11 October 2011	Used to estimate the travel distance of debris from the cliffs.
GNS Science cliff collapse database	Location, date and size of debris associated with cliff collapses mapped from aerial photographs (utilising the NZAM 26 February 2011 10 cm ground resolution), and from field mapping.	GNS Science and University of Canterbury	Last updated December 2013	Used to estimate the travel distance of debris from the cliffs.
Christchurch City Council recorded house hits	Data on the numbers of houses hit and penetrated by debris from cliff collapses triggered during the 2010/2011 earthquakes.	Engineering consultants working for CCC.	Received 22 November 2011	Used to assess the vulnerability of people in the homes affected by cliff collapse.

Data	Description	Data source	Date	Use in this report
GNS Science landslide database	Approximate location, date, and probably trigger of newsworthy landslides	GNS Science	Updated monthly	Used to estimate the likely numbers and volumes of pre-earthquake cliff collapses in the areas of interest.
Earthquake Commission claims database	Location, date and brief cause of claims made in the Port Hills of Christchurch since 1993.	Earthquake Commission (EQC)	1993–August 2010	Used to estimate the likely numbers and volumes of pre-earthquake cliff collapses in the areas of interest.
Ground-acceleration records for the 2010/2011 Canterbury earthquakes	Ground accelerations recorded at the GeoNet strong motion sites located in the Port Hills.	GeoNet	From 22 February 2011	Used to correlate with the estimated volumes of material leaving the cliffs in response to the 2010/11 Canterbury earthquakes.
Synthetic earthquake time/accelerations	Earthquake time acceleration history's for the four main 2011 earthquakes 22 Feb, 16 Apr, 13 Jun and 23 Dec.	GNS Science	February 2014	Used as inputs for the seismic site response analysis.
Composite seismic hazard model	The increased level of seismicity in the Canterbury region since 4 September 2010 has been quantified using a modified form of the national seismic hazard model.	GNS Science	Updated December 2013	Used to estimate the frequency of occurrence of a given peak ground acceleration.
Rainfall records for Christchurch	Rainfall records for Christchurch from various sources, extending back to 1873.	NIWA	1873–present	Used to assess the return periods of past storms triggering landslides of known magnitudes in the Port Hills.
Drillhole logs	The logs from cores extracted from holes bored into the cliff top areas covered by this report.	Tonkin and Taylor on behalf of EQC and Aurecon for CCC	February 2012 and February 2013	Used in generating the engineering geological models of the cliff interiors.
Downhole shear wave surveys	Downhole (drillhole) shear wave velocity surveys carried out in the Aurecon drillholes.	Southern Geophysical Ltd. (2013)	February 2014	Used to determine the dynamic properties of the materials in the slope for the seismic site response analysis.

Data	Description	Data source	Date	Use in this report
Geotechnical laboratory data	Geotechnical strength parameters for selected soil and rocks in the Port Hills.	GNS Science	February 2014	Used for static and dynamic slope stability analysis.
Field work	Field mapping of cliff collapses and ground truthing of the risk analyses.	GNS Science and the Port Hills Geotechnical group	22 February 2011–present	Used in generating the engineering geological models of the cliffs. Results from field checks used to update risk maps.
Traffic data	Numbers of cars passing along Wakefield Avenue.	CCC	2000–2012	Road-user risk assessment

3.0 SITE ASSESSMENT (RESULTS)

3.1 SITE HISTORY

3.1.1 Aerial photograph interpretation

Aerial photographs of the site are available for various dates since 1940. Table 4 summarises the photo details and main features noted.

Table 4 Summary of observations from aerial photographs used to assess the site history at Richmond Hill Road.

Date/scale of photo	Run/print number/resolution	Comments
1940 1:10,000 (approx.)	Moderate resolution	<p>Several large arcuate features – possible relict landslide scars – are apparent in the cliff face. Below these features are what appear to be corresponding accumulations of talus west of Wakefield Avenue. These features are labelled 1–8 on (Figure 4, and Appendix 2 Map 1). Several very large boulders are visible on the ground surface at the slope toe. At the southern end of Wakefield Avenue a possible boulder(s) can be seen adjacent to the current position of the western road edge.</p> <p>The croquet lawn, the church and a few possible farm buildings are apparent beyond the slope toe (west of Wakefield Avenue), but no buildings were present at the slope crest off Richmond Hill Road. Richmond Hill Road is present but appears to be a farm access track.</p> <p>Several small areas of bare ground (possible tunnel gullies) are present towards the west of the cliff top at the southern end of Wakefield Avenue.</p> <p>At the northern end of the Wakefield Avenue there is an area of bare ground or possible recent debris at the toe of the rock slope. This may be due to earthworks (a track is visible leading to the area) relating to the removal of talus debris.</p> <p>Several brighter areas are apparent on the cliff face; these may relate to relatively more recent failure of material from the cliff.</p>
30/05/1946 1:5,500 (approx.)	SN Good resolution	<p>At the northern end of Wakefield Avenue (adjacent to the bare area of ground in 1940) is now a building (possibly a workshop).</p> <p>Much of the cliff face is in shadow but vegetation (and possibly talus) at the southern end of the site (west of Wakefield Avenue at the slope toe) has been cleared for house construction.</p> <p>Several small possible landslide scars are apparent in the loess at the cliff top, with areas of tunnel gully erosion also visible in the same area.</p> <p>No buildings are present at the slope crest east of Richmond Hill Road.</p>
1973, 1:10,000 (approx.)	Poor resolution	<p>Most of the buildings currently present at the slope toe along Wakefield Avenue, and at the cliff top along Richmond Hill Road have now been constructed.</p> <p>Much of the cliff face and toe are in shadow.</p>
1975, 1:10,000 (approx.)	Poor resolution	No obvious change. Much of the cliff face and toe is in shadow.
1984, 1:6,000 (approx.)	Good resolution	No obvious change. Some new boulders appear to be present at the cliff toe that were not present in 1946.

3.1.2 Before the 2010/11 Canterbury earthquakes

- Historical (post-European settlement to recent) and pre-historical talus, formed of deposits of successive rockfalls from the slope, has accumulated on ancient former beach and sand-dune sediments along Wakefield Avenue at the toe of a former coastal cliff.
- Using the 2003 LiDAR survey digital elevation model of these slopes, and by projecting the rock slope face at the toe of the slope through the talus to intersect an assumed pre-talus ground surface, it was possible to estimate likely volumes of talus present before the 2010/11 Canterbury earthquakes. At Wakefield Avenue, about 52,500 ($\pm 10,000$) m³ of talus mixed with an unknown proportion of dune sand had accumulated at the toe of the slope prior to the date of LiDAR acquisition (Figure 4 and Appendix 2, Map 1). The likely age of the coastal beach surfaces on which this material was deposited may be about 3,500–3,700 calibrated radiocarbon years (McFadgen and Goff, 2005) suggesting rockfall accumulation rates averaging 14–15 m³/year. If it is assumed that dune sand is largely filling interstices between fallen boulders, the proportion of dune sand may be ignored.
- The debris along the foot of the cliff is largely located below just a few arcuate features in the slope face, which are interpreted as relict landslide scars (apparent in the 1940 aerial photos). Estimated debris volumes per arcuate feature range from 1,500–12,700 m³, each of which we assume fell as a result of a single landslide rather than as the accumulation from several smaller landslides (this assumption is justified only as a more conservative option).
- The cliff-top recession rate at Wakefield Avenue (adopting a rockfall accumulation rate averaging 14–15 m³/year, assuming no bulking factor from source to debris) would be about 0.5 and 0.6 m per 1000 years – assuming a slope-face area of 26,560 m², and that failures are evenly distributed across the face.
- However, the majority of cliff-top loss occurs in discrete events, as shown by the 2010/11 Canterbury earthquakes. It is possible that the pre-2003 talus accumulated mostly in past earthquakes (one of which may have triggered the large rockfall that blocked Monk's Cave about 500 years ago and the large rockfalls in Moa Cave around the same time).
- The GNS Science landslide catalogue records six landslides that mainly affected roads in the region between 1996 and 2011; about 0.4 events per year. These are all recorded as being small (<10 m³) and mainly initiated by rainfall. The GNS Science landslide catalogue records two homes hit by a rockfall in Wakefield Avenue (at the toe towards the southern end of the site) during rain on 13–14 August 2006. Insurance claim assessments carried out on behalf of the Earthquake Commission by a local consultant, Geotechnical Consulting Ltd., report the volume of rock that fell from the Wakefield Cliff in August 2006 was about 300 m³ (N. Traylen, personal communication 2011).

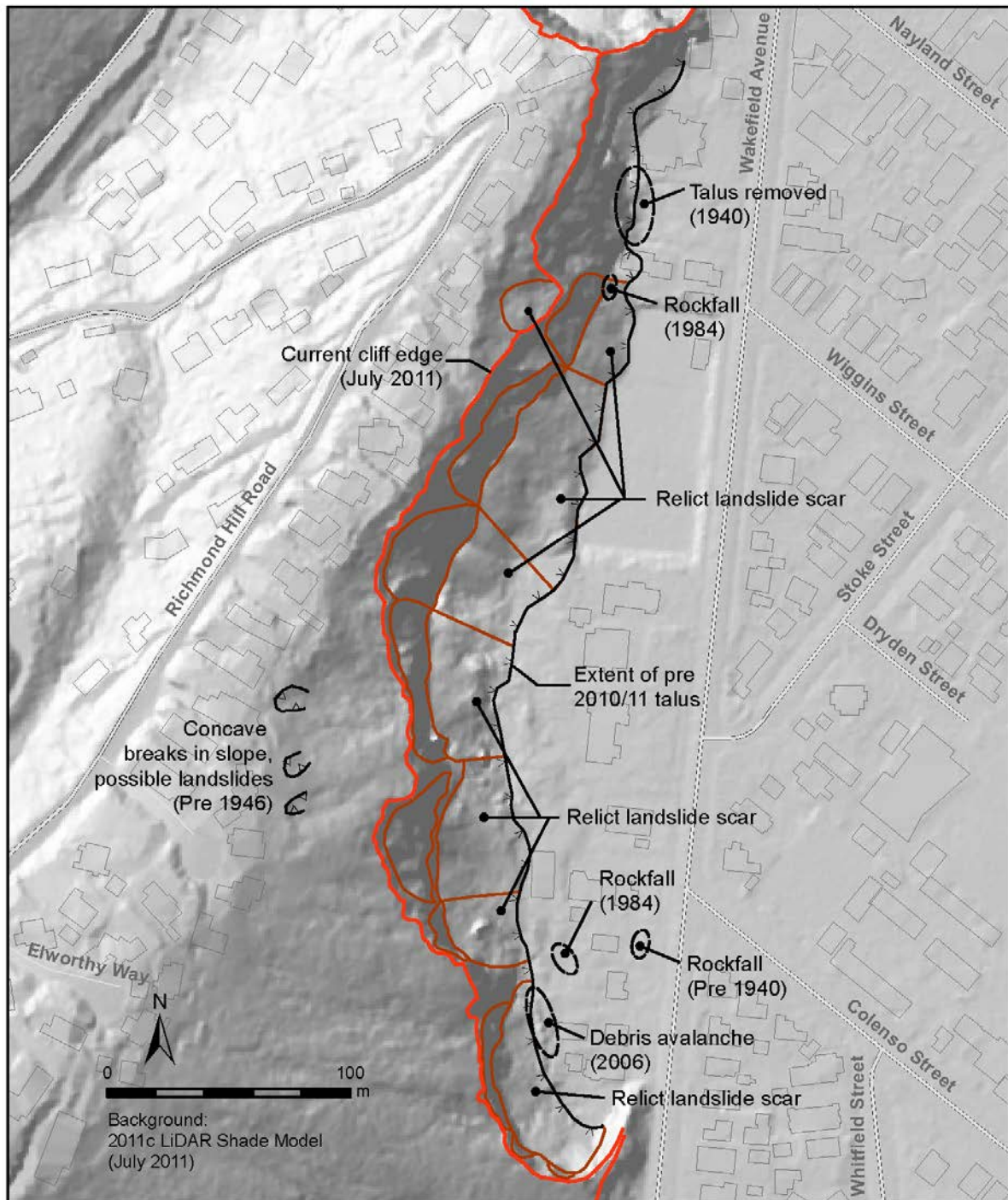


Figure 4 Main features identified at the site from field mapping and the interpretation of historical aerial photographs.

3.1.3 During the 2010/11 Canterbury earthquakes

- *4 September 2010 (Darfield) earthquake:* No 2010 displacement of the cliff top has been reported to GNS Science. Approximately 40 m³ of debris is estimated to have fallen from the cliff face (M. Yetton, personal communication 2011).
- *22 February 2011 earthquakes:* Some cracking at the cliff top (in loess) was reported to the Port Hills Geotechnical Group (PHGG) consultants following this earthquake. These cracks were assessed at the time as being superficial, and of little significance to the stability of the cliff. During this earthquake approximately 5,260 (±1,000) m³ of rock fell from the slope (Table 3), onto residential and commercial properties at the

bottom of the slope, killing one person who was working immediately below the cliff. In some locations the cliff edge receded up to 3 m. Many cracks were visible in the cliff face after these events (Massey et al., 2012a).

- *16 April 2011 earthquake:* No displacement of the cliff top or opening of the mapped cracks was reported or detected by GNS Science. About 920 (± 80) m³ of rock fell from the cliff, some of it onto dwellings at the bottom (Appendix 3).
- *13 June 2011 earthquake:* The mapped crack distributions (in loess) at the cliff top (shown on the maps in the Stage 1 report) were mainly generated by the 13 June 2011 earthquake. These include those related to the loess slump, a Class II mass movement, number 3B shown on Figure 1. Horizontal permanent displacement of the cliff top in response to this earthquake (inferred from analysis of geodetic surveys and measuring of crack apertures) varied between 200 and 800 mm towards the east, with vertical displacements of 200–400 mm. During this earthquake, about 10,120 ($\pm 1,050$) m³ of rock fell off the cliff, some onto dwellings and other buildings at the bottom, which were unoccupied following the 22 February 2011 earthquake. The cliff edge receded by up to 5 m in some locations (Massey et al., 2012a) and many more cracks appeared on the cliff face.
- *23 December 2011 earthquake:* Monitored survey marks at the cliff top indicate horizontal displacements relative to adjacent land of about 80 mm to the east and vertical displacement of 50 mm downward. Re-survey of crack apertures – by PHGG consultants – showed further opening of existing cracks. During this earthquake about 1,400 (± 130) m³ fell from the cliff, on to unoccupied dwellings at the bottom (Appendix 3).

3.1.4 After the 2010/11 Canterbury earthquakes

- Analysis of survey results subsequent to the 2010/11 Canterbury earthquakes shows that horizontal displacement of the cliff edge locally reaches 30 mm towards the east with vertical displacement up to about 20 mm. These displacements occurred over seven days between 11 and 17 August 2012, following a large rainstorm.
- The survey results also reveal slow displacement of the cliff edge, at almost constant rates (of about 25 mm/yr) over the past two years (July 2011–present). The area affected and cause of this movement is currently unknown.
- About 440 (± 160) m³ of rock fell from the slope face between January 2012 and January 2013 as a series of small events rather than one larger event. No notable ground accelerations were recorded during this interval in the local area. However, a notable rainstorm of 61 mm (24-hour rainfall total) occurred on 13 August 2012.
- Several small (typically less than 50 m³) debris/earth flows originating from the loess at the cliff top have been identified after rainfall. Surface water has been observed flowing down the cliff face during rain. It may be assumed that storm water and sewer pipes within the cracked mass at the slope crest are broken and leaking (runoff from some deformed paved areas may now drain to the cliff if the drainage gradient has reversed) and may be contributing to these types of landslide.

3.2 SITE INVESTIGATIONS

3.2.1 Geomorphological mapping

The results from the field mapping of slope morphology, interpreted surface materials and their genesis, surface deformation mapping and other relevant information are shown in Figure 5.

The site consists of an asymmetric north trending spur with a very steep eastern flank (cliff face) and a gentler sloping western flank. The width and height of the spur decreases towards the north, from cross-section 7 to cross-section 1 (Figure 5). The cliff is about 70 m high, 540 m long with a slope angle of 50–90°. The northern part of the cliff has a main aspect towards 110° and the southern part towards 80° indicating a general arcuate shape. The steeper cliff on the eastern side is a relict or former coastal cliff.

Richmond Hill Road is located at the slope crest about 50 to over 100 m away from the cliff edge. Wakefield Avenue is located some 40–100 m out (east) from the talus at the foot of the cliff.

3.2.2 Subsurface trenching and drilling

Subsurface information is available from the four drillholes carried out by Tonkin and Taylor Ltd., for the Earthquake Commission in 2011 (designated BH-RHR-01 to 03 and shown in Figure 6), and the three drillholes carried out by Aurecon New Zealand Ltd., as part of this project (BH-RHR-01 to BH-RHR-03, Figure 6). Details are summarised in Table 6.

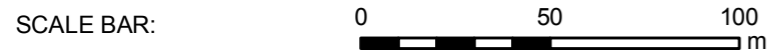
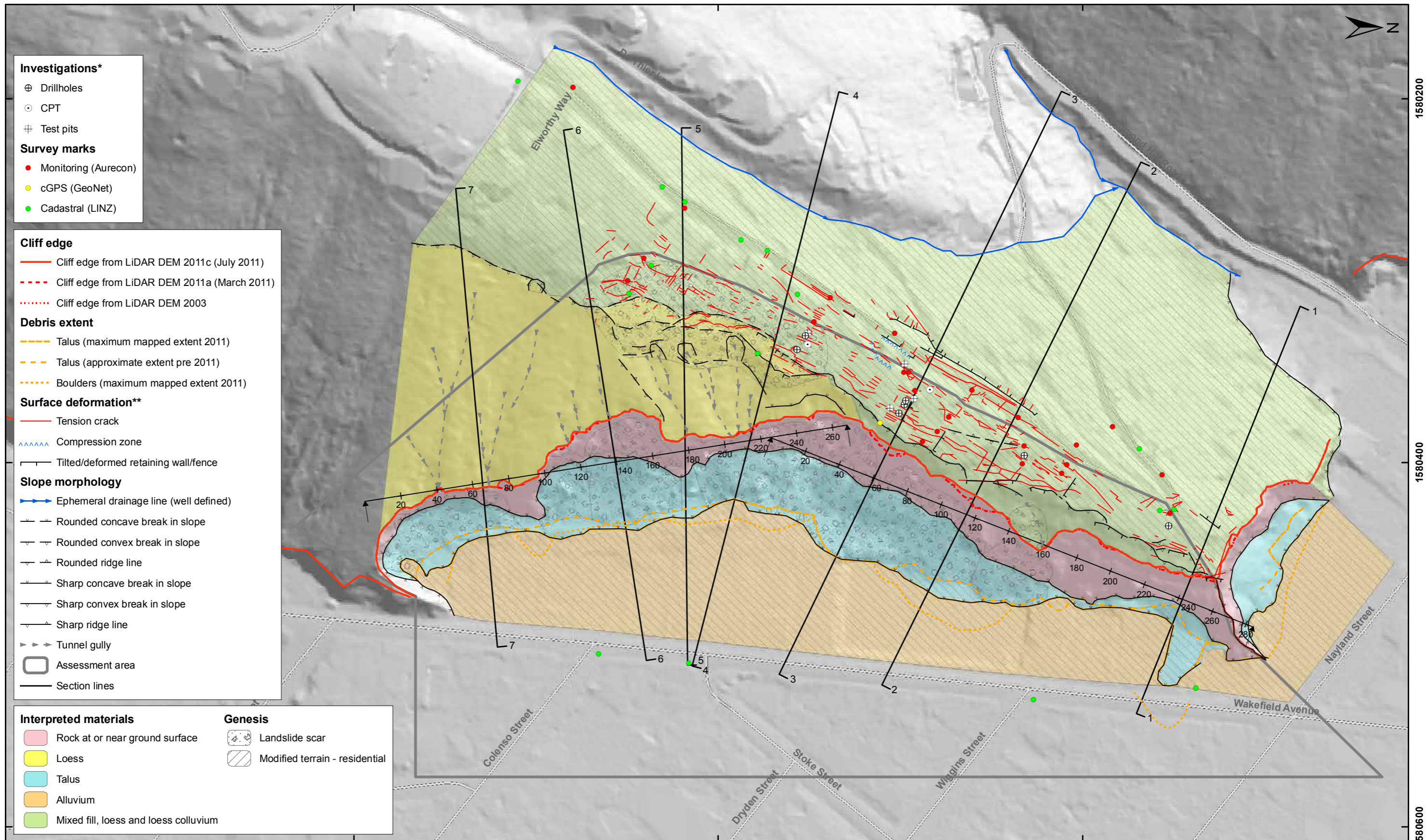
The Tonkin and Taylor Ltd drillholes were relatively shallow and did not extend deeper than the upper rock unit. In addition Tonkin and Taylor Ltd carried out two cone penetrometer holes (CPT-RHR-01 and CPT-RHR-02) (Figure 6). The logs and core photos from these drillholes are available in Tonkin and Taylor (2012a). The three Aurecon New Zealand Ltd. drillholes went deeper and extended to the base of the cliff. The logs and core photographs are presented in Revell and Pletz (2013).

Cross-sections through the site showing the location and depth of the drillholes are presented in Figure 7 (cross-sections 1–7).

Tonkin and Taylor Ltd. also excavated four test pits in soil (loess) at the slope crest (Figure 6). These were carried out to investigate at depth particular tension cracks visible on the surface in order to assess the depths (below ground level) to which these features extended.

Table 5 Summary of the ground investigations carried out at the site by Aurecon NZ Ltd. (Revell and Pletz, 2013) and Tonkin and Taylor Ltd. (Tonkin and Taylor, 2012a).

ID	Data source	Type	Depth (m below ground level)	Instrumentation
BH-RHR-01	Aurecon NZ Ltd.	Cored hole	80	Inclinometer
BH-RHR-02	Aurecon NZ Ltd.	Cored hole	74	Piezometer/seismometer
BH-RHR-03	Aurecon NZ Ltd.	Open hole	80	Inclinometer
BH-RHR-01	Tonkin and Taylor Ltd.	Cored hole (inclined 48°)	40	None
BH-RHR-02	Tonkin and Taylor Ltd.	Cored hole (inclined 45°)	35	None
BH-RHR-03	Tonkin and Taylor Ltd.	Cored hole (inclined 45°)	30	None
BH-RHR-04	Tonkin and Taylor Ltd.	Vertical	10	Standpipe
CPT-RHR-01	Tonkin and Taylor Ltd.	Cone penetrometer	6	Standpipe
CPT-RHR-02	Tonkin and Taylor Ltd.	Cone penetrometer	6	Standpipe
TP01, TP02, TP03 and TP04	Tonkin and Taylor Ltd.	Test pits	Variable 1.8–4 m	N/A



EXPLANATION:
 * For details refer to site investigation map
 ** Taken from report 2012/317
 Background shade model derived from NZAM post earthquake 2011c (July 2011) LiDAR survey resampled to a 1 m ground resolution.
 Roads provided by Christchurch City Council (20/02/2012).
 PROJECTION: New Zealand Transverse Mercator 2000

DRW:
BL
 CHK:
CM



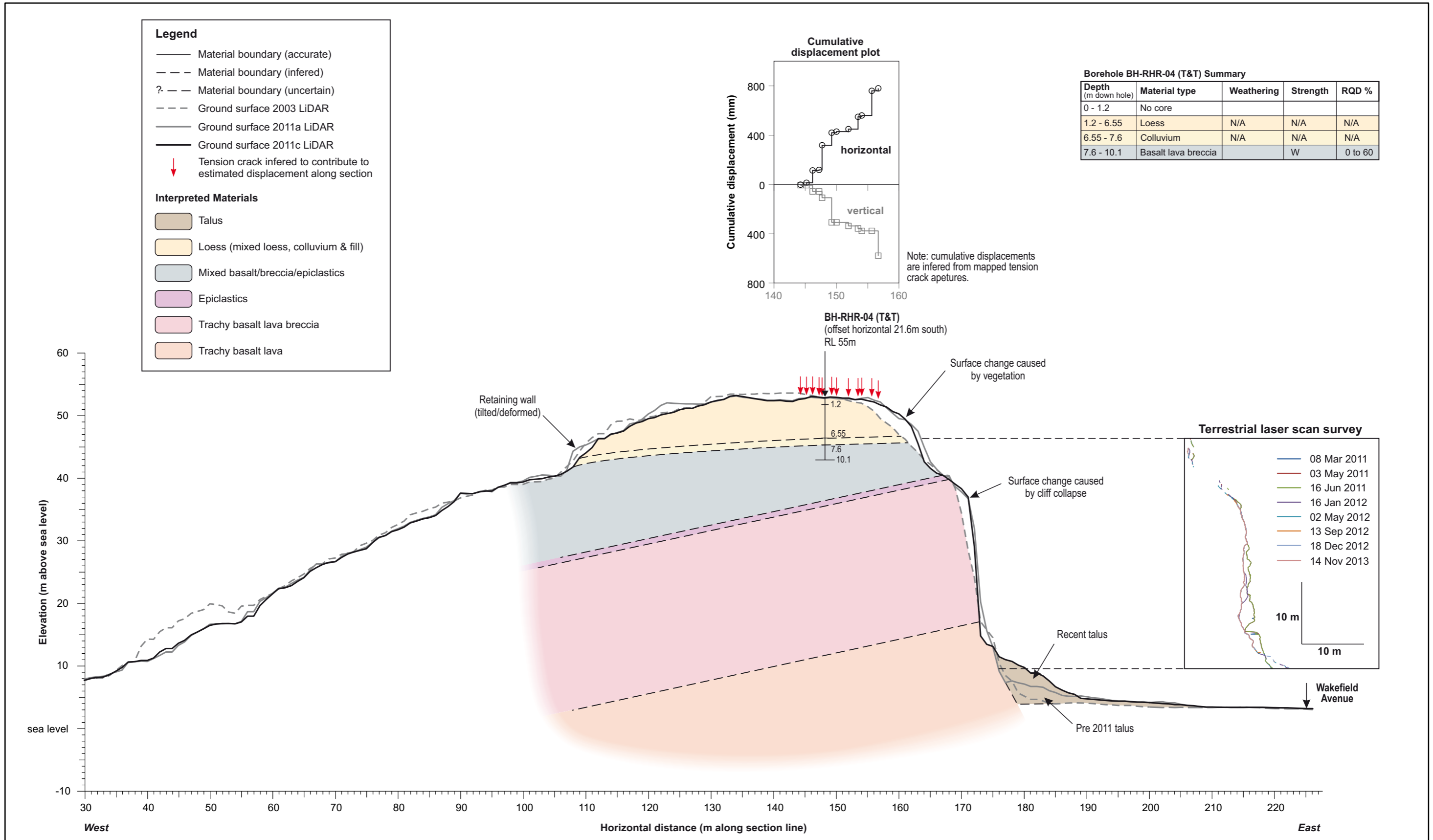
ENGINEERING GEOLOGY MAP


**Richmond Hill Road
Christchurch**

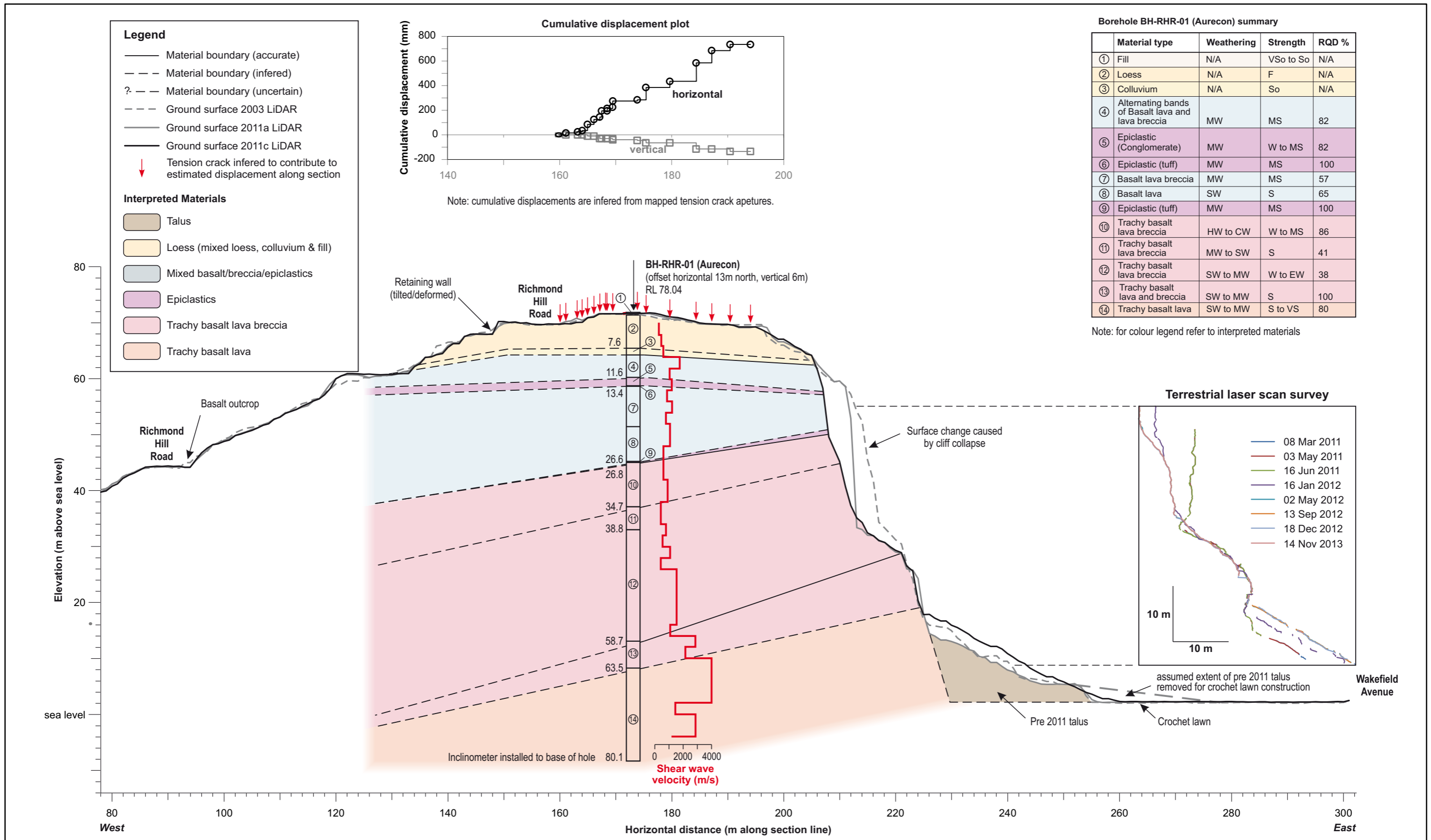
FIGURE 5

FINAL

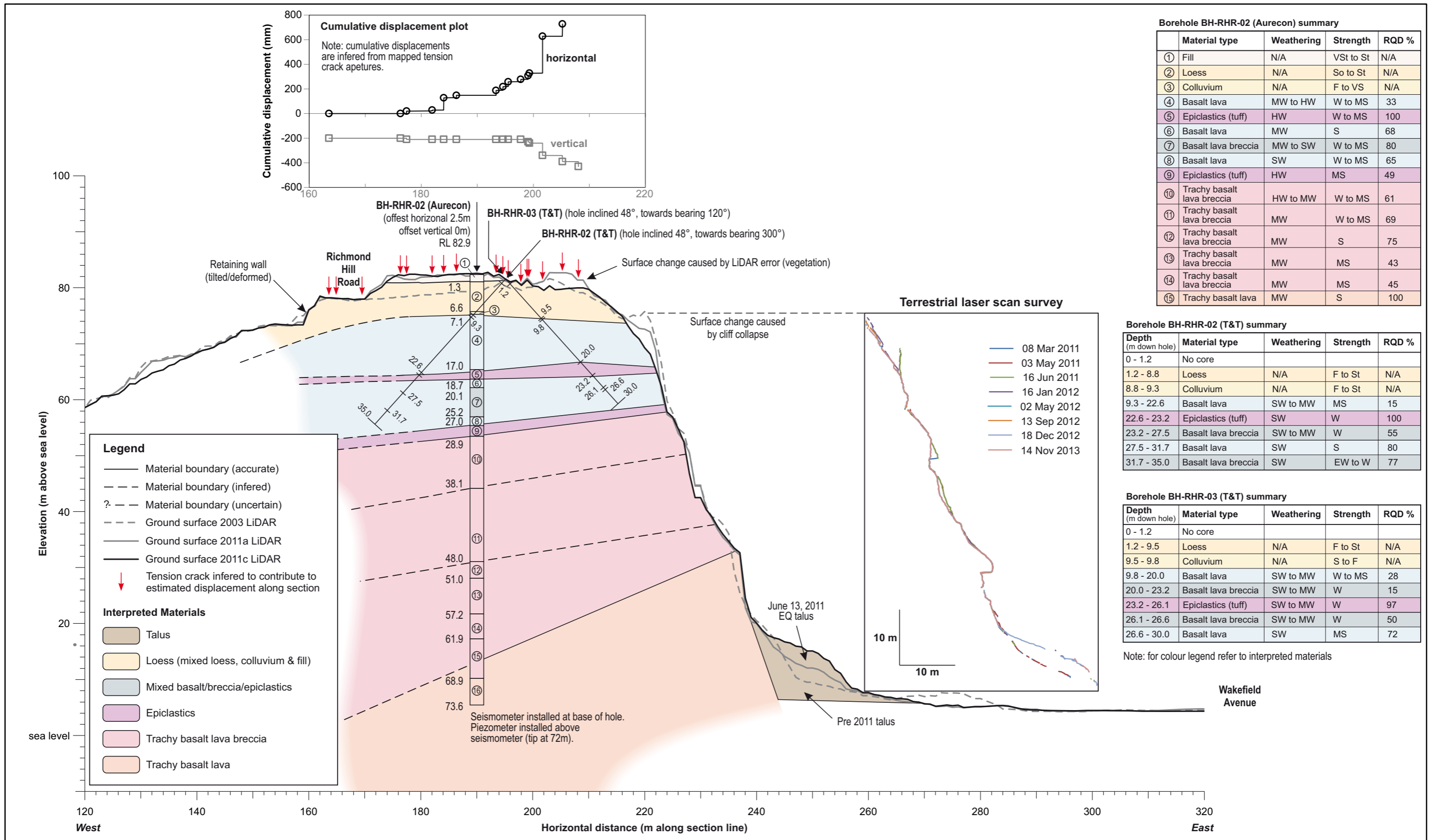
REPORT:
CR2014/34 DATE:
June 2014

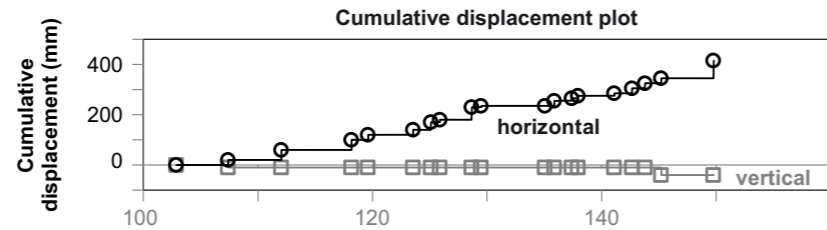


Weathering (adopting NZGS (2005) terminology): CW completely weathered; HW highly weathered; MW moderately weathered; SW slightly weathered; UW unweathered. Rock Strength (field strengths adopting NZGS (2005) terminology): EW extremely weak; VW very weak; W weak; MS moderately strong; S Strong; VS very strong; extremely strong. Soil strength (field strengths adopting NZGS (2005) terminology): Coarse soils – VL very loose; L loose; MD medium dense; D dense, VD very dense. Cohesive soils – H hard; VSt very stiff; St stiff; F firm; So soft; VSo very soft. RQD: Rock quality designation	DRW: PC		ENGINEERING GEOLOGY CROSS SECTION 1		FIGURE 7	
	CHK: CM/FDP		Richmond Hill Road Christchurch		FINAL	
			REPORT: CR2014/34	DATE: June 2014		



Weathering (adopting NZGS (2005) terminology): CW completely weathered; HW highly weathered; MW moderately weathered; SW slightly weathered; UW unweathered. Rock Strength (field strengths adopting NZGS (2005) terminology): EW extremely weak; VW very weak; W weak; MS moderately strong; S Strong; VS very strong; extremely strong. Soil strength (field strengths adopting NZGS (2005) terminology): Coarse soils – VL very loose; L loose; MD medium dense; D dense, VD very dense. Cohesive soils – H hard; VSt very stiff; St stiff; F firm; So soft; VSo very soft. RQD: Rock quality designation	DRW:		ENGINEERING GEOLOGY CROSS SECTION 2		FIGURE 7	
	PC		Richmond Hill Road Christchurch		FINAL	
	CHK:				REPORT:	DATE:
CM/FDP	CR2014/34	June 2014				





Note: cumulative displacements are inferred from mapped tension crack apertures.

Borehole BH-RHR-01 (T&T) Summary

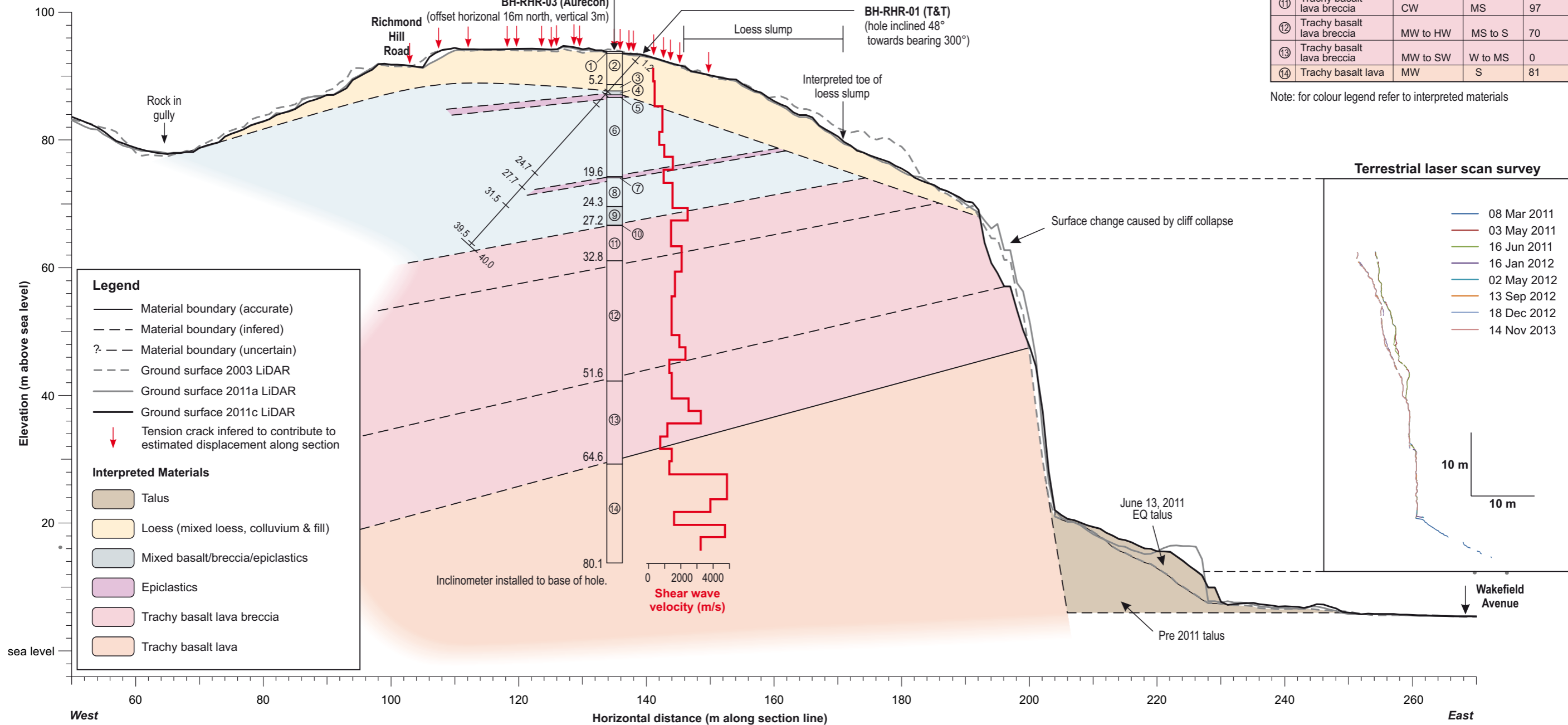
Depth (m down hole)	Material type	Weathering	Strength	RQD %
0 - 1.2	No core			
1.2 - 7.6	Loess	N/A	F to St	N/A
7.6 - 8.2	Colluvium	N/A	St	N/A
8.2 - 10.3	Basalt lava breccia	SW to MW	W	97
10.3 - 24.7	Basalt lava	SW to MW	MS	50
24.7 - 27.7	Basalt lava breccia	SW to MW	W to EW	62
27.7 - 31.5	Basalt lava	SW	S	56
31.5 - 39.5	Basalt lava breccia	SW to MW	EW to W	35
39.5 - 40.0	Basalt lava	SW	S	60

Note: for colour legend refer to interpreted materials

Borehole BH-RHR-03 (Aurecon) Summary

	Material type	Weathering	Strength	RQD %
①	Fill	N/A	So to F	N/A
②	Loess	N/A	F	N/A
③	Colluvium	N/A	VSt to H	N/A
④	Basalt lava breccia	MW to HW	MS to S	84
⑤	Epiclastics (tuff)	MW to HW	S	N/A
⑥	Basalt lava	HW to MW	MS to S	50
⑦	Epiclastics (tuff)	MW	MS	N/A
⑧	Basalt lava	MW to SW	S to VS	93
⑨	Basalt lava breccia	MW to HW	MS to S	44
⑩	Epiclastics (tuff)	MW	MS	N/A
⑪	Trachy basalt lava breccia	CW	MS	97
⑫	Trachy basalt lava breccia	MW to HW	MS to S	70
⑬	Trachy basalt lava breccia	MW to SW	W to MS	0
⑭	Trachy basalt lava	MW	S	81

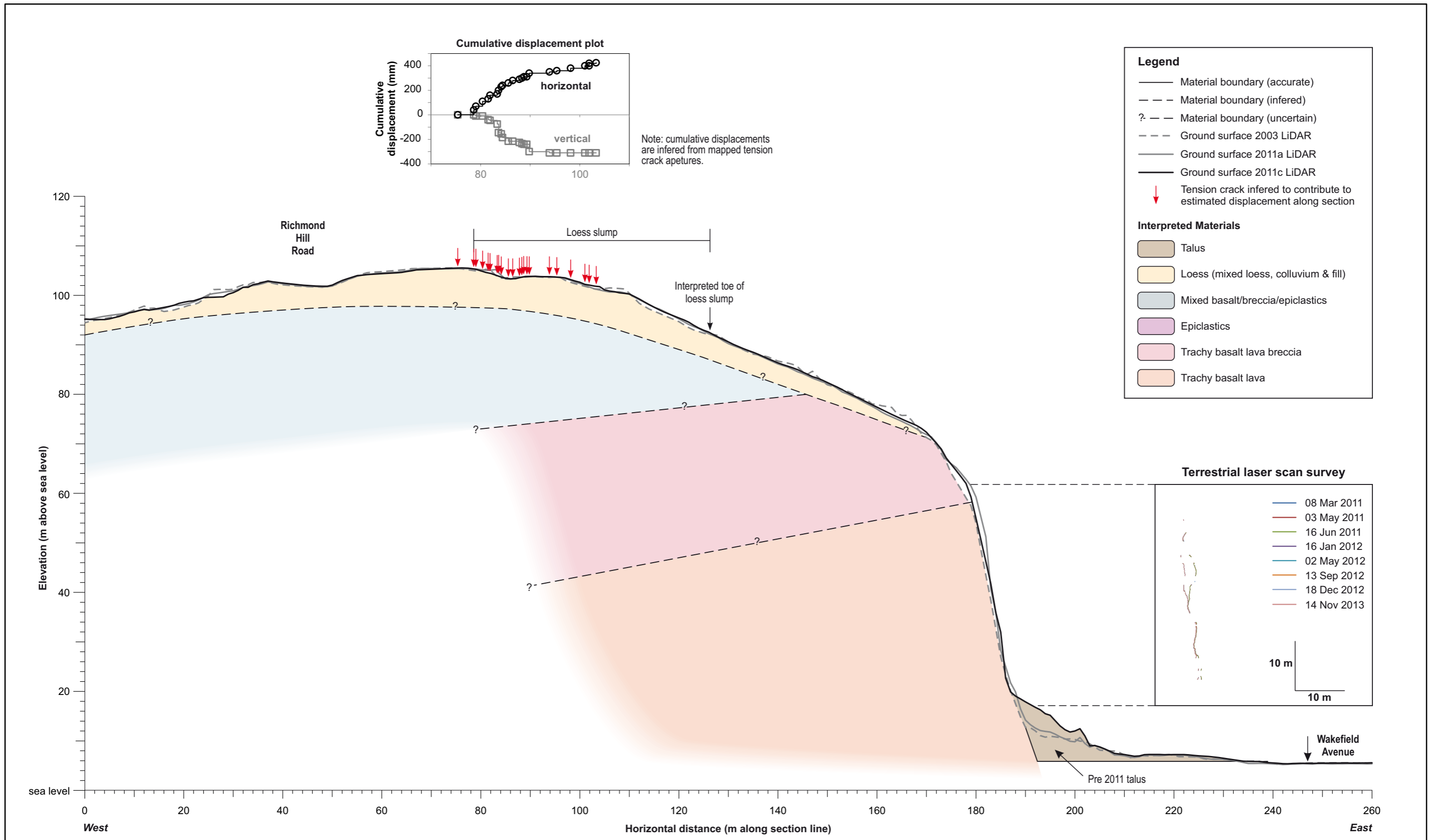
Note: for colour legend refer to interpreted materials




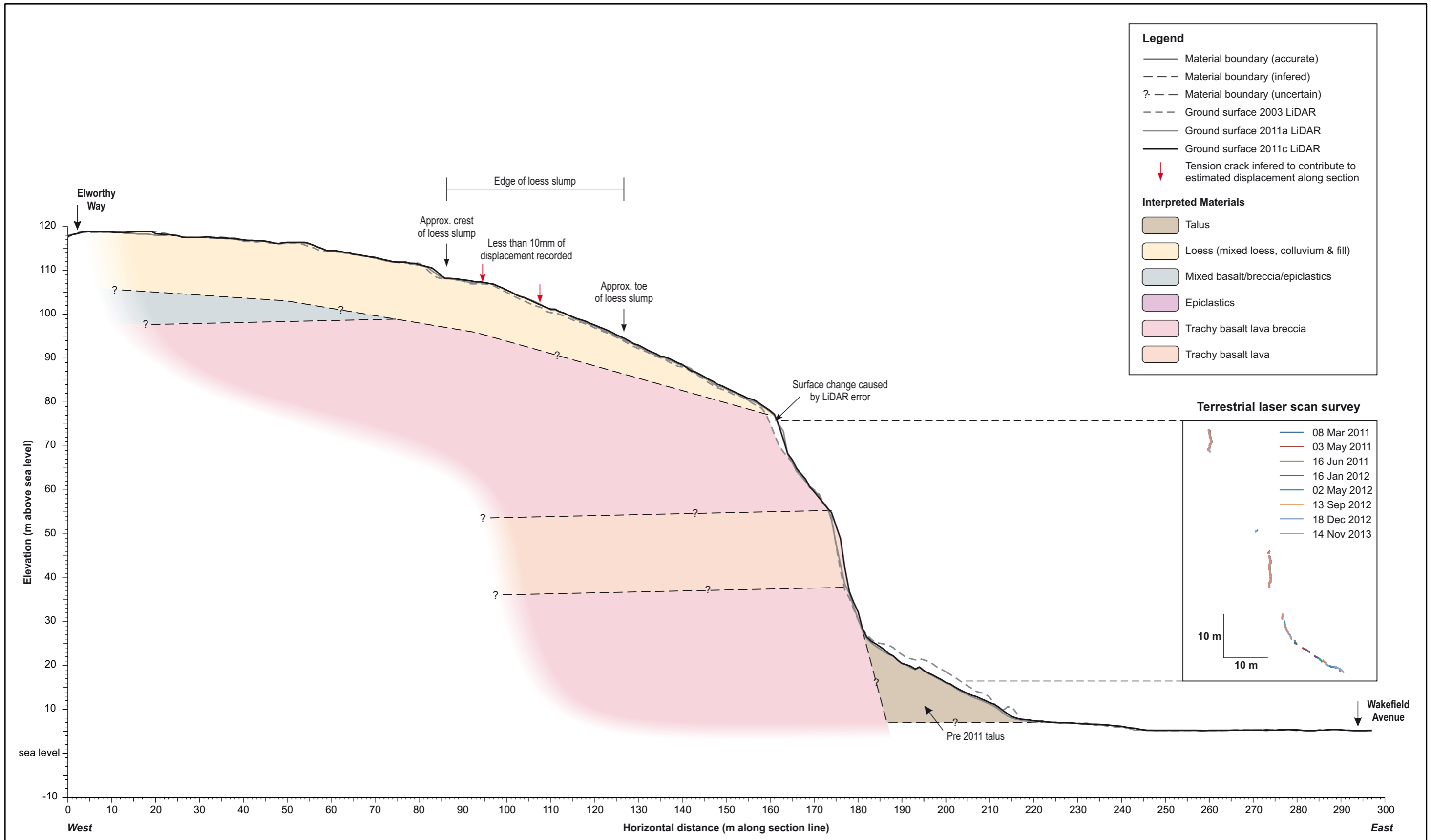
Terrestrial laser scan survey

- 08 Mar 2011
- 03 May 2011
- 16 Jun 2011
- 16 Jan 2012
- 02 May 2012
- 13 Sep 2012
- 18 Dec 2012
- 14 Nov 2013

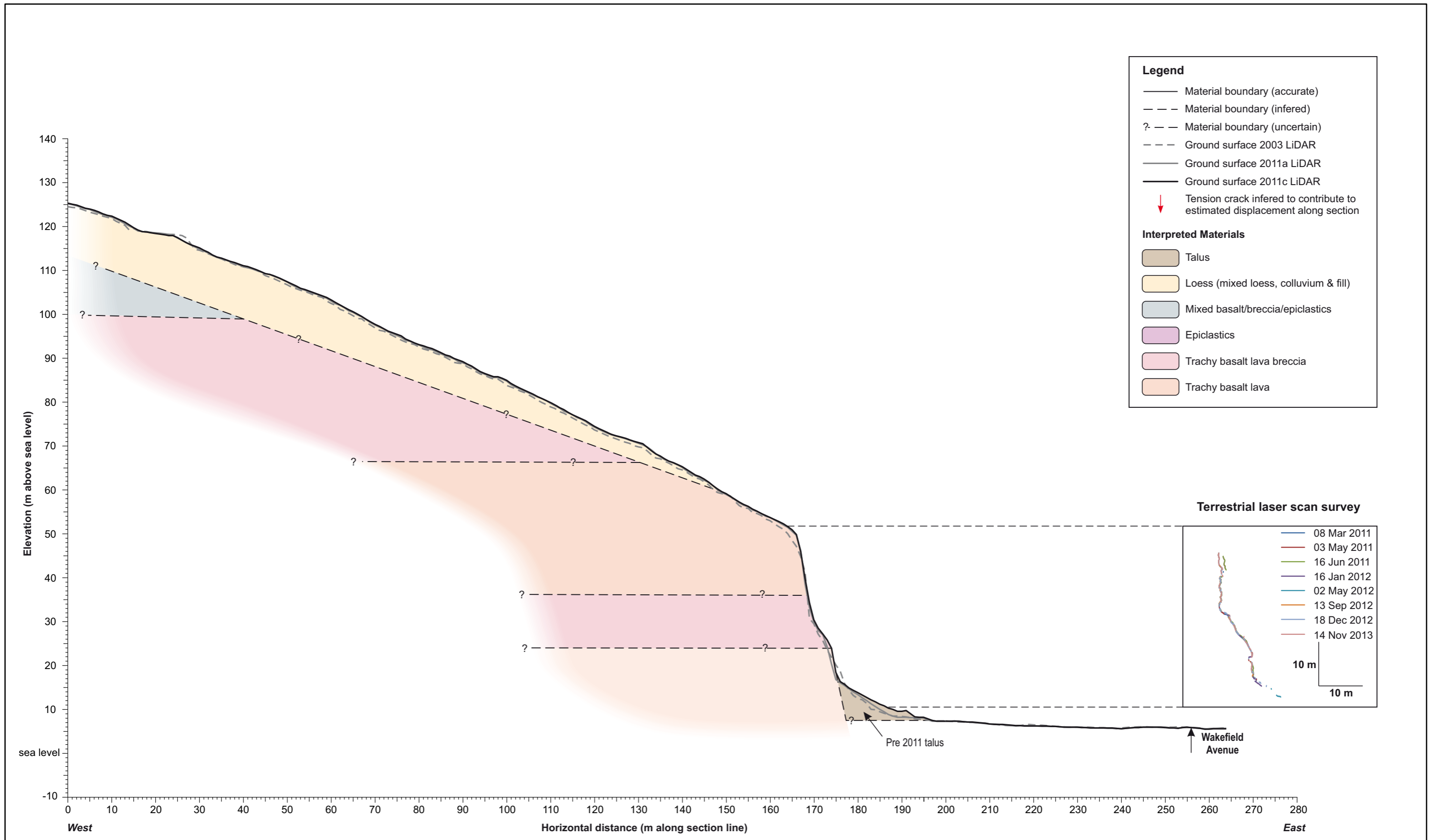
Weathering (adopting NZGS (2005) terminology): CW completely weathered; HW highly weathered; MW moderately weathered; SW slightly weathered; UW unweathered. Rock Strength (field strengths adopting NZGS (2005) terminology): EW extremely weak; VW very weak; W weak; MS moderately strong; S Strong; VS very strong; extremely strong. Soil strength (field strengths adopting NZGS (2005) terminology): Coarse soils – VL very loose; L loose; MD medium dense; D dense; VD very dense. Cohesive soils – H hard; VSt very stiff; St stiff; F firm; So soft; VSo very soft. RQD: Rock quality designation	DRW:		ENGINEERING GEOLOGY CROSS SECTION 4		FIGURE 7	
	PC		Richmond Hill Road Christchurch		FINAL	
	CHK:				REPORT:	DATE:
CM/FDP	CR2014/34	June 2014				




Weathering (adopting NZGS (2005) terminology): CW completely weathered; HW highly weathered; MW moderately weathered; SW slightly weathered; UW unweathered. Rock Strength (field strengths adopting NZGS (2005) terminology): EW extremely weak; VW very weak; W weak; MS moderately strong; S Strong; VS very strong; extremely strong. Soil strength (field strengths adopting NZGS (2005) terminology): Coarse soils – VL very loose; L loose; MD medium dense; D dense, VD very dense. Cohesive soils – H hard; VSt very stiff; St stiff; F firm; So soft; VSo very soft. RQD: Rock quality designation	DRW:		ENGINEERING GEOLOGY CROSS SECTION 5		FIGURE 7	
	PC					
	CHK:		Richmond Hill Road Christchurch		FINAL	
CM/FDP	REPORT:	DATE:				
			CR2014/34	June 2014		



Weathering (adopting NZGS (2005) terminology): CW completely weathered; HW highly weathered; MW moderately weathered; SW slightly weathered; UW unweathered. Rock Strength (field strengths adopting NZGS (2005) terminology): EW extremely weak; VW very weak; W weak; MS moderately strong; S Strong; VS very strong; extremely strong. Soil strength (field strengths adopting NZGS (2005) terminology): Coarse soils – VL very loose; L loose; MD medium dense; D dense, VD very dense. Cohesive soils – H hard; VSt very stiff; St stiff; F firm; So soft; VSo very soft. RQD: Rock quality designation	DRW: PC		ENGINEERING GEOLOGY CROSS SECTION 6		FIGURE 7	
	CHK: CM/FDP		Richmond Hill Road Christchurch		FINAL	
			REPORT: CR2014/34	DATE: June 2014		



Weathering (adopting NZGS (2005) terminology): CW completely weathered; HW highly weathered; MW moderately weathered; SW slightly weathered; UW unweathered. Rock Strength (field strengths adopting NZGS (2005) terminology): EW extremely weak; VW very weak; W weak; MS moderately strong; S Strong; VS very strong; extremely strong. Soil strength (field strengths adopting NZGS (2005) terminology): Coarse soils – VL very loose; L loose; MD medium dense; D dense, VD very dense. Cohesive soils – H hard; VSt very stiff; St stiff; F firm; So soft; VSo very soft. RQD: Rock quality designation	DRW: PC		ENGINEERING GEOLOGY CROSS SECTION 7		FIGURE 7	
	CHK: CM/FDP		Richmond Hill Road Christchurch		FINAL	
					REPORT: CR2014/34	DATE: June 2014

3.2.3 Surface movement

3.2.3.1 Inferred cliff top displacements from crack apertures

Displacements of the cliff top during the 22 February and 13 June 2011 earthquakes are mainly inferred from measured tension-crack apertures, following the method described in Massey et al. (2013). Crack apertures – relative displacements across cracks in both the horizontal and vertical directions – were measured with a tape measure at locations that were thought to best represent the overall displacement across the crack. Cracks with apertures of less than 5 mm were generally ignored, and so the inferred total displacements of the cliff edge are slightly underestimated.

Only minor cracking was identified by Port Hills Geotechnical Group consultants after the 22 February 2011 earthquake and so it is inferred that the displacements recorded across crack apertures are mainly in response to the 13 June 2011 earthquake. Therefore, displacement of the cliff top in response to this earthquake have been estimated for each cross-section, by adding together the mapped crack apertures (openings) along the cross-sections (Table 6 and Figure 7 cross-sections 1–7).

The logs from the test pits (Tonkin and Taylor, 2012a) located back from the cliff edge show that cracks in the loess, extend from the surface down, but do not reach into bedrock. This would suggest that the presence of cracks in loess do not necessarily imply cracking of the underlying rock. However, field mapping of exposures of loess at the cliff edge also show that cracks formed in the bedrock do not always extend into the loess, or to the ground surface (Figure 8).

The dip of the resultant vectors from the horizontal – adopting only those components with both vertical and horizontal displacement (Table 7) – suggests that the angle of displacement is significantly steeper than the loess/rock interface, and more consistent with displacement of the underlying rock rather than localised slumping of the loess along the loess/rock interface. Given these uncertainties, the displacements inferred from crack apertures are thought to represent upper bound estimates of the total permanent displacements of the cliff top during the 2010/11 Canterbury earthquakes. The displacements of the sections of cliff (nearest the cliff edge) that fell off during the earthquakes are unknown; however, they were likely to have been significantly greater than those recorded behind the cliff edge.

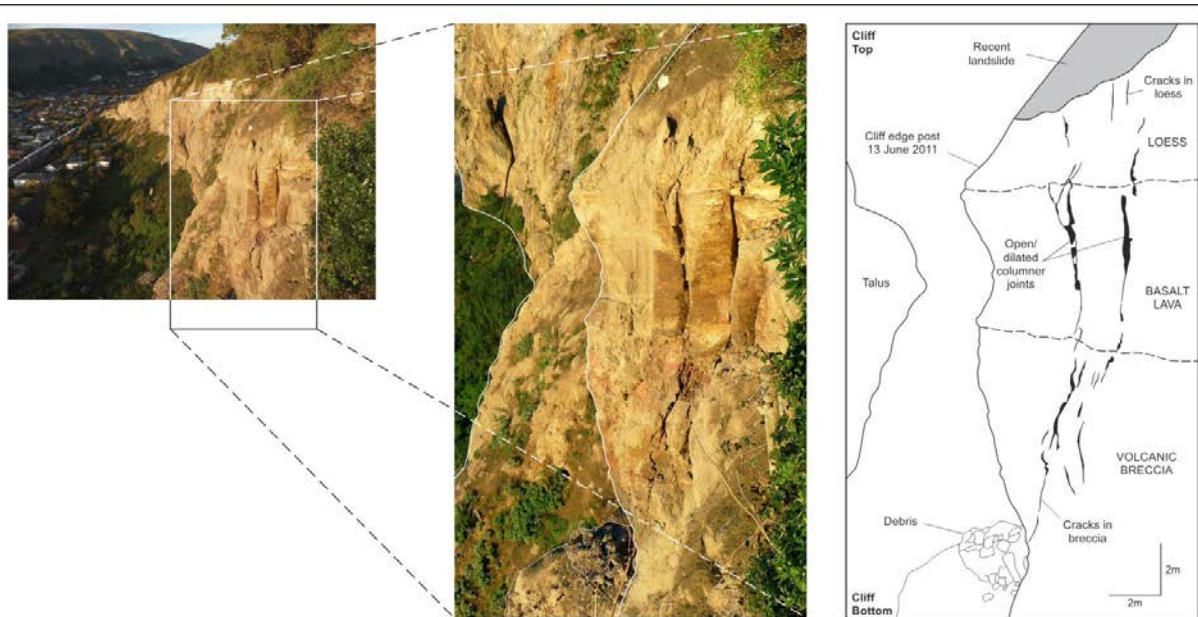


Figure 8 Cracks observed below the Richmond Hill cliff top near the interface between rock and loess. Photographs taken after the 23 December 2011 earthquake.

Two distinct crack patterns were identified in the loess (and fill) at the cliff top:

- Set 1 indicates mainly extensional (horizontal) displacements across cracks – occurring well back from the cliff edge – and are inferred to be a function of shallow inelastic response of the loess (and fill) above rock head during shaking (e.g., settlement, slumping).
- Set 2 indicates both horizontal and vertical displacement (up to 0.6 m of cumulative vertical displacement measured, Table 7), and are located closer to the cliff edge. These cracks are therefore inferred to relate to deeper-seated deformation in the underlying rock mass during shaking.

Table 6 Estimated cliff top displacements across crack apertures in response to the 22 February and 13 June 2011 earthquakes (mainly the 13 June earthquake). Displacements are estimated from field mapping of tension crack apertures. Errors are nominally estimated as being ± 5 mm. No cracks were identified behind the cliff edge along cross-sections 6 and 7 due to vegetation.

Cross-section	Cumulative crack apertures – horiz. component (m)	Cumulative crack apertures – vert. component (m)	Total disp. (m)	Translation angle (from horiz.)	Angle of loess/rock interface	Comment
1	0.77	0.57	0.96	37°	0° (flat)	Local retaining wall failure has contributed to total recorded disp.
2	0.65	0.14	0.66	11°	3° out of slope	
3	0.49	0.22	0.54	24°	3° out of slope	
4	0.41	0.04	0.41	6°	18° out of slope	
5	0.42	0.31	0.52	37°	18° out of slope	

Table 7 Estimated cliff top displacements as per Table 7a, but only for those cracks with both vertical and horizontal displacements across the apertures recorded for cross-sections 1–3 at the cliff top.

Cross-section	Cumulative crack apertures – horiz. component (m)	Cumulative crack apertures – vert. component (m)	Total disp. (m)	Translation angle (from horiz.)	Angle of loess/rock interface
1	0.55	0.57	0.57	46°	0° (flat)
2	0.44	0.14	0.46	17°	3° out of slope
3	0.49	0.22	0.54	24°	3° out of slope

3.2.3.2 Surveyed slope displacements

The survey monitoring data are presented in Appendix 4 and summarised below. There are three data sets:

1. Cadastral survey marks, details held by Land Information New Zealand (LINZ), i.e., property boundaries and roads footpaths etc.;
2. Monitoring survey marks installed by Aurecon NZ Ltd., for Christchurch City Council, to monitor surface displacement; and
3. Continuous GPS monitoring at one location at the cliff top, carried out by GeoNet.

All datasets adopt reference control marks outside the area of landslide movement, but still within the local area. Therefore, regional offsets caused by the tectonic displacements are largely removed from the data.

Cadastral marks (source: LINZ)

Available cadastral survey marks were resurveyed by GNS Science to detect absolute ground movements spanning the earthquake period from before the 22 February 2011 earthquakes (the pre-earthquake survey dates for each cadastral mark vary) to 30 October 2012, and therefore include total displacements of the survey marks in response to the earthquakes within this time period. No survey marks are located in the main area of cracking behind the slope crest, and therefore the overall movement of the slope is unknown.

The results of this survey are contained in Appendix 4 (Map 2). Two survey marks were installed on the loess slump (Figure 2). Vector displacements indicate permanent ground displacements in the order of about 0.08–0.15 m. Other displacements, outside error, are thought to represent localised displacement of the ground surface, as they are located outside the main area of cliff-top cracking.

Monitoring marks (source: Aurecon NZ Ltd. and GeoNet)

Surface movement at the slope crest has been monitored since January 2012 by Aurecon New Zealand Ltd using a network of survey pegs (Figure 6). Surface movement at one location is monitored by GNS Science using a continuous GPS (cGPS) receiver which was installed in June 2011 by GeoNet (Figure 6). All of this monitoring commenced after the 13 June 2011 earthquake and so did not capture displacement of the cliff top during the 22 February, 16 April and 13 June 2011 earthquakes. Assessment of the survey results is contained in Appendix 4.

Surface movement of the cliff top was identified from cGPS records in response to the 23 December 2011 earthquake. Recorded cGPS displacements at the time of the earthquake were 80 mm horizontal towards the east and 50 mm vertical (downwards) (Appendix 4); a translational angle of displacement of about 40° from the horizontal. Errors on a daily solution are about ±5 mm horizontal and ±10 mm vertical at one standard deviation.

Post-earthquake displacements of parts of the cliff top have been inferred from the monitoring measurements. Two types of displacement are inferred from the cGPS monitoring (Mark ID 25, Appendix 4): a relatively rapid period of displacement that occurred over 7 days between 11 and 17 August 2012 (30 mm towards the east with vertical displacement up to about 20 mm); and slow displacement at an almost constant rate (of about 25 mm/yr) that has occurred over the past two years (July 2011–present).

The period of more rapid displacement recorded by the cGPS is corroborated by the results from the survey network installed by Aurecon, where one of their survey marks (Mark ID 20 Appendix 4) shows a similar magnitude of displacement (13 ± 4 mm/yr), for the same period, although the vector of displacement is towards the north east. This survey mark is located about 20 m north of the cGPS in a similar topographic position near the cliff edge.

3.2.3.3 Volumes of debris lost from the cliffs

A summary of the volumes leaving the cliffs during the main earthquakes derived from airborne LiDAR and terrestrial laser scan surveys is contained in Table 8. Assessment results from the airborne LiDAR are presented in Appendix 2 and from the terrestrial laser scanning in Appendix 3.

Since the onset of the 2010/11 Canterbury earthquakes the 18,000 m³ of debris that has fallen from the cliff has in some locations increased the angle of the existing talus at the slope toe, and in other locations created new talus piles where there were originally none. In such cases, the slope morphology has changed, and could cause future debris to runout further from the cliff toe.

Table 8 Estimated volumes lost from the cliffs calculated from the terrestrial laser scan (TLS) and LiDAR surveys.

Change model	Volume leaving cliff (m ³)	Area of cliff face (m ²) ³	Volume loss per unit area (m ³ /m ²)	Probable trigger
Estimate by PHGG consultants after the earthquake	40 (±10)	26,560	0.002	4 September 2010 earthquake (M _w 7.2)
Airborne LiDAR: 2003–March 2011 (2011a) ¹	5,260 (±1,000)	26,560	0.20	22 February 2011 earthquake (M _w 6.2)
TLS: 8 March 2011–3 May 2011 ²	920 (±80)	26,560	0.03	16 April 2011 earthquake (M _L 5.6)
Airborne LiDAR: March 2011–July 2011 ¹	10,120 (±1,050)	26,560	0.38	13 June 2011 earthquake (M _w 6.2)
TLS: 16 June 2011–16 January 2011 ²	1,400 (±130)	26,560	0.05	23 December 2011 earthquake (M _w 6.1)
TLS: 16 January 2011–13 September 2012 ²	440 (±160)	25,560	0.02	No obvious trigger possible rainfall induced

¹ Change models derived from airborne LiDAR surveys carried out by AMM Hatch (2003) and Aerial New Zealand Mapping (2011a, March 2011 and 2011c, July 2011).

² Change models derived from terrestrial laser scan surveys carried out by GNS Science, refer to Appendix 3 for details.

³ A constant cliff-surface area has been adopted based on the overall extent of the cliff face surveyed.

Digital elevation models representing the ground surface at a given time were generated for each data set. For the LiDAR surveys, a 1 m grid (ground resolution) of elevations was generated from filtered scan data points supplied by the contractor. For each of the terrestrial laser scan surveys a 0.1 m grid was generated from the filtered point data. Filtering comprised removal of points representing vegetation and buildings from the supplied point data, thereby creating a “bare earth” or “filtered” point elevation data set. This was undertaken by GNS Science for the terrestrial laser scan survey data, and by the consultants AAM Hatch and New Zealand Aerial Mapping for the LiDAR datasets (these companies were commissioned by other parties, mainly the Earthquake Commission and the Christchurch City Council, to carry out the surveys).

Errors are assessed for each digital elevation model by comparing the modelled surface with the filtered point data used to generate it. Errors in the terrestrial laser scan survey data are generally ±0.05–0.09 m at one standard deviation and for the LiDAR data generally ±0.1–0.3 m (in height) for the New Zealand Aerial Mapping data sets (LiDAR surveys 2011a and 2011c), and ±0.2–0.5 m (in height) for the AAM Hatch data sets.

3.2.4 Sub-surface movement

Drillhole inclinometer tubes are used to monitor displacements at depth, assess whether movement is occurring along single or multiple slide-surfaces, and to independently verify the results of surface monitoring. Monitoring is undertaken manually by commercial contract (Geotechnics Ltd.).

Inclinometer tubes were installed in the two Aurecon NZ Ltd., drillholes (BH-RHR-01 and BH-RHR-03) at the cliff top in October 2012. Displacements of the slope indicator 85 mm diameter, plastic inclinometer casings (installed to the base of the drillholes), are measured based on test method ASTM D6230:05, using probe-type inclinometers with readings at 0.5 m intervals. Inclinometer accuracy is quoted as ± 6 mm over 25 m of tubing (Slope Indicator, 2005). Initial readings were conducted on 8 February 2013, when each inclinometer was read twice (Table 9).

The results from the survey are presented in Geotechnics (2014). No subsurface displacements outside of error have been identified to date. No inclinometer survey records from the Tonkin and Taylor drillholes have been provided to GNS Science.

Table 9 Summary of inclinometer details.

Inclinometer	Tube top (m AMSL)	Inclinometer depth ¹		First reading date	Subsequent reading dates
		(m bgl)	(m amsl)		
BH-RHR-01	78.04	79.54	-1.5	8/02/2013	3/04/2013, 9/07/2013
BH-RHR-03	99.78	79.5	20.3	6/02/2013	3/04/2013, 9/07/2013

¹ Metres below ground level (bgl) and above mean sea level (amsl).

3.2.5 Groundwater

All three of the Aurecon New Zealand Ltd. drillholes (BH-RHR-01 to BH-RHR-03) were reported by the driller as being dry, and loss of water flush in all three drillholes was recorded (Revell and Pletz, 2013). The piezometers installed in BH-RHR-02 currently show no measurable groundwater levels, other than moisture at the bottom of the piezometer tubes, which is interpreted as remaining fluid at the base of the installation following the drilling.

All three of the Tonkin and Taylor Ltd., standpipe piezometers show no measurable groundwater levels (Tonkin and Taylor, 2012a). The standpipe response zones for these piezometers are generally in the loess. A ground water level of about 5 m below ground level (tip of the piezometer is given as 5.19 m below ground surface), was recorded in the standpipe in CPT-RHR-02, in April 2012. There are only three measurements recorded and the other two are consistent with the depth of the standpipe tip, indicating it was dry at these times. It is possible that groundwater is present in the other standpipes, but that the poor temporal resolution has not allowed its presence to be resolved.

3.3 ENGINEERING GEOLOGICAL MODEL

An engineering geological map is presented in Figure 5, site investigation map in Figure 6 and cross-sections 1–6 in Figure 7. The map and cross-sections are based on the interpretation of features identified in aerial photographs, field mapping and ground investigation data.

3.3.1 Slope materials

Slope materials interpreted from the logging of drill-cores samples and mapping of the cliff face along Nayland Street and Wakefield Avenue indicate seven key units – using the classification of Bell and Trangmar (1987) – these comprise: 1) Fill (mixture of topsoil, overburden, loess and other materials); 2) Talus; 3) Loess colluvium and mixed loess/volcanic colluvium; 4) Loess; 5) Basalt lava and lava breccia; 6) Trachy basalt lava breccia; and 7) Trachy basalt lava.

The boundaries and locations of the materials interpreted from the drillholes and field mapping are shown on cross-sections 1–7 in Figure 7. Cross-section locations are shown on Figure 5 and a geological log of the cliff face along Wakefield Avenue is presented in Appendix 3. A face log of the cliff along Nayland Street is presented in Massey et al. (2012a).

3.3.1.1 Fill and Loess

The slope crest and toe are heavily modified by construction of residential homes. It is not possible to identify and map each individual area of fill, or modified ground.

The loess mantling the cliff top at Richmond Hill Road is similar to other areas of the Port Hills. It is a relatively cohesive silt-dominated soil with only minor clay mineral content and the strength of loess is largely controlled by the soil-moisture content (Bell et al., 1986; Bell and Trangmar, 1987; McDowell, 1989; Yetton, 1992; Carey et al., 2014). The loess in the main zone of cracking at the cliff top is unsaturated and relatively strong where exposed. Similarly, the thin layer of loess/volcanic colluvium sometimes present above the bedrock and at the base of the loess does not appear particularly weak or wet. The thickness of the loess, inferred from drillhole records and field mapping, varies between 7 m at the slope crest to less than a metre near the cliff edge, where it pinches out against bedrock.

3.3.1.2 Colluvium

A layer, of sandy silt containing boulders and gravel with minor clay was logged by Aurecon NZ Ltd. in drillholes BH-RHR-01, BH-RHR-02 and BH-RHR-01 (Revell and Pletz, 2013), and by Tonkin and Taylor Ltd. in drillholes BH-RHR-01, BH-RHR-02, BH-RHR-03 and BH-RHR-04 (Tonkin and Taylor 2012a). Revell and Pletz (2013) describe this material as highly variable and dominated by either silts or gravel and cobbles. The thickness of the colluvium varies from about 0.2–1 m.

It is thought to represent the deposits of debris from past landslides and other erosion processes. The material derives mainly from weathered volcanic breccia and lava and remobilised loess. In drillholes and field exposures, the colluvium is highly variable. It ranges from gravel to boulder-sized clasts of volcanic basalt with a loess and clay matrix, to remoulded loess with occasional gravel and boulders.

3.3.1.3 Talus

The talus at the toe of the cliff – present before the 2010/11 earthquake-induced talus accumulations – comprises several car-sized boulders along with many smaller boulders of volcanic rock that have fallen from the cliff. Much of this material has slaked – due to wetting and drying cycles – indicating that the original rockfall volumes were larger than the volume of talus currently present.

The recent accumulations of talus and boulders triggered by the 2010/11 Canterbury earthquakes are shown on Figure 5. Site observations – post-2010/11 earthquakes – indicate that these volcanic materials are already slaking. Sampling for particle size distributions of the talus has not been carried out for health and safety reasons. However, estimates made from photographs suggest the majority of the debris comprises boulders of diameter greater than 0.5 m.

3.3.1.4 Bedrock

The cliff face comprises gently dipping (and locally steeply dipping) interlayered variations of four main rock types – in order from the cliff edge to cliff bottom: 1) Blocky columnar-jointed basalt lava interlayered with more massive basalt lava breccia; 2) epiclastic layers within the basalt-breccia/lava sequence ranging from coarse poorly sorted conglomerates and sandstones to tuffaceous clays and silts and rare but prominent palaeosols (Figure 9). The materials within the layers are highly variable both laterally and vertically but the layers are laterally persistent along most of the cliff); 3) trachy-basalt breccia; and 4) trachy-basalt lava. Descriptions of the main units are given in Table 10.

The general dip/dip direction of the volcanic sequence in the north of the site is dip of 10–15° towards dip direction 290–320°, which is well constrained by the rock exposures in the cliff face along Nayland Street (Massey et al., 2012a). This dip becomes less to the south, where it is essentially horizontal and some areas appear to dip out of the slope. However, there are significant variations within the sequences. In the central part of the cliff the trachy basalt lavas form a steeply inclined dome (possible lava dome) locally dipping into the slope at about 60°.

Discontinuity data derived from photogrammetric surveys of the Richmond Hill cliff and kinematic assessment of the various discontinuity-controlled failure modes is contained in Appendix 5.

Table 10 Engineering geological descriptions of the main geological units forming the cliffs (descriptions as per New Zealand Geotechnical Society, 2005).

Unit name	Description
Basalt lava	Dark greenish grey to black, unweathered to moderately weathered, sometimes vesicular, Basalt, very strong with variably developed columnar joints, widely to very widely spaced (1.5–5 m), typically giving large to very large block sizes that are columnar in shape. Columnar joints are often radial to flow margins, and lavas have gradational contacts with lava breccia at their upper and side margins. Joint faces are generally rough to very rough, stepped or irregular, commonly manganese oxide or calcite coated, and only rarely have clay or silt fill. Individual flows form lensoidal bodies throughout the cliffs, ranging from 0.5 to 2–4 m thick. Columnar jointing is well expressed where flows are thick, and gives way to thin, platy flow orientated jointing where flows are thin.
Basaltic lava breccia	Slightly weathered to highly weathered, light grey to dark grey when slightly weathered to orange or red-brown when highly weathered, massive, brecciated Basaltic Lava Fragments, moderately strong to strong (but varies to weak or very weak when highly or completely weathered), with very widely spaced irregular discontinuities. At all sites basaltic lavas have flowed within thick carapaces of brecciated lava, with the breccia often exceeding the thickness of its source lava (brecciated units may be 2 to >10 m thick.). Breccias are poorly graded, angular lava fragments with a fine to coarse matrix supporting unsorted cobbles, blocks and often 1–5 m diameter megablocks of broken lava. Breccia fragments are often more vesicular and scoriaceous than the source lava, and prone

Unit name	Description
	to weathering due to high porosity. Bedding is massive, poorly jointed, with lower boundaries gradational with the source lava and upper boundaries roughly planar. Weathering expression is cavernous and spheroidal, of fine and coarse blocks respectively, and in some cases development of cliff parallel exfoliation joints/cracks. Freshly exposed breccia faces show extensive interstitial clay weathering and deposition of clay within vesicles and between clasts.
Epiclastic deposits	Moderately to highly weathered or oxidised brown to red-brown or yellow-brown thinly bedded Tuff or Tuffaceous Sandstone, intercalated with or grading into fine to coarse pebbly Lapilli Tufts or Gravelly Sandstone and conglomerate, with occasional cobble-sized blocks and bombs of basalt, moderately strong to weak, very weak to extremely weak when highly weathered. Rarely jointed, prone to cracking on exposed surfaces and easily eroded. Bedding is thin (0.1–2 m) and discontinuous, disrupted by overlying lavas. In all sites, these layers of red-oxidised pyroclastic and epiclastic paleosol material are found between lava flows and breccias, usually at the top of the preceding lava breccia, and oxidised/baked by the overlying lava flow. The thinly bedded ash and lapilli, with occasional blocks and bombs, is discontinuous due to re-working by water-driven epiclastic processes or re-working by overlying lava flows. The pyroclastic material exposed in the cliffs is often vegetated or a focus for fluid flow, being relatively impermeable compared to the overlying jointed lavas and porous breccias. Contacts are often gradational into lava breccia or lahar/debris-flow deposits.
Trachy basalt breccia	Slightly weathered to highly weathered, dark grey when fresh, weathering to pale tan, yellow or mauve patches with spheroidal and cavernous weathering structures; massive and unsorted brecciated trachy basalt Lava fragments, moderately strong to extremely weak and the highly weathered material appears stronger than the slightly weathered material. The breccia can change rapidly from being clast-supported to matrix-supported. The trachy basalt Lava on Wakefield Avenue has flowed within a thick upper and lower carapace of autobrecciated lava, up to 4–5 m thick below the main lava, and up to 10 m thick above it, with gradational contacts between the lava and its breccia. Massive and poorly jointed, but with extensive leaching and clayey alteration present in upper parts below top contact with overlying tufts and basalt lavas, and at lower contact below the lava at South Wakefield Avenue. Weathering expression is cavernous and spheroidal, with extensive clayey alteration and oxidation of clasts in some locations (South Wakefield Avenue). Freshly exposed faces by Wakefield Avenue Croquet Club show interstitial clay deposition and shrinkage cracks on exposure, and examples of polished slickensides (Iron and manganese oxide stained slickensides have been observed in blocks of lava breccia that have fallen from the Wakefield Avenue slope face during the 2010/11 Canterbury earthquakes).
Trachy basalt lava	Unweathered to moderately weathered, pinkish brown to grey brown when fresh, flow-banded trachy basalt, very strong, with pronounced anastomosing flow parallel banding and joints that are closely spaced (approximately 0.1–0.25 m spacing), typically giving large to very large block sizes that are tabular shaped. Columnar joints are either very poorly developed or absent. Lower contact with its own breccia is often sharp, upper contact is gradational into autobreccia.



Figure 9 View to the west onto the northern cliff at Wakefield Avenue. The homes are accessed from Richmond Hill Road. The loess/fill, which is thickly covered by tall shrubs, overlies rock at the slope crest (**A**). The rock exposed in the upper part of the cliff (**B**) is columnar jointed basalt lava and breccia. The persistently recessed layer beneath this is the epiclastic deposit (**C**), and the material below this is massive trachy basalt lava breccia (**D**). Photograph C. Massey GNS Science (July 2011).

3.3.2 Geotechnical material properties

Strength parameters have been assigned to the materials forming the cliff based on the results from in-house laboratory tests (on drillhole core samples and fallen boulders) and other published testing results (Carey et al., 2014). The parameters for loess (and fill) are derived mainly from ring and direct shear testing as well as unconfined compression testing with strain gauge measurements. The intact strength parameters for rock samples are derived mainly from unconfined compressive strength testing with shear gauge measurement and tensile testing.

For rock strengths – in order to derive rock mass strength parameters that take into account the nature of the discontinuities – the geological strength index (Hoek, 1999) has been adopted to reduce the strengths derived from the laboratory testing of intact samples by using the Rocscience RocLab software. The geological strength index values adopted for the main rock units are shown in Figure 10.

Two estimates of strength parameters have been adopted from the laboratory testing and field assessments: 1) an “average” estimate; and 2) a reasonable “lower” estimate. These are summarised in Table 11. Table 11 shows the reduced (rock mass) strengths derived from using the geological strength index.

In general the parameters adopted for the “average” estimates of material strength were derived from the testing of borehole cores, whilst those adopted for the “lower” estimate were derived from cores taken from boulders that fell off the slope face during the 2010/11 earthquakes.

The *in situ* shear modulus of the materials was derived from the downhole (drillhole) shear-wave surveys carried out by Southern Geophysical Ltd. (Southern Geophysical Ltd., 2013) in Aurecon NZ Ltd., drillholes BH-RHR-01 and BH-RHR-03.

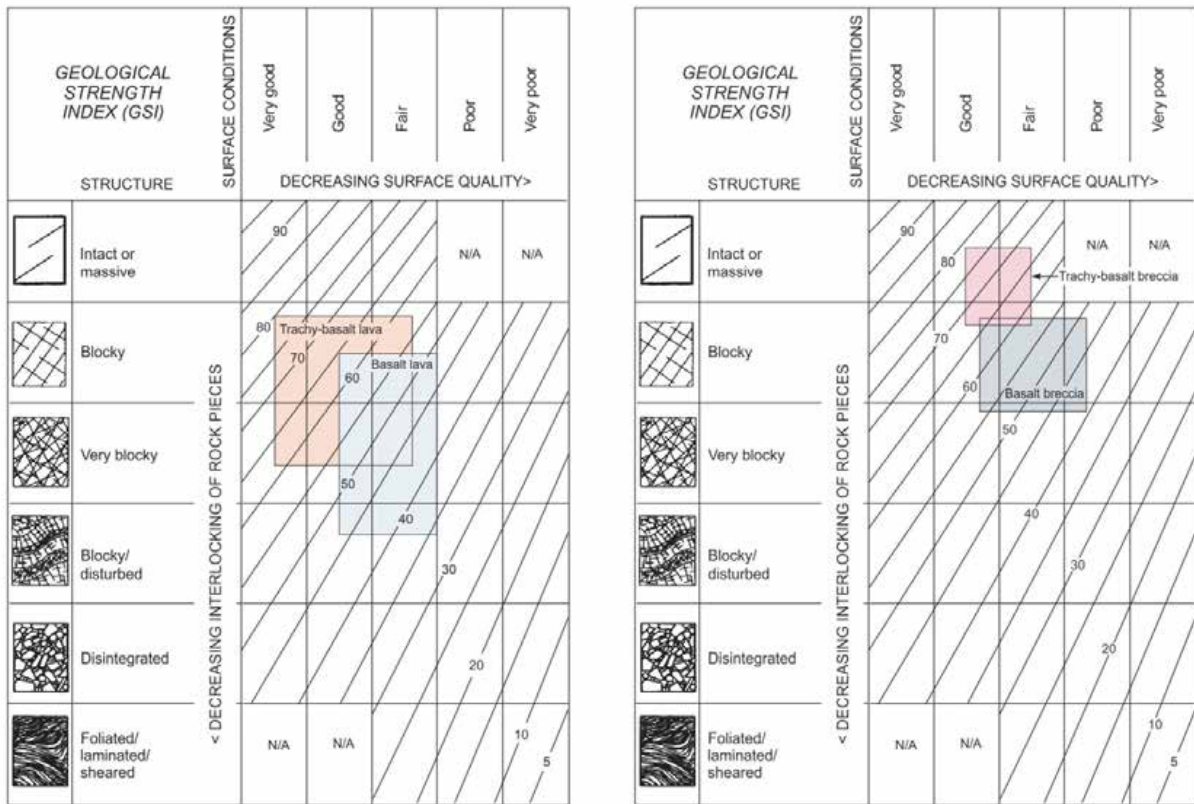


Figure 10 Geological strength index plot for basalt and trachy-basalt lavas and basalt and trachy-basalt lava breccias exposed on the cliffs at Wakefield Avenue (Modified after Hoek, 1999).

Table 11 Geotechnical material parameters derived from testing and used for the modelling.

Unit	Depth to base of layer (m)	Lab UCS (MPa)	GSI ¹	Unit weight (kN/m ³)	MI ²	Tensile (MPa)	Intact modulus E _i (MPa)	Poisson's ratio	Shear modulus ³ G _s (kPa)	Rock mass parameters used for modelling ⁴			
										Cohesion c (MPa)	Friction ϕ (°)	Tensile strength (MPa)	Rock mass modulus E _M (MPa)
Model 1: Material properties													
Loess	7	0.4	N/A	17	N/A	N/A	30	0.3	275,700	0.015	32	0.05	N/A
Basalt Lava (Incl. basalt breccia)	20	55	55	28	11	5.7	12,000	0.25	6,422,000	0.6	57	0.17	4900
Trachy basalt lava breccia	35	5	75	20	7	0.7	3,800	0.3	4,587,200	0.28	41	0.11	3100
Trachy basalt Lava	55	160	60	26	15	10.5	13,000	0.2	13,984,400	2	61	0.52	6,700
Model 2: Material properties													
Loess	7	0.2	N/A	17	N/A	N/A	10	0.4	161,900	0.01	30	0.03	N/A
Basalt Lava (Incl. basalt breccia)	20	20	40	28	6	5.7	10,000	0.25	2,311,900	0.18	42	0.04	1600
Trachy basalt lava breccia	35	3	65	20	4	0.7	970	0.3	733,900	0.14	30	0.05	600
Trachy basalt lava	55	101	50	26	9	10.5	10,000	0.2	13,984,400	1	53	0.26	3100
Model 3: Material properties, as model 2 except for:													
Trachy basalt lava breccia	35	3	55	20	4	0.7	970	0.3	733,900	0.1	28	0.03	400

¹ Geological strength index (GSI) – rock mass properties derived using the GSI, but not for the loess, where laboratory tests are used.

² The mi values shown, represent the range in the ratio of unconfined compressive strength to tensile strength, derived from tested samples of basalt lavas and basalt lava breccias (Carey et al., 2014), and not the ratio of unconfined compressive strength to tensile values shown in the table.

³ Shear modulus is defined using the shear wave velocity derived from the downhole (drillhole) shear wave surveys (Southern Geophysical Ltd., 2013).

⁴ Mohr-coulomb parameters (cohesion and friction) were derived from RocLab by line fitting over the appropriate stress range of the slope.

3.3.2.1 Shear Modulus

The *in situ* shear moduli of the materials were derived from:

1. Results from the downhole shear-wave velocity surveys carried out by Southern Geophysical Ltd. (Southern Geophysical Ltd., 2013) based on the survey results from drillholes BH-MB-01 and BH-MB-02 carried out by Aurecon NZ Limited at the site; and
2. Results from the dynamic probing of the loess and loess colluvium carried out by Tonkin and Taylor for the Earthquake Commission at Clifton Terrace (Tonkin and Taylor, 2012b).

The range of shear moduli for the different materials was calculated by using the relationship between the shear wave velocity and material density:

$$G = \rho \cdot V_s^2 \quad \text{Equation 2}$$

Where ρ is the density of the material and V_s is the shear wave velocity.

The shear-wave velocity profiles carried out by Southern Geophysical Ltd. (Southern Geophysical Ltd., 2013) in drillholes BH-MB-01 and BH-MB-02 are shown on cross-sections 2, 3 and 4 in Figure 7.

The strengths of the samples derived from the boulders that fell off the slope during the 2010/11 earthquakes are generally lower than for the same lithologies from drillhole samples, and the strengths of drillhole core samples taken from BH-RHR-01, closer to the cliff face – about 30 m – are generally lower than those from samples taken of the same lithologies from drillhole BH-RHR-03 – about 60 m from the cliff face (Carey et al., 2014).

This is also true of the shear wave velocity profiles. The mean shear wave velocities recorded in BH-RHR-01 are much lower than those for the same materials in BH-RHR-03 (Table 12). These data suggest that in general the strength of the rock mass deteriorates towards the cliff face.

Table 12 Shear wave velocity profiles (measured in the Aurecon NZ Ltd. drillholes).

Unit	BH-RHR-01 (30 m from cliff edge) Mean shear wave velocity (m/s)	BH-RHR-03 (60 m from cliff edge) Mean shear wave velocity (m/s)
Loess	260	340
Basalt lava (Incl. basalt lava breccia)	900	1,500
Trachy basalt lava breccia	600	1,500
Trachy basalt lava	2,300	3,600

3.3.3 Rainfall and groundwater response

In general, groundwater has two main effects on the stability of rock slopes that need to be considered: 1) rising groundwater within the slope rock mass leading to an increase in pore pressures in joints and a reduction in the effective stress of the materials; and 2) infiltration from high intensity and prolonged rainfall, leading to increased water pressures in tension cracks and open joints. The first effect is not thought to be the main one affecting the slope at

Richmond Hill, as the materials forming the slope are relatively free draining and there is a limited catchment area above the slope. The second effect is thought to be the most important from a stability perspective, as the open tension cracks in the overlying loess would allow water to readily infiltrate any open cracks in the underlying rock mass. It should be noted that there is currently no monitoring of groundwater levels within the rock mass.

The relationship between rainfall and landslides in the Port Hills has been summarised by McSaveney et al. (2014). Heavy rain and long-duration rainfall have been recognised as potential landslide triggers on the Port Hills for many years.

A long historical landslide record has been gathered by searching “Paperspast” (<http://paperspast.natlib.govt.nz>). This electronically searchable record of daily and weekly newspapers covers the period 1860–1926, but its landslide information is very incomplete, being only what newspapers of those times considered to be “newsworthy”.

Rockfalls were frequent enough before the era of wider urban development in the Port Hills that extensive shelter belts of usually macrocarpa or other trees were planted below rockfall areas to protect livestock and orchards.

A list of Earthquake Commission claims for landslide (rockfall) damage was examined for the interval 1997–2010, and a Geotechnical Consulting Ltd. landslide investigations list covers the interval 1992–2009. Any duplicate records for the period 1997–2009 contained in the data sets were removed. These records, though incomplete with respect to all of the landslides that occurred over those intervals, may be approximately complete with respect to the episodes of rain associated with landslide occurrences that damaged homes and urban properties (Figure 11).

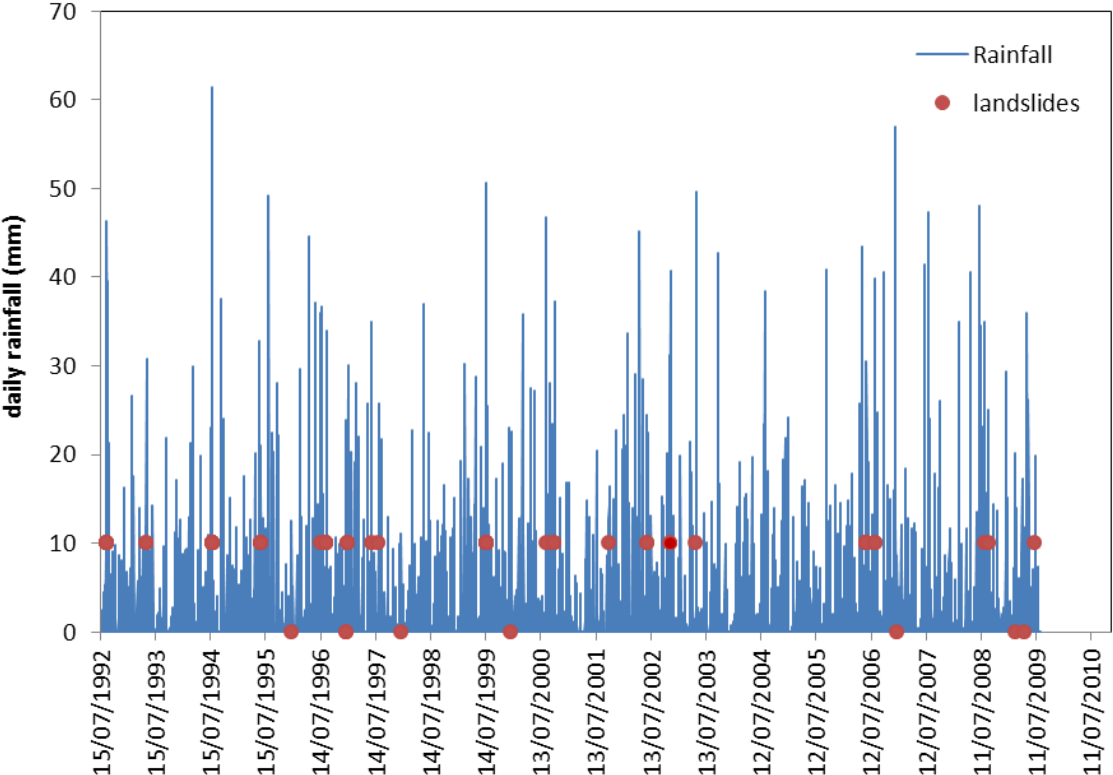


Figure 11 Daily rainfalls at Christchurch Gardens and landslides in the Port Hills. Daily rainfalls at Christchurch Gardens and landslides in the Port Hills investigated by Geotechnical Consulting Ltd, or listed by the Earthquake Commission as causing damage to homes. Landslides without rain are plotted at 0 mm, all others are plotted at 10 mm of rain (the minimum rainfall for triggered landslides).

McSaveney et al. (2014) conclude that the comparison of the record of damaging landslides (including rockfalls) and daily rainfall for the period 1992–2010 shows that:

1. Landslides can occur without rain, but the probability of landslides occurring increases with increasing intensity of rainfall;
2. Landslides occurred much more frequently on days with rain, but there were many rainy days when no landslides were recorded; and
3. As the amount of daily rainfall increased, a higher proportion of the rainy days had recorded landslides.

Following the 2010/11 Canterbury earthquakes there have been two notable rainfall events (Table 13):

- 11–17 August 2012: occurred at the end of winter following a long period of wet weather. During this period a total of 92 mm of rainfall was recorded at the Christchurch Gardens. The maximum daily rainfall (24 hourly rainfall recorded 9 am–9 am) during this period occurred on 13 August 2012 and totalled 61 mm.
- 3–5 March 2014: occurred at the end of a period of dry weather. During these three days, a total of 118 mm of rain was recorded at the GNS Science rain gauge installed at Clifton Terrace in the Port Hills (approximately 2 km west of Deans Head). The maximum daily rainfall (24 hourly rainfall recorded 9 am–9 am) during this period occurred on 5 March 2014 and totalled 89 mm.

The frequency of high-intensity rainfalls in Christchurch has been well studied (e.g., Griffiths et al., 2009, Figure 12, and McSaveney et al., 2014). Griffiths et al. (2009) use rainfall records for the period 1917–2008 from gauges all over Christchurch. McSaveney et al. (2014) use a composite rainfall record, for the period 1873–2013, mainly from the Christchurch Gardens gauge, but substituting averages for other nearby stations where gaps in the Christchurch Gardens data exist.

The annual frequencies estimated for four recent heavy rainfall events, including the two notable events are given in Table 13. Rainfall depth-duration-return period relations for Christchurch Gardens and Van Asch St, Sumner are taken from Griffiths et al. (2009) and for Christchurch Gardens from McSaveney et al. (2014).

Table 13 Annual frequencies of given rainfall in the Christchurch for four main events following the 2010/11 Canterbury earthquakes (rainfalls are calculated daily from 09:00 to 09:00 NZST).

Date	Total rainfall (mm)	Station	Max daily rainfall/date	Annual frequency Christchurch Gardens Griffiths et al. (2009)	Annual frequency Christchurch Gardens McSaveney et al. (2014)	Annual frequency Van Asch, Sumner Griffiths et al. (2009)
11–17 August 2012	92	Christchurch Gardens (CCC/NIWA)	61 mm, 13 August 2011	92 mm = no data available 61 mm = 0.5 (once every 2 years)	92 mm = 0.4 (once every 2.7 years) 61 mm = 5 (5 times per year)	N/A
3–5 March 2014	118	Clifton Terrace (GNS Science)	89 mm, 5 March 2014	N/A	N/A	118 mm = 0.1 (once every 10 years) 89 mm = 0.1 (once every 10 years)
3–5 March 2014	141	Christchurch Gardens (NIWA)	130 mm 5 March	141 mm = 0.05–0.02 (once every 20–50 years) 130 mm = 0.02–0.01 (once every 50–100 years)	141 mm = 0.05 (once every 20 years) 130 mm = (>0.01) less than once every 100 years	N/A
18 April 2014	68	Lyttelton (NIWA)	68 mm	N/A	N/A	68 mm = 0.5 (once every 2 years)
29 April 2014	20	Clifton Terrace (GNS Science)	20 mm	N/A	N/A	Greater than 0.5 (occurs frequently every year)

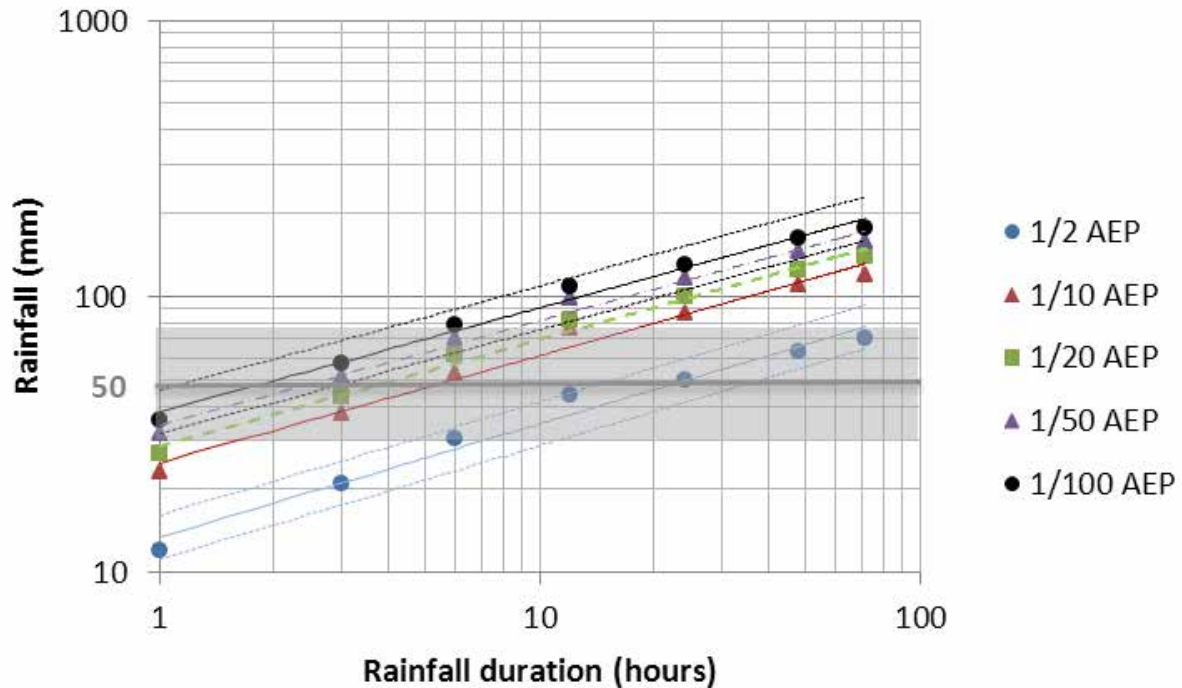


Figure 12 Rainfall depth-duration-return period relations estimated for Christchurch Gardens by Griffiths et al. (2009) using recorded rainfall data. Error limits of 20% are shown by dotted lines for the 1/2 and 1/100 AEP curves. Shaded area covers the range of 30–75 mm of rainfall over which the expected number of soil landslides in the Port Hills rises from very few to many. Rockfalls can occur without rain, but the probability of rockfalls occurring increases with increasing intensity of rainfall.

Laser scan surveys covering this (3–5 March 2014) period were carried out, but the data are not available at the time of writing this report, although field observations indicate many small failures of rock occurred from the slope. Results from earlier terrestrial laser scan surveys (between January 2012 and November 2013) indicate considerable volumes of material (100–670 m³/year) continue to fall from the slope, during periods when no notable earthquakes occurred, although the rates may be decreasing (e.g., 670 m³/year in 2012 to 100 m³/year in 2013).

Regardless of the rainfall data-sets used, the rainfall data suggest that the heavy rainfalls recorded in the Port Hills following the 2010/11 Canterbury earthquakes are unexceptional. Although the three-day rainfall of 118 mm had an annual frequency of 0.05–0.1 (once every 10 years), it occurred at the end of summer when the ground would have had a seasonally low water content.

However, given the historical rates of rainfall triggered rockfall for the slope of about 5–6 m³/year, although the maximum recorded rate is about 50 m³/year in any one year (estimated from historical data by Massey et al., 2012a), the current rates of rockfalls triggered by rainfall are considerably higher. These increased rates are not unexpected, as the rock mass forming the slope has been considerably weakened by earthquake-induced cracking. The historical and recent rainfall-induced rockfalls from the slope tend to be local and relatively small in volume (mean volumes of discrete failures tend to be <0.1 m³ based on the results from terrestrial laser scan surveys), and are randomly distributed across the slope.

It is not known whether the recorded cGPS movement at the cliff top (11–17 August 2012) was related to shallow movement of the loess/fill overlying bedrock, or to deeper-seated movement in the cliff. It is also not known what the groundwater conditions in the area were at the time of movement.

3.4 SLOPE FAILURE MECHANISMS

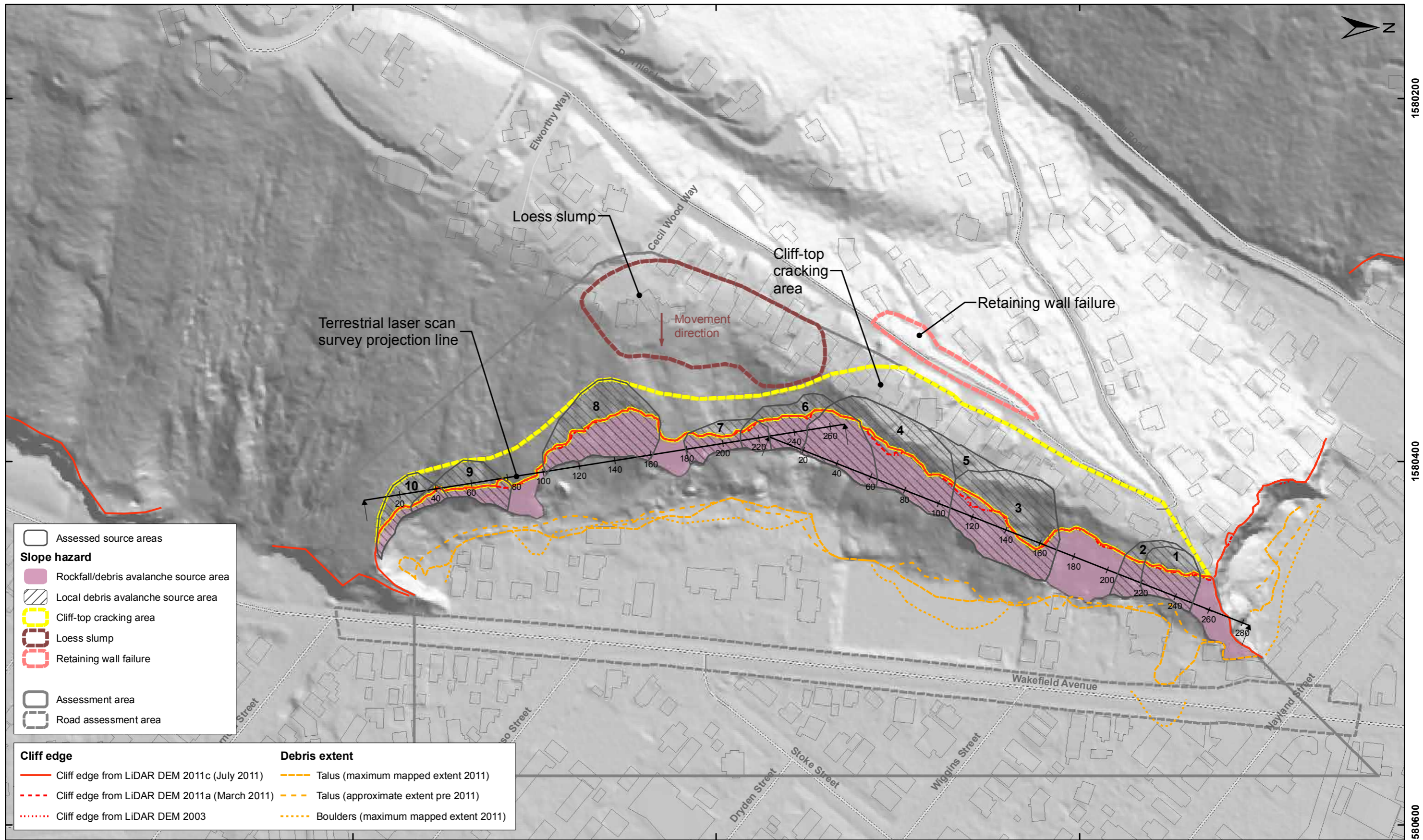
3.4.1 Landslide types affecting the site

Based on the aerial photograph interpretation, engineering geological mapping, cross-sections and site observations and measurements of the impacts of the 2010/11 Canterbury earthquakes, it is anticipated that any future landslides in the study area will occur under either static or dynamic conditions, but under static conditions they are likely to be smaller in volume.

Four potential landslide types have been identified that could affect the site:

1. Debris avalanches – ranging from a single rockfall to many thousands of cubic metres of rock falling from the cliff.
2. Cliff-top recession, deformation and cracking – in response to deformation of the rock mass in the slope.
3. Slumping of loess (and fill) at the cliff top. The slump features, thought to be predominantly in loess, may also reactivate during or shortly after very wet weather.
4. Earth/debris flows originating in loess above the cliff edge. Rain or snowmelt and ingress of water through tension cracks can wet the fill, loess and loess colluvium at the crest of the slope overlying rock head, causing loss of strength leading to earth/debris flows. To date (post-2010/11 earthquakes), such flows have been relatively small at this location ($<10 \text{ m}^3$) with limited runout of debris down the cliff face.

Based on the past performance of the cliffs in the study area, cliff collapse hazards (cliff-top recession and debris avalanches) pose the greatest landslide hazard and therefore landslide risk to people at the cliff top and cliff toe. These slope-instability processes form the basis of the following hazard and risk assessments, and their potential source areas are shown on Figure 13.



SCALE BAR: 0 50 100 m

EXPLANATION:

Background shade model derived from NZAM post earthquake 2011c (July 2011) LiDAR survey resampled to a 1 m ground resolution.
 Roads and building footprints provided by Christchurch City Council (20/02/2012).
 PROJECTION: New Zealand Transverse Mercator 2000

DRW:
BL
CHK:
CM



ENGINEERING GEOLOGY MODEL

**Richmond Hill Road
Christchurch**

FIGURE 13

FINAL

REPORT:
CR2014/34

DATE:
June 2014

3.4.1.1 Cliff collapse

The majority of past failures, pre-2010/11 earthquakes and those during the 2010/11 Canterbury earthquakes have occurred within the trachy basalt breccia, which has the lowest strength of the rocks tested at the site. The large arcuate features (relict landslide scarps inferred from the aerial photograph interpretation and field mapping) are predominantly in this material. Failures during the recent earthquakes also occurred in other materials forming the slope, although these failures tended to be smaller in volume than those in the trachy basalt breccia.

The static strength of the rock slope and its loess mantle at the slope crest is considered to have been weakened from its pre-earthquake state by earthquake-induced cracking and deformation of the rock-mass and loess. The newly exposed slope is considered to be more prone to failure than was the former slope which had had many hundreds of years to shed its less stable material after the penultimate earthquake sequence. Significant rock-mass degradation is supported by post-earthquake down-hole geophysical surveys, laboratory strength tests of drill core samples and boulders, and identification of significant cracks and areas of deformation on the cliff face that were visible after the 13 June 2011 earthquake (Figure 14).

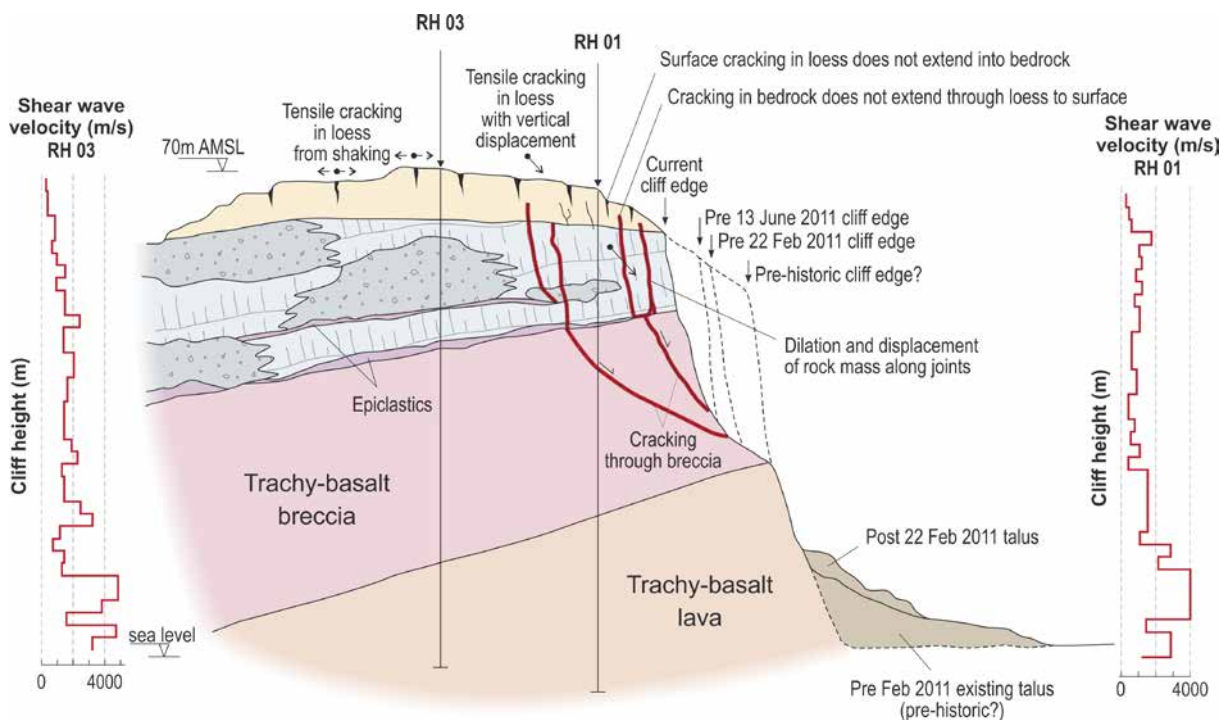


Figure 14 Schematic cross-section (cross-section 2, Figure 7) of the cliff showing the inferred failure mechanisms and differences in rock mass strength derived from the downhole shear wave surveys.

The field evidence supporting the possibility of larger failures comprises the presence of relict (pre-2010/11 Canterbury earthquakes) failure scarps on the cliff face and corresponding debris at the cliff toe, and large discrete cliff failures occurred at other similar cliffs during the 2010/11 earthquakes. The largest, with a failure volume of about 35,000 m³ occurred at Shag Rock Reserve during the 13 June 2011 earthquake (Massey et al., 2012a).

In addition to cliff-top cracking and debris avalanches from the cliff face, several retaining walls along the western side of Richmond Hill Road were damaged in the 2010/11 earthquakes. The stability of retaining walls has not been assessed in this study.

3.4.2 Cliff collapse failure mechanisms

3.4.2.1 Static conditions

Potential failure mechanisms occurring at Richmond Hill Road under static conditions comprise:

- Ravelling of loose rock from the cliff. This is on-going and occurs during rain and at other times without an obvious trigger. Ravelling has involved (to date) only small volumes of rock (and soil) at a time. However, the post-earthquake accumulation rate of debris at the base of the cliff is about 670 m³ per year (based on terrestrial laser scan surveys).
- Larger, non-seismic debris avalanches could occur from this slope if rock mass strength continues to deteriorate as a cumulative result of effects such as water ingress, cycles of wetting and drying and deterioration in future earthquakes.

3.4.2.2 Dynamic conditions

Buildings at the cliff top towards the northern end of the spur – where the width of the spur is thinnest – showed major shaking damage, indicating that significant amplification of ground shaking occurred in these areas (Figure 15).



Figure 15 View to the south along Richmond Hill after the 13 June 2011 earthquake. Photograph taken by C. Gibbons, Aurecon New Zealand Ltd.

The magnitude of permanent earthquake-induced displacement of the cliff top and the volume of debris that could fall from the cliffs, depends on the magnitude and duration of earthquake-induced ground accelerations and the critical yield acceleration of the cliff.

Failure mechanisms that occur at Richmond Hill Road under dynamic conditions are:

- Permanent cliff displacement in future strong shaking – similar to those recorded during the 2010/11 Canterbury earthquakes, However, these may be larger than those recorded during the recent earthquakes, because of the accumulated strength degradation of the rock mass behind the cliff caused by the earthquake-induced cracking and deformation. Localised cracking of the loess above rock head can also occur.
- It is expected that future strong earthquakes will trigger further cliff collapses and rockfall volumes could be larger than those triggered during the 22 February, 16 April, 13 June and 23 December 2011 earthquakes.

Engineering geological mapping, air photograph interpretation and measurements of cracking, deformation and the volumes of debris leaving the slope during the 2010/11 Canterbury earthquakes, suggests that it is possible for larger cliff collapses (larger in volume than those triggered recently at this site during the earthquakes) to occur at the site. Three potential source areas have been identified, where the crack patterns suggest larger failures could occur. If these were to occur, their debris could travel further downslope than the debris from previous failures.

4.0 HAZARD ASSESSMENT RESULTS

4.1 SLOPE STABILITY (SOURCE AREAS 1–10)

For assessed source areas 1–10, the engineering geological cross-sections in Figure 7 were used as the basis of the numerical slope stability modelling. Geotechnical material strength parameters used in the modelling are from Table 11, and models using variable shear strength parameters for the key materials were run to assess the sensitivity of the slope – along a given cross-section – to failure, and to take into account the on-going degradation of the rock mass in response to earthquake-induced fracturing.

Stability assessments were carried out adopting two different geotechnical material strength parameter models (“average” and “lower” parameters, Table 11). Strength reduction was simulated by reducing the geological strength index values to simulate the observed increased fracturing of the rock mass through the 2010/11 Canterbury earthquakes (Figure 16) and by varying the intact strengths of the rock materials based on the differences between the testing results from the boulders and drillcores (Carey et al., 2014). The condition of the rock mass at the onset of the 2010/11 earthquakes was inferred from photographs of the cliff taken (by M. Yetton, Geotech Ltd.) immediately after the 4 September 2010 (Darfield) earthquake.

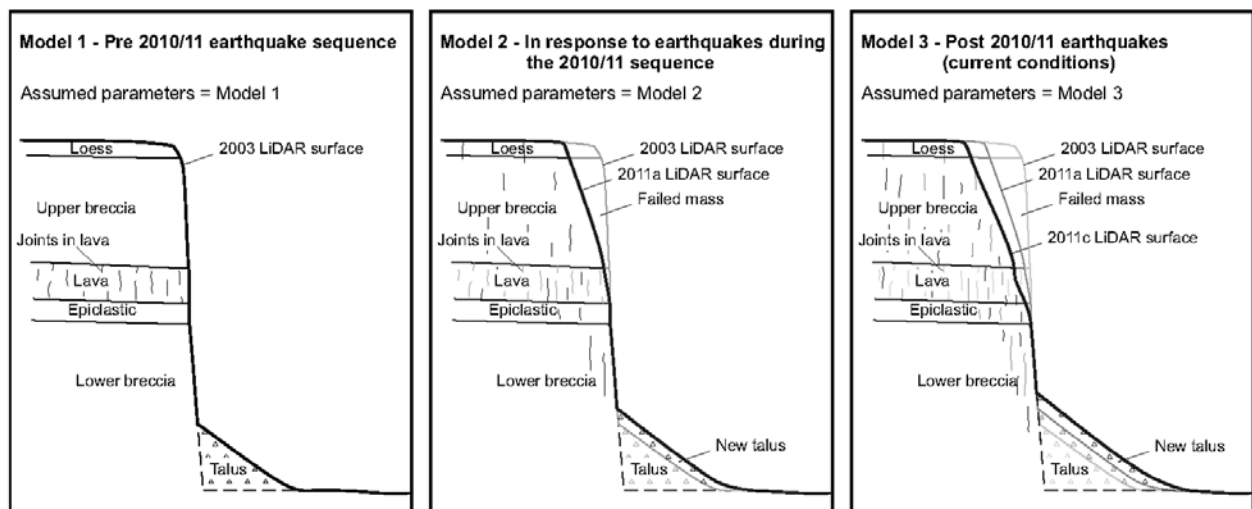


Figure 16 Schematic diagram showing the increasing frequency of defects in the slope in response to the successive 2010/11 Canterbury earthquakes.

Earthquake-induced cracks are unlikely to extend far back from the slope face near the toe of the slope, but are likely to extend further back from the slope face with increasing height from the toe. This is mainly because the amplification of shaking at the cliff top is substantially greater than at the cliff toe.

4.1.1 Slope stability – Static conditions (deep-seated failures)

The stability of the cross-sections under static conditions is assessed by assuming the slope is drained with no permanent water table. This was because no groundwater had been recorded in the piezometers or encountered during drilling, and noting that the area is a prominent spur with only a very limited catchment area. All models were assessed using the current slope surface geometry, derived from the LiDAR survey 2011c.

Figure 17 shows the results from the limit equilibrium modelling for slide surfaces constrained to the loess, and Figure 18 shows the results for the critical slide surface defined as the one with the lowest factor of safety for the cross-section, where the slide surface is not confined to a particular material. The adopted shear strength parameters for the loess are at the lower end of the range considered to be reasonable (Carey et al., 2014 and Della Pasqua et al., 2014). These parameters take into account that the material could have increased moisture – and therefore lower shear strength – during periods of wet weather typical of most winters.

Results from the limit equilibrium and finite element modelling (Table 14) show that there is a good correlation between the shape and location of critical slide surfaces derived from the limit equilibrium modelling and the zones of increased shear strain from the finite element modelling assessment (Figure 19) for those failures through the rock mass. The static factors of safety and the shear strength reduction factors are also comparable.

Static factors of safety for the cross-sections are lower for those shallow failure surfaces (although still deep seated) within the rock than for those confined to the loess. The cross-sections 1 and 7 – at the very northern and southern end of Wakefield Avenue respectively – have the lowest static factors of safety and shear strength reduction factors. This is because these cross-sections are steepest in angle and are formed of the weaker trachy basalt breccia.

Note that for cross-sections 4 and 5 the slide surfaces through the loess have lower factors of safety and stress reduction factors than the rock. These cross-sections and failure geometries correspond to the location and geometry of the identified loess slump (mass movement 3B; Figure 2).

Table 14 Example results from the static slope stability assessment adopting model 2 material strength estimates.

Cross-section	Slide surface	FoS/SRF ¹	Method ²	FoS with water filled tension cracks	Slide surface depth	Depth ³ (m)	Width ³ (m)	Material
1	1	1.4	LEM Path	1.1	Shallow	13	42	Rock
1	2	1.6	LEM Path		Deep	15	53	Rock
1	3	2.7	LEM Path		Shallow	2	6	Loess
1	4	3.4	LEM Path		Deep	3	9	Loess
1	5	1.4	FEM SRF		Shallow	12	44	Rock
2	1	1.5	LEM Path	1.0	Shallow	14	37	Rock
2	2	2.0	LEM Path		Deep	20	54	Rock
2	3	2.5	LEM Path		Shallow	2	11	Loess
2	4	2.7	LEM Path		Deep	4	15	Loess
2	5	1.6	FEM SRF		Shallow	12	45	Rock
3	1	1.5	LEM Path	1.0	Shallow	16	54	Rock
3	2	1.7	LEM Path		Deep	24	68	Rock
3	3	1.7	LEM Path		Shallow	2	13	Loess
3	4	2.0	LEM Path		Deep	5	16	Loess
3	5	1.5	FEM SRF		Shallow	13	56	Rock
4	1	1.9	LEM Path	1.6	Shallow	11	35	Rock

Cross-section	Slide surface	FoS/SRF ¹	Method ²	FoS with water filled tension cracks	Slide surface depth	Depth ³ (m)	Width ³ (m)	Material
4	2	1.7	LEM Path		Shallow	5	38	Loess
4	3	1.9	LEM Path		Deep	6	61	Loess
4	4	2.0	LEM Path		Deep	12	65	Rock
4	5	1.8	FEM SRF		Deep	5	46	Loess
5	1	3.0	LEM Path	2.7	Shallow	10	42	Rock
5	2	3.9	LEM Path		Deep	18	75	Rock
5	3	1.7	LEM Path		Shallow	5	38	Loess
5	4	1.9	LEM Path		Deep	7	58	Loess
5	5	2.0	FEM SRF		Shallow	4	41	Loess
6	1	1.8	LEM Path	1.1	Shallow	9	35	Rock
6	2	1.9	LEM Path		Deep	18	51	Rock
6	3	1.8	LEM Path		Shallow	13	43	Rock
6	4	1.9	LEM Path		Shallow	5	61	Loess
6	5	1.4	FEM SRF		Deep	15	50	Rock
7	1	1.4	LEM Path	1.0	Shallow	8	27	Rock
7	2	1.7	LEM Path		Deep	13	46	Rock
7	3	1.7	LEM Path		Shallow	5	75	Loess
7	4	1.5	FEM SRF		Deep	11	44	Rock

¹ FoS is the factor of safety derived using the GLE Morgenstern and Price (1965) method. Where the cross-section has been assessed using the FEM, the stability of the cross-section is assessed in terms of the stress reduction factor (SRF) (Comment: The Shear Strength Reduction (SSR) method is used to determine the Stress Reduction Factor (SRF) or factor of safety value that brings a slope to the verge of failure (Dawson et al., 1999).

² LEM is the limit equilibrium method adopting the “path search” slide surface function, and FEM is the finite element method.

³ Estimated failure depth (perpendicular to slide surface) and failure length (crown to toe of failure) based on slide surface geometry.

4.1.1.1 Model sensitivity to groundwater

The sensitivity of the factor of safety to transient changes in ephemeral ground water (pore pressure) has been simulated by modelling pore pressures acting within tension cracks, where the tension cracks are assumed to extend from the surface to the base of the upper basalt lava unit (for cross-sections 1–3 and 7), from the surface to the base of the upper trachy-basalt lava unit (cross-sections 4 and 5) and from the surface to the base of the upper trachy-basalt breccia unit (cross-section 6) – corresponding to the main areas of cliff-face cracking. Tension cracks were assumed to be 100% filled.

The results show that the inclusion of water filled tension cracks within the model decreases the factor of safety for cross-sections 1–3, 6 and 7 to just above 1.0 (Table 14). These are thought to be lower bound estimates as tension cracks were assumed to be 100% filled.

If a slope has a static factor of safety of one, then the slope is assessed as being unstable. Slopes relating to structures designed for civil engineering purposes are typically designed to achieve a long-term factor of safety of 1.5 under drained conditions, as set out in the New Zealand Building Code. Results from the stability assessment indicate that under current conditions the factors of safety of the assessed slope cross-sections 2–7 are greater than 1.5. The exception is cross-section 1, where the factor of safety is 1.3.

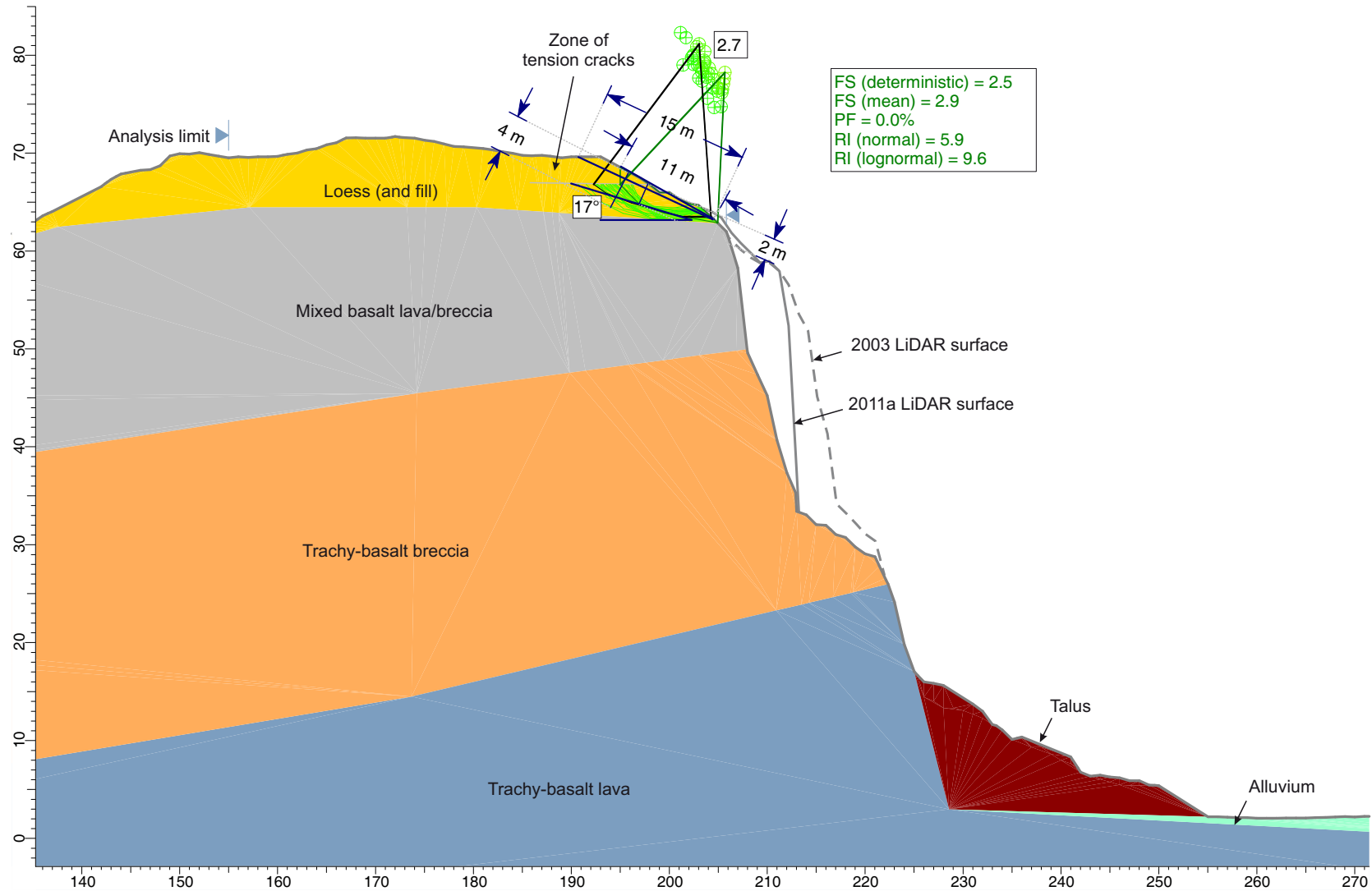
Although the static factors of safety are relatively high, under current drained conditions it is still possible that deep-seated failure of the rock mass for cross-sections 1–3, 6 and 7 (adopting the assessed slide surfaces in Figure 20–Figure 22) could occur without an earthquake, given the sensitivity of the modelled cross-sections to surface water infilling tension cracks. It should be noted that material strengths – and therefore the slope factors of safety – could reduce with time, and the occurrence of future large earthquakes.

It should also be noted that the stability assessment results presented are for relatively deep-seated slide surfaces through the rock mass. However, much of the slope face appears unstable and rocks fall from the slope with no apparent trigger, indicating that parts of the slope face are only marginally stable to unstable, with factors of safety much less than those assessed for the deep-seated failures.

4.1.1.2 Model sensitivity to slope geometry

The sensitivity of the factor of safety to changes in the slope geometry was assessed by adopting the different slope-surface geometries from the LiDAR surveys for cross-sections, 2, 4 and 6, where material from the cliff fell off during the 2010/11 Canterbury earthquakes, causing the slope geometry to change.

Results show that as material falls from the cliffs the factors of safety increase slightly, as the slope angles reduce. However, any increase in stability caused by reducing slope angles, may be counterbalanced by fracture-induced weakening of the rock mass.



Slip surfaces shown with factor of safety < 3
 Factor of safety calculated adopting the GLE Morgenstern and Price (1965) method

DRW:
PC
CHK:
CM



**SECTION 2 LIMIT EQUILIBRIUM
 STABILITY ASSESSMENT
 Soil (loess) failure**

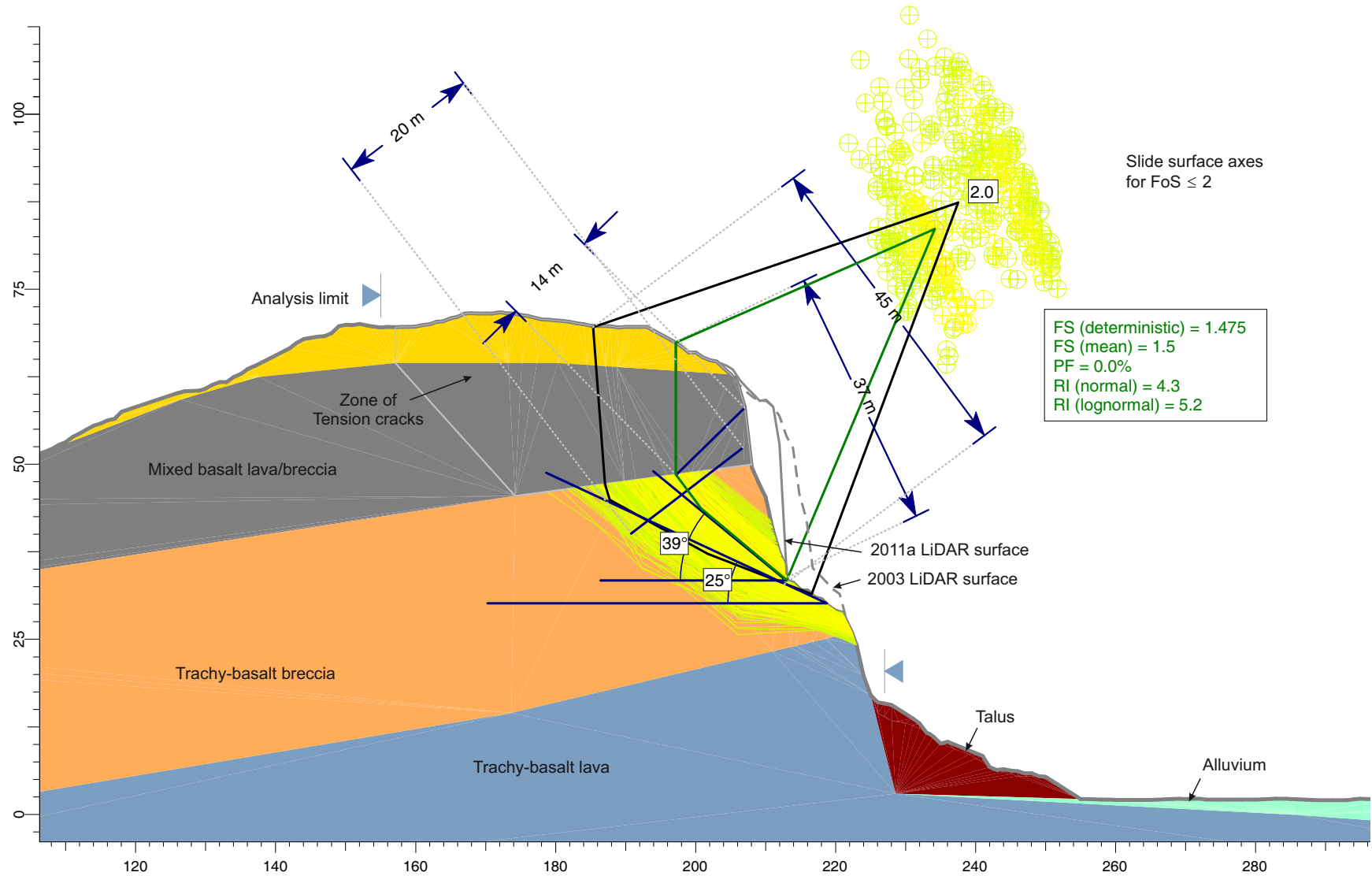
**Richmond Hill Road
 Christchurch**

FIGURE 17

FINAL

REPORT:
CR2014/34

DATE:
June 2014



Slip surfaces shown with factor of safety < 2
 Factor of safety calculated adopting the GLE Morgenstern and Price (1965) method

DRW:
PC
 CHK:
CM



SECTION 2 LIMIT EQUILIBRIUM STABILITY ASSESSMENT

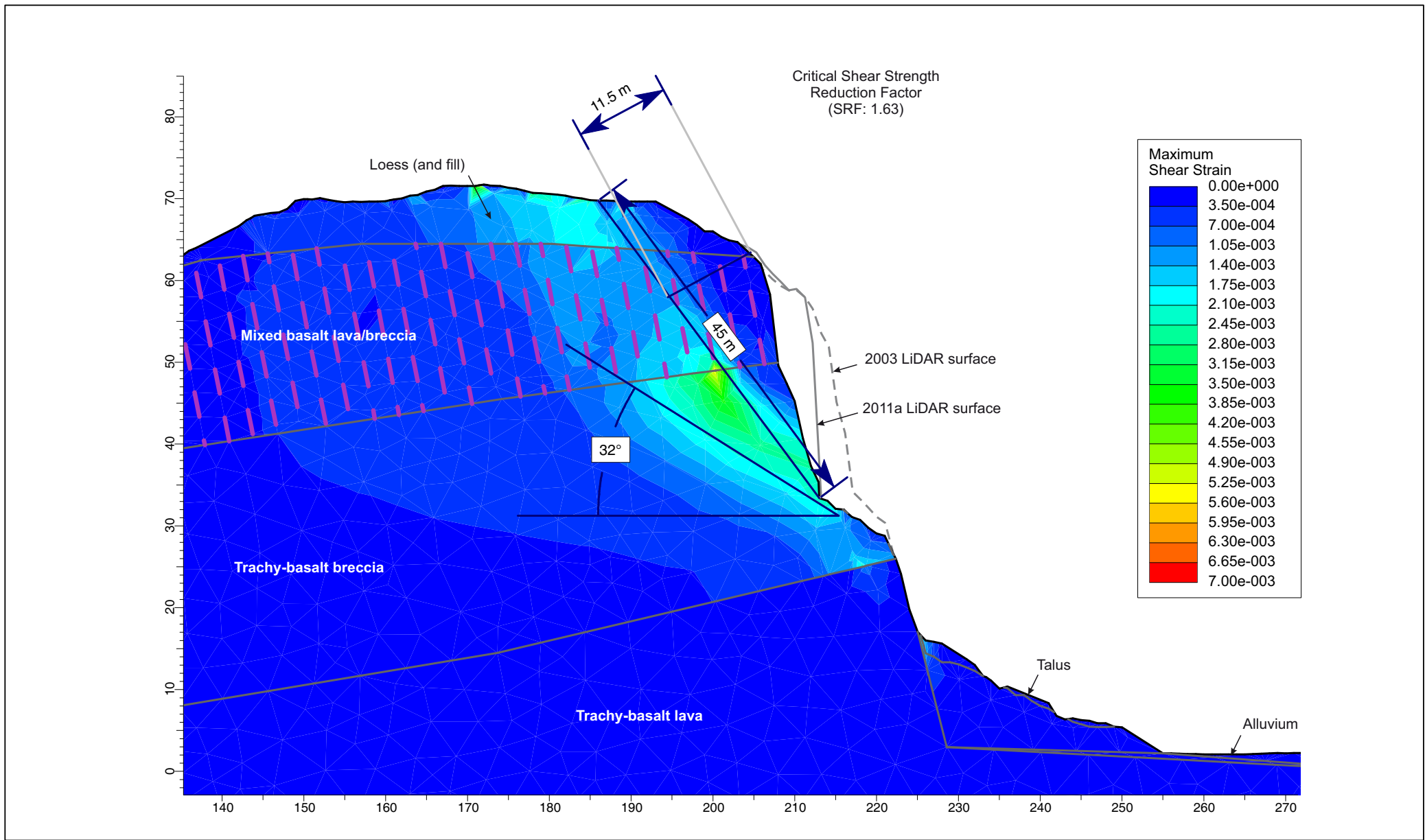
Richmond Hill Road
Christchurch

FIGURE 18

FINAL

REPORT:
CR2014/34

DATE:
June 2014



DRW:
PC

CHK:
CM



SECTION 2 FINITE ELEMENT STABILITY ASSESSMENT

**Richmond Hill Road
Christchurch**

FIGURE 19

FINAL

REPORT:
CR2014/34

DATE:
June 2014

4.1.2 Slope stability – Dynamic conditions

Dynamic stability assessment comprised: 1) back-analysing the performance of the slope during the 2010/11 Canterbury earthquakes to calibrate the models and check that the calculated displacements were consistent with the displacements inferred during the earthquakes; and 2) using the calibrated models to forecast the likely magnitudes of future displacements under given levels of peak ground acceleration.

Cross-section 2 (representing assessed source areas 3, 4 and 5) has been assessed under dynamic conditions, assuming a drained slope, using the decoupled method. The likely yield accelerations for cross-sections (1 and 3–7) were assessed using the pseudostatic method.

4.1.2.1 Amplification of ground shaking

The first stage of the assessment was to calculate the maximum acceleration at the cliff top (A_{MAX}) to quantify any amplification effects. Results from the dynamic site response assessment are contained in Appendix 6. This was done for cross-section 2, as it best represents the shape and geology of the overall slope, and the largest cliff top recession occurred in this area during the 2010/11 Canterbury earthquakes.

Results from this assessment have shown that the relationship between the peak ground acceleration of the free field input motion (A_{FF}) and the corresponding modelled peak acceleration at the cliff edge (A_{MAX}), is approximately linear up to an input peak acceleration of about 0.4 g. In this range of peak accelerations the amplification factor is typically in the order of about three times the input free field peak acceleration. Above peak ground accelerations of 0.4 g the relationship becomes non-linear, where the amplification factor reduces to about 1.5 times the input free field peak acceleration (Appendix 6). The rock input peak accelerations are those derived from the synthetic free field rock outcrop earthquake time acceleration histories (Holden et al., 2014). The results of the dynamic response analyses mirror trends reported by others, e.g., Bray and Rathje, (1998) and Kramer (1996). In general, the mean modelled horizontal peak accelerations at the cliff edge are about two to three times larger than the free field peak horizontal rock outcrop input accelerations.

The results suggest that the modelled ground accelerations increase with increasing height above the toe of the slope, but that the peak horizontal accelerations (for all modelled earthquakes) concentrate around the convex break in slope, defined as A_{MAX} .

4.1.2.2 Back-analysis of permanent slope deformation

Earthquake-induced permanent displacements were calculated using the decoupled method (Makdisi and Seed, 1978) and the Slope/W software. The failure mechanism assessed was failure of the slope through the rock mass. A range of slide surfaces were assessed adopting the “block search” and “semi-circular” functions. Permanent displacements was estimated along each slide surface, where the displacing mass was treated as a rigid-plastic body and no internal plastic deformation of the mass was accounted for, and the mass accrued no displacement at accelerations below the yield acceleration.

The out-of-phase synthetic rock outcrop earthquake time acceleration histories from the 22 February and 13 June 2011 earthquakes were used as inputs for the modelling, as permanent coseismic displacement of the Richmond Hill slopes were inferred during these events, and large volumes of materials fell from the slopes. Variable material strength parameters were used for the main materials present, adopting models 1–3 parameters (Table 11).

For this assessment the displacements measured from crack apertures (0.5–0.6 m, based on the combined crack apertures with both vertical and horizontal components) are assumed to represent the displacement of the cliff top during the 22 February, 13 June and 23 December 2011, earthquakes – mainly the 13 June 2011 earthquake. The calculated displacements of the slope for the 16 April and 23 December 2011, earthquakes were 0 m, where actual inferred displacements of the cliff top were about 0 m and 0.1 m respectively.

For the assessments the slope surface at the time of the earthquake was used adopting the LiDAR survey data. For example, back-analysis of the 22 February 2011 earthquake uses the slope surface from the 2003 LiDAR survey, and back-analysis of the 13 June 2011 earthquake uses the 2011a LiDAR survey. All forecast modelling uses the 2011c LiDAR slope surface model.

Results from the assessment show that if the model 1 material strength parameters are adopted the modelled displacements for the cross-section are too low when compared to the actual inferred displacements of greater than 0.5–0.6 m. The calculated displacements – adopting the model 2 and model 3 estimates of the material strength parameters – are more consistent with the actual recorded displacements at the cliff top for the for the 22 February and 13 June 2011 earthquakes – mainly the 13 June 2011 earthquake (Figure 20).

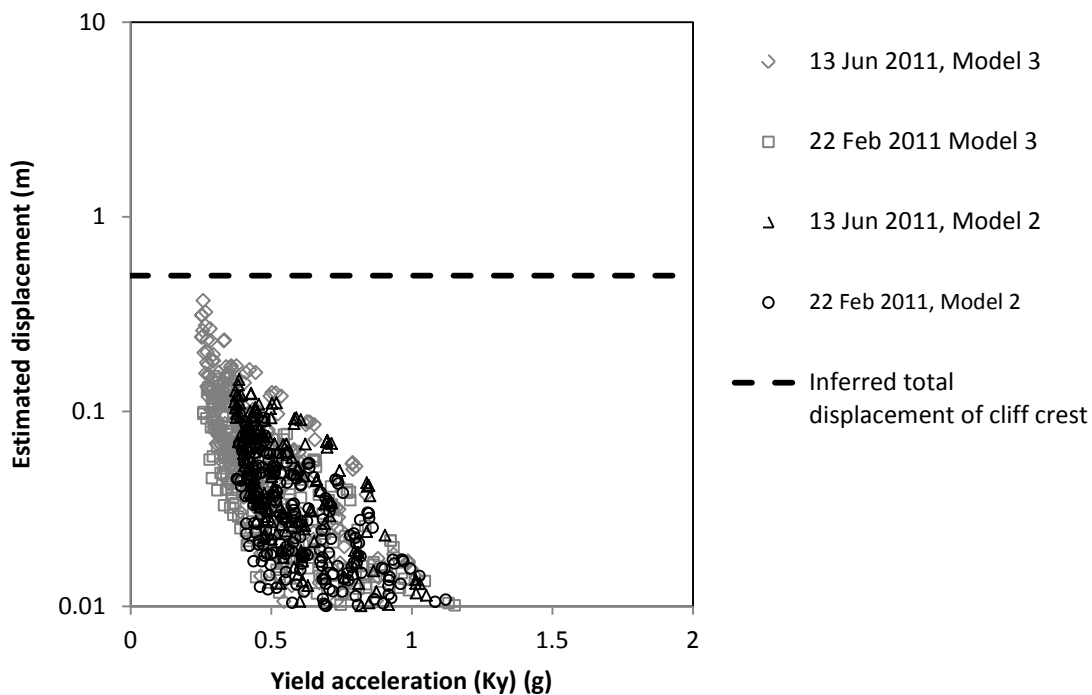


Figure 20 Modelled Slope/W decoupled displacements for cross-section 2 Richmond Hill Road, adopting the model 2 and 3 estimates of the material strengths. Each data point represents a modelled slide surface and the corresponding estimate of its displacement as a result of the 22 February, 13 June and 23 December 2011 earthquakes – adopting the synthetic free-field rock outcrop earthquake acceleration time histories. Data points are for slide surfaces mainly in rock.

Estimated displacements for slide-surface geometries confined within the loess are shown in Figure 21. These results adopt strength parameters for the loess of friction (ϕ) of 30° and cohesion (c) of 10 kPa, which are thought to be at the lower end of the range considered to be reasonable. Comparison of the results from Figure 20 and Figure 21 show that the modelled critical slide surfaces – those with the lowest factors of safety and largest displacement magnitudes – are those through the rock mass and not those through the loess.

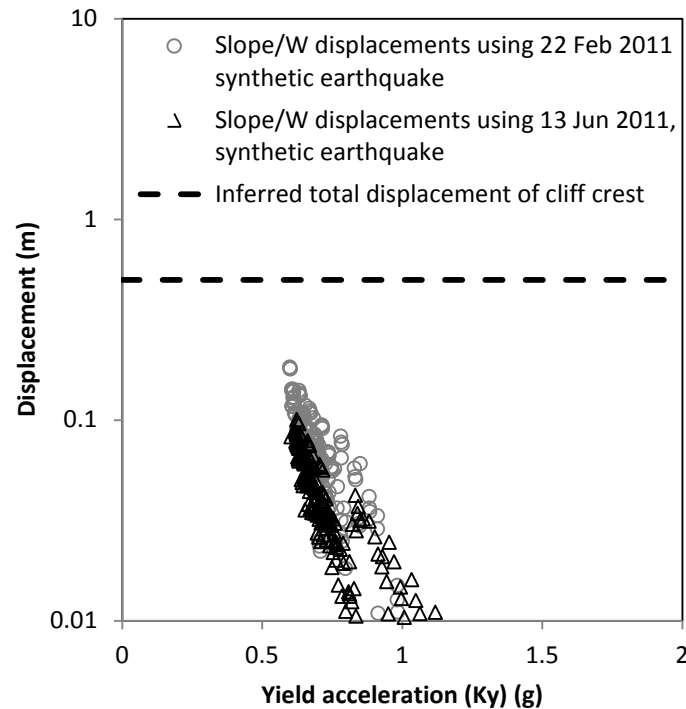


Figure 21 Modelled Slope/W decoupled displacements for cross-section 2 Richmond Hill Road, adopting loess shear strength of friction (ϕ) of 30° and cohesion (c) of 10 kPa, where the slide surfaces are constrained to the loess only. Each data point represents a modelled slide surface and the corresponding estimate of its displacement under the 22 February and 13 June earthquakes – synthetic adopting the free-field rock outcrop earthquake acceleration time histories.

For comparison purposes only, the estimated Newmark displacements adopting the recorded time acceleration histories from the GeoNet stations at Lyttelton Port Company (LPCC) and Godley Head (GODS) instruments have been used as inputs for a Newmark (1965) rigid block assessment, adopting Equation 23 of the 1965 paper. These results are shown on Figure 22 and Figure 23, along with the decoupled displacements shown in Figure 20, for the 22 February and 13 June earthquakes. The location and geometry of the modelled slide surfaces presented in Figure 20 are illustrated in Figure 24 and Figure 25.

The horizontal peak ground acceleration (PGA) recorded at station LPCC for the 22 February 2011 earthquake was 8.6 m/s/s (0.88 g) maximum single component. The instrument is located on the surface in the free field – on flat land – and the instrument is located on several meters of rock fill overlying *in situ* rock, which is recorded as site class B (in NZ standard 1170). Even though the instrument is located several kilometres away from the Richmond Hill site and further from the 22 February 2011 earthquake epicentre, it is the closest instrument to the Richmond Hill site that recorded the 22 February 2011 earthquake (refer to Holden et al., 2014, for further discussion).

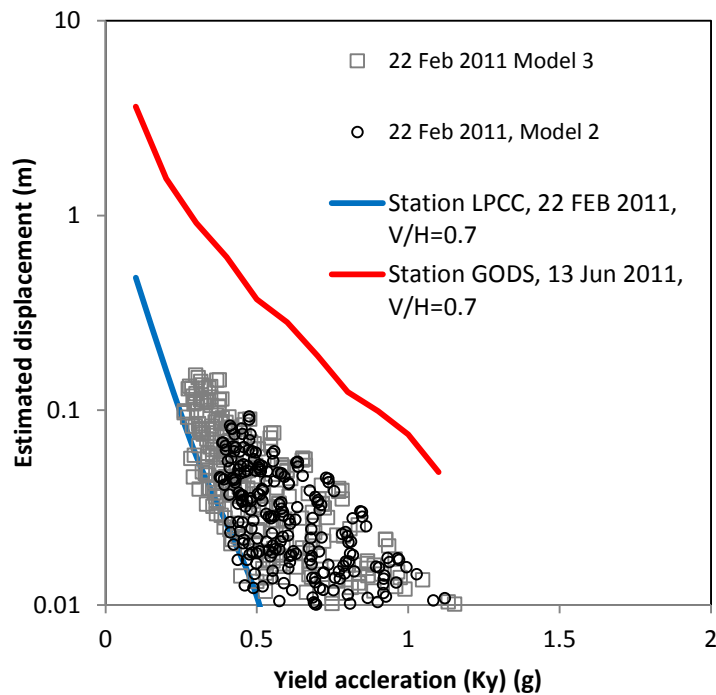


Figure 22 Estimated displacements of the Richmond Hill slope (cross-section 2) during the 22 February 2011, earthquake. Results show the decoupled displacements estimated using Slope/W adopting the 22 February 2011, synthetic earthquake time acceleration history. For comparison purposes the results from a classic Newmark (1965) sliding block analysis are also shown. The estimated Newmark displacements are based on the time acceleration histories (largest single component) recorded at instrument site LPCC during the 22 February 2011 earthquake, and site GODS during the 13 June 2011 earthquake. Newmark displacements using the instrumental records were estimated using Equation 23 of Newmark (1965), adopting a vertical component of $V/H = 0.7$. The vertical component is 70% of the horizontal and was derived from the Quake/W site response assessment.

The horizontal peak ground acceleration (PGA) recorded at station GODS for the 13 June 2011 earthquake was 18.2 m/s/s (1.9 g) maximum single component. This is a motion recorded by a sensor on the surface at the top of a slope, and is located on rock (recorded as Site class B, 1170). The instrument is about 1 km to the east from the Richmond Hill site and was located closer to the 13 June 2011 epicentre. Station GODS rather than PARS (Figure 1) was used as GODS is located in a slope crest setting, and was closest to the 13 June 2011 earthquake epicentre.

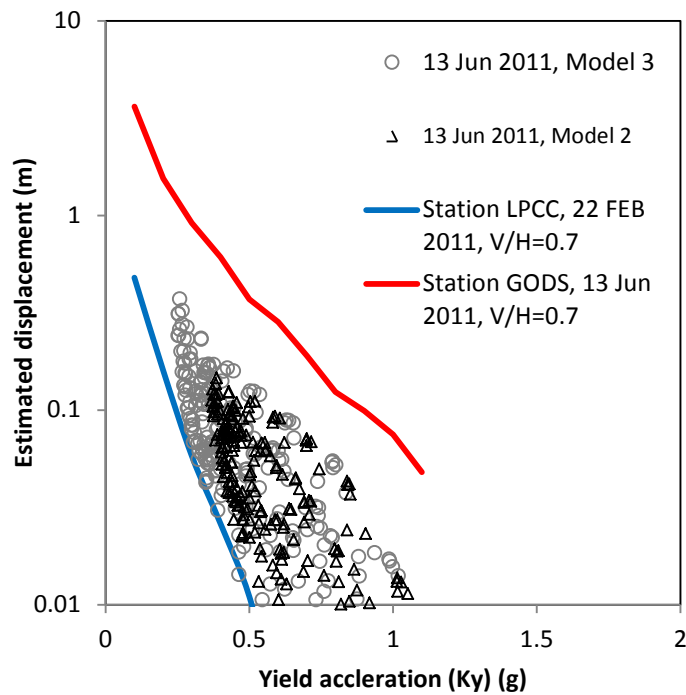


Figure 23 Estimated displacements of the Richmond Hill slope (cross-section 2) during the 13 June 2011 earthquake. Results show the decoupled displacements estimated using Slope/W adopting the 13 June 2011 synthetic earthquake time acceleration history. For comparison purposes the results from a classic Newmark (1965) sliding block analysis are also shown. The estimated Newmark displacements are based on the time acceleration histories (largest single component) recorded at instrument site LPCC during the 22 February 2011 earthquake, and site GODS during the 13 June 2011 earthquake. Newmark displacements using the instrumental records were estimated using Equation 23 of Newmark (1965), adopting a vertical component of $V/H = 0.7$. The vertical component is 70% of the horizontal and was derived from the Quake/W site response assessment.

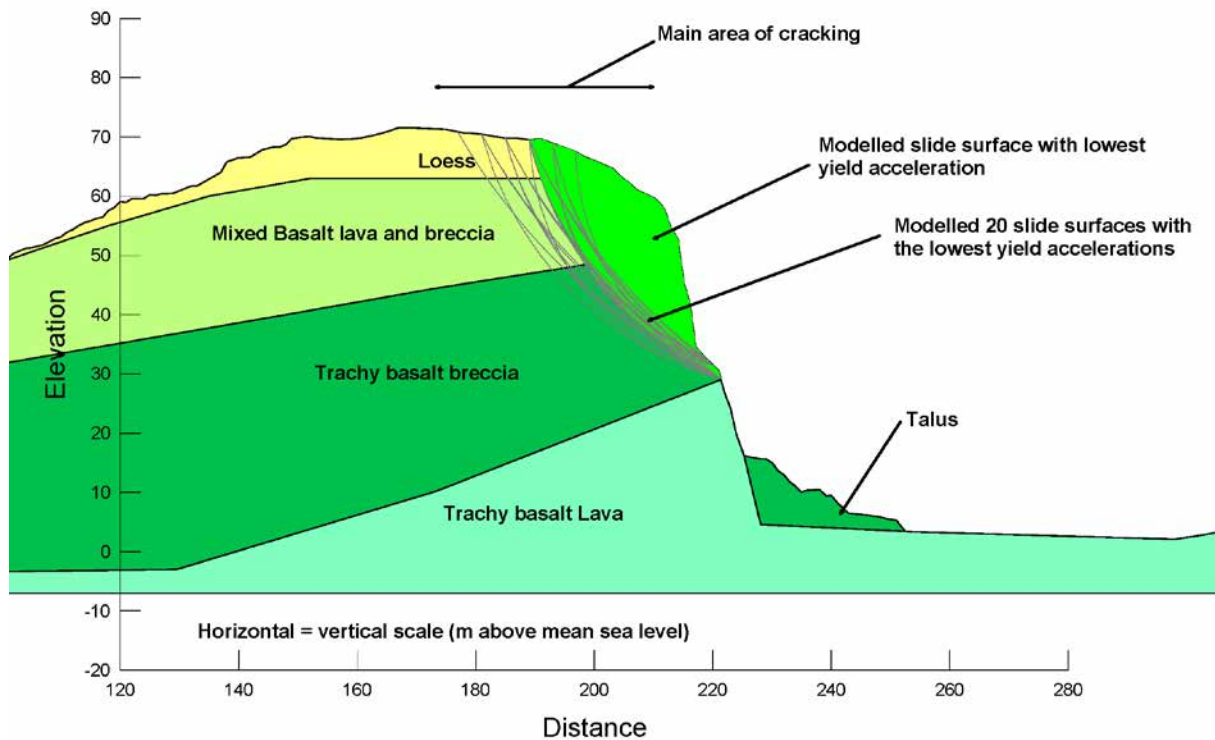


Figure 24 Cross-section 2 seismic slope stability assessment for the 22 February 2011 earthquake.

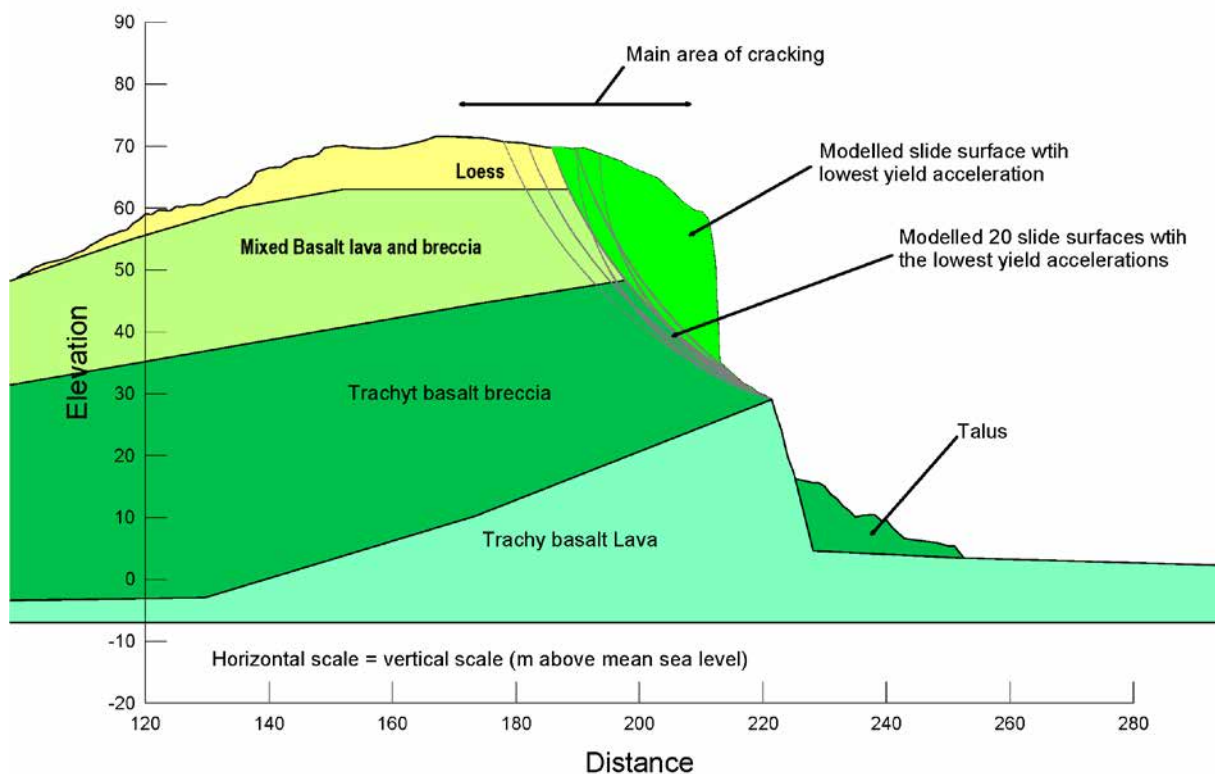


Figure 25 Cross-section 2 seismic slope stability assessment for the 13 June 2011 earthquake.

The results show that:

- A good correlation between the inferred permanent coseismic displacements from crack apertures and modelled displacements of the slope for the 13 June 2011 earthquakes was obtained adopting the model 2 and 3 material strength parameters.
- A good relationship between the decoupled displacements (derived from Slope/W) and the Newmark (1965) rigid block displacements (even though they are different techniques), across the range of yield accelerations.
- The largest displacements were estimated for the 13 June 2011 earthquake, which caused the largest measured volume of material to fall from the cliffs.
- The slide surfaces with the lowest yield accelerations adopting the model 1 and 2 material strength parameters were mainly in the trachy-basalt breccia.
- The slope material strength parameters may be reducing after each significant earthquake, as a result of the earthquake-induced fracturing of the rock mass and that as the material strength parameters degrade, the volume of any potential failure could increase.
- There is a good correlation between the locations and shape of the slide surfaces derived from the limit equilibrium and finite element static stability modelling, and those from the dynamic modelling.

4.1.2.3 Forecast modelling of permanent slope deformation

Permanent displacements, from the decoupled assessment of results from the 22 February and 13 June 2011 modelled earthquakes, were calculated for a range of slide-surface geometries with different ratios of yield acceleration (K_y) to the maximum average acceleration of the failure mass (K_{MAX}) for a given slide surface. The maximum average

acceleration (K_{MAX}) was calculated for each selected slide surface by taking the maximum value of the average acceleration time history from the response to the synthetic earthquake. About 20 slide surfaces (with the lowest value of critical yield acceleration K_y) were chosen to represent the results from each earthquake input motion, adopting the model 2 and 3 estimates of the shear strength of the main materials (Table 11).

The results from the assessment are shown in Figure 26 for those slide surfaces shown in Figure 24 and Figure 25. The results show that at similar ratios of K_y/K_{MAX} the calculated permanent displacements for cross-section 2 are larger for the 13 June 2011 earthquake than those calculated for the 22 February 2011 earthquake. This is thought to be because:

- Proximity of the site to the 13 June 2011 earthquake epicentre.
- The 22 February 2011 synthetic ground acceleration history (Holden et al., 2014) is dominated by one large acceleration peak of relatively short duration. This is reflected in the response of the cross-section to this earthquake, where the maximum average acceleration peak (K_{MAX}), of a given modelled slide surface, is significantly larger than any of the other acceleration peaks contributing to the cumulative permanent displacement.
- The 13 June 2011 synthetic ground acceleration history (Holden et al., 2014) is dominated by several large acceleration peaks of relatively short duration. This is reflected in the response of the cross-section to this earthquake, where, for a given slide surface, there are several peaks in the average acceleration history that are similar in amplitude to the maximum average acceleration peak (K_{MAX}), which contribute to the overall cumulative displacement of the given slide mass.

The results show that between K_y/K_{MAX} values of 0.2–0.6, and K_y/A_{FF} values of 0.4–1.0, the data are well fitted to a straight line (exponential trend line) in semi-log space, where the coefficient of determination (R^2) is 0.9 for K_y/K_{MAX} (both earthquakes) and 0.6 and 0.7 for K_y/A_{FF} for the 22 February and 13 June 2011 earthquakes, respectively. The gradients of the fitted K_y/K_{MAX} lines for both earthquakes are similar.

The peak ground acceleration of the input motion (A_{FF}) does not take into account amplification effects caused by the slope geometry (Appendix 6). From the data in Figure 26, the mean ratio of K_{MAX} to A_{FF} for cross-section 2 is 2.0 (± 0.1 at one standard deviation), meaning that K_{MAX} is on average 2.0 times greater than the peak horizontal ground acceleration of the input motion, assuming a linear relationship.

The shape of the K_y/A_{FF} trend is consistent with the results reported by Jibson (2007), where the data from Richmond Hill plot between the ranges of data for earthquake Magnitudes M6.5–7.5 reported by Makdisi and Seed (1978) and plotted by Jibson (2007).

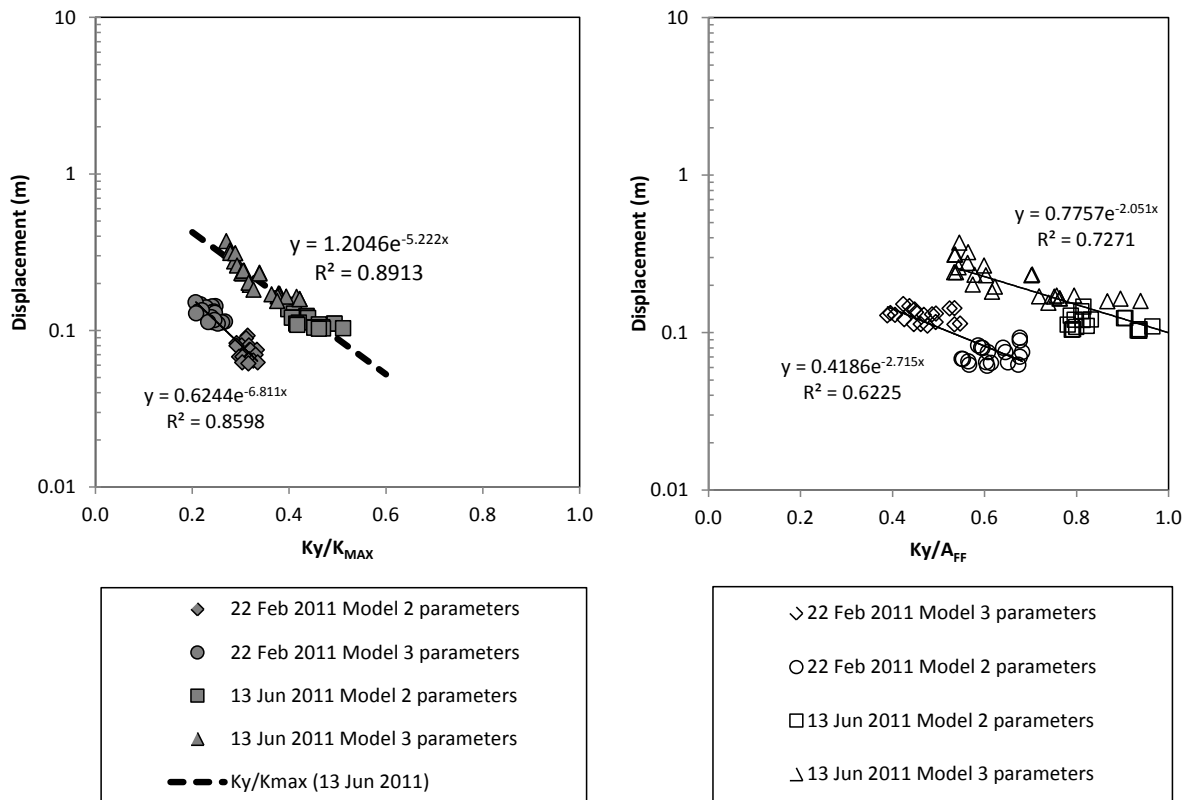


Figure 26 Decoupled Slope/W displacements calculated for different ratios of yield acceleration to maximum average acceleration of the mass (Ky/K_{MAX}), and maximum acceleration of the mass (Ky/A_{FF}), for selected slide-surface geometries, for cross-section 2. A_{FF} is the peak acceleration of the input earthquake time acceleration history. Synthetic rock outcrop time acceleration histories for the 22 February and 13 June earthquakes were used as inputs for the assessment. ($N = 80$). The black dashed lines are exponential trend line fitted to the semi-log data. The formula and the coefficient of determination (R^2) for the trend lines are shown.

The results from the decoupled assessment show that the magnitude of permanent slope displacement during an earthquake will vary in response to:

1. the shear strength of the rock mass at the time of the earthquake;
2. pore pressures within tension cracks and the rock mass, at the time of the earthquake; and
3. duration and amplitude of the earthquake shaking.

For cross-section 2, the relationship between the yield acceleration and the maximum average acceleration (from Figure 26) has been used to determine the likely range of displacements of a given failure mass with an adopted yield acceleration (Ky) at given levels of peak free field horizontal ground accelerations (A_{FF}) and the equivalent maximum average ground acceleration (K_{MAX}). For cross-sections 1 and 3–7, the pseudostatic method of assessing the yield acceleration of each cross-section was used (the results are shown in Table 15). The pseudostatic method was used to check the yield acceleration of section 2, derived from the decoupled assessment method; the results from both methods were comparable.

The K_y/K_{MAX} relationship (Figure 26), established for cross-section 2, adopting the results from the 13 June 2011 earthquake, was used to determine the likely magnitude of permanent displacement for each cross-section in a future earthquake. This has been done using the seven earthquake event bands, used to represent the range of earthquake events the slopes could be subjected to in the future.

The results are shown in Table 16. Conservative yield accelerations have been adopted, assuming the model 1 material strength parameters, to take into account the possibility that the current shear strength of the materials is now degraded as a result of the past movement and cracking.

Displacement of the slide mass will not occur at maximum average accelerations (K_{MAX}) less than the critical yield acceleration. However, the critical yield acceleration depends upon the strength of the slide surface at the time of the earthquake.

Table 15 Calculated factors of safety and yield accelerations for cross-sections 1–7, adopting model 2 and 3 material strength parameters (Table 11).

Cross-section	Model 2		Model 3	
	Factor of safety ¹	Yield acceleration ² (Ky)	Factor of safety	Yield acceleration (Ky)
1	1.35	0.35	1.07	0.30
2	1.48	0.40	1.13	0.20
3	1.47	0.32	1.16	0.15
4	1.93	0.50	1.51	0.38
5	3.01	0.80	2.30	0.65
6	1.84	0.30	1.33	0.28
7	1.35	0.23	1.07	0.10

¹ Factor of safety derived from limit equilibrium modelling adopting the semi-circular path search function in slide.

² Yield acceleration calculated using the pseudostatic slope stability method

Table 16 Forecast modelling results from the dynamic slope stability assessment for cross-sections 2, 4 and 6, adopting model 3 material parameters, and no water in tension cracks. Estimated displacements are rounded to the nearest 0.1 m and are based on the K_y/K_{MAX} relationship established using the results in Figure 26 for the 13 June 2011 earthquake.

		Earthquake event band	1	2	3	4	5	6	7
		Peak ground acceleration range of band (g)	0.1–0.3	0.3–0.5	0.5–0.8	0.8–1.2	1.2–1.6	1.6–2.0	2.0–3
		Representative free field peak ground acceleration (A_{FF}) for each band (g)	0.2	0.4	0.65	1.0	1.4	1.8	2.5
		Adopted K_{MAX}^1 to A_{FF}^2 ratio	2.1 (mean plus one standard deviation)						
Cross-section	Adopted yield ³ acceleration (K_y) (g)	Representative equivalent maximum average acceleration (K_{MAX}) of each band (g)	0.4	0.8	1.4	2.1	2.9	3.8	5.2
1	(0.3)	Estimated permanent displacement (m)	0.0	0.2	0.4	0.6	0.7	0.8	0.9
2	0.2	Estimated permanent displacement (m)	0.1	0.3	0.6	0.7	0.8	0.9	1.0
3	(0.2)	Estimated permanent displacement (m)	0.2	0.5	0.7	0.8	0.9	1.0	1.0
4	(0.4)	Estimated permanent displacement (m)	0.0	0.1	0.3	0.5	0.6	0.7	0.8
5	(0.7)	Estimated permanent displacement (m)	0.0	0.0	0.1	0.2	0.4	0.5	0.6
6	(0.3)	Estimated permanent displacement (m)	0.0	0.2	0.4	0.6	0.7	0.8	0.9
7	(0.1)	Estimated permanent displacement (m)	0.3	0.6	0.8	0.9	1.0	1.0	1.1

¹ K_{MAX} represents the maximum average acceleration of the given slide surfaces with the lowest yield accelerations.

² A_{FF} represents the peak horizontal ground acceleration of the free field input motion, rounded to the nearest 0.1 g.

³ Where shown in brackets, the yield acceleration was calculated using the pseudostatic slope stability method. The yield acceleration for section 2 was derived from the decoupled method of assessment.

4.1.3 Slope stability – Summary of results

The main results from the static and dynamic stability assessment for cross-sections 1–7 are:

1. Under current conditions, it is possible for failure of the example slide surfaces to occur under either static or dynamic conditions. Material strengths – and therefore the slope factors of safety – may reduce with time (weathering), water content, and further movement of the slope under either static or dynamic conditions.
2. Under static and dynamic conditions the slide surfaces with the lowest factors of safety and those with the lowest yield accelerations (K_y) are those associated with small failures at the crest and face of the slope, especially when water-filled tension cracks are included.
3. The most critical modelled slide surfaces are those with the lowest factors of safety and yield accelerations passing through the rock mass, particularly where the rock mass comprises trachy basalt lava breccia.
4. Estimated dynamic slope displacements (from the decoupled method) behind the cliff edge using the model 1 material strength parameters are too low when compared to the inferred displacements from crack apertures (with vertical components) – indicating that the rock mass nearer the slope face is significantly weaker.
5. Seismic site response assessment suggests that the peak ground amplification factors between the peak synthetic rock outcrop free field accelerations and the modelled peak accelerations at the cliff edge are about three for both horizontal and vertical motions, and that the relationship is non-linear.
6. Given the relatively low static factors of safety, an increase in pore water pressures in open tension cracks within the overlying loess and joints within the underlying rock mass could lead to instability of the slope under static conditions (i.e., short duration high intensity rain).
7. Given the relatively low yield acceleration of the slope (estimated to be about 0.1–0.2 g for cross-sections 2, 3 and 7), it is likely that future earthquakes could reactivate the slope, leading to permanent displacements that could be large. The magnitude of any coseismic permanent displacements will depend upon:
 - a. The shear strength of the materials at the time of the earthquake;
 - b. The pore pressure/water content conditions within the slope at the time of the earthquake; and
 - c. The duration and amplitude of the earthquake shaking at the site.
8. Earthquake-induced failures are likely to be larger in volume and the debris travel further, than rainfall-induced failures.

It is inferred that parts of the cliff top have already undergone more than 0.6 m of permanent slope displacement, during the 2010/11 Canterbury earthquakes. Given the relative stability of loess compared to the underlying rock mass, it is possible that much of the inferred cliff-crest displacement can be attributed to displacement of the underlying rock mass, even though displacement of the loess, above rockhead and unrelated to displacement of the underlying rock, is likely to have also occurred. This displacement may have reduced the shear strength of critical materials in the slope, making the slope more susceptible to future earthquakes. In addition, there may be an unknown amount of further displacement that the slopes may be able to undergo before failing catastrophically (i.e., where the magnitude of displacement causes the failure mass to break down to become a mobile failure).

4.2 RUNOUT DISTANCE

4.2.1 Potential future source volume estimation

4.2.1.1 Earthquake volumes

The total volumes of cliff-collapse debris likely to be generated in an earthquake representative of each peak ground acceleration band was determined from the relationship between the volumes of material leaving the cliffs during the 2010/11 Canterbury earthquakes (per square metre of cliff face), and the calculated free field rock outcrop peak ground acceleration at the Richmond Hill site (Holden et al., 2014) (Table 17 and Figure 28).

Table 17 The volumes of debris leaving the slope during each of the 2010/11 earthquakes and the earthquake's estimated peak ground acceleration, at the Richmond Hill site – horizontal (PGA H) and vertical (PGA V) components are listed separately.

Earthquake	PGA H (m/s/s)	PGA V (m/s/s)	Origin ¹	Volume leaving slope (m ³)	Source slope surface area (m ²)	Volume/slope area (m ³ /m ²)
4 September 2010	3.1	1.1	GeoNet LPCC	40 (±10)	26,560	0.002
22 February 2011	6.9	4.1	Synthetic	5,260 (±1,000)	26,560	0.20
16 April 2011	0.5	0.3	Synthetic	920 (±80)	26,560	0.03
13 June 2011	4.6	3.4	Synthetic	10,120 (±1,050)	26,560	0.38
23 December 2011	1.9	1.0	Synthetic	1,400 (±130)	26,560	0.05

¹ With the exception of the 4 September 2010 earthquake, peak ground accelerations were taken from the synthetic time acceleration histories (free field rock outcrop motions) derived from earthquake source modelling (Holden et al., 2014), for the Richmond Hill site. For the 4 September 2010 earthquake the instrumental record (maximum single component) from the GeoNet station LPCC was used.

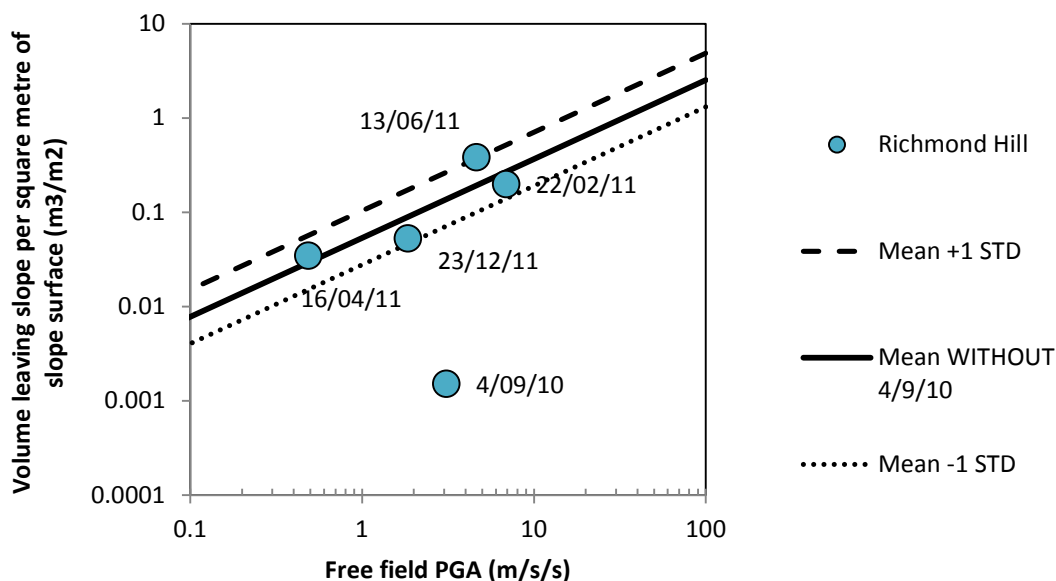


Figure 27 Relationship between free field peak ground accelerations at Richmond Hill and the volume of debris leaving the Richmond Hill slope.

The observed rockfall volumes correlate well with horizontal peak ground accelerations, with the exception of the 4 September 2010 earthquake. The data are well fitted by a power law, with a coefficient of determination (R^2) of 0.9, if the 4 September 2010 earthquake data is removed, and an R^2 of 0.1 if left in, indicating a poor correlation. In the 4 September 2010 earthquake much smaller volumes were generated (at all Port Hills sites) than for the other, later earthquakes. This difference is presumed to be because of the more fractured nature of the rock slopes following the 22 February 2011 earthquake (consistent with ground observations and measured cracks).

The ground conditions are likely to have weakened further after the 22 February 2011 earthquake. Earthquake induced fracturing and strength degradation of the rock during each subsequent earthquake will have caused further deterioration to rock-mass quality, but the amount of degradation likely in each earthquake is not known.

The 4 September 2010 datapoint is treated as anomalous and was not included in the correlations used to estimate rockfall production as a function of peak ground acceleration.

Seven peak ground acceleration bands are chosen for the assessment and the volumes generated in each band have been estimated from the relationship shown in Figure 27, adopting the mean, the mean -1 STD (standard deviation) and the mean +1 STD, as the middle, lower and upper volume estimates respectively (Table 18).

Table 18 The estimated volumes of debris leaving the slope for different bands of peak ground acceleration (PGA). STD is the standard deviation of the mean based on the correlation in Figure 27.

PGA Band (g)	0.1–0.3	0.3–0.5	0.5–0.8	0.8–1.2	1.2–1.6	1.6–2.0	2.0–3
Midpoint of PGA band (g)	0.2	0.4	0.65	1	1.4	1.8	2.5
Midpoint of PGA band (m/s/s)	1.96	3.92	6.38	9.81	13.73	17.66	24.53
Upper volume: MEAN +1 STD (m ³) ¹	4,823	8,615	12,936	18,552	24,588	30,346	39,951
Middle volume: MEAN (m ³) ¹	2,496	4,459	6,695	9,602	12,726	15,705	20,676
Lower volume: MEAN -1 STD (m ³) ¹	1,292	2,308	3,465	4,969	6,586	8,128	10,701

¹ Only the first digit in the number is significant.

Analysis shows that the total volume of material leaving the cliff will be dominated by infrequent and local large failures. In the case of the 13 June 2011 landslide volumes, one landslide accounted for about 60% of the total volume of all of the surveyed cliff collapses in the Port Hills. At Richmond Hill, there were two discrete local cliff collapses with a combined volume of about 3,500 m³) which accounted for about 35% of the total volume of debris leaving the slope in response to the 13 June 2011 earthquake.

The 13 June 2011 cliff collapse data shows that 40% of the total failure volume came from many small randomly distributed failures and 60% from a few very large local failures, with a change in rate at a failure volume of about 2,500–3,000 m³ (Figure 28).

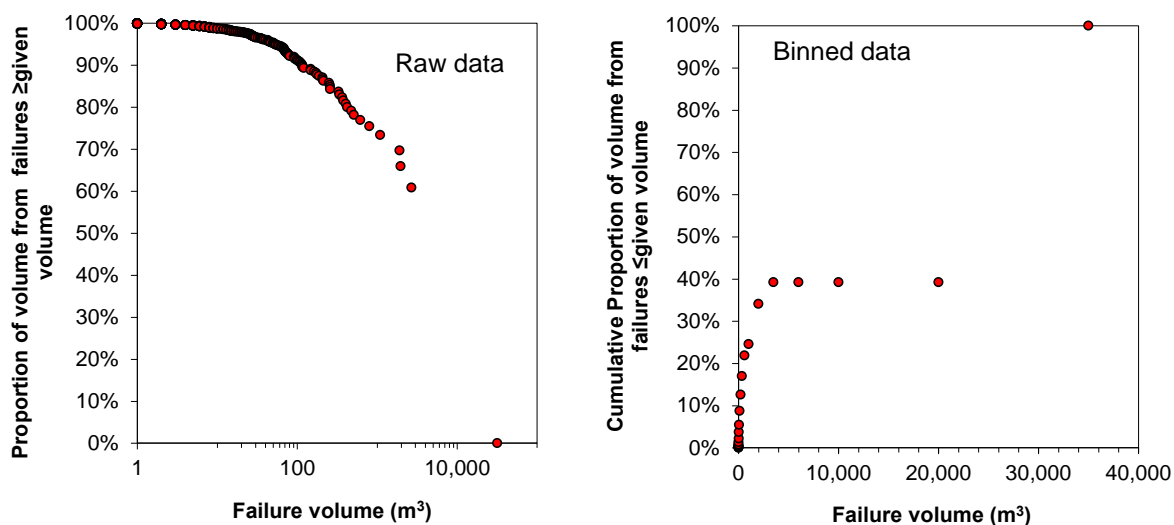


Figure 28 Proportion and cumulative proportion of volume from cliff collapses in the Port Hills greater than or equal to a given volume. Data from the 2011 cliff collapse volumes triggered by the 13 June 2011 earthquakes, derived from terrestrial laser scan change models of Richmond Hill, Shag Rock Reserve and Redcliffs. The different plots represent raw data and binned data.

Local sources (assessed source areas 1–10)

The likely locations and volumes of potential source areas (1–10) have been estimated based on:

1. Numerical stability analysis results;
2. Mapped crack distributions relating to the 2010/11 Canterbury earthquakes; and
3. Engineering geology and morphology of the slope.

Three possible failure volume estimates – lower, middle and upper range estimates – have been calculated for each potential source area. The variation in failure volumes reflects the uncertainty in the source shape (depth, width and length dimensions) estimated from site conditions and the modelling.

Volumes were calculated by estimating the shape of any future failures as quarter-ellipsoids (half-spoon shaped) (following the method of Cruden and Varnes, 1996) (Figure 29). Estimated volumes are shown in Table 19.

Table 19 The mean and mean-minus-one-standard-deviation (-1 STD) fahrboeschungs (F-angles) for each source area (1–10) and each volume (lower, middle and upper estimates).

Source area	Volume ¹	Talus F-angle (°)		Boulder roll F-angle (°)	
		Mean	Mean - 1 STD	Mean	Mean - 1 STD
1 lower	4,712	43.5	37.0	39.2	33.6
1 middle	7,756	42.4	36.0	38.6	33.0
1 upper	10,800	41.7	35.3	38.2	32.6
2 lower	7,925	42.4	35.9	38.6	33.0
2 middle	12,016	41.5	35.1	38.1	32.5
2 upper	16,106	40.8	34.5	37.7	32.2
3 lower	8,526	42.2	35.8	38.5	32.9
3 middle	13,554	41.2	34.8	37.9	32.4
3 upper	18,583	40.5	34.2	37.5	32.0
4 lower	12,342	41.4	35.0	38.0	32.5
4 middle	18,086	40.6	34.2	37.6	32.1
4 upper	23,831	40.0	33.7	37.2	31.8
5 lower	31,986	39.3	33.1	36.9	31.4
5 middle	45,216	38.6	32.4	36.5	31.1
5 upper	58,446	38.1	31.9	36.2	30.8
6 lower	5,882	43.0	36.5	38.9	33.3
6 middle	10,074	41.8	35.4	38.3	32.7
6 upper	14,266	41.1	34.7	37.9	32.3
7 lower	5,882	43.0	36.5	38.9	33.3
7 middle	10,074	41.8	35.4	38.3	32.7
7 upper	14,266	41.1	34.7	37.9	32.3
8 lower	7,643	42.4	36.0	38.6	33.0
8 middle	11,702	41.5	35.1	38.1	32.5
8 upper	15,761	40.9	34.5	37.7	32.2
9 lower	1,714	45.7	39.2	40.4	34.7
9 middle	3,391	44.2	37.7	39.6	34.0
9 upper	5,068	43.3	36.9	39.1	33.5
10 lower	2,437	44.9	38.4	40.0	34.3
10 middle	4,522	43.6	37.1	39.2	33.6
10 upper	6,607	42.8	36.3	38.8	33.2

¹ Only the first digit in the number is significant (e.g., for a volume of 5,006 m³, the first digit in the number, which is the significant number, meaning that the volume is about 5,000 m³).

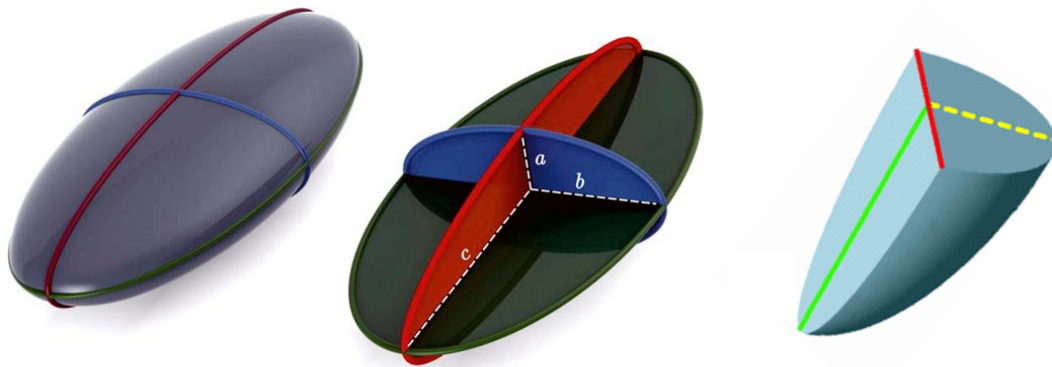


Figure 29 Estimation of landslide volume assuming a quarter-ellipsoid shape.

The credibility of these potential failure volumes has been evaluated by comparing them with estimated volumes of individual debris avalanches that fell from the slopes at Richmond Hill Road, Shag Rock Reserve and Redcliffs (Massey et al., 2012a) during the 13 June 2011 earthquakes (Figure 28). These volumes were derived from the terrestrial laser scan change models.

The estimated potential failure volumes of assessed source areas 1–10 are within the upper volume range of data from relict failures and those that fell in the 13 June 2011 earthquakes. This suggests that such failure volumes could occur, but they are likely to be very infrequent and few in number during a single strong earthquake.

4.2.1.2 Non-earthquake volumes

Non-earthquake volumes and rates of cliff collapse were taken from Massey et al. (2012a) and are based on historical data. The historical data used to infer these rates is summarised in Table 20.

Table 20 Information used to estimate event volumes contributing to the total risk from non-seismic rockfall triggering events, all sites.

Time period (years)	Type of events	Description
<1–15	Rainstorms/frosts that occur frequently.	Cliff collapses tend to be small and localised from events with this high frequency of occurrence. Estimated volumes of events derived using Earthquake Commission claims, local consultant files and the GNS Science database.
15–100	Rainstorms with larger intensities and durations that occur once every 15–100 years on average.	Cliff collapses occur but their volumes tend to be limited and localised. Estimated volumes of events derived using historical newspapers and consultant reports.
100–1,000	Rainstorms with very large intensities and durations that occur once every 100–1,000 years on average.	Cliff collapses will be widespread. Estimated volumes of events derived using old newspaper reports.
1,000–10,000	Rainstorms with extreme intensities and durations exceeding Cyclone Bola (1988) and the Manawatu storm (2004) that occur once every >1,000 years on average.	These events might trigger a large number of cliff collapses over a wide area and may be large in volume. However, cliff collapse risk would be low compared with risk from flooding or debris flows.

4.2.2 Runout modelling

4.2.2.1 Randomly distributed cliff collapses

For distributed cliff collapses triggered by earthquakes and for non-earthquake cliff collapses, the volume of debris passing through each 2 m by 2 m grid cell was estimated using the volumes of material that passed a given fahrboeschung angle from debris avalanches triggered by the 22 February and 13 June 2011 earthquakes, at Richmond Hill. The values contained in Massey et al. (2012a), have been revised based on reassessment of the LiDAR data sets. Results are presented in Figure 30.

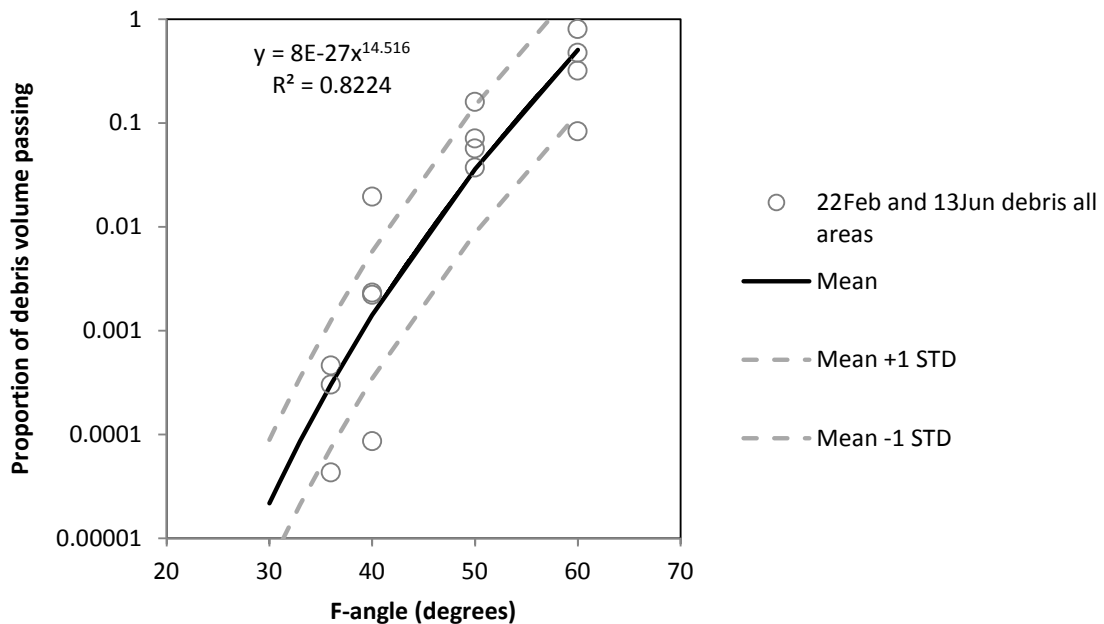


Figure 30 Proportion of debris volume passing a given fahrboeschung angle line, from debris avalanches triggered during the 22 February and 13 June 2011 earthquakes at Richmond Hill/Wakefield Avenue, Shag Rock Reserve and Redcliffs.

For these randomly distributed cliff collapses, the volume of debris passing through a given 2 m by 2 m grid cell below the slope was derived from the relationship in Figure 30, for each volume estimate (lower, middle and upper). For the risk assessment the volume was converted into an equivalent number of boulders, where 1 m³ of debris comprised about 15 boulders.

4.2.2.2 Local cliff collapses (assessed source areas 1–10)

The runout of debris from the assessed source areas 1–10 was assessed both empirically and numerically.

For local cliff collapses the maximum volume of debris passing through a given 2 m by 2 m gridcell below the source was derived from the RAMMS model outputs for each assessed source area (1–10) for each volume estimate (lower, middle and upper). For the risk assessment the volume was then converted into an equivalent number of boulders, as per the randomly distributed debris volumes.

The runout distances estimated from RAMMS were checked using empirical runout relationships measured from discrete debris avalanches that occurred in the Port Hills during the 2010/11 Canterbury earthquakes.

Empirical method

The procedure followed for estimating the empirical run-out distance, in terms of the fahrboeschung angle, is detailed in Appendix 1.

A total of 45 sections through specific debris avalanches triggered by the 22 February and 13 June 2011 earthquakes have been assessed. For each section the fahrboeschung for “talus” (where the ground surface is obscured by many boulders) and “boulder roll” (individual boulders) have been defined based on field mapping. The results are shown in Figure 31 as ratios of H/L where H is the height of fall and L is the length, or runout distance, of the mapped rockfalls and debris avalanche deposits (talus).

These fahrboeschung relationships are based on debris avalanches that fell from cliffs in the wider Port Hills area during the earthquakes, and not just from the Richmond Hill site. They therefore reflect all of the different types of slope shape that could affect the debris avalanche runout.

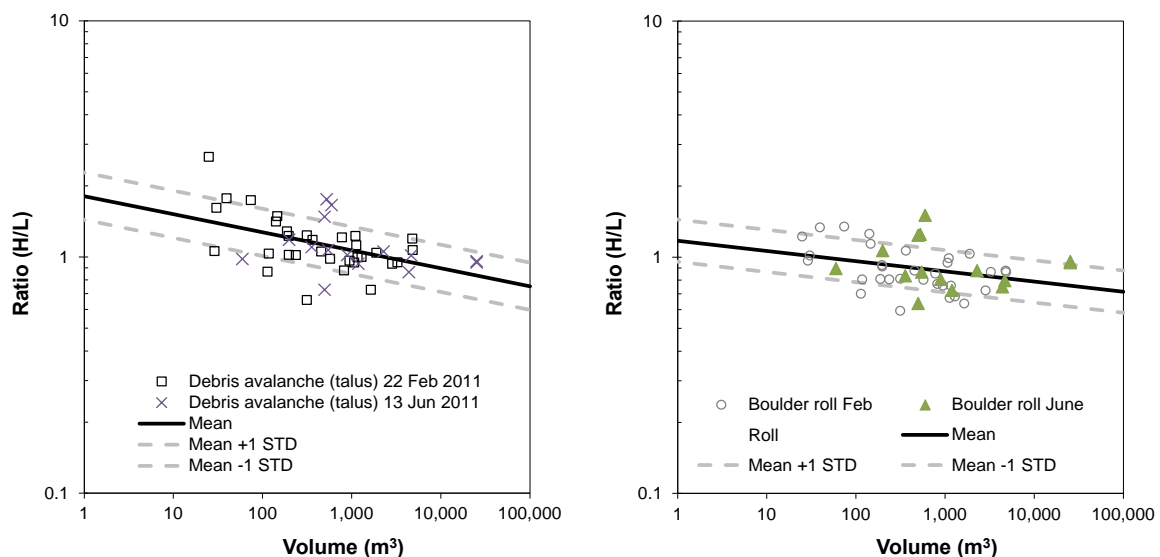


Figure 31 The empirical fahrboeschung relationships, expressed as the ratio of height (H) to length (L) for debris avalanche talus and boulder roll (rockfalls), recorded in the Port Hills. N = 45 sections. Errors are expressed as the mean \pm one standard deviation (STD).

Numerical method – RAMMS®

The RAMMS software (RAMMS, 2011) takes into account the site slope geometry when modelling debris runout. The physical model of RAMMS Debris Flow uses the Voellmy friction law. This model divides the frictional resistance into two parts: a dry-Coulomb type friction (coefficient μ) that scales with the normal stress and a velocity-squared drag or viscous-turbulent friction (coefficient ξ). The RAMMS model parameters were calculated from the back-analysis of 23 debris avalanches (ranging in volume from 200 to 35,000 m³) that fell from the slopes at Richmond Hill Road, Shag Rock Reserve and Redcliffs during the 22 February and 13 June 2011 earthquakes. The modelled parameters μ (μ) and ξ were optimised to obtain a good correlation between the modelled versus actual runout and deposited debris heights (Figure 32).

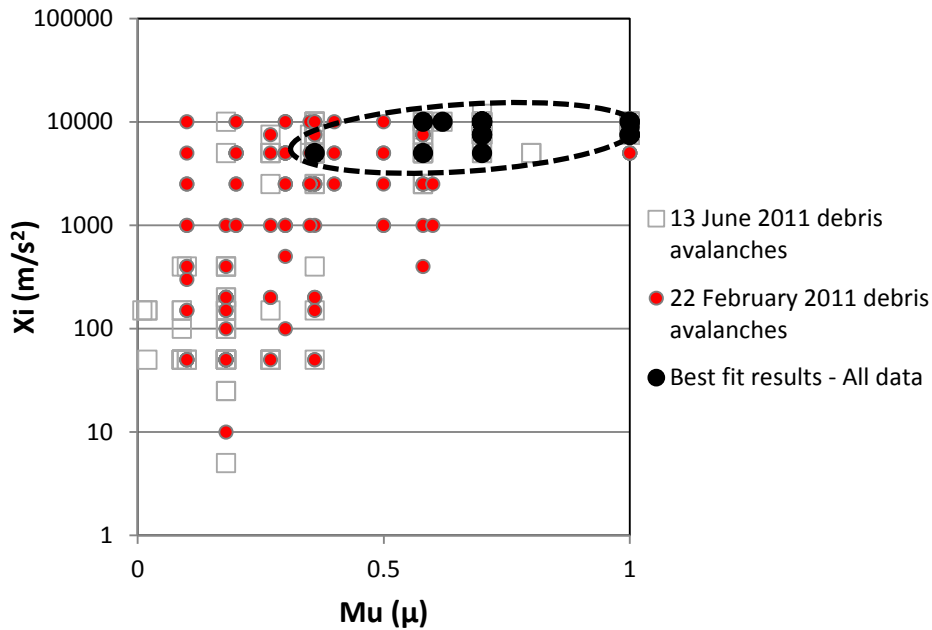


Figure 32 Range of parameters used to back-analyse the runout of debris avalanches in the Port Hills triggered by the recent earthquakes using the RAMMS software (RAMMS, 2011).

The model parameters that gave the “best fits” between modelled and actual runout distances and heights when: $\mu = 0.7$ and $xi = 7,500 \text{ m/s}^2$. The xi values are comparable to results from other assessments compiled by Andres (2010) for rockfalls (debris avalanches), but the μ values are larger than those shown by Andres (2010), possibly because the Port Hills debris avalanches are more clast-dominated (Figure 33).

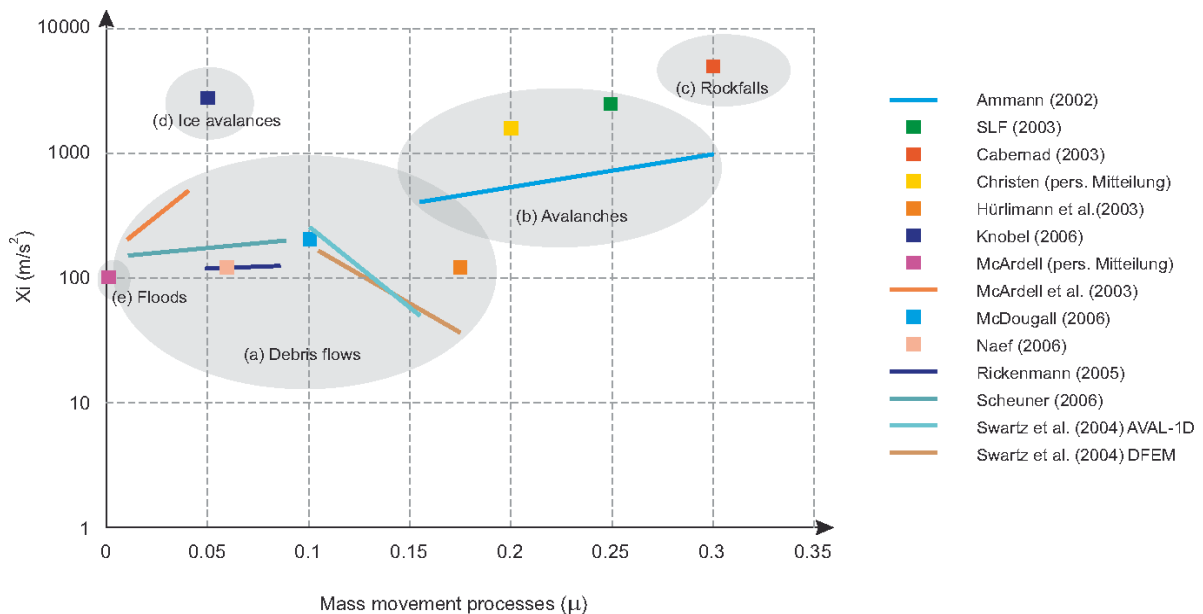


Figure 33 Range of parameters for different mass movement processes: a) debris flows, b) snow avalanches, c) snow avalanches, d) ice avalanches, e) debris floods. Modified from Andres (2010).

For each back-analysed debris avalanche, the modelled final debris thicknesses were compared to the actual deposit thicknesses interpolated from difference models derived from the airborne LiDAR surveys using a 1 m grid. For debris avalanches triggered by the 22 February 2011 earthquakes the deposit thicknesses were estimated from differences between the 2011a (March 2011) LiDAR survey and the 2003 LiDAR survey. For debris

avalanches triggered by the 13 June 2011 earthquakes the 2011c (July 2011) and 2011a LiDAR surveys were used. Statistics from the comparison give a mean difference of 0.5 (± 0.4) m^3 , with a mode of 0.2 m^3 (Figure 34) for the 1 m^2 grid cells.

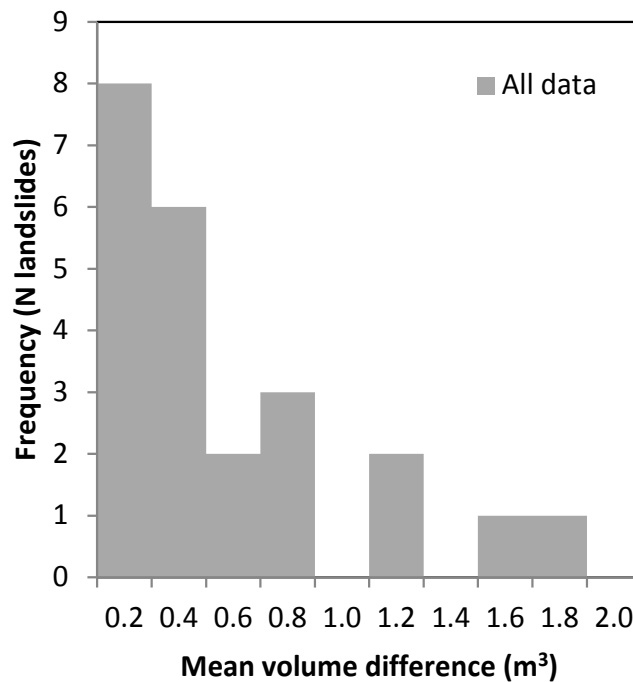


Figure 34 Mean volume difference between the RAMMS modelled volumes and the actual recorded volumes per 1 m^2 grid cell. N = 23 debris avalanches triggered by 22 February and 13 June 2011 earthquakes.

For the 23 debris avalanches, the performance of the RAMMS and fahrboeschung models (based on the compiled 45 sections shown in Figure 31) were assessed against the actual field mapped runout distances. The RAMMS model performed well with a gradient of 1.01 (± 0.04) at one standard deviation and coefficient of determination (R^2) of 0.3 indicating the data are scattered. The empirical fahrboeschung model performed about the same as the RAMMS model, where the gradient was 1.06 (± 0.05) at one standard deviation but the coefficient of determination (R^2) of 0.5 indicates less scatter (Figure 35).

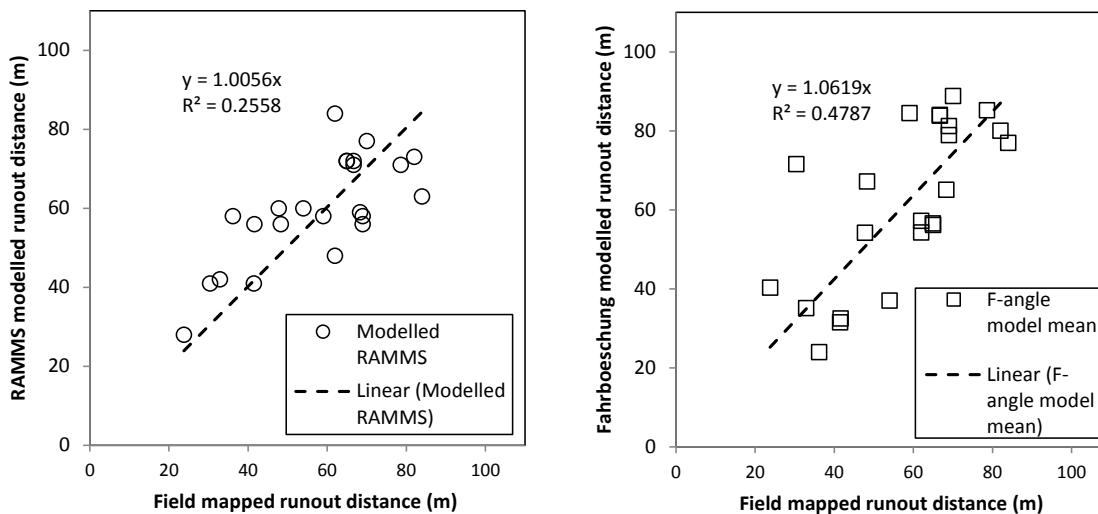


Figure 35 Comparison between the RAMMS modelled and the empirical modelled debris runout (Figure 32), and the actual recorded runout for debris avalanches triggered by the 22 February and 13 June 2011 earthquakes. N = 23 debris avalanches.

4.2.3 Forecast runout modelling

A hazard map (Figure 36) presents the empirical and numerical runout limits from the modelling. Figure 36, Map 1, shows the cliff collapse hazard map for the randomly distributed source areas, and the fahrboeschung angles from 60° to 31°. The 31° fahrboeschung angle is the runout limit of rocks from debris avalanches triggered by the 2010/11 Canterbury earthquakes from the assessed cliffs (Redcliffs, Shag Rock Reserve, and Richmond Hill/Wakefield Avenue) by Massey et al. (2012a).

Figure 36, Map 2, shows the cliff collapse hazard map for the localised source areas 1–10 for the upper volume estimates (Scenario A). The mean and mean minus one standard deviation fahrboeschung angles for each source area assuming the upper volume estimates, are also shown (Table 19). The estimated runout distances from the RAMMS modelling for the same source areas are also shown for the upper volume estimates. These show the likely runout limits of the debris from the assessed debris avalanche source areas.

RAMMS runout models are contained in Appendix 7 (debris height) and Appendix 8 (debris velocity), for sources 1–3 (upper, middle and lower source volume estimates), along with the corresponding mean and mean minus one standard deviation fahrboeschung angles.

In general, there is a good correlation between the fahrboeschung angles and RAMMS runout limits for the assessed source areas. The RAMMS modelled debris from source areas 1, 2, 9 and 10 exceed the runout limits defined from the empirical fahrboeschung model (mean minus one standard deviation), this is due to the topography channelling the debris, causing it to runout further, and the presence of talus ramps at the slope toe. However, it should be noted that debris heights in these distal areas are low (less than 0.5 m high), and although shown as a continuous deposits are more likely to comprise many individual boulders.

RAMMS models the runout of the debris as flow using the two-parameter Voellmy relation to describe the frictional behaviour of the debris (RAMMS, 2011). In reality some part of the debris may be acting as a flow, but the distal part of the debris is not – being formed of many individual boulders. Therefore the RAMMS velocities in these distal areas are not representative of the debris emplacement process.

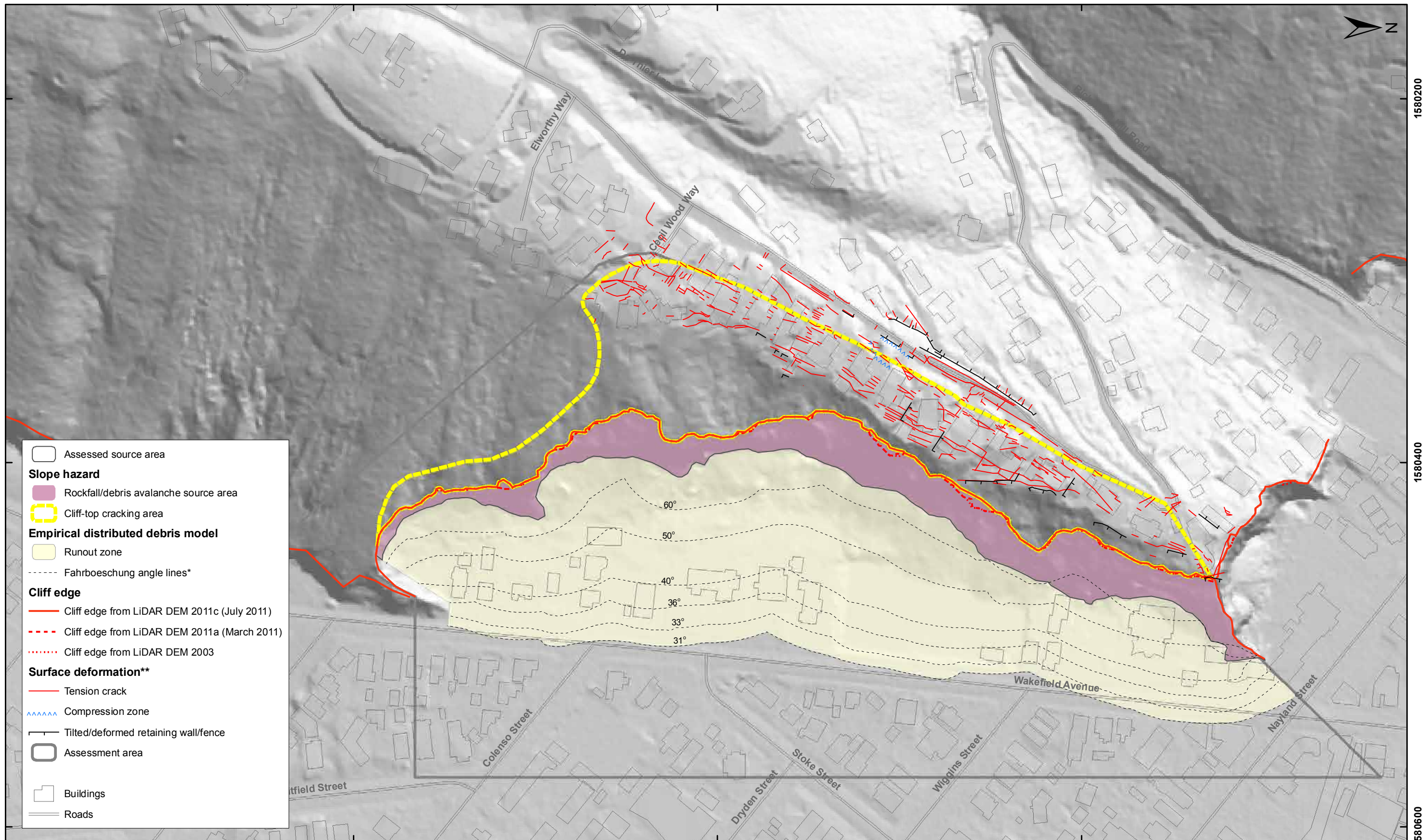
For source areas 3–8 the RAMMS derived runout limits do not exceed the limits defined from the empirical fahrboeschung model (the mean nor the mean – 1 standard deviation limits). This is because in these areas the debris is free to disperse without any channelizing effects.

4.2.3.1 Numerical method – Rocfall®

In order to better define the debris velocities and to check the RAMMS runout distances in the distal runout zone, the two-dimensional rockfall modelling software RocFall, developed by RocScience has been used, as RocFall treats the debris as individual particles, while RAMMS treats the debris as an aggregated flow. The results of Rockfall run out simulations for Richmond Hill cross-sections 1 and 7 are shown in Appendix 9 with the corresponding “end-points” histograms indicating the farthest point reached by the simulation. Cross-sections 1 and 7 have been modelled, adopting the parameters detailed by Massey et al. (2012c). Results are shown in Appendix 9.

The RocFall software program was used by Massey et al. (2012c) to analyse the runout limits of individual boulders that fell during the 2010/2011 Canterbury earthquakes. This was done to derive material parameters by back-analysis of the observed rockfall runouts, which were then subsequently used for forecasting rockfall runout in areas where little rockfall data were available.

Results for cross-section 1 show that boulders could reach the western side of Wakefield Avenue, supporting observations made of debris runout from debris avalanches triggered by the 22 February 2011 earthquakes. For cross-section 7, the results show that boulders are unlikely to make it past the western edge of Wakefield Avenue, however, relict boulders have been mapped on the eastern edge of Wakefield Avenue at the southern end of the site.



5175400 5175600 5175800 1580200 1580400 1580600

SCALE BAR: 0 50 100 m

EXPLANATION:
 * Taken from report CR2012/57
 ** Taken from report CR2012/317
 Background shade model derived from NZAM post earthquake 2011c (July 2011) LiDAR survey resampled to a 1 m ground resolution.
 Roads and building footprints provided by Christchurch City Council (20/02/2012).
 PROJECTION: New Zealand Transverse Mercator 2000

DRW:
BL
 CHK:
CM, FDP



**CLIFF COLLAPSE HAZARD MAP
(Randomly distributed debris)**

**Richmond Hill Road
Christchurch**

FIGURE 36

Map 1

FINAL

REPORT: CR2014/34 DATE: June 2014

5.0 RISK ASSESSMENT RESULTS

5.1 TRIGGERING EVENT FREQUENCIES

Failure of the assessed sources could be triggered by earthquakes (dynamic conditions) or by water ingress (static conditions).

5.1.1 Frequency of earthquake triggers

For earthquake triggers, the frequency of a given free-field peak ground acceleration (A_{FF}) occurring is obtained from the New Zealand National Seismic Hazard Model (Table 21) (Stirling et al., 2012). The increased level of seismicity in the Christchurch region is incorporated in a modified form of the 2010 version of the National Seismic Hazard Model (Gerstenberger et al., 2011).

For these assessments, peak ground acceleration is used to represent earthquake-shaking intensity, as peak ground acceleration is the ground-motion parameter considered to be most directly related to coseismic landslide initiation (Wartman et al., 2013).

Table 21 The annual frequency of a given peak ground acceleration (PGA) band occurring on rock (Site Class B) for different years from the 2012 seismic hazard model for Christchurch (G. McVerry, personal communication 2014). Note: these are free field rock outcrop peak ground accelerations.

PGA Band (g)	0.1–0.3	0.3–0.5	0.5–0.8	0.8–1.2	1.2–1.6	1.6–2.0	2.0–3
Year 2012 annual frequency	0.3405	0.0874	0.0329	0.0084	0.0016	0.0004	0.0001
Year 2016 annual frequency	0.1381	0.0322	0.0119	0.0030	0.0006	0.0001	0.00005
Next 50-year average annual frequency	0.0729	0.0148	0.0054	0.0014	0.0003	0.0001	0.00002

To take into account the possibility of larger local failures of the slope the total volume of debris generated in each band was partitioned between: 1) random uniformly distributed failures of the cliff face comprising 40% of the total volume, that may fall from anywhere on the slope; and 2) local (non-random) larger failures comprising 60% of the total volume, corresponding to assessed source areas 1–10 (Table 22). Volumes were estimated based on the upper, middle and lower total volume estimates of debris generated in each band.

Table 22 Proportion of the total debris volume per peak ground acceleration band allocated to distributed and local failures, for upper, central and lower estimates of volume.

Estimated debris avalanche volumes ¹ (m ³)	Peak ground acceleration band (g)						
	0.1–0.3	0.3–0.5	0.5–0.8	0.8–1.2	1.2–1.6	1.6–2.0	2.0–3
Distributed debris: Upper volume	1,929	3,446	5,174	7,421	9,835	12,138	15,980
Localised debris: Upper volume	2,894	5,169	7,761	11,131	14,753	18,207	23,970
Distributed debris: Middle volume	998	1,784	2,678	3,841	5,090	6,282	8,271
Localised debris: Middle volume	1,498	2,675	4,017	5,761	7,635	9,423	12,406
Distributed debris: Lower volume	517	923	1,386	1,988	2,634	3,251	4,280
Localised debris: Lower volume	775	1,385	2,079	2,982	3,952	4,877	6,421

¹ Only the first digit in the number is significant.

5.1.1.1 Peak ground acceleration and permanent slope displacement

The probability of each local source area (1–10) being triggered in a given earthquake was based on the calculated permanent displacement, estimated from the decoupled results.

It is difficult to estimate the probability of triggering failure, leading to catastrophic slope collapse, where the debris runs out down slope forming a debris avalanche. It is also possible that permanent slope displacements could cause catastrophic damage to dwellings located at the cliff top, even if the debris does not leave the source. The level of displacement chosen to differentiate between safe and unsafe behaviour (Abramson et al., 2002) differs between authors. Some examples are:

- a. Hynes-Griffin and Franklin (1984) suggest that up to 0.1 m displacements may be acceptable for well-constructed earth dams.
- b. Wieczorek et al. (1985) used 0.05 m as the critical parameter for a landslide hazard map of San Mateo County, California.
- c. Keefer and Wilson (1989) used 0.1 m for coherent slides in southern California.
- d. Jibson and Keefer (1993) used a 0.05–0.1 m range for landslides in the Mississippi Valley.
- e. The State of California (1997) finds slopes acceptable if the Newmark displacement is less than 0.15 m. A slope with a Newmark displacement greater than 0.3 m is considered unsafe. For displacements in the “grey” area between 0.15 and 0.3 m, engineering judgement is required for assessment.

The estimated magnitude of permanent slope displacement of the assessed sources in a future earthquake was based on the decoupled assessment results. The permanent displacement of each source at a given level of free-field peak ground acceleration (A_{FF}) was estimated from the relationship between the yield acceleration (K_y) and the maximum average acceleration of the mass (K_{MAX}) (Figure 26). Different levels of peak ground acceleration were adopted based on the seven earthquake event bands, and each multiplied by the site-specific ratio of K_{MAX} to A_{FF} (assuming the mean plus one standard deviation) to estimate the equivalent maximum average acceleration of the mass (K_{MAX}) for the given value of A_{FF} . For example, an A_{FF} of 0.4 g would have an equivalent K_{MAX} of 0.8 g, assuming a ratio of 2.1 (Table 23).

5.1.1.2 Permanent slope displacement and likelihood of catastrophic slope failure

The probability of occurrence of each local source area (1–10) was based on the estimated permanent displacement, estimated from the decoupled results (Figure 26), as follows:

- If the estimated displacement of the source area is ≤ 0.1 m then the probability of catastrophic failure = 0.
- If the estimated permanent displacement of the source area ≥ 1.0 m then the probability of catastrophic failure = 1.
- If the estimated permanent displacements are between 0.1 m and 1 m then the probability of failure (P) is calculated based on a linear interpolation between $P=0$ at displacements of 0.1 m, and $P = 1$, at displacements of 1 m.

It should be noted that the displacements at different ratios of K_y/K_{MAX} , were calculated using the synthetic earthquake acceleration time histories for 13 June 2011 earthquake. This event was a near-field earthquake of short duration, but high amplitude. The calculated displacements in Figure 26 represent displacements in response to these earthquakes (adopting material parameters for model 3). Earthquakes of longer duration may affect the site in different ways, for example the response of the loess and volcanic colluvium (at higher water contents representative of winter conditions) may be non-linear, and could lead to larger permanent displacements. Conversely, the peak amplitudes relating to longer duration earthquakes from more distant sources are likely to be lower and may not trigger displacement of the slope.

Table 23 Forecast modelling results from the dynamic slope stability assessment for cross-sections 2, 4 and 6, adopting model 3 material parameters, and no water in tension cracks. Estimated displacements are rounded to the nearest 0.1 m.

				1	2	3	4	5	6	7
Earthquake event band										
Peak ground acceleration range of band (g)				0.1–0.3	0.3–0.5	0.5–0.8	0.8–1.2	1.2–1.6	1.6–2.0	2.0–3
Free field peak ground acceleration (A_{FF}) for representative event in band (g)				0.2	0.4	0.65	1.0	1.4	1.8	2.5
Year 2016 annual frequency of representative event in band				0.1381	0.0322	0.0119	0.0030	0.0006	0.0001	0.00005
Adopted K_{MAX} to A_{FF}¹ ratio				2.1 (mean plus 1 standard deviation)						
Source area	Representative cross-section	Adopted yield² acceleration (K_y) (g)	Representative equivalent maximum average acceleration (K_{MAX}) of each band (g)³	0.4	0.8	1.4	2.1	2.9	3.8	5.2
1	1	(0.30)	Probability of failure	0.0	0.1	0.3	0.5	0.7	0.8	0.9
2	1	(0.30)	Probability of failure	0.0	0.1	0.3	0.5	0.7	0.8	0.9
3	2	(0.20)	Probability of failure	0.0	0.3	0.5	0.7	0.8	0.9	1.0
4	3	(0.15)	Probability of failure	0.1	0.4	0.6	0.8	0.9	1.0	1.0
5	3	(0.15)	Probability of failure	0.1	0.4	0.6	0.8	0.9	1.0	1.0
6	4	(0.38)	Probability of failure	0.0	0.0	0.2	0.4	0.6	0.7	0.8
7	4	(0.38)	Probability of failure	0.0	0.0	0.2	0.4	0.6	0.7	0.8
8	6	(0.28)	Probability of failure	0.0	0.1	0.3	0.6	0.7	0.8	0.9
9	7	(0.10)	Probability of failure	0.3	0.6	0.8	0.9	1.0	1.0	1.0
10	7	(0.10)	Probability of failure	0.3	0.6	0.8	0.9	1.0	1.0	1.0

¹ A_{FF} represents the peak horizontal ground acceleration of the free field input motion, rounded to the nearest 0.1 g.

² Where shown in brackets, the yield acceleration was calculated using the pseudo-static slope stability method.

³ Rounded to the nearest 0.1 g.

5.1.1.3 Deaggregation of the National Seismic Hazard Model

The seismic performance of the slope in future earthquakes was inferred from assessing its performance in past earthquakes, mainly the 22 February, 16 April, 13 June and 23 December 2011 earthquakes, using the relationship established between peak ground acceleration and the amount of permanent slope displacement. These earthquakes varied in magnitude between M5.2 and M6.3, and were “near-field”, i.e., their epicentres were very close, within 10 km, of the Richmond Hill site.

The annual frequencies of a given level of peak ground acceleration occurring in the area are given by the National Seismic Hazard Model of New Zealand (Stirling et al., 2012). The National Seismic Hazard Model combines all of the various earthquake sources that could contribute to the seismic hazard at a given location. The National Seismic Hazard Model estimates for the Port Hills are based on a combination of different earthquake sources: 1) subduction zone; 2) mapped active faults; and 3) unknown or “background” earthquakes. For the risk assessment it is important to deaggregate the National Seismic Hazard Model to assess which earthquake sources contribute the most to it.

Buxton and McVerry (personal communications, 2014) suggest that it is magnitude M5.3–6.3 earthquakes on unknown active faults, within 20 km of the site that contribute most to the National Seismic Hazard Model. These earthquakes are similar to the 22 February, 16 April 13 June and 23 December 2011 earthquakes.

5.1.2 Frequency of rainfall triggers

As discussed in Section 4.1, it is possible that local source areas (1–10) could be triggered under non-seismic (static or natural) conditions, as strength degradation caused by future earthquakes and/or periodic wetting and drying of the slope face could lead to larger static failures in the future.

However, it is unlikely that a rainstorm will trigger a comparable number and volume of cliff collapses over an area similar to a large magnitude earthquake (typically $>M_w$ 6). This is because earthquake loading can greatly exceed the rock mass strength resulting in slope factors of safety of $\ll 1.0$, while intense rain can only reduce rock mass strength until it becomes unstable (factor of safety = 1.0).

Debris avalanche rates triggered by non-seismic events were taken from Massey et al. (2012a). The results from Massey et al. (2012a) for Richmond Hill are shown in Table 24.

Table 24 Representative annual event frequency of debris avalanches occurring, and the representative volume of the avalanche, for each time-period band. These represent the estimated volumes of the material leaving the cliffs per site with a given frequency, for non-seismic triggers. Taken from Massey et al. (2012a) for Richmond Hill, using historical data.

Location	Return period (years)	Number of events in band	Annual frequency of events	Mean event volume (m ³)	Annual accumulation rate (m ³ /year)
Richmond Hill	1–15	5.5	0.37	5	1.8
	15–100	1.3	0.0133	170	2.3
	100–1,000	0.7	0.0007	1,500	1.0
	1,000–10,000	0.3	0.00003	10,000	0.3

Given the historical rates of rainfall triggered rockfall for the slope of about 5–6 m³/year (estimated from historical data by Massey et al. 2012a), the current rates of rockfall triggered by rainfall are considerably higher (670 m³ per year for 2012 and 100 m³/year for 2013). To take the increased non-seismic rockfall rates into account a factor of 2 has been applied to the annual rate in Table 24, based on the measured rates of rockfall from the terrestrial laser scan surveys.

At present the non-seismic rockfall rates derived from terrestrial laser scan surveys are considerably higher than 10–12 m³/year (historical rate multiplied by a factor of 2), but these rates are expected to reduce with time as the more unstable boulders are removed from the slope. The rates recorded from the terrestrial laser scan surveys represent cumulative volumes of debris for a single year. Historically, a maximum yearly rate of up to 50 m³ has been recorded, but this reduces once divided over a longer time period.

If the site were to be affected in the near future by another large earthquake, it is probable that these currently high rates would continue to persist for much longer.

5.1.3 Dwelling occupant risk

The results from the risk assessment are shown in Figure 37 (Maps 1–3) as the annual individual fatality risk for scenarios A, B and C (Table 2), adopting the input parameters as shown in Table 2. Map 1 shows the annual individual fatality risk estimated for cliff collapses (debris avalanches and cliff-top recession) adopting the upper debris volume and runout estimates (scenario A). Map 2 shows the estimated annual individual fatality risk for cliff collapses adopting the middle debris volume and runout estimates (scenario B). Map 3 shows the annual individual fatality risk adopting the lower debris volume and runout estimates (scenario C).

5.1.4 Variables adopted for the risk assessment

Other variables used in the risk assessment were discussed at a workshop with Christchurch City Council on 18 March 2014. Based on the results from the workshop the risk estimates presented in Figure 37 adopt the following main variables:

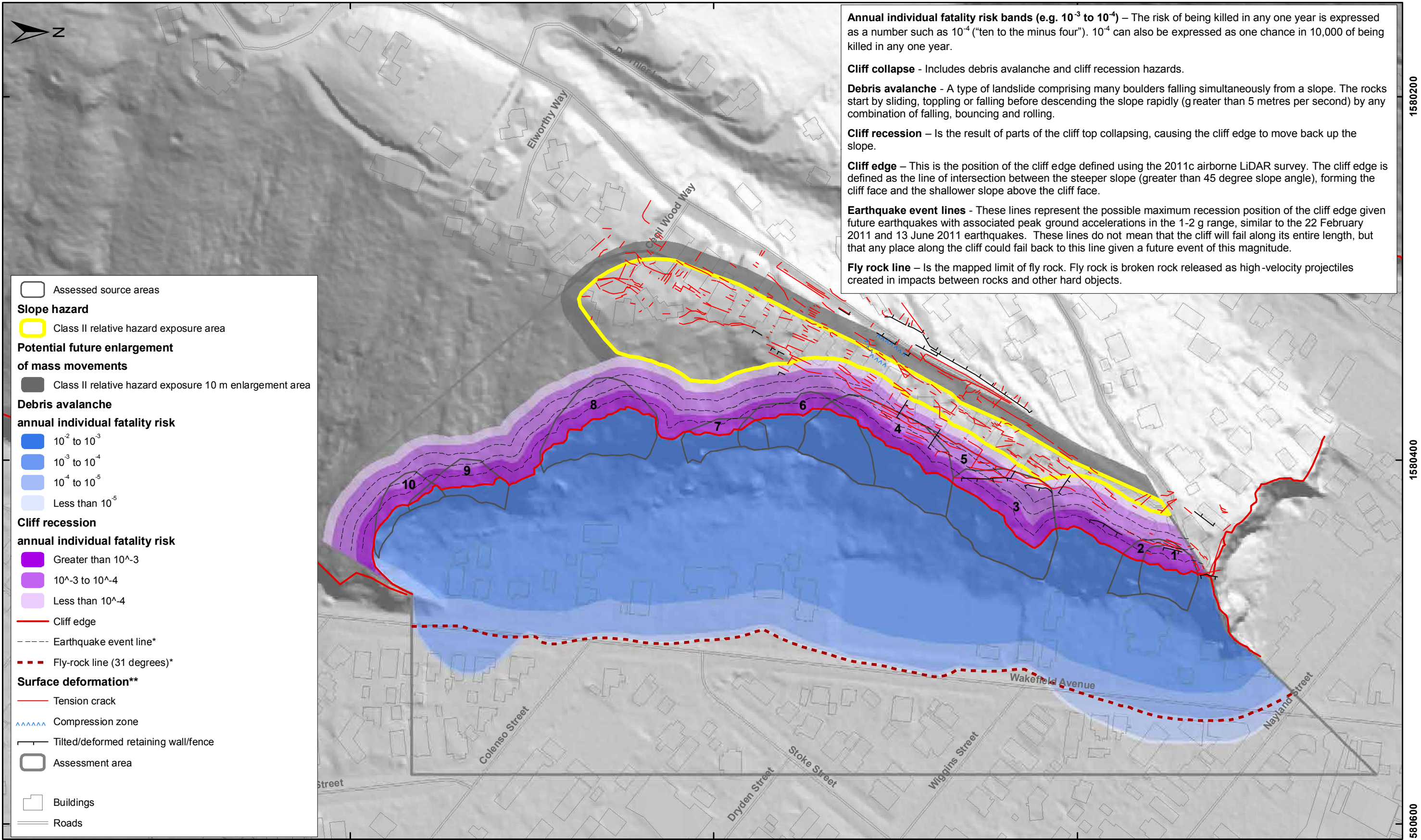
- $P_{(H)}$ for earthquake triggers the annual frequency of the triggering event adopt the 2016 seismic hazard model results, which include aftershocks.
- $P_{(S:H)}$ the probability that a person, if present, is in the path of the debris is based on variable (lower, middle and upper) estimates of the debris volume that could be triggered in an event.
- $P_{(T:S)}$ the probability that a person is present at a particular location, as the debris moves through it, of 67 %. Assuming an “average” person spends 16 hours a day at home. For this assessment, GNS Science has assumed the same “average” occupancy rate value adopted by the Canterbury Earthquake Recovery Authority.
- $V_{(D:T)}$ the vulnerability of a person, if present and inundated by debris, is a constant vulnerability factor of 70% has been adopted for this risk assessment as it was the factor adopted by the Canterbury Earthquake Recovery Authority (CERA) for the previous risk assessments.

5.1.5 Debris avalanche

For comparison purposes the effect of including the three assessed source areas in the risk assessment are shown, by including an estimation of the risk without these three source areas, where all of the debris generated in the peak ground acceleration bands is uniformly distributed across the slope (Figure 38).

Other parameters such as the probability of a person being present ($P_{(T:S)}$) and the vulnerability of a person if present and hit are held constant across all scenarios where $P_{(T:S)} = 0.67$ and $V_{(D:T)} = 0.7$.

Graphs showing the results for each scenario with/without local seismic sources are shown in Figure 39. The number of 2 m by 2 m cells shown in the graphs indicates the spread of the risk at different levels of annual individual fatality risk between the scenarios.



SCALE BAR: 0 50 100 m

EXPLANATION:
 * Modified from report CR2012/57
 ** Taken from report CR2012/317
 Background shade model derived from NZAM post earthquake 2011c (July 2011) LiDAR survey resampled to a 1 m ground resolution. Roads and building footprints provided by Christchurch City Council (20/02/2012).
 PROJECTION: New Zealand Transverse Mercator 2000

DRW:
BL
 CHK:
CM, FDP



**CLIFF COLLAPSE
 ANNUAL INDIVIDUAL FATALITY RISK
 (Scenario A)**

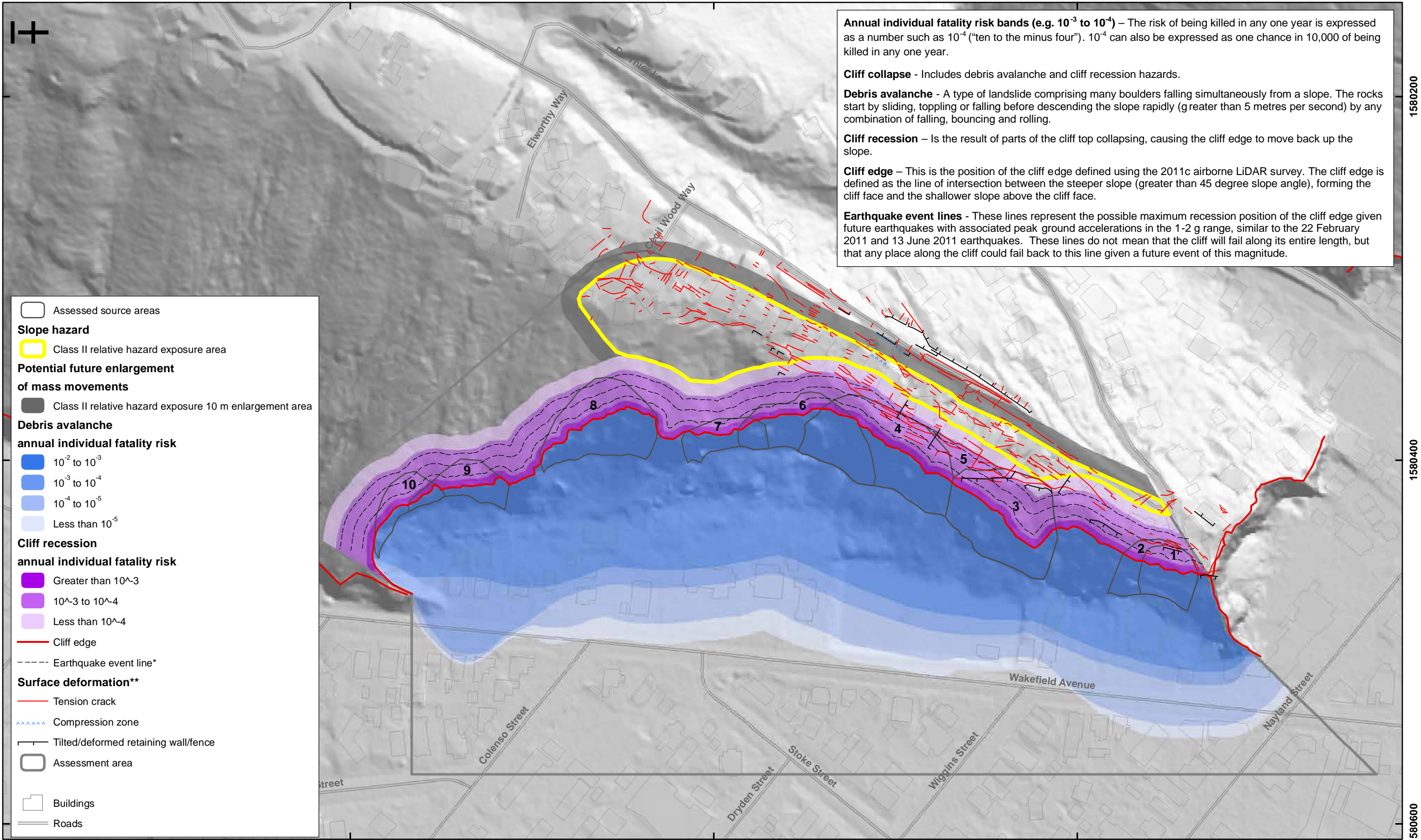
**Richmond Hill Road
 Christchurch**

FIGURE 37

Map 1

FINAL

REPORT: CR2014/34 DATE: June 2014



Annual individual fatality risk bands (e.g. 10^{-3} to 10^{-4}) – The risk of being killed in any one year is expressed as a number such as 10^{-4} (“ten to the minus four”). 10^{-4} can also be expressed as one chance in 10,000 of being killed in any one year.

Cliff collapse - Includes debris avalanche and cliff recession hazards.

Debris avalanche - A type of landslide comprising many boulders falling simultaneously from a slope. The rocks start by sliding, toppling or falling before descending the slope rapidly (g greater than 5 metres per second) by any combination of falling, bouncing and rolling.

Cliff recession – Is the result of parts of the cliff top collapsing, causing the cliff edge to move back up the slope.

Cliff edge – This is the position of the cliff edge defined using the 2011c airborne LiDAR survey. The cliff edge is defined as the line of intersection between the steeper slope (greater than 45 degree slope angle), forming the cliff face and the shallower slope above the cliff face.

Earthquake event lines - These lines represent the possible maximum recession position of the cliff edge given future earthquakes with associated peak ground accelerations in the 1-2 g range, similar to the 22 February 2011 and 13 June 2011 earthquakes. These lines do not mean that the cliff will fail along its entire length, but that any place along the cliff could fail back to this line given a future event of this magnitude.

- Assessed source areas
- Slope hazard**
- Class II relative hazard exposure area
- Potential future enlargement of mass movements**
- Class II relative hazard exposure 10 m enlargement area
- Debris avalanche**
- annual individual fatality risk**
- 10^{-2} to 10^{-3}
- 10^{-3} to 10^{-4}
- 10^{-4} to 10^{-5}
- Less than 10^{-5}
- Cliff recession**
- annual individual fatality risk**
- Greater than 10^{-3}
- 10^{-3} to 10^{-4}
- Less than 10^{-4}
- Cliff edge
- - - - Earthquake event line*
- Surface deformation****
- Tension crack
- ▲▲▲▲▲ Compression zone
- Tilted/deformed retaining wall/fence
- Assessment area
- Buildings
- Roads

SCALE BAR: 0 50 100 m

EXPLANATION:
 * Modified from report CR2012/57
 ** Taken from report CR2012/317
 Background shade model derived from NZAM post earthquake 2011c (July 2011) LiDAR survey resampled to a 1 m ground resolution.
 Roads and building footprints provided by Christchurch City Council (20/02/2012).
 PROJECTION: New Zealand Transverse Mercator 2000

DRW:
BL

CHK:
CM, FDP



**COMBINED CLIFF COLLAPSE
 ANNUAL INDIVIDUAL FATALITY RISK
 (Scenario B)**

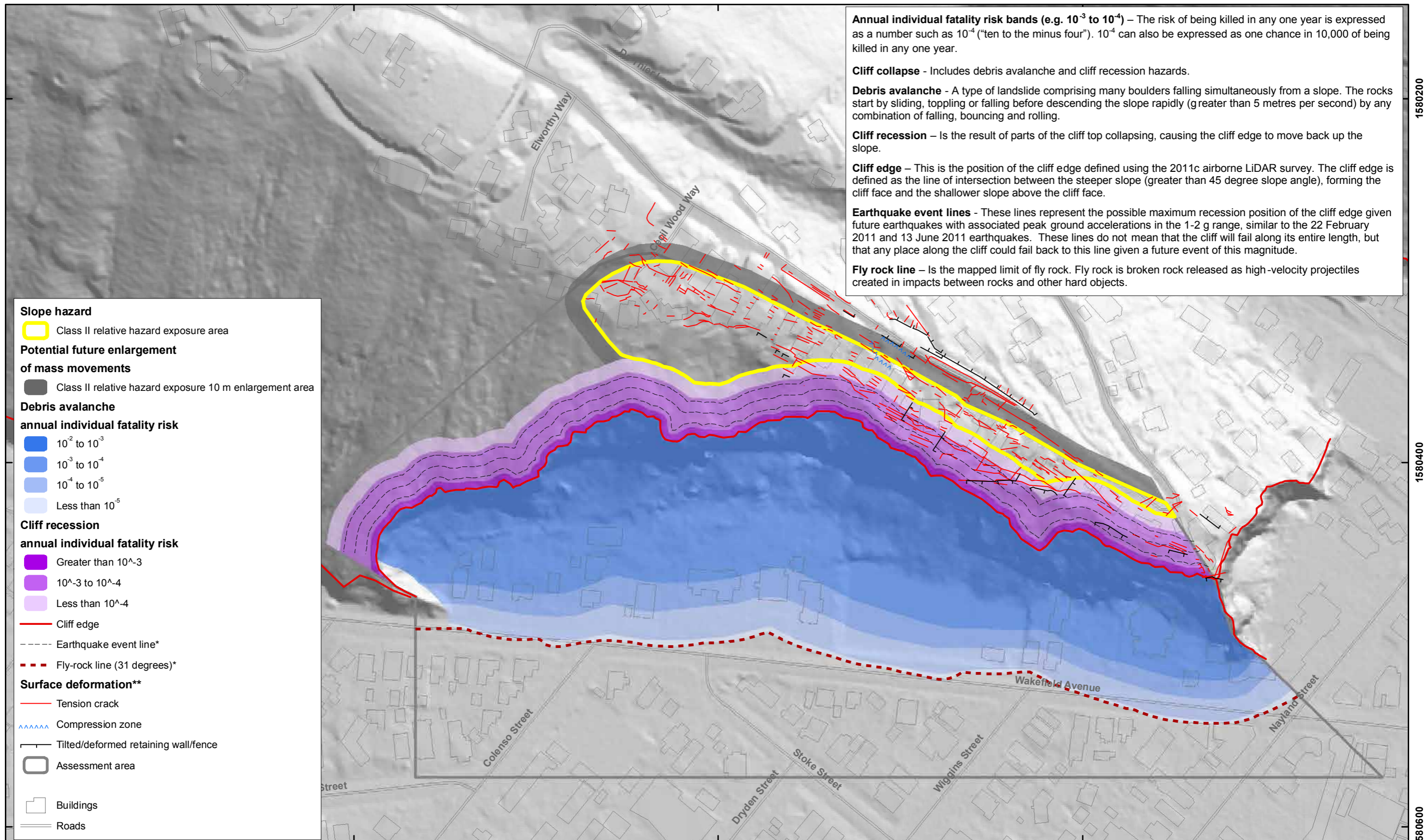
**Richmond Hill Road
 Christchurch**

FIGURE 37

Map 2

FINAL

REPORT: CR2014/34 DATE: June 2014



Annual individual fatality risk bands (e.g. 10^{-3} to 10^{-4}) – The risk of being killed in any one year is expressed as a number such as 10^{-4} (“ten to the minus four”). 10^{-4} can also be expressed as one chance in 10,000 of being killed in any one year.

Cliff collapse - Includes debris avalanche and cliff recession hazards.

Debris avalanche - A type of landslide comprising many boulders falling simultaneously from a slope. The rocks start by sliding, toppling or falling before descending the slope rapidly (greater than 5 metres per second) by any combination of falling, bouncing and rolling.

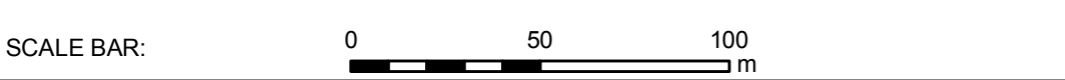
Cliff recession – Is the result of parts of the cliff top collapsing, causing the cliff edge to move back up the slope.

Cliff edge – This is the position of the cliff edge defined using the 2011c airborne LiDAR survey. The cliff edge is defined as the line of intersection between the steeper slope (greater than 45 degree slope angle), forming the cliff face and the shallower slope above the cliff face.

Earthquake event lines - These lines represent the possible maximum recession position of the cliff edge given future earthquakes with associated peak ground accelerations in the 1-2 g range, similar to the 22 February 2011 and 13 June 2011 earthquakes. These lines do not mean that the cliff will fail along its entire length, but that any place along the cliff could fail back to this line given a future event of this magnitude.

Fly rock line – Is the mapped limit of fly rock. Fly rock is broken rock released as high-velocity projectiles created in impacts between rocks and other hard objects.

- Slope hazard**
- Class II relative hazard exposure area
- Potential future enlargement of mass movements**
- Class II relative hazard exposure 10 m enlargement area
- Debris avalanche annual individual fatality risk**
- 10^{-2} to 10^{-3}
 - 10^{-3} to 10^{-4}
 - 10^{-4} to 10^{-5}
 - Less than 10^{-5}
- Cliff recession annual individual fatality risk**
- Greater than 10^{-3}
 - 10^{-3} to 10^{-4}
 - Less than 10^{-4}
- Cliff edge
 - Earthquake event line*
 - Fly-rock line (31 degrees)*
- Surface deformation****
- Tension crack
 - Compression zone
 - Tilted/deformed retaining wall/fence
 - Assessment area
 - Buildings
 - Roads



EXPLANATION:
 * Modified from report CR2012/57
 ** Taken from report CR2012/317
 Background shade model derived from NZAM post earthquake 2011c (July 2011) LiDAR survey resampled to a 1 m ground resolution.
 Roads and building footprints provided by Christchurch City Council (20/02/2012).
 PROJECTION: New Zealand Transverse Mercator 2000

DRW:
BL
 CHK:
CM, FDP



**CLIFF COLLAPSE
 ANNUAL INDIVIDUAL FATALITY RISK
 (Scenario B, 100% distributed)**

**Richmond Hill Road
 Christchurch**

FIGURE 38

FINAL

REPORT: CR2014/34 DATE: June 2014

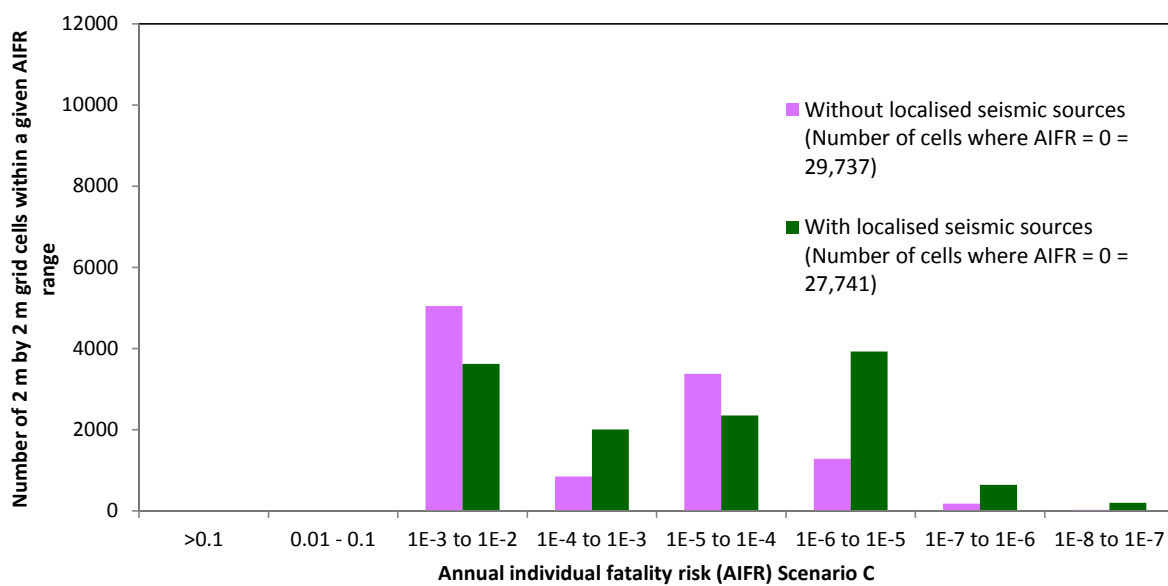
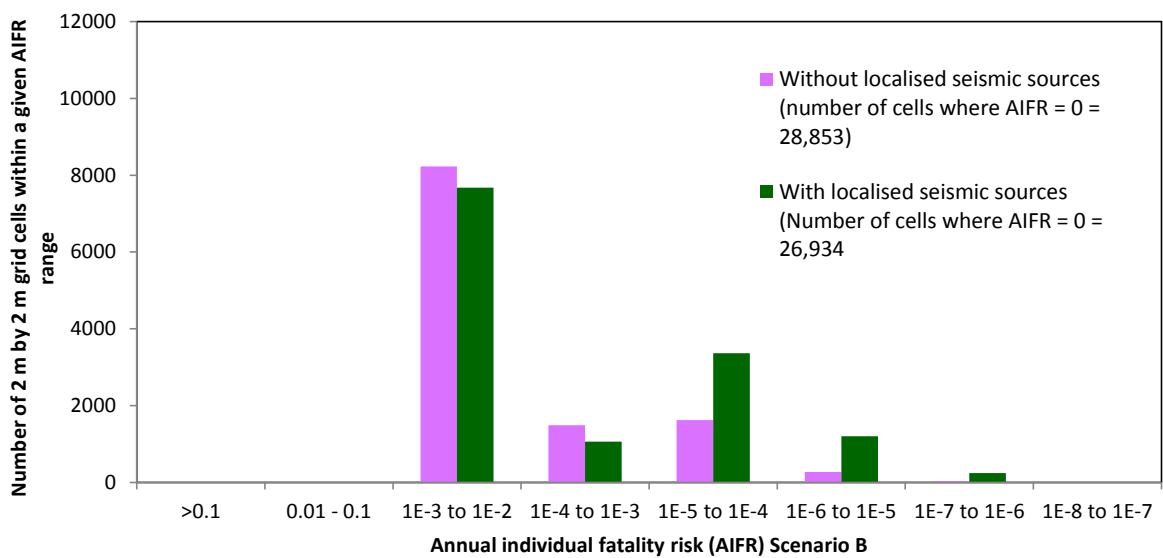
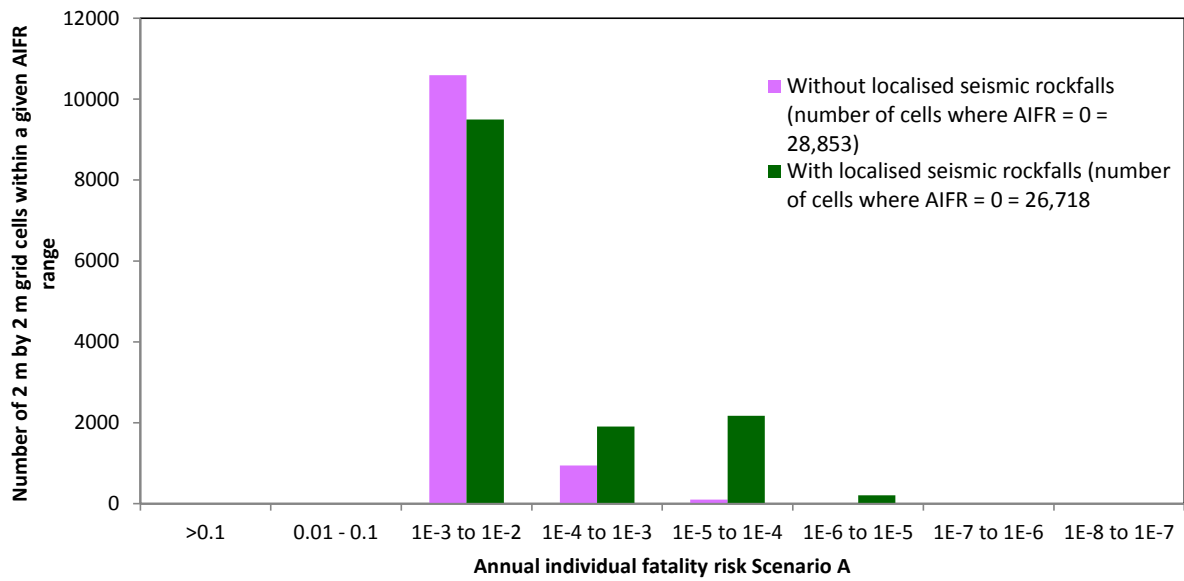


Figure 39 Results from the debris avalanche risk assessment per scenarios A, B and C (dwelling occupant).

5.1.6 Cliff-top recession

The area of cliff top lost per event was estimated using a 0.019 ratio of area lost to volume leaving the cliff face (from Massey et al., 2012a) (Tables 25 and 26).

Table 25 Area of cliff top lost per peak ground acceleration (PGA) band for upper, middle and lower volume estimates. Note only the first digit in the estimated area lost is significant, areas have been rounded to the nearest 10 m².

Area of cliff top lost (m ²)	PGA Band (g)						
	0.1–0.3	0.3–0.5	0.5–0.8	0.8–1.2	1.2–1.6	1.6–2.0	2.0–3
Distributed upper volume	37	65	98	141	187	231	304
Localised upper volume	55	98	147	211	280	346	455
Distributed middle volume	19	34	51	73	97	119	157
Localised middle volume	28	51	76	109	145	179	236
Distributed lower volume	10	18	26	38	50	62	81
Localised lower volume	15	26	40	57	75	93	122

Table 26 Volume of debris and area of cliff top lost per non-seismic band (based on historical rockfall rates in Massey et al., 2012a).

Time period (years)	Number of events in band	Annual frequency of events	Mean event volume (m ³)	Area lost (m ²)
1–15	5.5	0.37	5	0.1
15–100	1.3	0.0133	170	3
100–1,000	0.7	0.0007	1,500	30
1,000–10,000	0.3	0.00003	10,000	200

For distributed sources the proportion of land area lost at a given distance back from the cliff edge was estimated from the LiDAR change models. The method and results are detailed in Appendix 1 and in Massey et al. (2012a).

For local source areas 1–10, the land area lost at given distance back from the edge was estimated from the geometry of the potential source areas. To do this, the cliff top was considered as a series of 1 m by 1 m cells arranged parallel to the cliff edge. The numbers of 1 m cells within each source area – at 1 m intervals back from the current cliff edge – were counted, ensuring that for areas where different potential sources overlapped, the cells were only counted once. The annual individual fatality risk at given distances back from the cliff edge, for scenarios A–C, are shown in Figure 40. The position behind the cliff edge of the 10⁻⁴ risk contour changes between scenarios. As expected, the 10⁻⁴ contour for scenario A is the furthest back from the cliff edge (about 25 m) as this scenario comprises the upper volume estimates per assessed source, compared to scenario C (about 18 m).

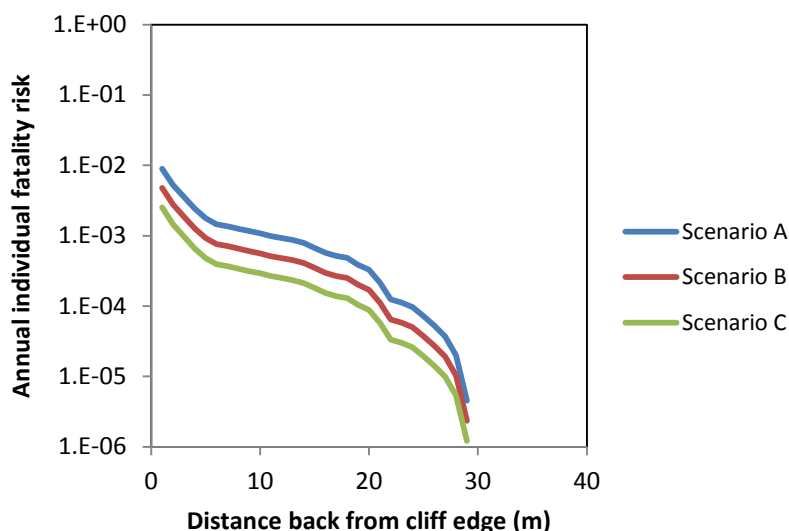


Figure 40 Results from the cliff top recession risk assessment, per scenarios A, B and C (dwelling occupant). Refer to Table 25 for details of the each scenario.

5.1.6.1 Slumping and cracking

The area of slope between the cliff-top recession risk zone and the mapped extent of cracking that was highlighted in the Stage 1 report as a Class I area, has now been reassessed as being in a Class II area. A Class II area is defined in the Stage 1 report (Massey et al., 2013) as:

- Coherent slides and slumps of predominantly loess with associated cumulative inferred displacement of the mass of greater than 0.3 m, where dwellings and critical infrastructure is present within the moving mass. It is possible that renewed movement may severely impact critical infrastructure and dwellings. The level of disruption to critical infrastructure and dwellings is likely to be a function of where they are within the feature. The most hazardous places are the mainly extensional and compressional areas. Given the magnitudes of displacement it is unlikely that damage to dwellings would pose an immediate life risk to their occupants.

A 10 m wide area has been added to the inferred boundary of the Class II hazard exposure area, where the area of slumping and cracking could potentially in the future enlarge in an up-slope or lateral direction beyond the currently recognised boundary. This has been termed a “Class II relative hazard exposure 10 m enlargement area”.

5.2 ROAD USER RISK

Risk to road users is calculated per journey, along the length of Wakefield Avenue in front of the cliff (Figure 2). The factors determining that risk are explained in Section 5.2.1. Other risk parameters are calculated from the risk per journey in Section 5.2.2:

- Annual individual fatality risk for heavy users of the road (by multiplying by trips per year made by individual such users);
- Aggregate total expected fatalities per year (by multiplying by the total number of trips per year made by relevant users); and
- Frequency of a fatal accident (by working out the probability that all trips by relevant users will result in a non-fatal outcome).

5.2.1 Risk per Journey

Summaries of the risk assessment results for all road user groups modelled – travelling along Wakefield Avenue in the study area (Figure 2) – in terms of risk per 100 million journeys under rockfall scenarios A, B and C, are presented in Figure 41.

Figure 41 shows three bars for each road user group, representing the rockfall risk on the uphill (West) and downhill (East) sides of the road, and (in red) the motor vehicle crash risk such road users would face on a trip of equal length on an average New Zealand road.

The risk per journey, and its relativity to motor vehicle crash risk, varies significantly by user group. For car users and cyclists, the rockfall risk is broadly speaking comparable with the motor vehicle crash risk. For motorcyclists it is lower (because the existing crash risk is so high). For pedestrians the rockfall risk is comparable with or greater than the motor vehicle crash risk – this is largely because the exposure time to rockfall risk for pedestrians is substantially greater than that for other road users; their vulnerability is also somewhat greater than that of people in cars. Under any assumptions, the rockfall risk on the downhill side of the road is about half that on the uphill side for pedestrians.

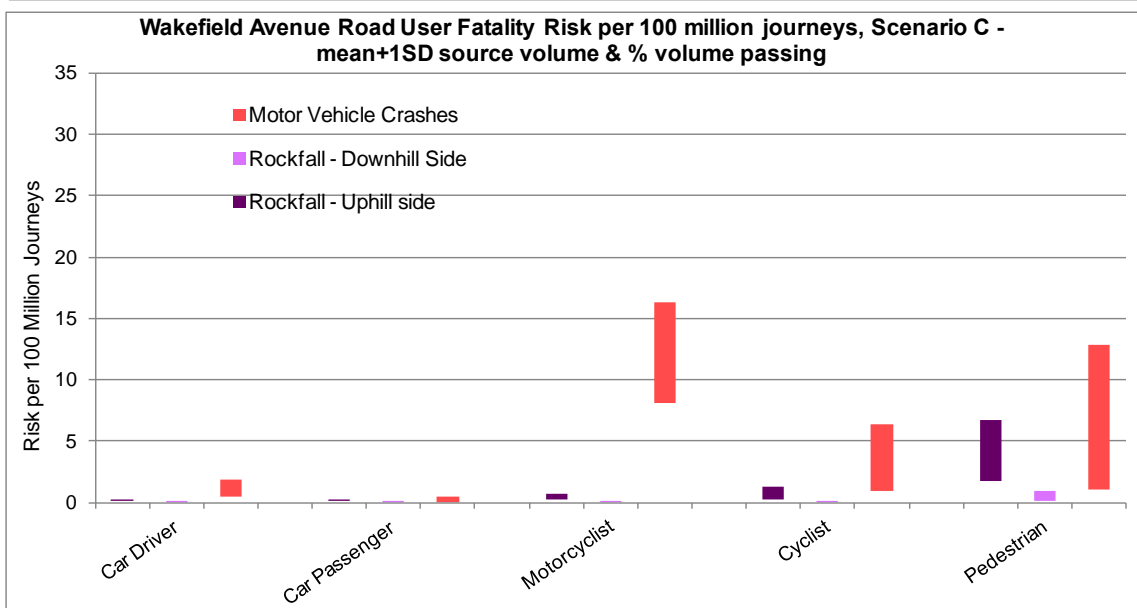
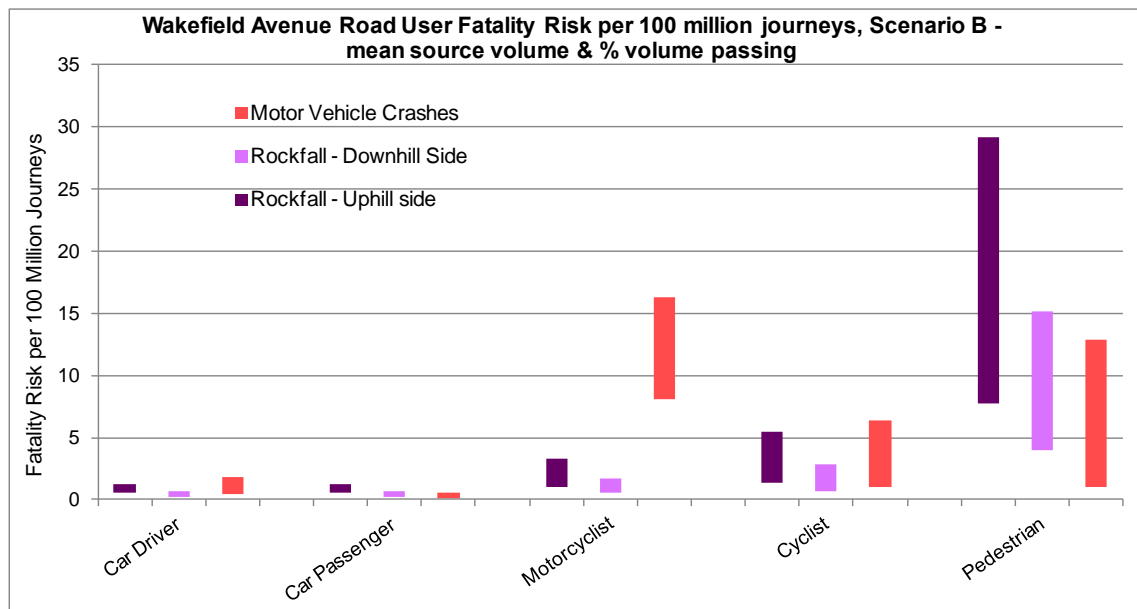
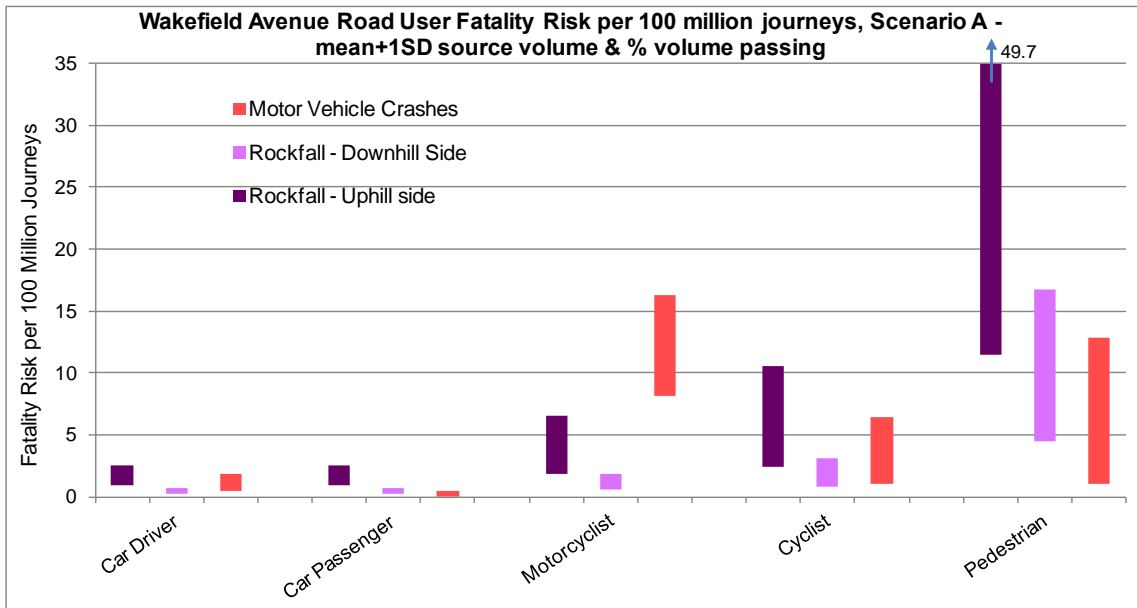


Figure 41 Risk per journey under rockfall scenarios A, B and C.

Figures 42a–c show where on the section of Wakefield Avenue that has been assessed the major risk contributions arise for the three rockfall scenarios (A, B and C) modelled.

Risk per 100 million journeys - Lower Risk per 100 million journeys - Upper
Scenario A - mean+1SD source volume & % volume passing

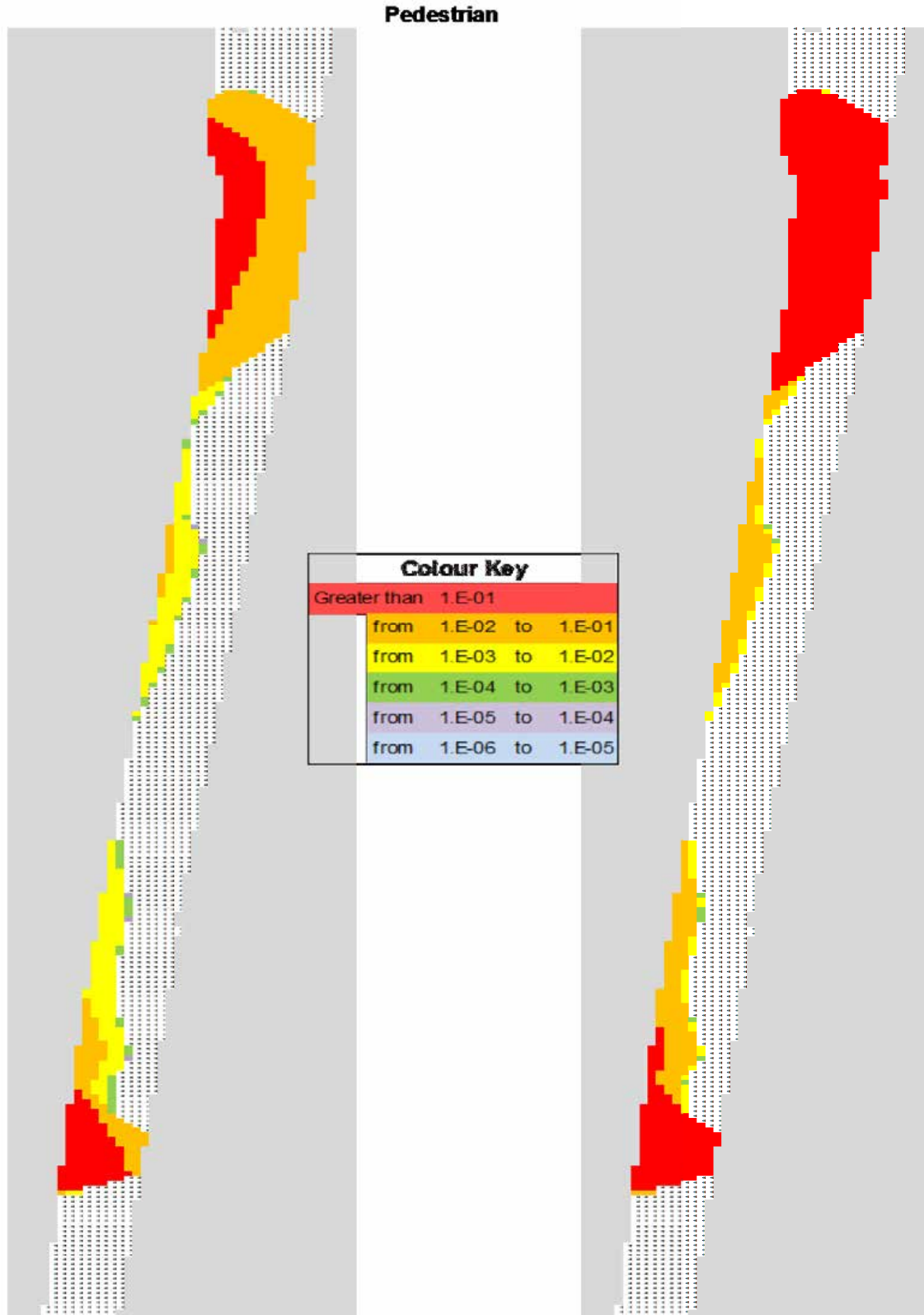


Figure 42a Road user risk contributions (per 100 million journeys) from individual cells – Scenario A.

Risk per 100 million journeys - Lower

Risk per 100 million journeys - Upper

Scenario B - mean source volume & % volume passing

Pedestrian

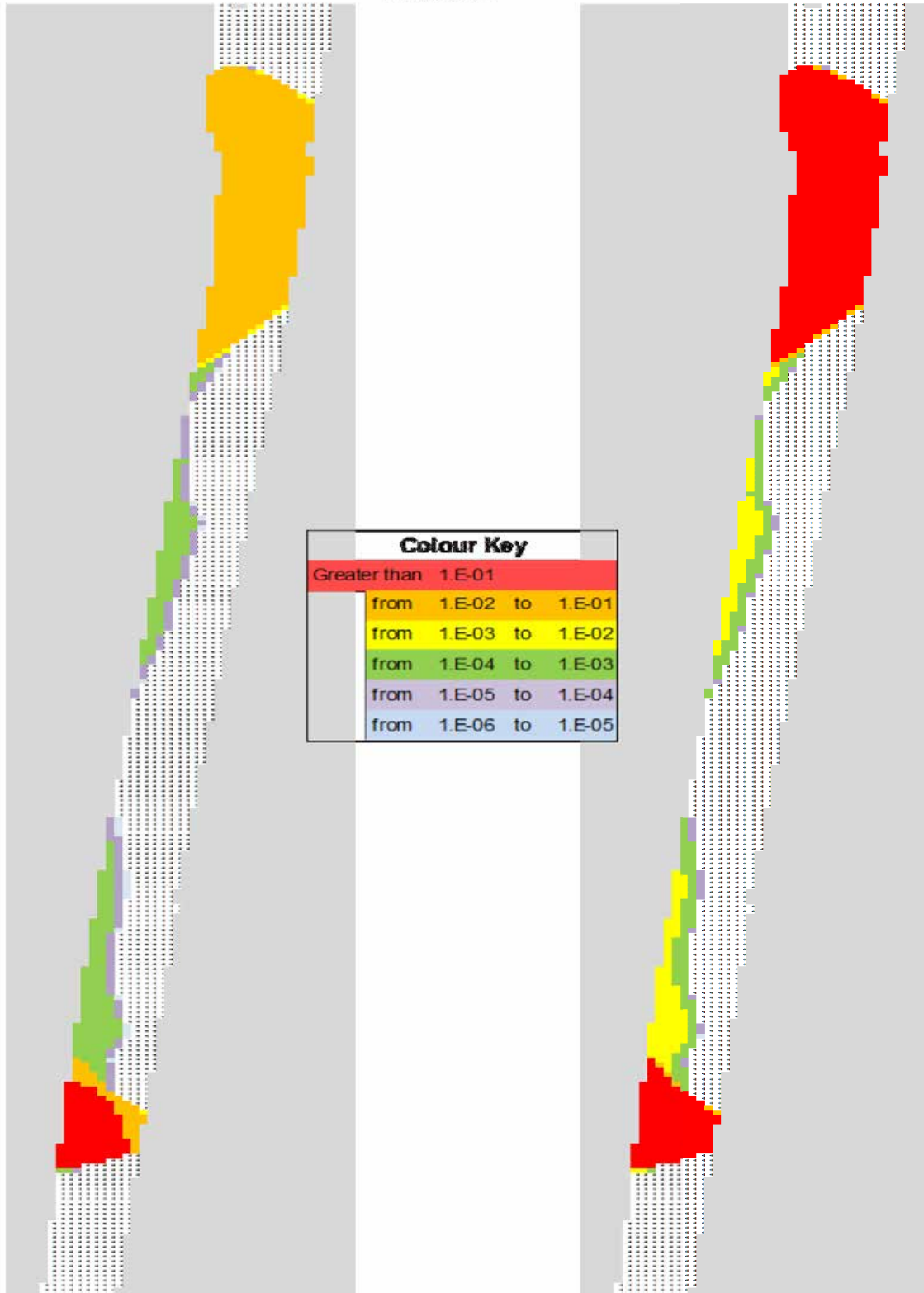


Figure 42b Road user risk contributions (per 100 million journeys) from individual cells – Scenario B.

Risk per 100 million journeys - Lower

Risk per 100 million journeys - Upper

Scenario C - mean+1SD source volume & % volume passing

Pedestrian

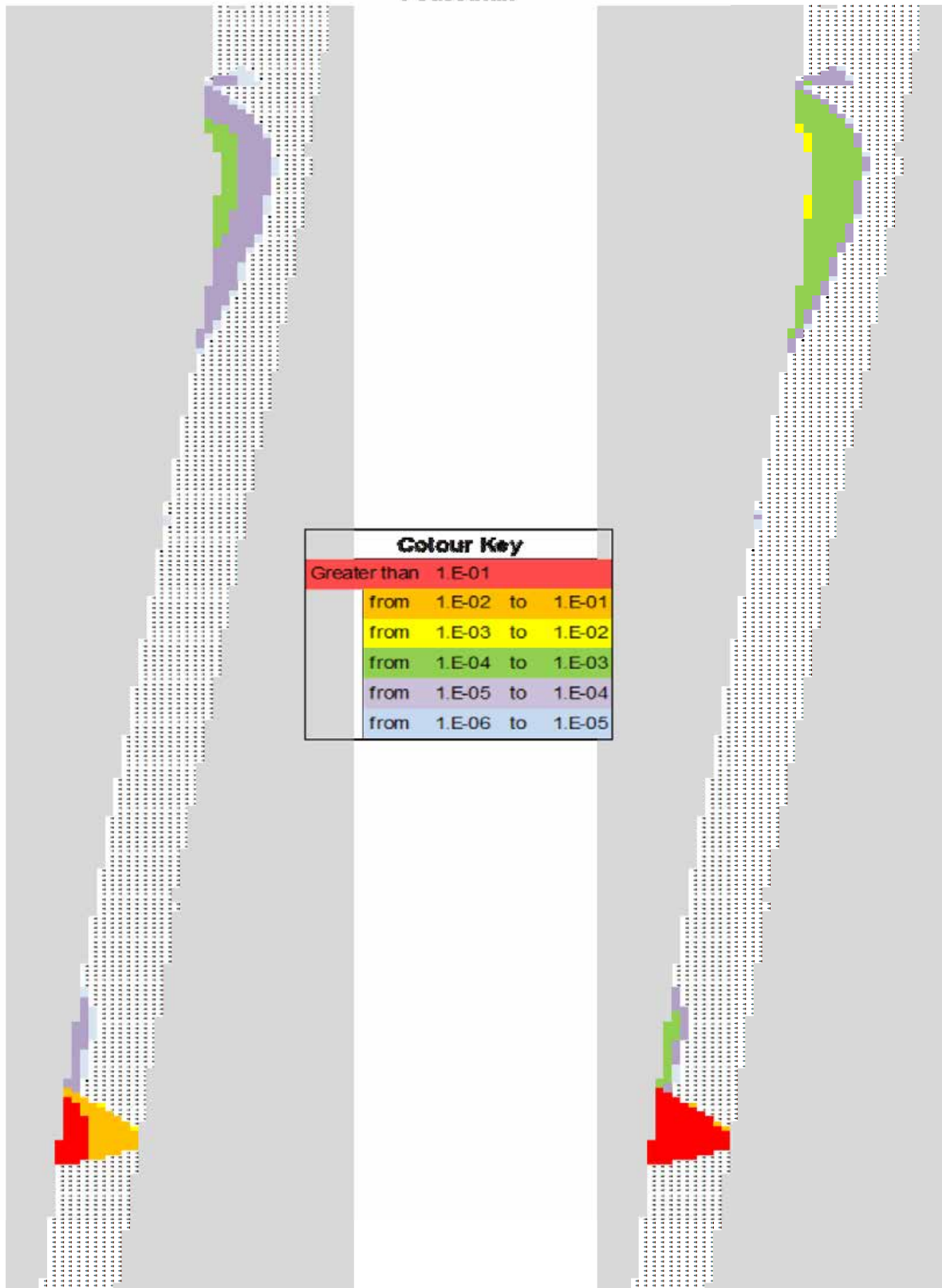


Figure 42c Road user risk contributions (per 100 million journeys) from individual cells – Scenario C.

The majority of the risk per journey is contributed by the two local sources at the top and bottom of Figures 42a–c. For large stretches of the road the risk is zero or minimal. This series of figures illustrates the high sensitivity of risk to both: 1) the rockfall runout uncertainty (represented by the difference across Figures 42a, 42b and 42c); and 2) the side of the road on which risk is assessed.

Neither of these sensitivities is surprising; the road was presumably originally located at what was judged to be a reasonably safe distance out from the foot of Richmond Hill, which would have been well recognisable from the boulders at its foot as a regular source of rockfalls. Events within the range of “normal expected rockfall” thus do not reach the road, whereas larger events (before European settlement in New Zealand, but now considered entirely plausible in the event of even modest ground shaking, given the state of the slope as discussed earlier in this report), by running out a few tens of metres farther, extend the hazard range across the road. The risk falls off steeply with distance from the foot of the hill, hence the large difference between risk on the west and on the east side of Wakefield Avenue.

The relative contributions to risk of the different rockfall triggers and of the two hazards to road users modelled (hazard 1 – the “hit by falling rock” and hazard 2 – the “crash into, or in avoiding, fallen rock”) is illustrated in Figure 43. This makeup is not sensitive to the rockfall runout scenario or to whether upper/lower risk estimates are examined.

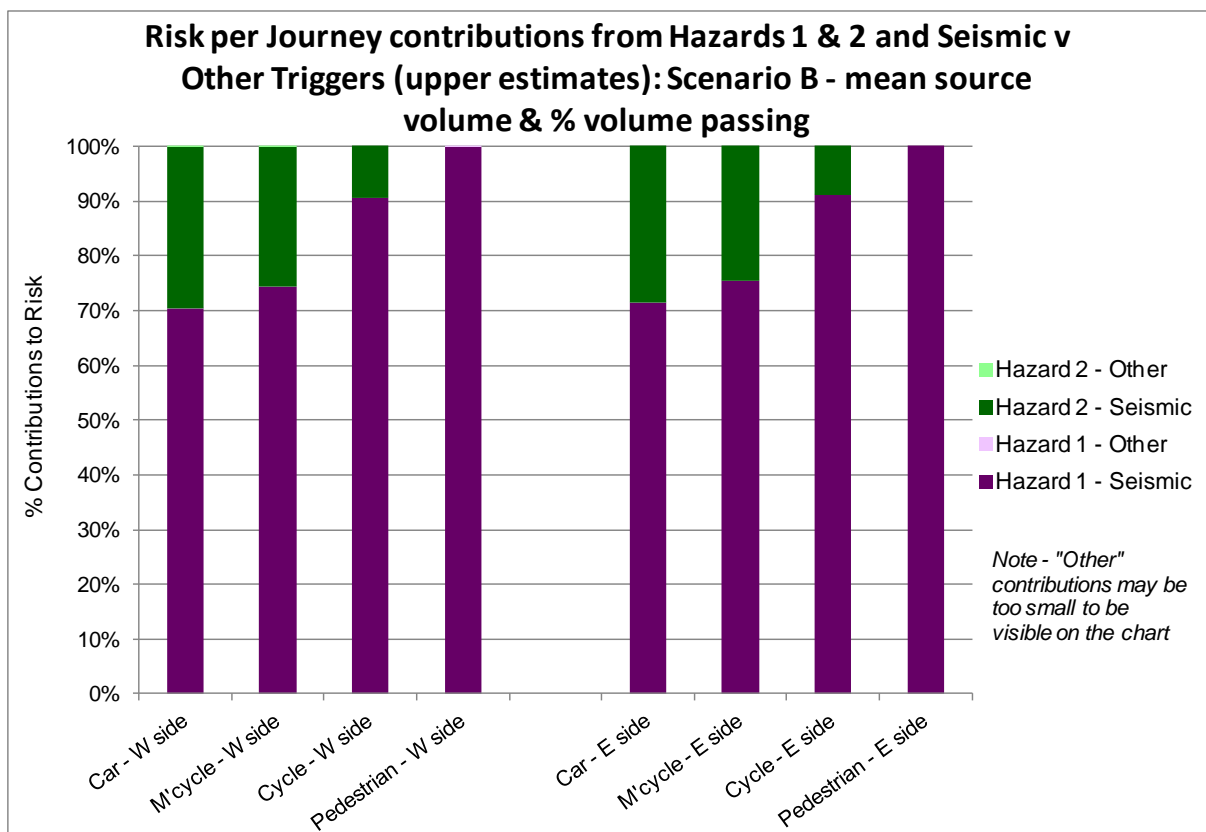


Figure 43 Risk contributions from hazards 1 and 2 and seismic versus other triggers.

In every case, the key observations are that:

- a. Hazard 1 (“hit by”) dominates over Hazard 2 (“crash into/avoiding”); and
- b. Seismic triggers greatly dominate over the non-seismic triggers, whose contribution to risk is so small as to be invisible in Figure 43.

The inclusion of the local rockfall sources in the current work, in comparison with our earlier work in which all rockfall was assumed to be uniformly, randomly distributed along the whole slope length, is clear from Figures 42a–c. The importance for road users of the local sources that have been characterised in this study is illustrated starkly in Figure 44, which shows the risk that would be assessed if all the rockfall were treated as distributed uniformly along the slope.

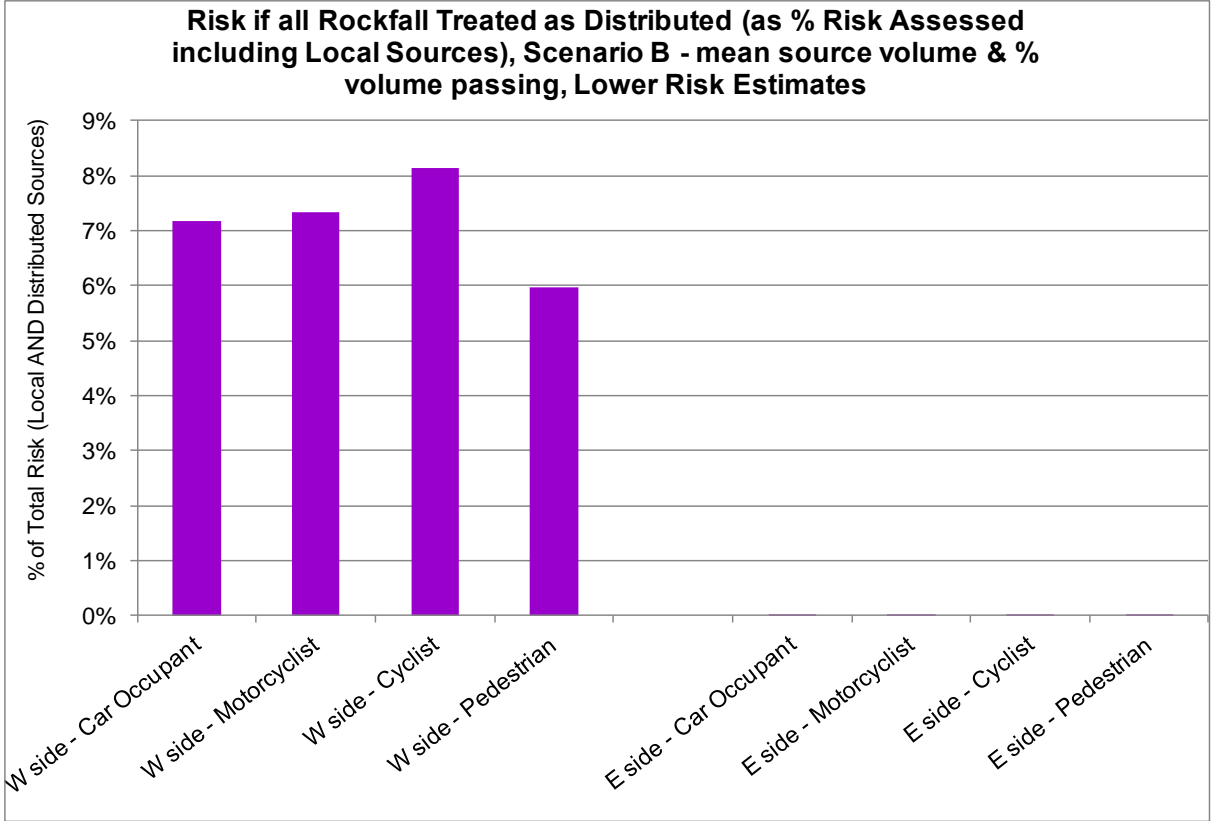


Figure 44 Effect of treating all rockfall as uniformly distributed along the cliff – Scenario B.

Without the large local sources being assessed, the risk on the downslope (east) side of the road virtually disappears. Under the central scenario B, the risk on the uphill side is a small fraction of that which would be assessed with local sources included. The virtual absence of risk on the downslope side of the road is not sensitive to the rockfall runout uncertainty. The ratio of risk (distributed sources only) to risk (distributed and local sources) on the uphill side of the road is sensitive to rockfall runout assumptions; as runout increases the ratio also increases, becoming greater than 1 for scenario A¹.

¹ This is because the risk in the local source areas on the road is no higher in places that would be inundated with rockfall from the local sources, whereas fewer cells on the upslope side of the road are free from boulders under the assumption of distributed sources only.

5.2.2 Alternative risk parameters for road users

Risk to individual road users is calculated in terms of annual individual fatality risk to heavy users of the road, whose usage is assumed to be as shown in Table 27.

Table 27 Number of trips per day for high road users.

Travel mode	High user trips per day	
	Lower risk	Higher risk
Car driver	2	4
Car passenger	2	4
Motorcyclist	2	4
Pedal cyclist	2	4
Pedestrian	2	4

The annual individual fatality risk is simply the number of trips per day (as in Table 27) multiplied by 365 (days in the year) and the risk per journey (as in Figure 43). The resulting annual individual fatality risk estimates, again shown alongside the corresponding motor vehicle crash risks for making the same number of journeys on an average New Zealand road, are shown in Figure 45. The observations as to the relativity of risk between road users and in relation to motor vehicle crash risk are identical to those made on Figure 41.

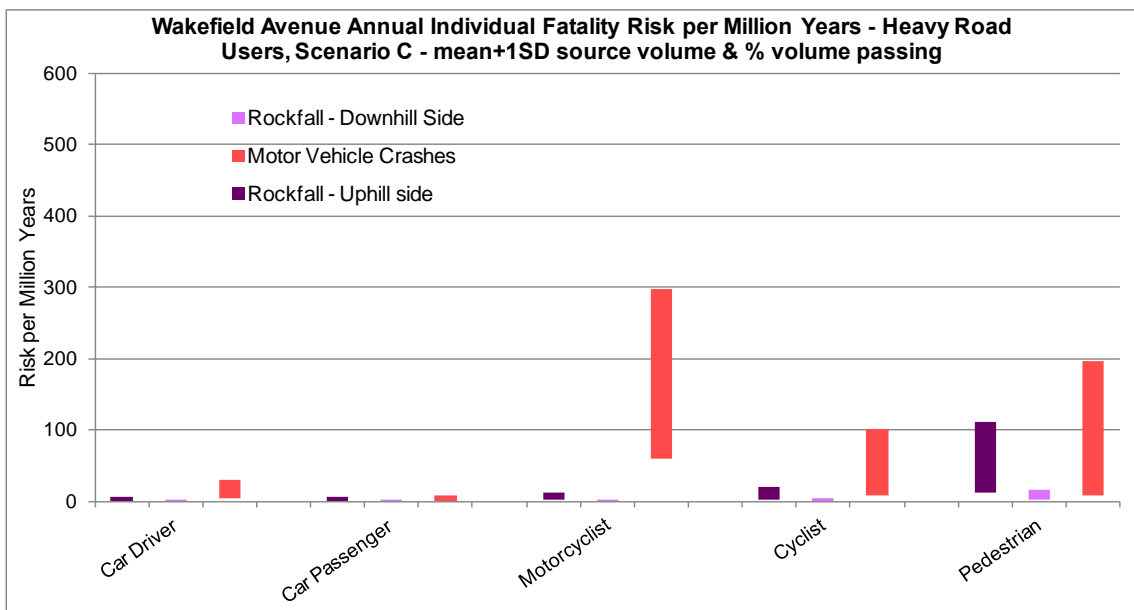
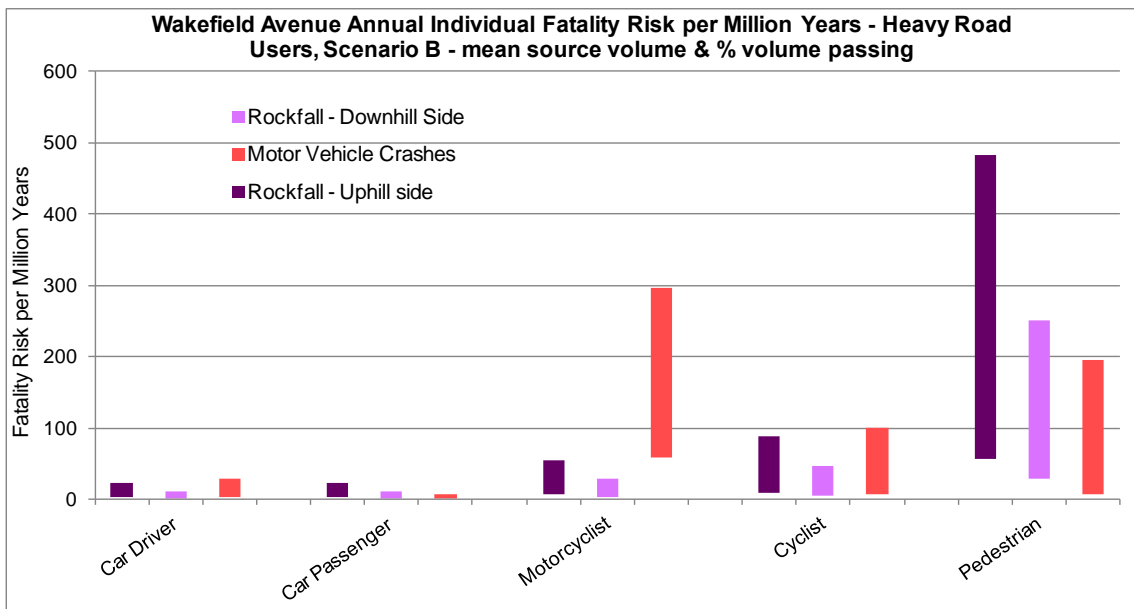
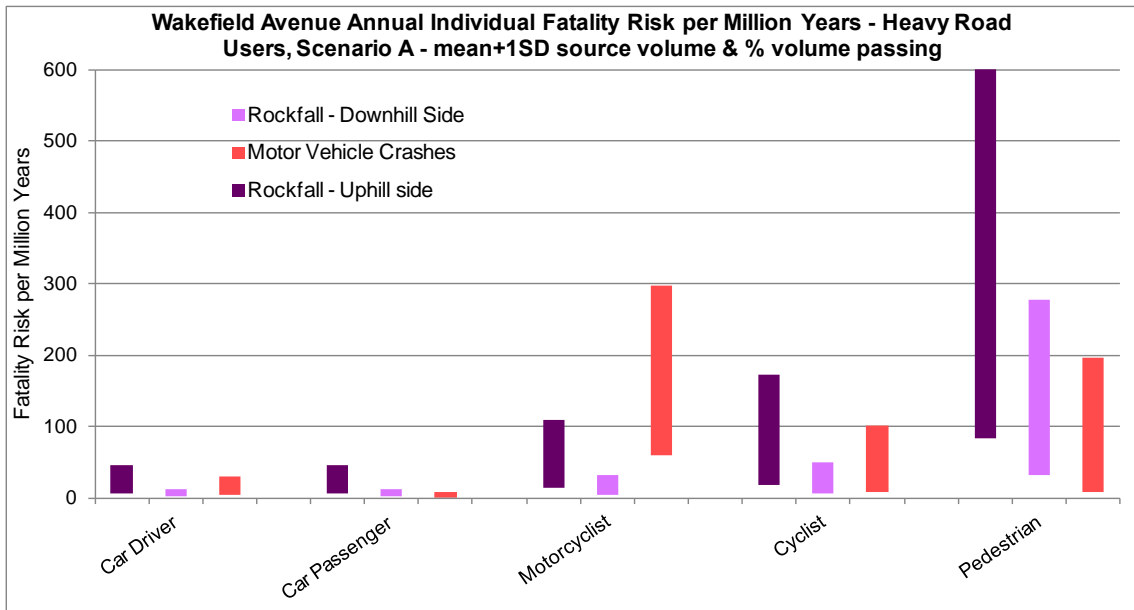


Figure 45 Annual individual fatality risk for heavy users of Wakefield Avenue, scenarios A, B and C.

Aggregate risk for all road users depends on the total number of journeys travelled by the different modes. Estimates for cars are available from Christchurch City Council traffic volume surveys², which have been carried out at the junction of Wakefield Avenue and Nayland Street at approximately 20-yearly intervals since the early 1990's. Prior to the earthquake traffic grew steadily up to about 6,400 vehicles per day (7-day, 24 hour average) in the 2010 survey. The 2012 figure dropped to about 2,500 vehicles per day, presumably reflecting reduced population and activity levels in the wake of the 2010 and 2011 earthquakes. A range from 2,500 to 7,000 vehicles per day (all assumed to be cars) has been assumed here, to ensure the estimates produced are robust to resumption of pre-earthquake population and activity levels.

Estimates for numbers of other road user trips per day were made in consultation with a number of GNS Science staff who shared occupancy of a house at the southern end of Wakefield Avenue for much of 2012 and 2013 and travelled daily, at different times, along the stretch of Wakefield Avenue in question. The total trips per day assumed in this study are shown in Table 28.

Table 28 Total trips per day for all road users.

User group	Total trips per day (all users)	
	Lower risk	Higher risk
Cars	2500	7000
Motorcycles	15	50
Bicycles	50	200
Pedestrians	100	250

The aggregate risk parameter calculated from these figures and the risks per journey (Figure 43 above) is the expected average annual fatalities per year for each road user group³. This is simply the risk per journey multiplied by total trips per year for the relevant road user group. The sum over all road users gives the total average expected fatalities per year.

The resulting average annual expected fatalities per year, by road user group and in total, are shown in Table 29.

² <http://www.ccc.govt.nz/CCC.Web.TrafficCount/cityleisure/projectstoimprovechristchurch/transport/trafficcount/volumecount.aspx>

³ Note – if the expected fatalities per year were higher we would also calculate the expected frequency of fatal accidents, but in this case, because the numbers are small, the figures are almost identical (the frequency of fatal accidents is marginally lower than the expected fatalities per year as a small proportion of accidents involve multiple fatalities).

Table 29 Average total expected deaths per year.

Average total expected deaths per year		
Scenario A – mean + 1 STD source volume and % volume passing		
(assumes trips evenly split between uphill and downhill sides of road)		
User group	Lower risk	Higher risk
Car drivers	5.6E-03	4.3E-02
Car passengers	3.3E-03	2.5E-02
Motorcycles	6.6E-05	7.6E-04
Bicycles	2.9E-04	5.0E-03
Pedestrians	2.9E-03	3.0E-02
TOTAL deaths/year	1.2E-02	1.0E-01
or on average one death every		10–82 years

Average total expected deaths per year		
Scenario B – mean source volume and % volume passing		
(assumes trips evenly split between uphill and downhill sides of road)		
User group	Lower risk	Higher risk
Car drivers	3.6E-03	2.5E-02
Car passengers	2.1E-03	1.5E-02
Motorcycles	4.2E-05	4.5E-04
Bicycles	1.9E-04	3.0E-03
Pedestrians	2.1E-03	2.0E-02
TOTAL deaths/year	8.0E-03	6.3E-02
or on average one death every		16–124 years

Average total expected deaths per year		
Scenario C – mean + 1 STD source volume and % volume passing		
(assumes trips evenly split between uphill and downhill sides of road)		
User group	Lower risk	Higher risk
Car drivers	6.2E-04	4.4E-03
Car passengers	3.7E-04	2.6E-03
Motorcycles	7.3E-06	7.9E-05
Bicycles	3.3E-05	5.3E-04
Pedestrians	3.6E-04	3.5E-03
TOTAL deaths/year	1.4E-03	1.1E-02
or on average one death every		90–723 years

Because there are so many more car users than other road users, the car users dominate the aggregate risk, making up 60–70% of the total. But the total, involving one death in an interval somewhere between 10 years and several hundred years, is very small in comparison with the overall road traffic accident rate on Christchurch roads.

The key conclusion here is that, while individual fatality risk associated with rockfall may be significant in comparison with road traffic accident risk, the aggregate rockfall risk to road users is small compared with the overall rate of road traffic accident risk in Christchurch.

6.0 DISCUSSION

6.1 DWELLING OCCUPANT RISK

Important points of note from the results of the risk assessment undertaken in this study include:

1. Earthquake-triggered debris avalanches contribute most to the risk, and large earthquake-triggered debris avalanches from local source areas dominate the earthquake contribution.
2. The inclusion of large local sources in the risk assessment increases the runout and hence the risk farther out from the toe of the slope, compared with the risk estimated assuming that the debris is uniformly distributed across the slope.
3. In particular, the annual individual fatality risk at the northern and southern ends of the site in scenarios A and B now extend across Wakefield Avenue, which is further (from the slope toe) than the original risk estimates shown by Massey et al. (2012a).
4. The inclusion of local earthquake triggered sources also increases the width of the cliff top recession risk zone. However, the revised cliff top recession annual individual fatality risk zone does not extend beyond the already “Red Zoned” properties that have already been zoned by the Canterbury Earthquake Recovery Authority.

6.2 ROAD USER RISK

Important points of note from the risk assessment results for road users along Wakefield Avenue include:

1. The rockfall risk is greatest for the slowest road users (pedestrians, then cyclists), because their slower travel exposes them to risk for longer on each journey.
2. The rockfall risk is significantly higher on the uphill (west) than on the downhill (east) side of the road.
3. The relativity between rockfall risk and road traffic accident risk is different for the different road user groups, in particular:
 - a. For car drivers and pedal cyclists the rockfall risk is in the same ball park as the road accident risk.
 - b. For car passengers the rockfall risk (assumed the same as for the driver) is higher than the road accident risk (which is a good deal smaller for car passengers than for drivers).
 - c. For motorcyclists, the road accident risk is greater than rockfall risk (because the former is so high).
 - d. For pedestrians, the rockfall risk on the uphill (west) side of the road is comparable with or greater than road accident risk, whereas on the downhill (east) side of the road it is comparable with or less than road accident risk.
4. The risk from seismic rockfall triggers dominates over that from non-seismic triggers, and the risk of being struck by rockfall dominates over the risk of crashing into (or whilst avoiding) rockfall on the road.

5. The consideration of local sources of rockfall introduced in this study in comparison with our previous work on road user risk on Wakefield Avenue (Taig and Massey, 2014) has substantially increased the assessed risk to road users.
6. While individual fatality risk from rockfall for some road users may be comparable with that of motor vehicle crashes, the aggregate risk from rockfall is small in relation to the aggregate risk of motor vehicle crashes for Christchurch.

6.3 RISK ASSESSMENT SENSITIVITY TO UNCERTAINTIES

In this section the sensitivity of the risk model to key uncertainties and reliability of the assessments are identified. The three sets of assumptions (used for scenarios A–C) are discussed, along with other variations in the input parameters not included in scenarios A–C.

The sensitivity of the estimated risk has been assessed to changes in the following:

6.3.1 Debris volumes

Volumes of debris triggered by the representative events for both seismic and non-seismic triggers:

- a. For seismically triggered debris avalanches three volume ranges have been used to account for any variation in the relationship between peak ground acceleration and volume leaving the slope.
- b. For non-seismically triggered debris avalanche volumes a scale factor of 2 has been used to take into account the likely increased rates of debris avalanches due to the now dilated and highly disturbed nature of the cliffs.

6.3.2 Area of cliff-top lost

Area of cliff top recessing as a result of the representative event for both earthquake and non-seismic triggers:

- a. For earthquake triggered recession this takes into account any variation in the relationship between peak ground acceleration and volume leaving the slope and the ratio of volume to cliff top area lost.
- b. For non-seismically triggered recession the scale factor (of 2) takes into account the likely increased rates of cliff collapse due to the now dilated and highly disturbed nature of the cliffs.
- c. The relationship between the volume leaving the cliffs and the area of cliff top lost from a ratio of 0.019 to a ratio of 0.025, i.e., for 100 m³ of debris leaving the cliff face the area lost would increase from 1.9 m² to 2.5 m².

6.3.3 Debris runout

Volume of material passing a given distance down the slope:

- a. For randomly-distributed failures the variation in the relationship between the volume passing a given fahrboeschung angle has been used.
- b. For earthquake-triggered local debris avalanches the volume of material passing a given distance – estimated using the RAMMS model – has been assessed using different source volumes in the model (upper, middle and lower volume estimates).

The results (Figure 37) show that largest impact on the risk is from the volumes of material that could be generated at different bands of peak ground acceleration; in particular, the volumes that could be generated from each potential local source area.

There are approximately two orders of magnitude difference (a factor of 100 times) in the risk between scenarios A and C, for the same location in the more distal ends of the debris runout zone (Figure 39, Maps 1 and 3). The risk in the zones closest to the slope toe does not change much between the scenarios.

6.3.4 Other sensitivities and uncertainties

The composite seismic hazard model provides the annual frequency of a debris avalanche-triggering earthquake occurring. The likelihood of such an earthquake occurring is much higher in the next few years, and will decrease over the next decade. The time-varying nature of the seismic hazard has been considered by comparing the differences in risk associated with the year 2016- and 50-year composite seismic hazard model results (50-years being consistent with the design life used in typical seismic hazard analysis for residential building construction).

The risk estimates reduce by a factor of between two and three – for the same location in the more distal ends of the debris runout zone – when adopting the year 2016 annual frequencies compared to the 50-year average annual frequencies (including aftershocks). There is little difference to the risk closer towards the slope toe (Figure 39, Maps 1 and 3).

6.3.5 How reliable are the results?

Potentially significant uncertainties noted and their likely implications for risk are summarised in Table 30.

Table 30 Uncertainties and their implications for risk.

Issue	Direction and scale of uncertainty	Implications for risk
a. Under-prediction of annual frequency for a given peak ground acceleration by the composite seismic hazard model.	Upward, potentially considerable – but geomorphological evidence in the Port Hills suggests there is a sensible cap that can be placed on the upward uncertainty, which is about an order of magnitude. Refer to Massey et al. (2012b) for details.	Risk due to earthquakes could be systematically under- or over-estimated.
b. Choice of whether to use average earthquake annual frequencies for next 50-years, or higher frequencies for next 1-year.	Moderate uncertainty between the use of the year 2016 and 50-year average annual frequencies. Refer to Massey et al. (2012a) for details. The magnitude of uncertainty depends on the location of the dwelling within the risk zones. The distal ends are more uncertain than the zones closer to the toe of the slope.	Longer term risk is potentially 5 times lower in the distal runout zone.
c. Volume of debris produced in each peak ground acceleration band.	Largest uncertainty in either direction.	c) and d) combine to give two orders of magnitude uncertainty (factor of 100) in the upward direction, but lower in the downward direction.

Issue	Direction and scale of uncertainty	Implications for risk
d. Volume of debris produced by other (non-seismic) events.	Large uncertainty either way in the annual frequency, but constrained by the geomorphology suggesting such extreme events (that dominate the risk) are at the medium and low frequency end. However, current frequency of debris production is likely to be higher due to the disturbed nature of the rock masses. It may take many years for the frequency to drop back to pre-earthquake rates.	Factor of 1.1–1.5 uncertainty in the upward direction, but lower in the downward direction.
e. Ratio between the volume leaving the face and area of cliff top recessing.	Moderate uncertainty either way. However, ratios may increase as the rock masses become more disturbed as the earthquakes continue.	Factor of about 1.2 uncertainty in the upward direction, but lower in the downward direction.
f. Volume of debris travelling downslope and the number of boulders per m ³ of debris.	Quite well constrained and could be considerable but linked to the total volume of material leaving the slope.	Factor of about 1.4 uncertainty in the upward direction, but lower in the downward direction.
g. Occupancy (proportion of time people are at home)	Assumption of 100% occupancy instead of 67% would modestly increase the estimated risk.	Would increase by a factor of about 1.4.
h. Probability person killed if struck by debris.	Uncertainty potentially reducible but unlikely to make large difference – will always be fairly large given the volumes of debris involved or height of fall.	A change in the vulnerability from 70 to 100% would increase the risk by a factor of about 1.8.

The uncertainty in the risk estimated for dwelling occupants between scenarios A–C are shown graphically in the maps (Figure 39). The majority of the slope toe within the debris avalanche runout zone falls within the annual individual fatality risk of greater than 10^{-3} . The annual individual fatality risk in the distal runout zone changes between scenarios; in scenario A, a dwelling occupant in a particular area could be at risk of 10^{-3} or greater, but under scenario C the same person could be at risk of 10^{-5} , indicating significant uncertainty in the risk estimates at the distal margins of debris runout.

The risks to the pedestrian (the road user exposed to the highest level of risk) estimated for scenario A – the highest risk scenario – are comparable with or less than road accident risk.

7.0 REPORT CONCLUSIONS

7.1 HAZARD

The strength of the rock mass forming the slope at Richmond Hill has been reduced by earthquake-induced fractures and movement and it will continue to weaken over time due to factors such as physical and chemical weathering, wetting and drying and further ground movement. Failures, of volumes of rock greater than those that failed during the 2010/11 earthquakes, from the cliff are now more likely to be triggered by future earthquakes or by non-earthquake triggers such as rain. Failure volumes triggered by earthquakes may now be larger than any that fell during the 2010/11 Canterbury earthquakes; they could be more similar in size to past failures (from the same slope) identified from pre-1940 aerial photographs and pre-2010/11 earthquakes slope geometry.

7.2 Risk

7.2.1 Dwelling occupant

1. There are very few additional dwellings in the debris avalanche or cliff recession zones that do not already have “red zone” offers made by the Canterbury Earthquake Recovery Authority.
2. Earthquake-triggered cliff collapses contribute most to the risk.
3. The results show that the most critical uncertainty in the risk assessment is the volumes of material that could be generated at different bands of peak ground acceleration. There are approximately two orders of magnitude difference (a factor of 100 times) in the risk estimates between the upper and lower failure volume estimates (scenarios A and C respectively) in the distal ends of the risk zone.
4. The inclusion of the assessed local source areas 1–10 in the risk assessment increases the runout and hence the risk farther out from the toe of the slope.
5. The revised cliff-top recession risk maps show that the inclusion of local source areas 1–10 has also extended the cliff-top-recession risk zone further from the cliff edge.

7.2.2 Road user

1. The section of Richmond Hill Road at the cliff top in the assessment area is unlikely to be lost through cliff-top recession. However, further cracking and deformation of the road, retaining-wall failures and local small landslides (in loess/fill materials) could occur again in future earthquakes and affect the operation of the road.
2. For users of Wakefield Avenue, the rockfall risk increases directly with their time spent on the road and is greatest for the slowest road users (pedestrians, then cyclists), because slower travel exposes them to risk for longer on each journey.
3. The rockfall risk to road users has been compared with risk from road accidents for a journey of the same length on average New Zealand urban roads. The relativity between rockfall risk and road traffic accident risk is different for the different road user groups, in particular:

- a. For car drivers and pedal cyclists the rockfall risk is similar to the road accident risk;
- b. For car passengers the rockfall risk (assumed the same as for the driver) is higher than the road-accident risk (which is much smaller for car passengers than for drivers);
- c. For motorcyclists, the road-accident risk is greater than rockfall risk (because the former is so high); and
- d. For pedestrians, the rockfall risk on the side of the road closer to the slope (West) is comparable with or greater than road-accident risk, for Scenarios A (upper failure volume estimates) and B (middle failure volume estimates), but is comparable with or less than road-accident risk for Scenario C (lower failure volume estimates).
- e. The risks to the pedestrian (the user exposed to the highest level of risk) are substantially lower (typically by a factor of two or more) on the eastern side of Wakefield Avenue road compared to the western side.

8.0 RECOMMENDATIONS

GNS Science recommends that based on the results of this study, Christchurch City Council:

8.1 POLICY AND PLANNING

1. Decide what levels of life risk to dwelling occupants and road users will be regarded as tolerable.
2. Decide how Council will manage risk on land and roads where life risk is assessed to be at the defined threshold of intolerable risk and where the level of risk is greater than the threshold.
3. Prepare policies and other planning provisions to address risk lesser than the intolerable threshold in the higher risk range of tolerable risk.

8.2 SHORT-TERM ACTIONS

8.2.1 Hazard monitoring strategy

1. Include the report findings in a slope stability monitoring strategy with clearly stated aims and objectives, and list how these would be achieved, aligning with the procedures described by McSaveney et al. (2014). In the meantime, extend the current survey network (by increasing the number of slope monitoring marks) further up the slope (particularly into source area 1), so as to maintain awareness of changes in the behaviour of the slope.
2. Ensure that the emergency management response plan for the area identifies the dwellings that could be affected by movement and runout, and outlines a process to manage a response.
3. Although not assessed as part of this study, the slump (in loess – mass movement 3B), should also be routinely inspected to assess any potentially dangerous trends in its movement.

8.2.2 Risk monitoring strategy

Monitoring the slope for early warning of potentially dangerous trends in groundwater or slope movement as part of a hazard warning system is not recommended. Monitoring alerts for slope deformation and groundwater changes cannot be relied upon to provide adequate early warning as experience from Port Hills and elsewhere shows that deformation and groundwater changes can occur rapidly, with little warning.

8.2.3 Surface/subsurface water control

1. Reduce water ingress into the slopes, where safe and practicable to do so, by:
 - a. Identifying and relocating all water-reticulation services (water mains, sewer pipes and storm water) inside the identified mass-movement boundaries (at the slope crest) to locations outside the boundary, in order to control water infiltration into the slope. In particular, the broken household storm water pipes at the crest of the slope; and
 - b. Filling the accessible cracks on the slope and providing an impermeable surface cover to minimise water ingress.
2. These measures alone are not thought sufficient to address the risk and longer-term solutions should be explored.

8.2.4 Pavement closure

1. Maintain the closure of the pavement on the slope-side of the road, and continue to divert pedestrians onto the footpath on the other side of the road.
2. It is not known how effective the current temporary containers would be if impacted by a sizable debris avalanche (as per those discussed in this report). The effectiveness of such temporary risk management measures should be reassessed to ensure they are “fit-for-purpose”.

8.3 LONG-TERM ACTIONS

8.3.1 Engineering measures

1. Explore the technical cost and effectiveness of engineering solutions, for example (but not limited to) earth bunds (check dams) at the northern and southern ends of the site (along the western side of Wakefield Avenue) to prevent any debris from impacting the dwellings on the eastern side of Wakefield Avenue. Such works would require a detailed assessment and design and to be carried out by a certified person.
2. For the sections of Main Road within the risk zone, liaise with whoever is responsible for roading in this area to ensure that the debris avalanche risk is taken into account in any road design (or in the design of modifications to the road).

8.3.2 Reassessment

Reassess the risk and revise and update the findings of this report in a timely fashion, for example:

- a. in the event of any changes in ground conditions; or
- b. in anticipation of further development or land use decisions.

9.0 ACKNOWLEDGEMENTS

GNS Science acknowledges: Mark Yetton (Geotech Consulting Ltd.) for advice during the assessment. The authors also thank Nicola Litchfield, Mauri McSaveney, Danielle Mieler, and Rob Buxton (GNS Science) for reviewing this report; and Dr Laurie Richards, Dr Joseph Wartman and Tony Taig for their independent reviews.

10.0 REFERENCES

- Andres, N. 2010. Unsicherheiten von Digitalen Geländemodellen und deren Auswirkungen auf die Berechnung von Gletscherseeausbrüchen mit RAMMS (Dr. R. Purves, D. Schneider, Dr. C. Huggel)
- Ashford, S.A., Sitar, N. 2002. Simplified method for evaluating seismic stability of steep slopes. *Journal of Geotechnical and Geoenvironmental Engineering* DOI: 10.1061/(ASCE)1090-0241(2002)128:2(119).
- Australian Geomechanics Society 2007. Practice Note Guidelines for Landslide Risk Management. *Journal and News of the Australian Geomechanics Society* 42(1): 63–114.
- Barlow B., Niemirska M., Gandhi, R.P. 1983. Ten years of experience with falls from a height in children. *Journal of Paediatric Surgery* Volume 18:509.
- Bell, D.H., Trangmar, B.B. 1987. Regolith materials and erosion processes on the Port Hills, Christchurch, New Zealand: Fifth International Symposium and Field Workshop on Landslides. Lausanne, A.A. Balkema. Volume 1: 77–83.
- Bell, D.H., Glassey, P.J., Yetton, M.D. 1986. Chemical stabilisation of dispersive loessical soils, Banks Peninsula, Canterbury, New Zealand. *Proceedings of the 5th International Congress of the International Engineering Geological Society* 1: 2193–2208
- Bray, J.D., Rathje, E. M. 1998. Earthquake-induced displacements of solid-waste landfills. *Journal of Geotechnical and Geoenvironmental Engineering*. March 1998. pp. 242–253.
- Bray, J. D., Travasarou, T. 2007. Simplified procedure for estimating earthquake-induced deviatoric slope displacements. *Journal of Geotechnical Engineering and Environmental Engineering*. DOI: 10.1061/(ASCE)1090-0241(2007)133:4(381).
- Bunce, C.M., Cruden, D.M., Morgenstern, N.R. 1997. Assessment of the hazard from rock fall on a highway. *Canadian Geotechnical Journal* 34(3): 344–356.
- California, State of 1977. Analysis and Mitigation of Earthquake-Induced Landslide Hazards, Guidelines for Evaluation and Mitigation of Seismic Hazards in California, Division of Mines and Geology, California Department of Conservation Special Publication 117, Chapter 5, 15 p.
- Carey, J., Santanu, M., Bruce, Z., Barker, P. 2014. Canterbury Earthquakes 2010/11 Port Hills Slope Stability: Laboratory testing factual report. GNS Science report CR2014/53.
- Choi, W.K. 2008. Dynamic properties of Ash-Flow Tuffs. PhD Thesis, The University of Texas at Austin.
- Chopra, A.K. 1966. Earthquake effects on dams. PhD Thesis, University of California, Berkeley.
- Corominas J. 1996. The angle of reach as a mobility index for small and large landslides. *Canadian Geotechnical Journal* 33: 260–271.
- Craig, R.F. 1997. *Craig's Soil Mechanics*, 6th Edition, Spon Press, London.

- Cruden, D.M., Varnes, D.J. 1996. Landslide types and processes. *Landslide: investigation and mitigation*. Turner, K.A.; Schuster, R.L. (eds.). Special report, Transportation Research Board, National Research Council, 247. Chapter 3, 36–75.
- Dawson, E.M., Roth, W.H., Drescher, A. 1999. Slope stability analysis of by strength reduction. *Geotechnique* 122(6) 835–840.
- Della Pasqua, F.; Massey, C. I.; Lukovic, B.; Ries, W.; Archibald, G. 2014. Canterbury Earthquakes 2010/11 Port Hills Slope Stability: Earth/Debris flow risk assessment for Defender Lane. GNS Science Consultancy Report 2014/67. 109 p.+ Appendices
- Du, J., Yin, K., Nadim, F., Lacaqsse, S. 2013. Quantitative vulnerability estimation for individual landslides. *Proceedings of the 18th International Conference on Soil Mechanics and Geotechnical Engineering, Paris 2013*. pp. 2181–2184.
- Eurocode 8. EN1998-5. 2004. Design of structures for earthquake resistance Part 5: Foundations, retaining structures and geotechnical aspects.
- Finlay, P.J., Mostyn, G.R., Fell, R. 1999. Landslides: Prediction of Travel Distance and Guidelines for Vulnerability of Persons. *Proceedings of the 8th Australia New Zealand Conference on Geomechanics, Hobart*. Australian Geomechanics Society, ISBN 1 86445 0029, Vol 1, pp.105–113.
- Geotechnics Ltd. 2014. GNS Science, Port Hills Inclinometers, Christchurch. Job No. 720085.001/REP.
- Gerstenberger, M., Cubrinovski, M., McVerry, G., Stirling, M., Rhoades, D., Bradley, B., Langridge, R., Webb, T., Peng, B., Pettinga, J., Berryman, K., Brackley, H. 2011. Probabilistic assessment of liquefaction potential for Christchurch in the next 50 years. *GNS Science Report 2011/15*.
- Griffiths, G., Pearson, C., McKerchar, A.I. 2009. Review of the frequency of high intensity rainfalls in Christchurch. NIWA Client Report: CHC2009-139 for Christchurch City Council. 26 pp.
- Hoek, E. 1999. Putting Numbers to Geology – an Engineer’s Viewpoint. *The Second Glossop Lecture, Quarterly Journal of Engineering Geology* 32(1): 1–19.
- Holden, C., Kaiser, A., Massey, C. I. 2014. Broadband ground motion modelling of the largest M5.9+ aftershocks of the Canterbury 2010–2011 earthquake sequence for seismic slope response studies *GNS Science Report 2014*.
- Hynes-Griffin, M.E., Franklin, A.G. 1984. Rationalizing the seismic coefficient method. *Miscellaneous Paper No. G.L. 84-13, U.S. Army Engineer Waterways Experiment Station, Vicksburg, Mississippi*.
- Ishibashi, I., Zhang, X. 1993. Unified dynamic shear moduli and damping ratios of sand and clay. *Soils and Foundations* 3(1): 182–191.
- Jibson, R.W. 2007. Regression models for estimating coseismic landslide displacement. *Engineering Geology* 91: 209–218.
- Jibson, R.W., Keefer, D.K. 1993. Analysis of the seismic origin of landslides: Examples from the New Madrid Seismic Zone. *Geological Society of America Bulletin* 21: 521–536.
- Keefer, D.K., Wilson, R.C. 1989. Predicting earthquake-induced landslides, with emphasis on arid and semi-arid environments. *Proceedings of Landslides in a Semi-Arid Environment, Vol. 2, Inland Geological Society, Riverside, California*, pp. 118–149.
- Keylock, D., Domaas, U. 1999. Evaluation of topographic models of rockfall travel distance for use in hazard applications. *Antarctic and Alpine Research* 31(3): 312–320.

- Kramer, S.L. 1996. Geotechnical earthquake engineering. Prentice Hall, Upper Saddle River, New Jersey.
- Makdisi, F.I., Seed, H.B. 1978. Simplified procedure for evaluating embankment response. *Journal of Geotechnical Engineering Division. American Society of Civil Engineers* 105(GT12): 1427–1434.
- Massey, C.I., Della Pasqua, F. 2013. Canterbury Earthquakes 2010/11 Port Hills Slope Stability: Working Note 2013/04 on the interim findings from investigations into the Richmond Hill mass movement. GNS Science Letter Report CR2013/252LR
- Massey, C.I., McSaveney, M.J., Yetton, M.D., Heron, D., Lukovic, B., Bruce, Z.R.V. 2012a. Canterbury Earthquakes 2010/11 Port Hills Slope Stability: Pilot study for assessing life-safety risk from cliff collapse. GNS Science Consultancy Report 2012/57.
- Massey, C.I., Gerstenberger, M., McVerry, G., Litchfield, N. 2012b. Canterbury Earthquakes 2010/11 Port Hills Slope Stability: Additional assessment of the life-safety risk from rockfalls (boulder rolls), GNS Science Consultancy Report 2012/214.
- Massey, C.I., McSaveney, M.J., Heron, D., Lukovic, B. 2012c. Canterbury Earthquakes 2010/11 Port Hills Slope Stability: Pilot study for assessing life-safety risk from rockfalls (boulder rolls). GNS Science Consultancy Report 2011/311.
- Massey, C.I., Yetton, M.J., Carey, J., Lukovic, B., Litchfield, N., Ries, W., McVerry, G. 2013. Canterbury Earthquakes 2010/11 Port Hills Slope Stability: Stage 1 report on the findings from investigations into areas of significant ground damage (mass movements), GNS Science Consultancy Report 2012/317.
- McDowell, B.J. 1989. Site investigations for residential development on the Port Hills, Christchurch. MSc Thesis, University of Canterbury.
- McFadgen, B.G., Goff, J.R. 2005. An earth systems approach to understanding the tectonic and cultural landscapes of linked marine embayments: Avon-Heathcote Estuary (Ihutai) and Lake Ellesmere (Waihora), New Zealand. *Journal of Quaternary Science* 20(3): 227–237.
- McSaveney, M.J., Litchfield, N., Macfarlane, D. 2014. Canterbury Earthquakes 2010/11 Port Hills Slope Stability: Criteria and procedures for responding to landslides in the Port Hills, GNS Science Consultancy Report 2013/171.
- Moon, A.T., Wilson, R.A., Flentje, P. 2005. Developing and using landslide size frequency models. <http://ro.uow.edu.au/engpapers/384>.
- Morgenstern, N.R., Price, V.E. 1965. The analysis of the stability of general slip surface. *Geotechnique* XV(1): 79–93.
- Newmark, N. 1965. Effects of earthquakes on dams and embankments. *Geotechnique* 15: 139–160.
- New Zealand Geotechnical Society 2005. Field description of soil and rock. Guideline for the field classification and description of soil and rock for engineering purposes.
- New Zealand Transport Agency (NZTA), 2013. Bridge manual (SP/M/022). 3rd edition. July 2013.
- RAMMS, 2011. A modelling system for debris flows in research and practice. User manual v1.4 Debris Flow. WSL Institute for Snow and Avalanche research SLF.
- Revell, T., Pletz, Z. 2013. Richmond Hill Road Ground Investigation Report. Aurecon New Zealand Ltd. Rev 2. 12 July 2013.

- Schanbel, P.B., Lysmer, J. Seed, H.B. 1972. SHAKE; a computer program for earthquake response analysis of horizontally layered sites. Report No. EERC 72-12, University of California, Berkeley.
- Slope Indicator, 2005. Digitilt inclinometer probe. Data sheet. Geo Slope Indicator. <http://www.slopeindicator.com/pdf/digitilt-vertical-inclinometer-probe-datasheet.pdf>
- Slope/W, 2012. Stability modelling with Slope/W. An engineering methodology. November 2012 Edition. GEO-SLOPE International Ltd.
- Southern Geophysical Ltd., 2013. Geophysical investigation: Borehole shear-wave testing, Port Hills, Christchurch. Southern Geophysical Ltd. Report for GNS Science.
- Stirling, M., McVerry, G., Gerstenberger, M., Litchfield, N., Van Dissen, R., Berryman, K., Barnes, P., Wallace, L., Bradley, B., Villamor, P., Langridge, R., Lamarche, G., Nodder, S., Reyners, M., Rhoades, D., Smith, W., Nicol, A., Pettinga, J., Clark, K., Jacobs, K. 2012. National Seismic Hazard Model for New Zealand: 2010 Update. Bulletin of the Seismological Society of America 102: 1514–1542.
- Taig, T., Massey, C. 2014. Canterbury Earthquakes 2010/11 Port Hills Slope Stability: Estimating rockfall (boulder roll) risk for the road user along part of Wakefield Avenue. GNS Science Consultancy Report 2013/30.
- Tonkin and Taylor. 2012a. Christchurch Earthquake Recovery Geotechnical Factual Report Richmond Hill. Report prepared for the Earthquake Commission.
- Tonkin and Taylor 2012b. Christchurch Earthquake Recovery Geotechnical Factual Report Kinsey / Clifton. Report prepared for the Earthquake Commission. Ref 52010.0400.
- Wartman, J., Dunham, L., Tiwari, B., Pardel, D. 2013. Landslides in eastern Honshu induced by the 2011 Tohoku Earthquake. Bulletin of the Seismological Society of America 103: 1503–1521, doi: 10.1785/0120120128.
- Wieczorek, G.F., R.C. Wilson, Harp, E.L. 1985. Map showing slope stability during earthquakes in San Mateo County, California. Miscellaneous Investigations Map I-1257-E, U.S. Geological Survey.
- Yetton, M.D. 1992. Engineering Geological and geotechnical factors affecting development on Banks Peninsula and surrounding areas – Field guide. Bell, D.H. (ed.): Landslides - Proceedings of the Sixth International Symposium, Christchurch, 10–14 February 1992, Rotterdam, A.A. Balkema, Vol. 2(3).

APPENDICES

This page is intentionally left blank.

A1 APPENDIX 1: METHODS OF ASSESSMENT

A1.1 HAZARD ASSESSMENT METHOD

A1.1.1 Slope stability modelling

The purpose of the stability assessment was to determine the likelihood of cliff collapse of assessed source areas 1–10, under both static (non-earthquake) and dynamic (earthquake) conditions.

The key output from the static stability assessment is a factor of safety (the ratio between the driving and resisting forces in a slope) of the given source area and associated volume, while the key output from the dynamic assessment is the magnitude of permanent slope displacement of the given source area expected at given levels of earthquake-induced ground acceleration. These two assessments are then used to determine: 1) the likely local source volumes of material that could be generated under the different conditions; and 2) probability that they will be generated in an earthquake event.

A1.1.2 Static slope stability

If a slope has a static factor of safety of 1.0 or less, the slope is assessed as being unstable. Slopes with structures designed for civil engineering purposes are typically designed to achieve a long-term factor of safety of at least 1.5 under drained conditions, as set out in the New Zealand Transport Agency (NZTA) 3rd edition of the bridge manual (NZTA, 2013).

Static assessment of the slope was carried out by limit equilibrium method using the Rocscience SLIDE[®] software and the general limit equilibrium method (Morgenstern and Price, 1965). The failure surfaces were defined using the path search feature in the SLIDE[®] software, and a zone of tension cracks was modelled corresponding to mapped crack locations on the surface and in exposures. For the assessment, tension cracks depths were defined: 1) based on the relationship of Craig (1997), where the depth of tensions cracks was determined by the software in order to satisfy the thrust line verification method in the numerical model; and 2) based on field observations of cracks, where the tension cracks were thought to extend from the surface, downwards through the upper basalt lava and breccia and into the underlying trachy-basalt lava breccia.

Models were run based on geological cross-sections 1–7, representing assessed source areas 1–10. The critical slide surface was determined based on the lowest calculated factor of safety. Sensitivity of the slope factor of safety to different geotechnical material strength parameters (models 1–3), was carried out. These strength parameters were derived from in-house laboratory testing on samples of materials taken from the site, and samples of similar materials taken from other sites in the Port Hills (Carey et al., 2014) and published information on similar materials. Strength parameters were also assessed by back-analysis in the limit equilibrium and dynamic analyses.

The finite element modelling adopts the shear strength reduction technique for determining the stress reduction factor or slope factor of safety (e.g., Dawson et al., 1999). Finite element modelling was undertaken on the same cross-sections adopted for the limit equilibrium modelling assessment, using the Rocscience Phase² finite element modelling software. This was done to check the outputs from the limit equilibrium modelling, because the finite element models do not need to have the slide-surface geometries defined.

A1.1.3 Dynamic stability assessment (decoupled method)

In civil engineering, the serviceability state of a slope is that beyond which unacceptably large permanent displacements of the ground mass take place (Eurocode 8, EN-1998-5, 2004). Since the serviceability of a slope after an earthquake is controlled by the permanent deformation of the slope; analyses that predict coseismic slope displacements (permanent slope displacements under earthquake loading) provide a more useful indication of seismic slope performance than static stability assessment alone (Kramer, 1996).

The dynamic (earthquake) stability of the slope was assessed with reference to procedures outlined in Eurocode 8 (EN-1998-5, 2004) Part 5. For the Richmond Hill assessed source areas, the magnitude of earthquake-induced permanent displacements was assessed for selected cross-sections adopting the decoupled method and using different synthetic earthquake time-acceleration histories as inputs.

The decoupled seismic slope deformation method (Makdisi and Seed, 1978) is a modified version of the classic Newmark (1965) sliding block method that accounts for the dynamic response of the sliding mass. The “decoupled” assessment is conducted in two steps:

1. A dynamic response assessment to compute the “average” accelerations experienced at the base by the slide mass (Chopra, 1966); and
2. A displacement assessment using the Newmark (1965) double-integration procedure using the average acceleration history as the input motion.

The average acceleration time history is sometimes expressed as the horizontal equivalent acceleration time history (e.g., Bray and Rathje, 1998), but they are both the same thing. The average acceleration time history represents the shear stress at the base of the potential sliding mass, as it captures the cumulative effect of the non-uniform acceleration profile in the potential sliding mass. The method assumes that the displacing mass is a rigid-plastic body, and no internal plastic deformation of the mass is accounted for.

The two steps above are described below in more detail.

1. Dynamic response assessment:
 - a. Two-dimensional dynamic site response assessment using Quake/W was carried out adopting synthetic time acceleration histories for the four main earthquakes known to have triggered debris avalanches, cliff-top deformation and cracking in the Port Hills. The modelled versus actual displacements inferred from survey results and crack apertures were compared to calibrate the models.
 - b. Synthetic out-of-phase vertical and horizontal free-field rock-outcrop horizontal and vertical time acceleration histories for the site – at 0.02 second intervals for the 22 February, 16 April, 13 June and 23 December 2011 earthquakes – were used as inputs for the assessment (refer to Holden et al. (2014) for details).

- c. The equivalent linear soil behaviour model was used for the assessment, using drained conditions. Strain-dependent shear-modulus reduction and damping functions for the rock materials were based on data from Schanbel et al. (1972) and Choi (2008). For the loess shear modulus and damping ratio functions from Ishibashi and Zhang (1993) were adopted assuming a plasticity index of 5 (Carey et al., 2014) and variable confining (overburden) stress, based on the overburden thickness of the loess at each cross-section assessed.
 - d. Shear wave velocity surveys were carried out by Southern Geophysical Ltd. for GNS Science (Southern Geophysical Ltd., 2013). These works comprised the surveying of a surface-generated shear wave signal at 2 m intervals between the surface and the maximum reachable depth inside drillholes BH-MB-01 and BH-MB-02.
2. Displacement assessment steps:
- a. The dynamic stress response computed with Quake/W – from each input synthetic earthquake time history – were assessed using Slope/W Newmark function to examine the stability and permanent deformation of the slope subjected to earthquake shaking using a procedure similar to the Newmark (1965) method (detailed by Slope/W, 2012).
 - b. For the Slope/W assessment, a range of material strength parameters was adopted (models 1–3) for the rock, colluvium and loess as per those used in the static stability assessment. This was done to assess the sensitivity of the modelled permanent deformation of the slope to changing material strength.
 - c. For each trial slide surface, Slope/W uses: 1) the initial lithostatic stress condition to establish the static strength of the slope (i.e., the static factor of safety); and 2) the dynamic stress (from Quake/W) at each time step to compute the dynamic shear stress of the slope and the factor of safety at each time step during the modelled earthquake. Slope/W determines the total mobilised shear force arising from the dynamic inertial forces. This dynamically driven mobilised shear force is divided by the total slide mass to obtain an average acceleration for a given slide surface at a given time step. This average acceleration response for the entire potential sliding mass represents one acceleration value that affects the stability at a given time step during the modelled earthquake.
 - d. For a given trial slide surface Slope/W:
 - i. Computes the average acceleration corresponding to a factor of safety of 1.0. This is referred to as the yield acceleration. The critical yield acceleration of a given slide mass is the minimum acceleration required to produce movement of the block along a given slide surface (Kramer, 1996). The average acceleration of the given slide mass, at each time step, is then calculated along the slide surface (base of the slide mass).
 - ii. Integrates the area of the average acceleration (of the trial slide mass) versus time graph when the average acceleration is at or above the yield acceleration. From this it then calculates the velocity of the slide mass at each time interval during the modelled earthquake.
 - iii. Estimates the permanent displacement, by integrating the area under the velocity versus time graph when there is a positive velocity.

- e. To calibrate the results, the permanent displacement of the slide mass for a given trial slide surface geometry (for a given cross-section) was compared with crack apertures and survey mark displacements, and also with the geometry and inferred mechanisms of failure that occurred during the 2010/11 Canterbury earthquakes. Those soil strength parameters that resulted in modelled displacements of similar magnitude to the recorded or inferred slope displacements were then used for forecasting future permanent slope displacements under similar earthquakes.

A1.1.3.1 Forecasting permanent slope displacements

To forecast likely slope displacements in future earthquakes, the relationship between the yield acceleration (K_y) and the maximum (peak) acceleration (K_{MAX}) of the average acceleration of a given slide mass, was used. Using the results from the decoupled (Slope/W) assessment, the maximum average acceleration (K_{MAX}) was calculated for each selected slide surface (failure mass), from the average acceleration versus time plot – where the average acceleration versus time plot is the response of the given slide mass to the input acceleration history. The decoupled assessment uses the 22 February and 13 June 2011 synthetic earthquake acceleration histories, as inputs (Holden et al., 2014), and the calibrated material strength parameters derived from back-analysis (bullet 2. e. above).

The K_y/K_{MAX} relationship was used to determine the likely magnitude of permanent displacement of a given failure mass – with an associated yield acceleration (K_y) – at a given level of average acceleration within the failure mass (K_{MAX}).

Permanent co-seismic displacements were estimated for a range of selected trial slide surfaces from each cross-section. These results were then used in the risk assessment to assess the probability of failure of a given range of slide surfaces.

A1.1.3.2 Forecasting probability of failure

The probability that the source areas 1–10 would fail during a given earthquake event was based on the estimated amount of permanent displacement of the failure mass, estimated from the decoupled results. For this assessment, the term “fail” refers to a state where the magnitude of permanent displacement causes the given failure mass to break down, forming a mobile debris avalanche.

For this assessment the following assumptions were adopted:

- If the estimated displacement of the source is ≤ 0.1 m then the probability of catastrophic failure = 0, assuming that the source area is unlikely to fail catastrophically if permanent displacements are ≤ 0.1 m. This was based on measurements of slopes that underwent permanent displacement (i.e., cracking) but where the displacement magnitudes were < 0.1 m and where catastrophic failure did not occur.
- If the estimated permanent displacement of the source ≥ 1.0 m then the probability of catastrophic failure = 1. Meaning that the source area is likely to fail catastrophically if displacements are ≥ 1 m. This was based on the magnitudes of displacement inferred from crack apertures at the cliff tops in the Port Hills. Cumulative displacements at the cliff edge, inferred from crack apertures and survey displacements, tended not to exceed 1 m when measured up to the cliff edge. However, in these locations the cliff edge had fallen away, indicating failure at cumulative displacements of greater than 1 m.

- If the estimated permanent displacements are between 0.1 m and 1 m then the probability of failure (P) is calculated based on a linear interpolation between $P=0$ at displacements of 0.1 m, and $P=1$, at displacements of 1 m.

A1.1.4 Estimation of slope failure volumes

The most likely locations and volumes of potential failures were estimated based on the numerical analyses, current surveyed displacement magnitudes, material exposures, crack distributions and slope morphology.

Three failure volumes (upper, middle and lower) were estimated for each potential source area to represent a range of source volumes. The credibility of these potential failure volumes was evaluated by comparing them against: 1) the volumes of relict failures recognised in the geomorphology near the site and elsewhere in the Port Hills; 2) historically recorded failures; and 3) the volumes of material lost from the Richmond Hill slope and other similar slopes, during the 2010/11 Canterbury earthquakes.

There are four main sources of information on historical non-seismic failures for the Port Hills:

1. Archived newspaper reports (paperspast.natlib.govt.nz). Papers Past contains more than three million pages of digitised New Zealand newspapers and periodicals. The collection covers the years 1839–1945 and includes 84 publications from all regions of New Zealand;
2. The GNS Science landslide database, which is “complete” only since 1996;
3. Insurance claims made to the Earthquake Commission for landslips which are “complete” only since 1996; and
4. Information from local consultants (M. Yetton, Geotechnical Consulting Ltd. and D. Bell, University of Canterbury) which incompletely covers the period from 1968 to present (McSaveney et al., 2014).

A1.1.5 Debris runout modelling

The potential runout of debris from the local assessed source areas 1–10 was assessed empirically by the fahrboeschung method and also by numerical modelling. The potential runout of debris from the distributed sources was assessed empirically by the fahrboeschung methods.

1. Empirical fahrboeschung method:
 - a. The fahrboeschung model is based on a relationship between topographical factors and the measured lengths of runout of debris (Corominas, 1996). The fahrboeschung⁴ (often referred to as the “travel angle”) method (Keylock and Domaas, 1999) uses the slope of a straight line between the top of the source area (the crown) and the furthest point of travel of the debris. The analysis assumes the slope crest to be the crown of each potential source area.
 - b. For distributed source areas, the volume of debris passing a given location within the study area is based on the volumes of material that fell and passed a given fahrboeschung angle, at Richmond Hill, during the 22 February and 13 June 2011 earthquakes.

⁴ Fahrboeschung is a German word meaning “travel angle” adopted in 1884 by a pioneer in landslide runout studies, Albert Heim. It is still used in its original definition.

- c. For local assessed source areas 1–10, an empirical relationship established from a compilation of 45 slope sections through discrete debris avalanches that were triggered by the 22 February and 13 June 2011 earthquakes, was used to check the limits of debris runout estimated by the numerical model. This relationship was not used to proportion debris down the slope, as the numerical RAMMS model was used for this.
2. Numerical methods – RAMMS:
- a. Numerical modelling of landslide runout was carried out using the RAMMS® debris-flow software. This software, developed by the Snow and Avalanche Research Institute based in Davos, Switzerland, simulates the runout of debris flows and snow and rock avalanches across complex terrain. The module is used worldwide for landslide runout analysis and uses a two-parameter Voellmy rheological model to describe the frictional behaviour of the debris (RAMMS, 2011). The physical model of RAMMS Debris Flow uses the Voellmy friction law. This model divides the frictional resistance into two parts: a dry-Coulomb type friction (coefficient μ) that scales with the normal stress and a velocity-squared drag or viscous-turbulent friction (coefficient ξ).
 - b. RAMMS software takes into account the slope geometry of the site when modelling debris runout. The RAMMS model parameters were calculated from the back-analysis of 23 debris avalanches (ranging in volume from 200 to 35,000 m³) that fell from the slopes at Richmond Hill Road, Shag Rock Reserve and Redcliffs during the 22 February and 13 June 2011 earthquakes.
 - c. The modelling results give likely debris runout, area affected, volume, velocity and the maximum and final height of debris in a given location at any moment in the runout.
 - d. The RAMMS modelling uses a “bare earth” topographic model, and so the runout impedance of buildings and larger trees is not considered (other than incidentally in back-analysis).

A1.2 RISK ASSESSMENT

The risk metric assessed is the annual individual fatality risk from cliff collapse and this is assessed for dwelling occupants and users of Main Road within the assessment area. The quantitative risk assessment uses risk-estimation methods that follow appropriate parts of the Australian Geomechanics Society framework for landslide risk management (Australian Geomechanics Society, 2007). It provides risk estimates suitable for use under SA/SNZ ISO1000: 2009.

A1.2.1 Fatality risk to dwelling occupants

The risk is based on the annual individual fatality risk and is assessed for dwelling occupants. The risk includes the assessment of the fatality risk to an individual in a residential home from: 1) debris avalanches (derived from the cliffs); and 2) cliff-top recession. The risk method was similar to the one detailed by Massey et al. (2012a), but now includes the possibility of larger debris avalanches occurring from local assessed source areas 1–10 on the cliff, which because they are larger, could travel further down slope were they to occur.

Annual individual fatality risk is the probability (likelihood) that a particular individual will be killed by a cliff collapse in spending one year at their place of residence. For most localities this probability is a small number. The report therefore makes extensive use of the scientific number format of expressing risk in terms of powers of ten. For example, the number 10^{-4} (“10 to the power of minus 4”) is the fraction 1/10,000, and the decimal number 0.0001; it may also be expressed as 0.01%. The units of risk are dimensionless probability per unit of time and the units of annual fatality risk are probability of death per year.

To investigate the influence of uncertainties in the input parameters used in the risk model, three risk-assessment scenarios were examined. These scenarios were based on: 1) an upper, central and lower estimate of the volumes of material that could fall from the slope; and 2) the volume of that debris passing a given distance down the slope. The other parameters represented GNS Science’s “best” and “reasonable but more cautious” estimates based on the range of uncertainties identified in the available data at the time of writing. The results for each scenario were modelled using the ArcGIS programme to produce the contoured maps of risk.

For debris avalanches and cliff top recession the risk assessment comprised the following steps:

1. Divide the study area into a series of 2 m by 2 m grid cells.
2. Consider the possible range of triggering events (following the method of Moon et al., 2005) in terms of a set of earthquake triggers and a set of non-seismic (e.g., rain) triggers.
3. Choose a small set of representative events for each type of trigger spanning the range of event severity, from the lowest to the highest.
4. For each representative event, estimate:

For debris avalanches:

- a. the frequency of the event and the volume of material produced in that event ($P_{(H)}$)
- b. the proportion of debris reaching or passing a given grid cell and the probability of a person at that location being in the path of at least one of the boulders in the debris – the earthquake events include debris from both the randomly distributed sources and the local assessed source areas 1–10 ($P_{(S:H)}$)
- c. the probability that a person is present at a given location in their dwelling as the debris moves through it ($P_{(T:S)}$)
- d. the probability that a person is killed if present and in the path of one or more boulders within the debris ($V_{(D:T)}$)

For cliff-top recession:

- a. the frequency of the event and the area of cliff top lost ($P_{(H)}$)
- b. the proportion of cliff top lost at a given distance back from the cliff edge and the probability that one of the N square metres of cliff top is lost at that location ($P_{(S:H)}$) factoring in both randomly distributed failures and the local assessed source areas 1–10
- c. the probability that a person is present at a given location at the cliff top as the material falls ($P_{(T:S)}$)

- d. the probability that a person if present on an area of cliff top that falls is killed ($V_{(D:T)}$)
5. Multiply 4(a)–(d) for debris avalanche and cliff-top recession to estimate the annual individual fatality risk to individuals at different locations below the cliff or at the cliff top, contributed by each representative event.
6. Sum the risks from all events (4(a)–(d) separately for debris avalanche and cliff-top recession to estimate the overall risk.
7. Enter the risk value for each grid cell (a 2 m by 2 m grid was used in this study) into a GIS programme and interpolate between the risks estimated in each grid cell to produce contours of equal risk across the GIS map.

A1.2.1.1 Non-seismic events

Rates of debris avalanches and rockfalls triggered without earthquakes, mainly rain, were taken from Massey et al. (2012a). These rates were used to estimate the contribution to total risk from non-seismic triggering events. Four representative event-trigger frequencies were used and the volumes of the debris triggered by events with these frequencies were estimated using a series of steps (frequency was expressed as its inverse, i.e., as return period):

Step 1 – Estimate the trigger frequency of events of a given size that have occurred over a given time period for all sites using the available data. Four event return-period bands were used: 1) 1–14 years; 2) 15–99 years; 3) 100–1000 years; and 4) >1000 (nominally 1000–10,000 years).

Step 2 – Assume a conservative volume of $N \text{ m}^3$ per “typical” event in each band, assuming the same volumes per event for all cliffs.

Step 3 – Estimate the annual frequency of a given volume event occurring in each band.

A1.2.1.2 For seismic events

Debris avalanche volumes likely to be generated in an earthquake were determined from the relationship between the volumes of material leaving the cliffs during the 2010/11 earthquakes (per square metre of cliff face), and the calculated free field rock outcrop peak ground acceleration at the Richmond Hill site (Holden et al., 2014).

Step 1 – Estimate the volumes of material that could be generated at different levels of peak ground acceleration adopting seven event bands, that cover the range of peak ground accelerations from 0.01 to 3 g. For each band adopt a representative event, in terms of the volume generated, by taking the midpoint of each band, and the corresponding volume generated (adopting upper, middle and lower volume estimates based on the statistical range of the data).

Step 2 – for each representative event (volume of debris), calculate the annual frequency of the event occurring. The frequency of a given free field peak ground acceleration band occurring is obtained from the National Seismic Hazard Model. The increased level of seismicity in the Christchurch region is incorporated in a modified form of the 2010 version of the National Seismic Hazard Model (Stirling et al., 2012), which incorporates the now-increased probabilities of rupture for major faults in the region (Gerstenberger et al., 2011).

The risk assessment adopts the year 2016 seismic hazard model results, assuming “aftershocks”.

This differs from the previous cliff collapse assessment in Massey et al., 2012a), which used the year 2012 model results (these were the available results at the time of that report). At the instruction of Christchurch City Council, for the risk assessment in this report the year 2016 model results have been adopted to take into account the currently elevated seismic hazard, which is elevated above the 50-year average due to the 2010/11 Canterbury earthquakes.

The model results used in this assessment also include the contributions from all earthquakes, including earthquakes that follow a main earthquake (aftershocks). This differs from the seismic hazard model results adopted by the Canterbury Earthquake Recovery Authority for land zoning purposes, where contributions from aftershocks were removed. Aftershocks were removed because the Canterbury Earthquake Recovery Authority policy makers assumed that people would be evacuated after a large earthquake, and therefore would not be present in their dwelling, and not exposed to cliff collapses triggered by subsequent aftershocks.

GNS Science has assumed the year 2016 seismic hazard model results including contributions from all earthquakes (including aftershocks), as it is not the role of GNS Science to recommend an evacuation policy after a large earthquake.

Step 3 – Take into account the possibility of larger local failure of assessed source areas 1-10. To do this the total volume of debris generated in each band was partitioned between: 1) Random uniformly distributed failures of the cliff face comprising 40% of the total volume, that fall from anywhere on the slope; and 2) Local (non-random) failures comprising 60% of the total volume, corresponding to assessed source areas 1–10.

Step 4 – Calculate the probability of each assessed source area occurring based on the results of the decoupled assessment and the estimated amount of permanent slope displacement (detailed in previous section A1.1.2.3).

Step 5 – Check that the total combined volume of assessed source areas 1–10 is not less than or greater than the 60% of the total volume attributed to these failures per band. For all event bands the total volume of all the assessed sources 1–10 significantly exceeds the estimated total debris avalanche volumes produced in the band. Therefore the probability (P) of each source occurring is calculated such that $P \times$ total volume of all assessed sources associated with earthquake events (V) = the expected total volume from the sources per given band (Figure A1.1). Thus, the summed volume of the assessed source areas per band cannot exceed 60% of the total volume produced in that band. However, if the total volume of all assessed source areas associated with a given band is less than the total expected volume in that band, the difference in volume is partitioned back to the distributed failures (Figure A1.1).

Expanded calculation of P(each localised source occurring)		
Prob of source i occurring given an earthquake =	P_i	
Relative probability of source i occurring =	p_i	based on estimated Newmark displacement
Total volume anticipated, all sources =	V	
Volume of source i	V_i	
The requirement is that	$V = \sum P_i \cdot V_i$	(summed over all sources)
But	$P_i = C \cdot p_i$	where C is a constant
So	$V = C \cdot \sum p_i \cdot V_i$	

Figure A1.1 Expanded calculation of the probability of each local source area “scoop” occurring.

A1.2.1.3 Impact from debris avalanches

$P_{F(S:H)}$ is the probability of the debris reaching or passing a portion of slope as it travels downhill from the source area. The probability of one boulder hitting an object when passing through a particular portion of the slope, perpendicular to the boulder path, is expressed as:

$$P_{F1(S:H)} = \frac{(D + d)}{L} \quad \text{Equation 2A}$$

where D is the diameter of the design boulder (assumed to be 0.5 m) that travels along a path either side of d , within which the boulder cannot miss, d is the diameter of an object such as a person or width of a building, and L is the unit length of slope perpendicular to the runout path, in this case L is 2 m which corresponds to the 2 m by 2 m grid-cell width adopted for the risk assessment.

However, the debris leaving the cliffs during the 2010/11 Canterbury earthquakes predominantly consisted of a mass of boulder- and cobble-sized blocks that were not all equal in volume. The distribution of block sizes within the debris has been simply quantified by counting and measuring boulders within the debris at the toe of the cliff. Based on this assessment a volume of 0.07 m³ has been adopted, which is based on a 50th percentile boulder width of 0.5 m and assuming that boulders are spherical. This means that each cubic metre of debris comprises about eight boulders (taking into account the space between the boulders). For the assessment, a conservative estimate of 15 boulders per cubic metre of debris has been adopted. If it is assumed that each cubic metre of debris comprises about 15 boulders of 0.07 m³ in volume, then the probability of one cubic metre of debris hitting an object when passing through a particular portion of the slope is expressed as.

$$P_{F15(S:H)} = 1 - \left(1 - \frac{(D + d)}{L}\right)^{15} \quad \text{Equation 3B}$$

The probability of one cubic metre of debris formed of 15 boulders reaching/passing the same portion of slope increases as a function of the volume of debris travelling down the slope. The probability of one cubic metre of N cubic metres of debris hitting an object when passing through that same portion of slope is then given, by:

$$P_{FN(S:H)} = 1 - (1 - P_{F15(S:H)})^N \quad \text{Equation 3C}$$

For the purposes of risk estimation, it is necessary to have a quantitative measure of the size of a person. In this report, a “person” is assumed to be a cylinder of 1 m diameter and unspecified height (no specification of height was required in the model). The assumed value covers the order-of-magnitude range from about 0.3 m (vertical e.g., the person is standing) to about 3 m (horizontal, e.g., the person is lying down).

For randomly distributed sources, the volume of debris passing a given distance down the slope is taken from the empirical relationship. For the local assessed source areas 1–10 the debris is distributed using the numerical RAMMS model (refer to previous Section A1.1.2.5).

A1.2.1.4 Cliff-top recession

For cliff-top recession, the recession of the cliff edge is approximately proportional to the cube root of the volume lost from the cliff face. The relationship between the volume lost from the cliff face and the corresponding area of cliff top lost during the 2010/11 Canterbury earthquakes is reported in Massey et al. (2012a) for Richmond Hill/Wakefield Avenue, Shag Rock Reserve and Redcliffs. From these data the ratio of area lost per unit of volume leaving the cliff face is about of $0.016 \pm 0.001 \text{m}^2/\text{m}^3$ (at one standard deviation). That is, for every 100 m^3 of cliff face lost, about 1.6 m^2 ($\pm 6\%$) of cliff top area is expected to be lost. For this assessment, however, a ratio of 0.019 was adopted, which is the ratio plus two standard deviations (95% error limit).

A1.2.1.5 Falling due to cliff-top recession

$P_{R(S:H)}$ is the probability of a particular location at the cliff top falling and a person falling with it should they be present in that location when the cliff top falls. The probability of a person if present at the cliff top falling, given one metre of cliff top recessing, perpendicular to cliff edge, is expressed as.

$$P_{R1(S:H)} = \frac{(2D)}{L} \tag{Equation 3A}$$

where D is the approximate area occupied by a person at the cliff edge, assumed to be 1 m^2 , and L is the unit length of cliff parallel to the cliff edge.

The probability of a person falling is dependent upon the total area of cliff edge that collapses during a given event, and how close the person is to the outer edge, as the proportion of cliff top that collapses in any event decreases away from the cliff edge. Therefore the probability of a person falling if one square metre of N square metres of cliff top were to fall is given by:

$$P_{RN(S:H)} = 1 - (1 - P_{R1(S:H)})^N \tag{Equation 4B}$$

For randomly distributed failures triggered by earthquakes and for non-seismic failures (both are assumed to be randomly distributed along the cliff), the proportion of cliff top lost per metre back from the cliff edge is based on what happened to the cliff edge at Richmond Hill during the 2010/11 earthquakes (Massey et al., 2012a). For assessed source areas 1–10 the proportion of cliff top lost per metre back from the cliff edge is calculated from the geometry of the source areas, adopting the lower, middle and upper area estimates.

Although the most likely locations of sources 1–10 have been determined, it is possible that such failures could occur from elsewhere along the steep cliff face, especially as the rock mass, forming the slope, is now open and dilated. Therefore the risk estimates including the local source areas 1–3 have been distributed across the cliff top in the assessment area and not just in the locations of the assessed source areas 1–10.

A1.2.1.6 Probability of a person being present

$P_{(T:S)}$ is the probability an individual is present in the portion of the slope when a boulder moves through it. It is a function of the proportion of time spent by a person at a particular location each day and can range from 0% if the person is not present, to 100% if the person is present all of the time.

For planning and regulatory purposes it is established practice to consider individual risk to a “critical group” of more highly-exposed-to-risk people. For example, there are clearly identifiable groups of people (with significant numbers in the groups) who do spend the vast majority of their time in their homes – the very old, the very young, the disabled and the sick.

The assumption used in the risk assessment (contained in Massey et al., 2012b) for judging whether risk controls should be applied to individual homes was thus that most-exposed individuals at risk would be those who spend 100% of their time at home.

In other international rockfall risk assessments (e.g., Corominas et al., 2005), values ranging from 58% (for a person spending 14 hours a day at home) to 83% (for a person spending 20 hours a day at home), have been used to represent the “average” person and the “most exposed” person, respectively. However, in reality the most exposed person is still likely to be present 100% of their time.

For the land zoning assessments carried out by the Canterbury Earthquake Recovery Authority – with regards to rockfall and debris avalanche risk – their policy adopted an “average” occupancy rate, to assess the average annual individual fatality risk from rockfall across the exposed population in order to estimate the risk to the average person.

For this assessment, GNS Science has assessed the sensitivity of the risk assessment results to a range of values representing the most exposed and average person. It has been assumed that the most exposed person spends 100% of their time at home, and that an average person spends on average 16 hours a day at home ($16/24 = 0.67$ or 67%).

When a person is at home they tend to spend more time in their home than in their garden. Whilst in their home they cannot occupy every part of it at the same time. To proportion the person across their home, GNS Science has assumed that Port Hills homes have a footprint area (assuming a single story dwelling) of $A_F = 100 \text{ m}^2$. The probability that a person will be occupying a given area within their home at any one time can be expressed as:

$$P_{(T:S)} = \frac{(0.67)}{(A_F / P_A)} \quad \text{Equation 4}$$

Where 0.67 (67%) is the proportion of time an average person spends in their home and P_A is the area of home occupied by a person at any one time. For this assessment, GNS Science has adopted the area of the grid used for the risk assessment, in this case a 2 m by 2 m (4 m^2) grid-cell to represent P_A . Therefore the probability of person being present in a given grid cell within their home is assumed to be 0.03 (3%) for the average person.

A1.2.1.7 Probability of the person being killed if hit or falling

This is the probability of a person being killed if present and either in the path of one or more boulders or on an area of cliff top that falls. Vulnerability (V) depends on the landslide intensity, the characteristics of the elements at risk, and the impact of the landslide (Du et al., 2013).

This probability is expressed as vulnerability, the term used to describe the amount of damage that results from a particular degree of hazard. Vulnerability ranges between 0 and 1 and for fatality risk represents the likelihood of an injury sustained by the individual being fatal (1) and the possibility of getting out of the way to avoid being struck.

Studies from Hong Kong (e.g., Finlay et al., 1999) summarised the vulnerability ranges and recommended likelihood of death “if struck by rockfall”. The vulnerability of an individual in open space if struck by a rockfall is given as 0.1–0.7, with a recommended value of 0.5, assuming that it may be possible to get out of the way. For people in homes, it would be unlikely that a person would be able to take evasive action as they would not see the boulder coming. However, this argument is counterbalanced by the level of protection a house may provide by stopping a boulder from entering it, but conversely, flying debris (shrapnel) inside a house may contribute to injury.

Data on homes damaged in the cliff-collapse areas of the Port Hills indicate they were struck by many boulders, and in some cases the building collapsed. Finlay et al. (1999) recommend using a vulnerability of 1.0 if a person is in a building and if the building is hit by debris and collapses, or is inundated with debris. However, Du et al. (2013) propose vulnerability ranges from 0.24 for timber buildings to 0.45 for masonry buildings indicating that somebody is more likely to survive in a timber building that has collapsed.

At Redcliffs one person was killed in their home when it was struck by many hundreds of boulders, which caused it to collapse and another person was hit by boulders and killed whilst in their garden. In other parts of the Port Hills, including one at Richmond Hill, a further three people died when they were buried by many boulders while outside.

The “landslide intensity” related to a debris avalanche is a function of the numbers of boulders passing through a given location and their velocity. In this risk assessment the probability of being in the path of one or more of N boulders within the debris (should a person be present) has been calculated separately as $P_{(S:H)}$.

Debris velocities derived from RAMMS model outputs are typically >5 m/s for most of the runout areas assessed. However, the velocity rapidly drops to <0.05 m/s in the distal limits of runout over a relatively short distance of several metres. These calculations are similar to field observations made from video footage although, some boulders within the distal debris fringe (mainly individual boulders) travelled at higher velocities, i.e., “fly rock”. Fly-rock may occur when moving blocks impact and fracture resulting in high velocity rock fragments being released (Figure A1.2).

The two-dimensional rockfall modelling (Appendix 9) suggests that boulder velocities in the distal runout zone are still in the range of about 3–5 m/s and not < 0.5 m/s as suggested by RAMMS. Such velocities are more consistent with field observations. At these boulder velocities, of about 5 m/s (18 km/hr), it is unlikely that a person could get out of the way of a boulder (Australian Geomechanics Society, 2007).



Figure A1.2 Debris avalanche at the northern end of Richmond Hill site triggered by the 22 February 2011 earthquakes. **A)** Photograph looking west across Wakefield Avenue – note debris in the foreground and some debris has been cleared from the road. **B)** Photograph looking east from Wakefield Avenue, opposite photograph A) showing fly-rock debris. Photographs taken by M. Yetton.

Based on these results, a constant vulnerability factor of 70% has been adopted for this risk assessment as it was the factor adopted by the Canterbury Earthquake Recovery Authority (CERA) for the previous risk assessments. A constant vulnerability value is thought reasonable as the velocity of the boulders, even in the distal runout zone are still relatively high with people unlikely to be able to get out of the way. The protective effects of buildings have not been taken into account, this is because most people killed by falling boulders during the 22 February 2011 earthquake were outside and therefore not protected by buildings. However, it is noted that buildings do have a sheltering effect as only 45% of buildings hit by boulders were penetrated (Massey et al., 2012c).

For a person falling from a cliff, the severity of injury increases with the height of fall, but it also depends on the age of the person, nature of the impact surface and how the body hits the surface. The chance of surviving increases if landing on a surface that can deform, such as snow or water. In a study by Barlow et al. (1983), the height at which 50% of children die from a fall is between 12 and 15 m. The cliffs in this study range from 40 to 70 m in height and the nature of the surface onto which a person would fall is boulder size debris formed of rock. Taking all these considerations into account, for this study, $V_{(D:T)}$, the probability of being killed if a person is on an area of cliff that falls, is assumed to be 0.7 as there might be a chance that a person could get away from the edge of the cliff before it falls.

A1.3 ROAD-USER RISK ASSESSMENT

The risk to road users has been expressed in multiple terms including: 1) annual individual fatality risk, based on an assumed number of trips per year; and 2) the risk per trip, for different types of road user mainly car occupant, motor cyclist, pedal cyclist and pedestrian. The risk method is similar to the one detailed in Taig and Massey (2014), but now also includes the possibility of non-random larger debris avalanches occurring at specific locations on the site.

Road users are susceptible to multiple hazards in the event of debris avalanches:

1. Direct impact of rockfall onto them or their vehicles;
2. Crashing into rockfall debris on the road, or crashing (into other vehicles that stop or swerve violently) while trying to avoid rockfall debris;
3. Being carried away in the collapse of a roadway during cliff-top recession or falling into an area of missing roadway.

For Wakefield Avenue at the toe of the slope, only the first two hazards are considered. The fourth is not relevant as there is no cliff below Wakefield Avenue at any point along the road length in question.

For Richmond Hill Road at the crest of the site, the fourth hazard is the only one that is relevant, although much of the road is on the limit of the study area and therefore unaffected by this hazard.

Road-user risk can be assessed for:

- a. motor-vehicle occupants (only occupants of light vehicles are considered, as there is little commercial or bus traffic along the stretch of road of interest);
- b. motorcyclists;
- c. cyclists; and
- d. pedestrians;

The event tree model used for assessment of risk is shown in Figure A1.3.

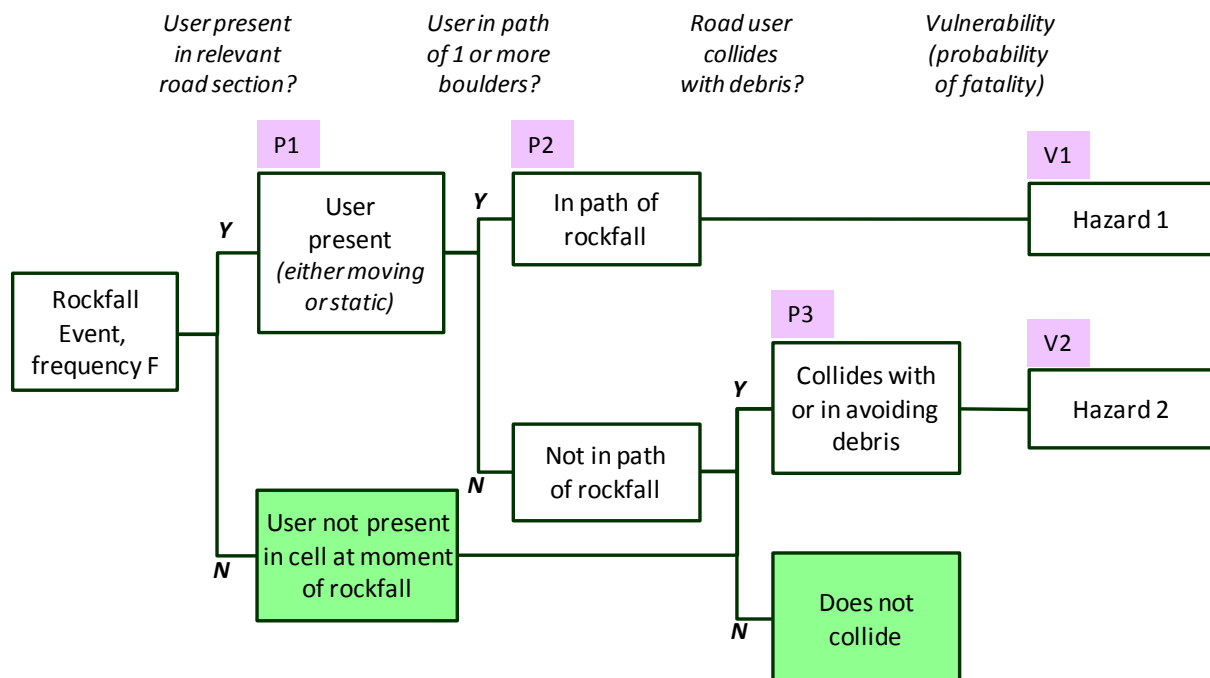


Figure A1.3 Event tree model for road user risk assessment – Wakefield Avenue.

The risk assessment methodology used here is developed from that described in the companion report (Taig and Massey, 2014). A summary of the derivation of the key input probabilities P_1 to P_3 , V_1 and V_2 is given in Section A1.4.

The assumptions used in estimating parameters for different road users in order to calculate the risk per single journey along the road are shown in Tables A1.1 and A1.2. The road traffic accident statistics used in estimating values for P_3 (the stopping time for a road user) and V_2 (the probability of death in the event of a road user collision with another object) are presented, based on the latest available road accident statistics. For parameter P_3 a threshold of 0.2 boulders per cell was used: above this value the probability of a collision for a road user within one stopping time/distance of rockfall debris on the road is assumed to be 1, below that value it is assumed to be zero.

Table A1.1 Derivation of key event tree parameters.

Parameter	Definition	Value/Formula	Basis of calculation
P ₁	Years per journey that road user is present within relevant cell, per single journey	$P1 = (\text{time in hours in cell per jny}) / (\text{hrs per yr}),$ $= (L/v) / (365.25 \times 24)$ where $v = \text{speed (m/hr)}$ $= V \times 1000$ PLUS annual time spent stationary / no. journeys	Time spent within cell length L metres, given average speed of travel V kph plus any time spent stationary (per year, divided by no. of journeys)
P ₂	Probability that a road user, if present within a given cell, will be in the path of one or more boulders in the event of a rockfall incident	$P2 = 1 - (1-P)^N, (N \geq 1)$ or $P2 = N.P (N < 1)$, where $P = \text{prob in path of 1 boulder passing through cell, and}$ $N = \text{no. boulders passing thru cell in given scenario}$ <i>(calculated for each cell individually)</i>	Basis is that probability of NOT being in the path of each of N boulders is 1-P. In turn $P = (d+D)/L$ (or 1 if $d+D > L$)
P ₃	Proportion of year per journey for which road user is in situation where collision occurs, = (Years per journey that road user is within safe braking distance of cell) x (Probability collision occurs if within safe braking distance)	$P3 = \text{Braking factor (time required to safely stop vehicle)}$ $\times \text{Collision Factor (P collision if within stop distance \& debris present)}$ $\times \text{Debris factor (1 if debris present > M boulders, 0 otherwise for each source)}$	If a road user is more than the stopping distance/time ahead of debris at the time it lands on road, collision is unlikely (though swerving may still be possible)
V ₁	Probability of death if in path of one or more boulders	Simple assumptions (compatible with those used in dwelling risk assessments)	Car user assumed to have minimal chance of avoiding boulders, but reasonably significant chance that impact with some parts of car will not be fatal
V ₂	Probability of death if collide with (or in swerving to avoid) rockfall debris on road	Derived from road traffic accident statistics for different types of collision with different objects	Based on NZ statistics on the proportion of collisions with different types of object (cars) or of different types of motorcycle accident, that are fatal, plus UK statistics on the % of cyclist injury accidents not involving motor vehicles that are fatal.

Table A1.2 Assumptions used in quantifying road user risk event tree.

Parameter	Definition	Road user	Key inputs	Key input values		Key output values		Important Assumptions
				V km/hr - lower risk	V km/hr - higher risk	P1 - lower risk	P1 - higher risk	
P ₁	Years per journey that road user is present within relevant cell, per single journey	Car occupant	Ave speed V kph	50	35	4.56E-09	6.52E-09	a) Time spent stationary on Wakefield Ave is insignificant - traffic is light and free-moving. b) V is constant along the length of the road. Appropriate for pedestrians & cyclists, but motor traffic may be slower at N end of Wakefield Ave.
		Motorcyclist		50	35	4.56E-09	6.52E-09	
		Cyclist		25	15	9.13E-09	1.52E-08	
		Pedestrian		4	2.5	5.70E-08	9.13E-08	
		Bus passenger		N/A	N/A	N/A	N/A	
				Effective road user diameter D (m)		P(in path of single boulder)		
				lower risk	higher risk	lower risk	higher risk	
P ₂	Probability that a road user, if present within a given cell, will be in the path of one or more boulders in the event of a rockfall incident	Car occupant	Effective road user diameter D metres	1	2	0.75	1.00	Rockfall behaves as a random set of discrete boulders of a given diameter.
		Motorcyclist		1	2	0.75	1.00	
		Cyclist		1	2	0.75	1.00	
		Pedestrian		0.5	1	0.50	0.75	
		Bus passenger		N/A	N/A	N/A	N/A	
				Stopping time t (seconds)		P3 when rockfall debris present		
				lower risk	higher risk	lower risk	higher risk	31557600 seconds/yr
P ₃	Proportion of year per journey for which road user is in situation where collision occurs, = (Years per journey that road user is within safe braking distance of cell) x (Probability collision occurs if within safe braking distance)	Car occupant	Stopping time t seconds	2.08	3.98	6.60E-08	1.26E-07	See Appendix A1.4 for derivation (linked to V above). Optimistic in ignoring swerving/collision with other object; Pessimistic in ignoring extra warning time seeing rockfall before reaches road
		Motorcyclist		1.82	3.48	5.75E-08	1.10E-07	
		Cyclist		1.41	3.12	4.47E-08	9.90E-08	
		Pedestrian		0	0	0	0	
		Bus passenger		N/A	N/A	N/A	N/A	
						V1 - lower risk	V1 - higher risk	
V ₁	Probability of death if in path of one or more boulders	Car occupant	Motorcyclist assumed to have greater vulnerability than car user, but similarly low chance of avoiding boulders.			0.2	0.3	For cyclists & pedestrians greater vulnerability offset by significant chance of seeing/hearing rockfall in time to avoid
		Motorcyclist				0.4	0.8	
		Cyclist				0.3	0.7	
		Pedestrian				0.3	0.7	
		Bus passenger				N/A	N/A	
						V2 - lower risk	V2 - higher risk	
V ₂	Probability of death if collide with (or in swerving to avoid) rockfall debris on road	Car occupant	The NZ statistics used are for urban roads so should represent the sort of ranges of speeds relevant to Wakefield Avenue.			1.4E-02	0.0E+00	No allowance is made for the possibility either a) of swerving into oncoming vehicles (would tend to increase V2) or b) of the time available from first seeing the rockfall/debris to take safe evasive action (would tend to reduce V2)
		Motorcyclist				0.0E+00	0.0E+00	
		Cyclist				1.1E+02	0.0E+00	
		Pedestrian				0.0E+00	0.0E+00	
		Bus passenger				N/A	N/A	

Note: Cells shaded gold are user input assumptions.

The parameters shown in Table A1.2 are uncertain and if anything are considered to err on the side of caution (overestimating risk) for Hazard 2 (the “crash into or in avoiding debris on road” hazard). As in our previous work on road user risk from rockfall, inputs and outputs are presented as ranges from “reasonable lower” to “reasonable upper” values. No statistical significance is attached to these ranges; the results are regarded as providing a sensible range, given the associated uncertainties, within which decision makers should assume the actual risk might lie.

The event tree is evaluated for each cell in the grid for each rockfall scenario considered, based on a number of boulders calculated as the ratio of the volume of rock passing through the cell (from RAMMS output) to average boulder volume (based on the assumption of average boulder size of 0.5m diameter). The grid used was simplified relative to that used in modelling dwelling risk by excluding cells that did not form part of the roadway in order to streamline the calculation process; in all other respects the rockfall modelling used to estimate individual road-user risk was identical to that used to estimate individual dwelling occupant risk.

As in the dwelling occupant assessment, the set of scenarios modelled covers:

- Seven seismic trigger scenarios ranging from 0.1–0.3 g PGA up to 3 g PGA, each characterised by: 1) a series of non-random large debris avalanches at specific locations constituting 60% of the total volume per event; and 2) random debris avalanches distributed uniformly across the entire length of the Richmond Hill site constituting the remaining 40% of the total volume per event;
- Four non-seismically triggered rockfall scenarios (corresponding to different severities of weather-induced rockfall).

As in the dwelling-occupant assessment, contributions to the probability of death per journey from seismic triggers were calculated separately for each cell for the local and the distributed rockfall scenarios. These were then combined to calculate an overall probability of death from each seismic hazard scenario for both hazards (the “hit by falling rock” and “crash into/while avoiding fallen rock” hazards) using the formula

$$P_{overall} = 1 - (1 - P_{hazard1}) \times (1 - P_{hazard2}) \quad \text{Equation 5}$$

The overall risk per journey contributed by each cell is then calculated as the sum of (frequency of triggering event scenario) x (probability of death per journey if the triggering scenario occurs) for all seven seismic and four non-seismic event triggers.

A1.4 ROAD USER RISK ASSESSMENT ILLUSTRATION

The calculational process is illustrated for a single grid cell and seismic event in Table A1.3 (hazard 1) and Table A1.4 (hazard 2). Table A1.5 then shows how various risk outputs of interest are calculated from the probabilities per journey for individual cells and for the whole length of road.

Table A1.3 Calculation process for risk from hazard 1 (single cell, per journey).

Example Calculation:	R1 - Risk from Hazard 1 (hit by falling rocks)					
Grid Cell no. 29805 (cell width L = 2m)						
Seismic scenario	Band 2, 0.3 to 0.5g PGA					
Contributing sources	Localised sources 1 & 2, plus distributed sources					
Formula for R1: =	F x P₁ x P₂ x V₁					
<i>where</i>						
F = frequency of Band 2 EQ =	0.032153 events per year					
P ₁ = time in cell/journey	from table XX2 (road user dependent)					
V ₁ = P _{death if in path of 1+rocks}	from table XX2 (road user dependent)					
P ₂ = P _{in path of 1 or more rocks}	from all sources (cell & scenario dependent, see below)					
Calculation of P2					Notes/Formulae	
Boulders passing	Source 1	Source 2	Distributed sources			
Volume rockfall passing, m ³	0.648	1.173	0.000833	V, from RAMMS		
Equivalent no. 0.5m boulders	9.90	17.92	0.0127	N = V / (4/3 π r ³)		
<i>which is combined with</i>						
P(in path of single boulder)	lower	upper				
Car	0.75	1.00	P _{one} = (d+D)/L (see Tables XX1 & XX2)			
Motorcycle	0.75	1.00				
Pedal cycle	0.75	1.00				
Pedestrian	0.50	0.75				
<i>to calculate</i>						
P(in path of 1 or more of N boulders, if source triggered)	Source 1	Source 2	Distributed sources	Upper value only shown		
Car	1	1	0.012733	for N>1		
Motorcycle	1	1	0.012733	P _N = 1 - (1 - P _{one}) ^N		
Pedal cycle	1	1	0.012733	for N<1		
Pedestrian	0.999999	1	0.00955	P _N = N.P _{one} (see Table XX1)		
<i>which is combined with</i>						
P(source triggered)	0.444	0.278	1.000	in Band 2 earthquake		
<i>to calculate, for sources individually, then in combination</i>						
P₂ = P(in path of 1 or more of N boulders - UPPER, Band 2 EQ)	Source 1	Source 2	Distributed sources	P2 (Any Source)		
Car	0.444	0.278	0.013	0.6039	P _(any source) = 1 - (1 - P _{source1}) x (1 - P _{source2}) x (1 - P _{sourceN}) etc.	
Motorcycle	0.444	0.278	0.013	0.6039		
Pedal cycle	0.444	0.278	0.013	0.6039		
Pedestrian	0.444	0.278	0.010	0.6026		
<i>this can now be combined with the other parameters to calculate R1</i>						
Calculation of R1	F	P_{1, upper}	P_{2, upper}	V_{1, upper}	R1_{upper}	R1 is dimensionless, P(death per journey)
Car	0.032153	6.5E-09	0.6039	0.3	3.8E-11	
Motorcycle	0.032153	6.5E-09	0.6039	0.8	1.0E-10	
Pedal cycle	0.032153	1.5E-08	0.6039	0.7	2.1E-10	
Pedestrian	0.032153	9.1E-08	0.6026	0.7	1.2E-09	

Table A1.4 Calculation process for risk from hazard 2 (single cell, per journey).

Example Calculation:	R2 - Risk of crashing into (or in avoiding) rockfall debris on road					
Grid Cell no. 29805 (cell width L = 2m)						
Seismic scenario	Band 2, 0.3 to 0.5g PGA					
Contributing sources	Localised sources 1 & 2, plus distributed sources					
Formula for R2: =	F x P₃ x V₂					
<i>where</i>						
F = frequency of Band 2 EQ =	0.032153 events/year					
P ₃ = time/journey within which collision will occur	= Debris factor x Collision Factor x Braking Factor (see below)					
V ₂ = P(death if collision occurs)	from table XX2 (road user dependent)					
Calculation of P3					Notes/Formulae	
(a) Debris factor	Source 1	Source 2	Distributed			
Boulders on or passing the road	9.90	17.92	0.0127	Debris factor = (1 if > 0.2 boulders on or passing road, 0 otherwise) x P(source triggered in Band 2 EQ)		
Debris factor if source triggered	1	1	0			
P(source triggered)	0.444	0.278	1.000			
Debris factor for each scenario	0.444	0.278	0.000			
Overall Debris factor	0.599			Overall debris factor = 1 - (1-P _{source1}) x (1-P _{source2}) x (1-P _{distrib sources})		
(b) Collision factor						
Current assumptions	0.500	for all road users except pedestrians			See text for derivation	
(c) Braking factor	lower	upper				
Car	2.08	3.98	= braking time (seconds) (see text & Appendix X for derivation)			
Motorcycle	1.82	3.48				
Pedal cycle	1.41	3.12				
Pedestrian	0.00	0.00				
<i>Combination of (a) x (b) x (c) (converted from seconds to years) gives P3 values as follows</i>						
P3 values	Debris factor	Collision factor	Braking factor (upper)	P_{3,upper}	Upper values only shown	
Car	0.599	0.500	3.98	3.78E-08	Note: braking factor is converted to years in order to use P3 with annual event frequencies to calculate R2	
Motorcycle	0.599	0.500	3.48	3.30E-08		
Pedal cycle	0.599	0.500	3.12	2.97E-08		
Pedestrian	0.599	0.000	0.00	0.00E+00		
<i>this can now be combined with the other parameters to calculate R2</i>						
Calculation of R2	F	P_{3, upper}	V_{2, upper}	R2_{upper}	R2 is dimensionless, P(death per journey)	
Car	0.032153	3.8E-08	0.0100	1.2E-11		
Motorcycle	0.032153	3.3E-08	0.0250	2.7E-11		
Pedal cycle	0.032153	3.0E-08	0.0170	1.6E-11		
Pedestrian	0.032153	0.0E+00	0.0000	0.0E+00		

Table A1.5 Calculation of risk parameters of interest from single cell risk per journey

Aggregation of Risk Parameters for Cells			
(a) Risk per journey			
Risk R_{ij} for road user j within cell i =	$R1_{ij} + R2_{ij}$		
Risk R_j per journey to road user j =	sum of R_{ij} for all relevant i (all cells on uphill side or downhill side of road, as appropriate)		
(b) Other key risk parameters			
Annual Individual Fatality Risk for user j	$= R_j \times M_{j,ind}$	$M_{j,ind} =$ Journeys/year by individual heavy road user of type j	
Average expected fatalities per year, user j	$= R_j \times M_{j,tot}$	$M_{j,tot} =$ Journeys/year by ALL road users of type j	
Probability of 1 or more fatal accidents/year (road user type j)	$= P_j = 1 - (1-R_j)^{M_{j,tot}}$		
Probability of 1 or more fatal accidents/year (among ALL road users)	$= 1 - (1-P_{car}) \times (1-P_{motorcycle}) \times (1-P_{cycle}) \times (1-P_{pedestrian})$		

Because the road is significantly wider than a single gridcell, gridcells were tagged on the uphill (closer to Richmond Hill) and downhill side of the road. The risk per journey is then aggregated for each side of the road, enabling the risk to be compared for journeys on either side, though it is noted that the pavement has now been closed on the uphill side so all pedestrian journeys should now involve the downhill side of the road.

As for the dwelling risk assessment, the calculations were repeated for three sets of rockfall scenarios to explore sensitivity to the key issue of how far rockfall will reach out from the slope toe. Scenario B uses central estimates of debris volume and runout. Scenario A uses upper estimates of debris volume and runout, while scenario C uses lower estimates of debris volume and runout.

Current New Zealand road traffic accident statistics were used to provide comparison information on the risk road users would face in their ordinary travel up and down Wakefield Avenue for a journey of the same length (540 m) as that covered in the risk assessment model.

A1.5 ROAD USER RISK – ADDITIONAL DISCUSSION ON MAIN ASSUMPTIONS

The parameters used in quantifying the event tree described in the main report, and the values or models appropriate for Wakefield Avenue, are briefly discussed in turn. Throughout, tables highlight in yellow the key user input assumptions which can readily be altered in our risk assessment model to explore sensitivities and uncertainties.

P_1 – proportion of a year which a road user spends in an individual model cell, per journey

The average time at risk for a road user is simply the distance travelled (in this case 2 m is the length of each cell) divided by the average journey speed (converted into appropriate units). In calculating risk, P_1 is to be converted into a risk per journey by multiplying by the initiating event frequency. Thus if that frequency is expressed in events per year, P_1 needs to be expressed as a proportion of a year (then years/journey x events/year = events/journey).

For roads in general the average journey speed needs to take into account both “normal” journeys when traffic flows smoothly, “congested” journeys where there is some speed reduction, and “delay events” when traffic is actually stopped. The impact of journey delay is greatest for motorised road vehicles; for pedestrians traffic congestion has minimal impact. In some cases it may be possible reliably to estimate the average journey time, taking all these factors into account. In others it may be appropriate to estimate the proportion of journeys falling into each category (normal, congested, subject to a delay event) and the journey time associated with each.

For Wakefield Avenue, though, where the road is straight, traffic is relatively light and it would be unusual to encounter significant delay at any point along the stretch of road of interest, the possibility of even quite significant delays is considered to be well covered by the range of average road user speeds we have assumed for the whole stretch of road (e.g., for car users we have considered a range of speeds from 35 to 50 km/hr, the latter corresponding to the speed limit on the road and, in the authors’ personal experience, to the general average speed travelled by cars there, and the former corresponding perhaps to a more cautious driver who encounters some delays at junctions along the route). The full set of average speeds used to quantify P_1 , and the P_1 values that result, are shown in Table A1.6.

Table A1.6 Average journey speeds and resulting values of P_1 (= 2m/speed converted to metres/year).

Road User	V km/hr – lower risk	V km/hr – higher risk	P_1 – lower risk	P_1 – higher risk
Car occupant	50	35	4.56E-09	6.52E-09
Motorcyclist	50	35	4.56E-09	6.52E-09
Cyclist	25	15	9.13E-09	1.52E-08
Pedestrian	4	2.5	5.70E-08	9.13E-08

P_2 – Probability a road user is in the path of one or more boulders, should a rockfall triggering event occur

As in previous studies (Taig and Massey, 2014) this is calculated from the assumed effective dimensions of road users and of boulders, and from the modelled flux of boulders into/through each cell.

A key difference between this work and our previous studies in this area is that the smallest road section lengths we have considered previously have been large in comparison with the potential target road users/vehicles. In this report, the RAMMS model has been used with 2 m square gridcells, which is of the same order as the size of a car or motorcycle, and only a factor of two greater than the assumed effective collision diameter of a pedestrian or cyclist. This significantly affects the validity of our approximate model for the probability of a potential target object being in the path of one or more rocks in the event of a rockfall, represented by the equations:

$$P_1 = (d+D)/L \quad \text{Equation 6}$$

and

$$P_2 = P_N = 1 - (1-P_1)^N \quad \text{Equation 7}$$

where

P_1 is the probability of a target object of effective diameter d being in the path of a single boulder of diameter D travelling randomly through a space of cross-slope width L , and

P_N ($= P_2$ in the event tree) is the probability of the target object being in the path of one or more boulders, if N boulders travel randomly through the same space.

There are two complications once $(d+D)$ becomes comparable with or larger than L . First, equation (A1) needs to be modified; this is done here by truncating P_1 to 1 if equation (6) suggests a value larger than 1⁵. Second, equation (7) provides a good approximation for $N < 1$ so long as P_1 is small, but no longer does so when P_1 becomes close to 1. In the limit, once $P_1 = 1$ (i.e., it is inevitable that the target will be within the path of a single boulder passing through the cell), equation (A7) would predict a certainty of the target being in the path of one or more boulders even when the number of boulders was zero.

For $N > 1$ equation (A7) remains valid for large values of P_1 , but for values of $N < 1$ it is modified to:

$$P_N = N \times P_1 \quad \text{Equation 8}$$

⁵ Strictly speaking a second modification should be introduced to account for the areas within a cell within which the target can avoid a rock (e.g., if a rock diameter 1 m falls with its centre down one side boundary of a cell of width 2 m, there is a 0.5 m space within which the centre of a 1 m diameter target can lie without being in the path of the boulder). This is compensated for by the contribution to the target being struck by boulders whose centres fall within cells either side. If the boulder flux is equal in the cells either side then equation (6) remains valid. Given the small number of cells within which there are large differences in boulder flux between adjacent cells it was not considered worthwhile introducing the major calculational complexity of modifying equation (6) and adding in contributions from boulders “in” adjacent cells – in the worst case this may introduce about a 25% error for an individual cell; averaged across all cells the error is considered likely to be at most a few %, which is tiny in comparison with the other uncertainties in the assessment.

Effectively, this means that a predicted rockfall volume passing through a cell which is a fraction of a single boulder is treated as though it were a single boulder, but with probability of arising in the cell equal to that fraction.

Values of P_2 are calculated for each possible rockfall source (for an earthquake event this means 10 possible local rockfall sources, and a distributed source assumed equally scattered along the whole length of the route). The overall value of P_2 for each seismic event scenario is then calculated as

$$P_2 = 1 - (1 - P_{N,source1} \times P_{source\ 1\ triggered}) \times (1 - P_{N,source2} \times P_{source\ 2\ triggered}) \times (1 - P_{N,source3} \times P_{source\ 3\ triggered}) \dots \text{(etc, to include all possible sources)} \quad \text{Equation 9}$$

A good way to visualise this combination is that for a road user NOT to be in the path of any source, they must not be in the path of rockfall from source 1, or from source 2, or source 3 (etc., etc).

P_3 – Probability of road user collision with (or in swerving to avoid) fallen rockfall on the road.

This is calculated as the product of three factors:

- a debris factor;
- a collision factor; and
- a braking factor.

The **debris factor** is a simple yes/no (1 or 0) factor corresponding to whether significant debris is present in the cell in question. This is modelled very simply as being 1 if the number of boulders in a cell is less than a user-defined threshold and zero otherwise. A threshold of 0.2 boulders is used in the calculations presented here; although this might present little hazard of itself, the primary concern is that even a very modest amount of rockfall appearing ahead of a road user could cause sudden braking and swerving, which is our primary concern in relation to this hazard. The results are in any case insensitive to the value of this parameter as the vast majority of risk is contributed by cells that are quite heavily inundated with rockfall.

The collision factor corresponds to the probability that the road user will experience a collision (either with the rockfall debris or with something else in swerving to avoid that debris), if they are within one braking distance of the rockfall debris when it appears on the road. The assumptions here are that for relevant road users the probability of collision varies as follows:

- at greater than 1 braking distance away, the probability is zero;
- at zero distance away when the rockfall lands on the road, the probability is 1; and
- the probability rises linearly from 0 to 1 with the time between the road user being one braking distance away and being zero distance away when the rockfall lands on the road.

The simple effect of these assumptions is that on average the probability of a collision occurring for relevant road users is 0.5 (the average of 0 at 1 braking distance and 1 at zero distance). This probability is assumed to apply to all road users except pedestrians, for whom this hazard is not considered significant in that both: 1) they can stop virtually instantly so are unlikely to walk into a boulder that has not struck them; and 2) if they were to walk into a boulder they would be very unlikely to suffer fatal injury.

There are numerous assumptions built into this calculation of P_3 . It is conservative (tends to overestimate P_3 and thus risk) in that it takes no account of road users' ability to see or hear boulders coming towards the road and take evasive action either before or after they come within a braking distance of the debris. It is also conservative in that the official estimates of braking times and distances that have largely been used to derive values here are generally based on conservative assumptions about the braking capacity of vehicles – many modern motor vehicles will be able to brake safely within shorter times/distances (this has been taken into account to some extent in our selection of the range of values between 'upper' and 'lower' estimates for braking times). On the other hand it may be optimistic (tends to underestimate P_3 and thus risk) in that it takes no account of being struck by another road user coming the other way, and assumes that road users within one braking distance of debris may have a reasonable chance of managing to brake and steer so as to avoid collision.

The values of P_3 resulting from this discussion are shown in Table A1.7.

Table A1.7 Stopping times and values of P_3 (when rockfall debris present on road).

Road User	Stopping time t (seconds)		P3 when rockfall debris present	
	lower risk	higher risk	lower risk	higher risk
Car occupant	2.08	3.98	3.30E-08	6.30E-08
Motorcyclist	1.82	3.48	2.88E-08	5.51E-08
Cyclist	1.41	3.12	2.24E-08	4.95E-08
Pedestrian	0	0	0.00E+00	0.00E+00

The stopping times are derived from estimates of a reasonable range of accelerations likely under braking, derived from published data and recommendations on braking distances and times, as summarised in Table A1.8A (general points and cars) and Table A1.8B (motorcycles and cycles).

Table A1.8A Derivation of stopping times for cars (+ general points).

General Points							
<i>Stopping distance/time is the sum of Thinking Time + Braking Time</i>							
<i>Note throughout that because risk is dominated by Hazard 1, "higher risk" and "lower risk" scenarios are defined throughout as those which maximise time at risk of impact from rockfall i.e. lower speed = higher risk scenario</i>							
<i>Within each scenario, "higher risk" for P3 corresponds to slower braking times</i>							
(a) Cars							
UK Highway Code Guidance							
20	ft	braking distance on dry road at		20	mph		
		with braking distance increased by factor of		2	in wet		
Corresponds to	6.10	metres from speed of	8.94	m/sec			
Which is equivalent to	6.56	m/s/s, or	0.6683901	g			
Adaptation to Modern NZ Conditions							
1. Thinking time of 2/3 second is used in UK Highway Code; can be 1-2 seconds but most people will manage 2/3s or better; consider range up to 1.5s							
2. UK Highway Code guidance (box above) is based on 1960's braking performance. Most modern cars can manage 1g or close to it on good roads (acceleration expressed as multiple of g, acceleration due to gravity)							
CONCLUSION							
Use range from	0.4	(worse) to	1	g, better for braking acceleration			
	1.5	(worse) to	0.667	s, better, for thinking time			
Resulting Speed vs Stopping Time Estimates (range used shown red-green)							
Speed (kph)	Thinking Time		Braking Time (sec)		Stopping time (sec)		Speed m/s
	lower	higher	lower	higher	lower	higher	
15	0.666667	1.5	0.42	1.06	1.09	2.56	4.17
20	0.666667	1.5	0.57	1.42	1.23	2.92	5.56
25	0.666667	1.5	0.71	1.77	1.37	3.27	6.94
30	0.666667	1.5	0.85	2.12	1.52	3.62	8.33
35	0.666667	1.5	0.99	2.48	1.66	3.98	9.72
40	0.666667	1.5	1.13	2.83	1.80	4.33	11.11
45	0.666667	1.5	1.27	3.19	1.94	4.69	12.50
50	0.666667	1.5	1.42	3.54	2.08	5.04	13.89

Table A1.8B Derivation of stopping times, motorcycles and pedal cycles.

(b) Motorcycles
 Useful general source on motorcycle braking: <http://www.bikesafer.com/detail/braketime.html>

Key Points relative to Cars

- Thinking/response time shorter as hands/foot already in situ on handgrip/brake pedal
 see e.g. "Evaluation of brake reaction times on a motorcycle",
 Report no. FMQ-BRT 0.154, Promocycle Foundation, Montreal, 2003.
- Braking performance based on published ranges
 see e.g. "Performance evaluation for various braking systems of street motorcycles"
 Promocycle Foundation, Montreal, 2003

Range of g in dry: 0.4 (worse) to 1 (better)
 Range of g in wet: 0.4 (worse) to 0.75 (better)

CONCLUSION
 Use range of braking performance as above (red to green, worse to better)
 Reduce car thinking times to 1 s (worse) to 0.4 s (better)

Resulting Speed vs Stopping Time Estimates (range used shown red-green)

Speed (kph)	Thinking Time		Braking Time (sec)		Stopping time (sec)		Speed m/s
	lower	higher	lower	higher	lower	higher	
15	0.4	1	0.42	1.06	0.82	2.06	4.17
20	0.4	1	0.57	1.42	0.97	2.42	5.56
25	0.4	1	0.71	1.77	1.11	2.77	6.94
30	0.4	1	0.85	2.12	1.25	3.12	8.33
35	0.4	1	0.99	2.48	1.39	3.48	9.72
40	0.4	1	1.13	2.83	1.53	3.83	11.11
45	0.4	1	1.27	3.19	1.67	4.19	12.50
50	0.4	1	1.42	3.54	1.82	4.54	13.89

(c) Pedal Cycles
Key Points relative to motorcycles

- Reaction times assumed to be similar to those for motorcycles (hands already in situ on brakes)
- Most pedal cycles will have brakes significantly less good than those on motorcycles

CONCLUSIONS
 Braking performance in range 0.2 g (worse) to 0.7 g (better)
 Thinking time in range 1 s (worse) to 0.4 s (better)

Resulting Speed vs Stopping Time Estimates (range used shown red-green)

Speed (kph)	Thinking Time		Braking Time (sec)		Stopping time (sec)		Speed m/s
	lower	higher	lower	higher	lower	higher	
15	0.4	1	0.61	2.12	1.01	3.12	4.17
20	0.4	1	0.81	2.83	1.21	3.83	5.56
25	0.4	1	1.01	3.54	1.41	4.54	6.94
30	0.4	1	1.21	4.25	1.61	5.25	8.33

V₁ – Probability of death if in the path of one or more boulders.

The probability of death depends on two factors:

- a. whether the road user is able to avoid the rockfall, despite being in its path; and
- b. the severity of injury if the rockfall cannot be avoided and strikes the vehicle or road user themselves.

As regards ability to avoid the rockfall, people on foot may well be able to hear and see rockfall before it reaches the road; the ability of people outdoors to take evasive action in the event of rockfall is well documented (refer to the discussion in the main text of the report on vulnerability). This ability should if anything be enhanced for a long straight road with good visibility such as Wakefield Avenue, where Richmond Hill to the West is the dominant visual feature of the landscape. Several respondents in a survey of the experience of residents of Port Hills red-zoned homes during the 22 February 2011 earthquake mentioned taking evasive action in response to hearing or seeing boulders approaching, and at least one person definitely saved their life by dodging boulders as they rolled downhill⁶.

Relative to pedestrians or cyclists, motor vehicle users are disadvantaged when it comes to hearing rockfall coming. They may of course feel ground movement in the event of an earthquake-induced rockfall event, but may not immediately associate this with the possibility of rockfall.

When it comes to surviving impact with one or more boulders, the positions of the car occupant and the pedestrian or cyclist are reversed. The “vulnerable road user” in road safety terms is also highly vulnerable to rockfall. On the other hand the car occupant may benefit from either or both of a) boulders striking a part of the vehicle other than that which is occupied, or b) some degree of protection from the vehicle structure.

The ability of car occupants to survive rockfall impact, and the conditions which are more or less lethal, are illustrated by a small survey of recent incidents (since 2010) carried out in a day via Google searching globally (in English) and in French and German for combinations of the terms “(motorist, cyclist, pedestrian), (killed, near miss), (rock, rockfall, rockslide)” from which incidents involving impact of one or more boulders with a road user or their vehicle could be identified. The set of relevant incidents identified is presented in full in Table A1.9.

⁶ “Survey of the experience of residents of Port Hills properties red-zoned for slope collapse during the 22 February 2011 earthquake”, Marian Taig et al, GNS Report in preparation

Table A1.9 Some recent incidents of rockfall contacting road (and track) users.

Incident No.	Road User Type	Date	Location	Circumstances	N fatal	N inj	N OK	Source
1	Car occupant	27/01/2014	nr Keremeos, Canada	3 cars struck by boulders in major rockfall on Highway 3 (not landslide inundation - clearly discreet boulders many in range 0.5-2m across). 1 driver hospitalised, others walked away.		1	2	http://www.cbc.ca/news/canada/british-columbia/b-c-rock-slide-survivor-2-seconds-close-to-not-being-here-1.2515400
2	Car occupant	03/01/14	nr Autouste, Pyrenees France	Pregnant woman killed when 0.5 te boulder fell onto car. Husband (driving, sitting next to her) was unhurt.	1		1	http://www.leparisien.fr/aquitaine/pyrenees-un-rocher-s-ecrase-sur-une-voiture-une-femme-enceinte-tuee-03-01-2014-3459597.php
3	Car occupant	18/10/2013	Tahiti	Small rock fell from cliff onto footpath, narrowly missing 2 children and struck a car; no-one injured.			2	http://www.ladepeche.pf/article/faits-divers-justice/un-rocher-secrase-pres-de-deux-enfants-et-finit-sur-une-voiture
4	Pedestrian	30/09/2013	nr Buena Vista, Colorado	5 out of 6 members of family hiking in the hills were killed by a massive rockslide; one teenager survived (thought to have been sheltered by her father from worst of impact, though was trapped under boulders)	5	1		http://edition.cnn.com/2013/09/30/us/colorado-hikers-rockslide/
5	Car occupant	31/08/2013	Taiwan	"Giant boulder hit car" headlines - actually driver swerved to avoid rockfall & was stationary when boulder toppled almost onto the car but then rocked back. Front & side of car crushed by multiple smaller flying rocks. (Video on "photos" link)			1	http://www.mirror.co.uk/news/weird-news/video-watch-moment-motorist-narrow-2241819
6	Car occupant	02/04/2013	Sausalito, California	Motorist drove through rockslide (numerous small boulders typically <= 0.5m max length); car suffered significant damage (all 4 tyres blown out) but motorist unhurt			1	http://www.marini.com/ci_23384119/101-motorist-escapes-injury-sausalito-rockslide
7	Car occupant	18/12/2012	Montréal-la-Cluse, Nantua, France	Three rocks, one of 2 meters in diameter, were detached from the cliff. One came crashing into the windshield of a car traveling on the main road. The injured driver was described as "more frightened than hurt". Traffic was stopped for more than a quarter of an hour. Note the accident happened around 6pm when it would have been quite dark.			1	http://www.leprogres.fr/faits-divers/2012/12/19/nantua
8	Car occupant	06/06/2012	Chongqing, Southwest China	5 cars destroyed, 3 people injured by 2 massive boulders falling onto road (it appears from press photos that several of the cars impacted were parked/empty)			3	http://usa.chinadaily.com.cn/china/2012-06/08/content_15488314.htm
9	Car occupant	02/03/2012	Ain, France	200 te rockfall killed a motorist in his car and destroyed the front of a house	1			http://videos.tf1.fr/jt-we/2012/un-automobiliste-tue-par-la-chute-d-un-rocher-dans-l-ain-7035165.html
10	Car occupant	25/01/2012	Arly Gorge, Savoie, France	Mitsubishi Shogun crushed by 20te rock; driver amazingly survived - was trapped & injured but not life-threateningly so.			1	http://www.leparisien.fr/lyon-69000/un-rocher-de-20-tonnes-s-ecrase-sur-sa-voiture-le-miracle-temoigne-09-02-2012-1853248.php
11	Car occupant	22/02/2010	Abingdon, VA, USA	Couple's car roof crushed by falling rocks; no injury			2	http://www.wjhl.com/story/20801477/rock-fall-near-abingdon-hits-car-sending-passengers-to-emergency-room

This survey provides good anecdotal corroboration of our expectations based on common sense, in particular:

1. Impact of a large boulder or mass of boulders directly onto the part of a vehicle occupied by a person is generally fatal (incidents 2 and 9, plus numerous earlier reports of accidents, e.g., in Réunion where 20 deaths from rockfall have occurred on one highway over the past 30 years)⁷.
2. Impacts of smaller boulders onto vehicles are seldom fatal (incidents 3, 11).
3. Vehicle occupants can often survive impacts of large boulders if these strike vehicle parts away from the passenger compartment (incidents 1, 7, 8).
4. Vehicle occupants can sometimes survive even large boulder impacts with the passenger compartment (incidents 2, 7, 10).

Motorcyclists get the worst of both worlds – they are both disadvantaged in their ability to hear rockfall coming relative to pedestrians and cyclists, and are similarly vulnerable (though they will typically be wearing head protection, the hazard of losing control in the event of rock impact is significantly more dangerous for faster moving vehicles).

Our conclusions as to the relative capability of different road users a) to avoid and b) to survive impacts should they find themselves in the path of one or more boulders are summarised in the graphic below (Figure A1.4).

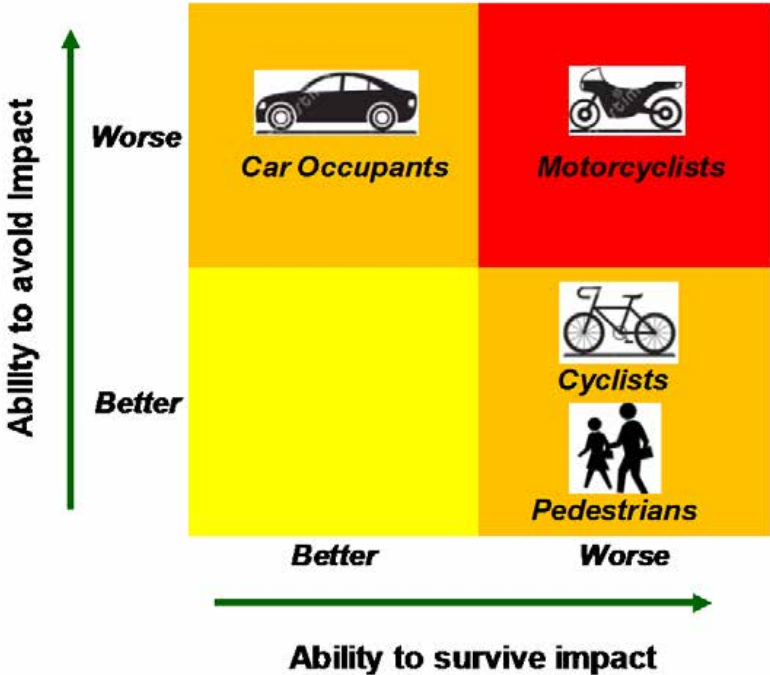


Figure A1.4 Overview of vulnerability factors for road users in path of rockfall.

The earlier report (Taig and Massey, 2014) used conservative values for the probability of a car occupant in particular being killed if their vehicle was struck by a boulder, in the range 0.5 to 0.7. After further consideration prompted by comments on that report and the discussion above, we would ideally like to adopt vulnerability values for car occupants that were dependent on the volume of rock/number of boulders passing through a given area. In the

⁷ See for example <http://forums.infoclimat.fr/topic/14228-eboulement-meurtrier-a-la-reunion/>

absence of good evidence on which to build a relationship between V_1 and magnitude of rockfall affecting the road user, we have adopted simple constant values, somewhat less conservative in comparison with those used in Taig and Massey (2014), as shown in Table A1.10. The value for car occupants is now closer to those used in earlier studies by other authors (e.g., Bunce et al., 1997).

Table A1.10 Vulnerabilities adopted for road users in path of rockfall.

Road User	V1 – lower risk	V1 – higher risk
Car occupant	0.2	0.3
Motorcyclist	0.4	0.8
Cyclist	0.3	0.7
Pedestrian	0.3	0.7

V₂: Probability of death in collision with (or in avoiding) rockfall debris on road

It has not been possible to collect substantial experience of collisions between road vehicles and rockfall debris in the course of this project, though incidents 5 and 6 in Table A1.9 above illustrate the possibility both of driving safely through/over substantial numbers of rocks on a road, and of swerving benignly to avoid rockfall.

In the absence of directly relevant data, and recognising that the risk associated with swerving to avoid debris will be highly location-dependent, this probability is estimated by comparison between road user collision with rockfall debris, possible accidents that might occur whilst swerving to avoid rockfall, and collisions with other New Zealand objects on and around the road. The New Zealand Ministry of Transport publishes statistics⁸ on:

- a. The proportion of all motor vehicle crashes that involve injury; and
- b. The proportion of all injury crashes that are fatal, broken down by different categories of collision target (cars) or collision type (motorcycles).

The approach used is as follows:

1. Estimate the proportion of car and motorcycle crashes that involve injury from NZ MOT data

FOR CARS

2. Rank collision targets in terms of their overall lethality (proportion of injury collisions that are lethal)
3. Compare rockfall debris and objects on and around Wakefield Avenue with the collision targets for which NZ MOT data is available and select a sub-set of those targets considered representative of typical potential collisions with or avoiding rockfall debris specifically on Wakefield Avenue
4. Informed by (3), decide a range of probabilities of injury collisions being lethal that should be applied to rockfall debris and/or objects with which a car might collide while swerving to avoid such debris (specific to Wakefield Avenue).

⁸ <http://www.transport.govt.nz/research/roadcrashstatistics/motorvehiclecrashesinnewzealand/motor-vehicle-crashes-in-new-zealand-2012/>

5. Multiply the proportion of car crashes involving injury by the proportion of injury crashes that are lethal to estimate the proportion of all car crashes that are lethal.

FOR MOTORCYCLES

6. Repeat steps 2–5 using corresponding motorcycle collision types (a smaller and less detailed set of information than is available for cars, reflecting the smaller numbers of motorcycles on the road).

FOR CYCLES

7. Estimate the proportion of injury accidents to cyclists NOT involving collision with a motor vehicle that were fatal (based on research for the UK Department for Transport), and the proportion of overall NZ cycling collisions that involve injury, and combine these as for cars and motorcycles to estimate the proportion of all cyclist collisions with objects other than motor vehicles that are likely to be fatal.
8. Compare this with the probability of a cyclist encountering one of the most lethal possible objects – a motor vehicle travelling in the opposite direction, to form a judgment as to the overall probability of a cyclist being killed in ANY collision with, or in swerving to avoid, rockfall debris.

The approach throughout relies on judgment and estimation informed by the New Zealand road accident statistics rather than pretending that there is any precise relationship between observations on other types of road collisions and those anticipated with (or in avoiding) rockfall debris. The significant possibility of road users taking some form of evasive action to mitigate collision impacts in the event of rockfall is not considered, which means that the estimated lethality of collisions with (or in avoiding) rockfall are likely to be generally conservative (over, rather than under-estimated). In the context of Wakefield Avenue a further pessimism built into this analysis is that the lethality of motor vehicle crashes increases rapidly with speed; the national aggregate data will certainly include a significant proportion of incidents involving much higher speeds than are travelled on Wakefield Avenue.

The first step in the process is to estimate the proportion of collisions that are lethal. MoT data was aggregated for 2000–2012 to produce the high-level breakdown of motor vehicle crashes shown in Table A1.11.

Table A1.11 Proportion of motor vehicle crashes involving injury.

Averages for 2000-2012 inclusive						
No. of Crashes*				No. of Casualties		
Fatal	Serious	Minor	Non-injury	Fatal	Serious	Minor
347.7	1965.4	8075.3	26191.2	396.5	2426.1	11388.5
* Note: a "crash" is a collision accident involving a motor vehicle of some sort (so include motorcycle collisions but not cycle-only or cycle/pedestrian accidents)						
Proportion of all crashes that are fatal =				0.95%		
Proportion of all crashes that are injury crashes =				28.40%		
Assumed proportion for CARS				25%		
Assumed proportion for MOTORCYCLES				50%		

Just under 1% of all crashes involve fatality, while just over 28% of crashes involve injury. It has been assumed that the proportion of motorcycle crashes involving injury will be significantly higher than that for four-wheeled vehicles. Thus the assumed proportion of crashes involving injury for cars has been rounded down from 28.4% to 25%, while the proportion of crashes involving injury for motorcycles has been estimated at twice this figure (50%).

Table A1.12 shows data aggregated for the years 2010, 2011 and 2012 to estimate the proportion of all injury crashes that are fatal. The upper table uses the NZ MOT classification of target objects, organised in descending order of lethality (averaged over all roads, as shown in the bold column towards the right of the table), and allocating a VH/H/M/L ranking to each object type. The lower table then shows the aggregated average lethality for those VH, H, M and L groupings of objects.

“Debris on the road” is one of the MOT categories which is clearly in the “low risk of fatality” group. While the debris involved in the MOT statistics may be less dramatic than a major rockfall incident, the lethality of collision with any sort of rockfall would be expected to be small, given the relatively low speeds on Wakefield Avenue and the major advances in vehicle crashworthiness that have been achieved in recent decades – only a very small proportion of motorists in modern vehicles are killed in road crashes at speeds of 50kph and below.

An important issue to be considered is “What else might a vehicle encounter if the driver swerves to avoid rockfall?” In this respect Wakefield Avenue is a relatively benign environment – there are no large drops, or water courses running alongside the road, or railways or bridges. The shaded portion of Table A1.11 represents the area considered more relevant to Wakefield Avenue.

Our judgment overall is that the lethality of objects which might be collided with on Wakefield Avenue in driving into (or swerving to avoid) rockfall debris on the road would be likely to lie somewhere in a range from the upper end of the “Low Risk” group of targets, to the lower end of the “High Risk” group of targets (in each case using statistics for urban roads, rather than for roads in general). We have accordingly adopted a range from 2% to 4% of injury accidents considered lethal. Multiplying by 25% of crashes that involve injury gives us a range from 0.5% to 2% of all car collisions in these circumstances that might prove lethal.

Table A1.11 Lethality of injury collisions with NZ MOT categories of target object.

Lethality Summary (in decreasing order of overall lethality, all roads)

Objects Struck	Urban Roads			Open Roads			Overall			Lethality Category	Lethality Index
	Overall	In Darkness	Not in Darkness	Overall	In Darkness	Not in Darkness	Overall	In Darkness	Not in Darkness		
Driven or accompanied animals	100.0%	0.0%	0.0%	0.0%	0.0%	0.0%	33.3%	0.0%	100.0%	VH	4
Into water river or sea	20.0%	25.0%	12.5%	11.2%	12.5%	10.2%	13.0%	15.9%	10.6%	VH	4
Train	5.9%	0.0%	9.1%	21.4%	33.3%	18.2%	12.9%	11.1%	13.6%	VH	4
Bridge or approach rails	5.0%	5.0%	5.0%	10.3%	11.1%	9.9%	9.0%	9.2%	8.9%	VH	4
Over bank or cliff	7.2%	5.2%	9.2%	7.4%	9.0%	6.5%	7.3%	8.0%	6.9%	H	3
Tree	3.9%	4.6%	3.0%	7.7%	8.6%	7.0%	6.0%	6.6%	5.5%	H	3
Slip washout or flood	0.0%	0.0%	0.0%	6.7%	0.0%	15.4%	5.7%	0.0%	12.5%	H	3
Other	1.7%	3.4%	0.0%	8.3%	8.4%	8.3%	5.6%	6.0%	5.2%	H	3
Traffic island or median	5.8%	6.2%	5.4%	3.8%	3.8%	3.7%	5.4%	5.8%	5.0%	H	3
Pole or post	3.7%	4.3%	2.9%	7.7%	10.1%	5.7%	5.4%	6.4%	4.2%	H	3
Roadworks signs or drums	0.0%	0.0%	0.0%	14.3%	20.0%	0.0%	5.3%	9.1%	0.0%	M	2
Phone boxes bus shelters etc	1.0%	2.0%	0.0%	17.1%	16.7%	17.4%	5.1%	4.9%	5.3%	M	2
Guard rail	3.2%	3.4%	3.0%	5.1%	6.4%	4.3%	4.8%	5.7%	4.1%	M	2
Fence letterbox hoarding etc	2.9%	3.1%	2.6%	5.0%	6.7%	3.9%	4.3%	5.3%	3.5%	M	2
Kerb	4.1%	5.9%	2.4%	5.1%	10.0%	2.6%	4.2%	6.3%	2.4%	M	2
House or building	4.1%	5.1%	3.2%	4.5%	7.7%	0.0%	4.2%	5.3%	3.0%	M	2
Traffic sign or signals	4.3%	5.6%	2.9%	3.9%	2.6%	4.8%	4.1%	4.2%	3.9%	M	2
Ditch	4.2%	5.6%	3.1%	3.8%	5.9%	2.6%	3.8%	5.8%	2.6%	M	2
Upright cliff or bank	1.7%	2.7%	0.7%	3.8%	4.6%	3.3%	3.5%	4.2%	3.0%	L	1
Broken down or accident vehicles	0.3%	0.0%	0.4%	6.5%	6.9%	6.3%	1.6%	2.3%	1.4%	L	1
Debris on the road	0.0%	0.0%	0.0%	1.5%	0.0%	1.9%	1.3%	0.0%	1.7%	L	1
Parked vehicle	1.1%	1.4%	0.9%	5.5%	0.0%	7.1%	1.3%	1.4%	1.2%	L	1
Stray or wild animals	0.0%	0.0%	0.0%	1.1%	1.4%	0.0%	1.1%	1.4%	0.0%	L	1

Lethality Summary by Lethality Category

	Urban Roads			Open Roads			Overall		
	Overall	In Darkness	Not in Darkness	Overall	In Darkness	Not in Darkness	Overall	In Darkness	Not in Darkness
VH	12.2%	14.0%	10.4%	11.2%	12.3%	10.6%	11.5%	12.8%	10.5%
H	4.0%	4.5%	3.4%	7.6%	8.9%	6.6%	5.9%	6.5%	5.3%
M	3.4%	4.2%	2.6%	4.7%	6.3%	3.7%	4.2%	5.4%	3.3%
L	1.1%	1.6%	0.8%	3.6%	3.9%	3.4%	2.3%	2.7%	2.0%

Table A1.12 provides corresponding information for motorcycles on the lethality of different types of accident, again aggregated for the period 2010–2012.

Table A1.12 Motorcycle accident lethality on New Zealand roads

Urban Roads 2010-2012 combined							
Movement Classification	Total No. of Collisions		No. of Fatal Collisions		% Injury Accidents that were Lethal		
	Total	In Darkness	Total	In Darkness	Overall	In Darkness	Not in Darkness
Overtaking or lane change	109	15	0	0	0.0%	0.0%	0.0%
Head on (not overtaking)	51	11	4	0	7.8%	0.0%	10.0%
LOSS OF CONTROL OR OFF ROAD:							
Loss of control - straight	189	61	1	1	0.5%	1.6%	0.0%
Loss of control - cornering	301	93	11	5	3.7%	5.4%	2.9%
Collision with obstruction	48	20	1	0	2.1%	0.0%	3.6%
Rear end	154	17	0	0	0.0%	0.0%	0.0%
INTERSECTIONS OR DRIVEWAYS:							
Intersections - turning	180	33	2	1	1.1%	3.0%	0.7%
Intersections - crossing (no turns)	149	33	2	0	1.3%	0.0%	1.7%
Intersections - crossing vehicle t	269	55	3	1	1.1%	1.8%	0.9%
Intersections - vehicles merging	89	21	0	0	0.0%	0.0%	0.0%
Intersections - right turn against	384	130	7	4	1.8%	3.1%	1.2%
Vehicle manoeuvring	242	58	4	1	1.7%	1.7%	1.6%
Pedestrian crossing road	46	12	0	0	0.0%	0.0%	0.0%
Pedestrian other	5	2	0	0	0.0%	0.0%	0.0%
Miscellaneous	8	3	0	0	0.0%	0.0%	0.0%
TOTALS	2224	564	35	13	1.6%	2.3%	1.3%

The range of accident types considered most relevant for collisions with, or in swerving to avoid, rockfall debris on Wakefield Avenue is shown shaded. The range considered appropriate for use in this analysis is from 2% to 5% of injury accidents proving lethal (providing approximately a +/- 1.5% range around the “not in darkness” figure for collision with obstructions, and extending up towards the highest figure, for accidents involving cornering in darkness). Combining this figure with the 50% estimate of the percentage of all motorcycle collisions that involve injury gives an estimate of **1% to 2.5%** of all motorcycle collisions with (or in avoiding) rockfall debris on Wakefield Avenue proving fatal.

As regards pedal cycles, we are not aware of any New Zealand statistics or research into the particular issue of cyclists colliding with objects other than motor vehicles. A UK study carried out in 2009⁹ investigated such collisions and found the following total numbers of injury accidents:

- 27 fatal;
- 257 serious; and
- 518 slight injury accidents.

On this basis about 3.4% (27 out of 802) of injury collisions with objects other than motor vehicles proved fatal.

⁹ "Collisions involving pedal cyclists on Britain's roads: Establishing the causes", J. Knowles, S. Adams, R. Cuerden, T. Savill, S. Reid and M. Tight, TRL(UK), PPR445, 2009 (published research report for UK Department for Transport)

The possibility also needs to be taken into account of a cyclist swerving to avoid rockfall only to collide with a motor vehicle travelling in the opposite direction. For a cyclist to be killed in this way would require:

- a. A motor vehicle to be present travelling in the opposite direction within a few seconds travel time from the cyclist;
- b. The cyclist to swerve into its path; and
- c. The resulting collision to prove fatal.

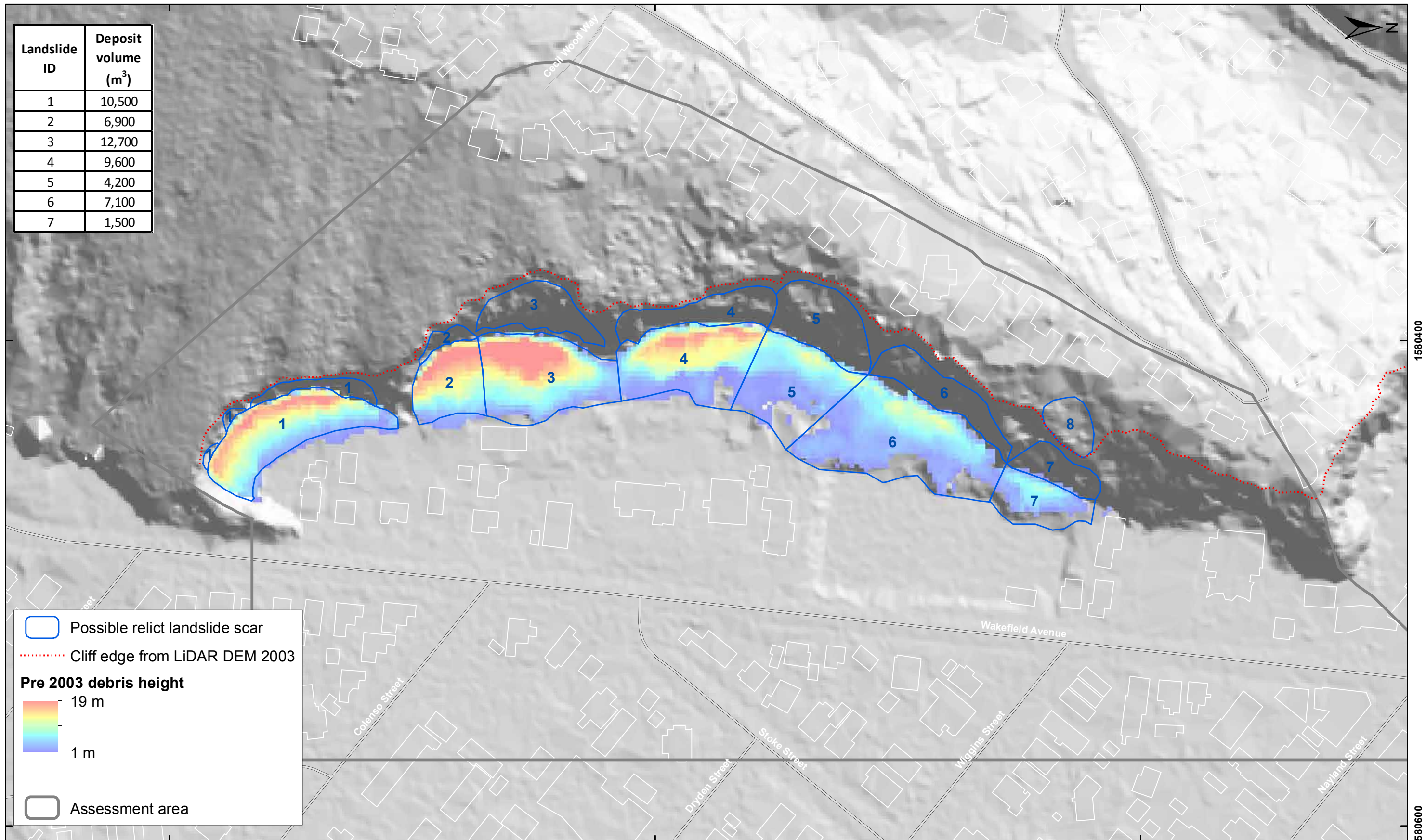
The latest published New Zealand statistics on cyclist injuries in motor vehicle crashes¹⁰ show 27 fatal and 2,425 injury accidents to cyclists in the three years 2010, 2011 and 2012 combined, suggesting that just over 1% of cyclist injury accidents involving a motor vehicle crash prove fatal.

On this basis it appears unlikely that, when combined with (a) and (b) above, collisions with motor vehicles while swerving to avoid rockfall would significantly add to the likelihood of fatality for a cyclist. Assuming that the proportion of cyclist collisions of any sort that involve significant injury is in the same range as that for cars and motorcycles (i.e., 25–50%), we have therefore combined this with the proportion of UK injury accidents (not involving collision with a motor vehicle) that were fatal to estimate a range of values of $\sqrt{2}$ for cyclists from **0.8% to 1.7%** (i.e., from 25 to 50% of 3.4%).

¹⁰ Cyclists CRASH STATISTICS FOR THE YEAR ENDED 31 DECEMBER 2012, Crash Factsheet November 2013, NZ Ministry of Transport. Available at <http://www.transport.govt.nz/assets/Uploads/Research/Documents/cycling-crashfacts-2013.pdf>

A2 APPENDIX 2: RESULTS FROM AIRBORNE LIDAR SURVEYS

Landslide ID	Deposit volume (m ³)
1	10,500
2	6,900
3	12,700
4	9,600
5	4,200
6	7,100
7	1,500



 Possible relict landslide scar
 Cliff edge from LiDAR DEM 2003
Pre 2003 debris height

 Assessment area



EXPLANATION:
 Background shade model derived from AAM 2003 LiDAR survey resampled to a 1 m ground resolution.
 Roads and building footprints provided by Christchurch City Council (20/02/2012).
 PROJECTION: New Zealand Transverse Mercator 2000

DRW:
BL
 CHK:
CM



**RESULTS FROM AIRBORNE LiDAR SURVEYS
 ESTIMATED TALUS DEPOSITS
 Pre 2003**

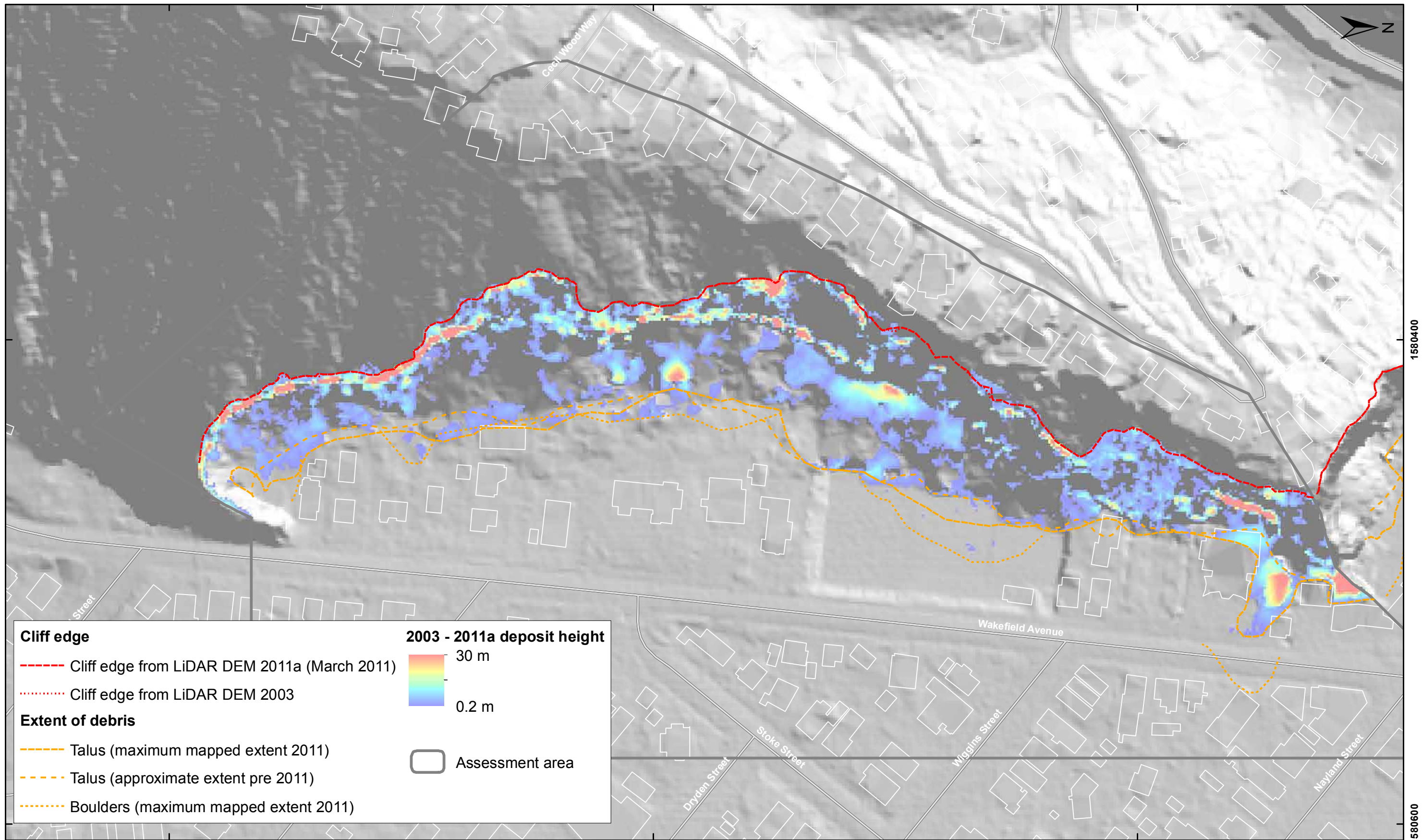
**Richmond Hill Road
 Christchurch**

APPENDIX 2

Map 1

FINAL

REPORT: CR2014/34	DATE: June 2014
----------------------	--------------------



Cliff edge	2003 - 2011a deposit height
----- Cliff edge from LiDAR DEM 2011a (March 2011)	30 m
..... Cliff edge from LiDAR DEM 2003	0.2 m
Extent of debris	Assessment area
----- Talus (maximum mapped extent 2011)	
----- Talus (approximate extent pre 2011)	
..... Boulders (maximum mapped extent 2011)	



EXPLANATION:
 Background shade model derived from NZAM post earthquake 2011a (March 2011) LiDAR survey resampled to a 1 m ground resolution.
 Roads and building footprints provided by Christchurch City Council (20/02/2012).
 PROJECTION: New Zealand Transverse Mercator 2000

DRW:
BL
 CHK:
CM



**RESULTS FROM AIRBORNE LiDAR SURVEYS
 ESTIMATED TALUS DEPOSITS
 2003 - March 2011**

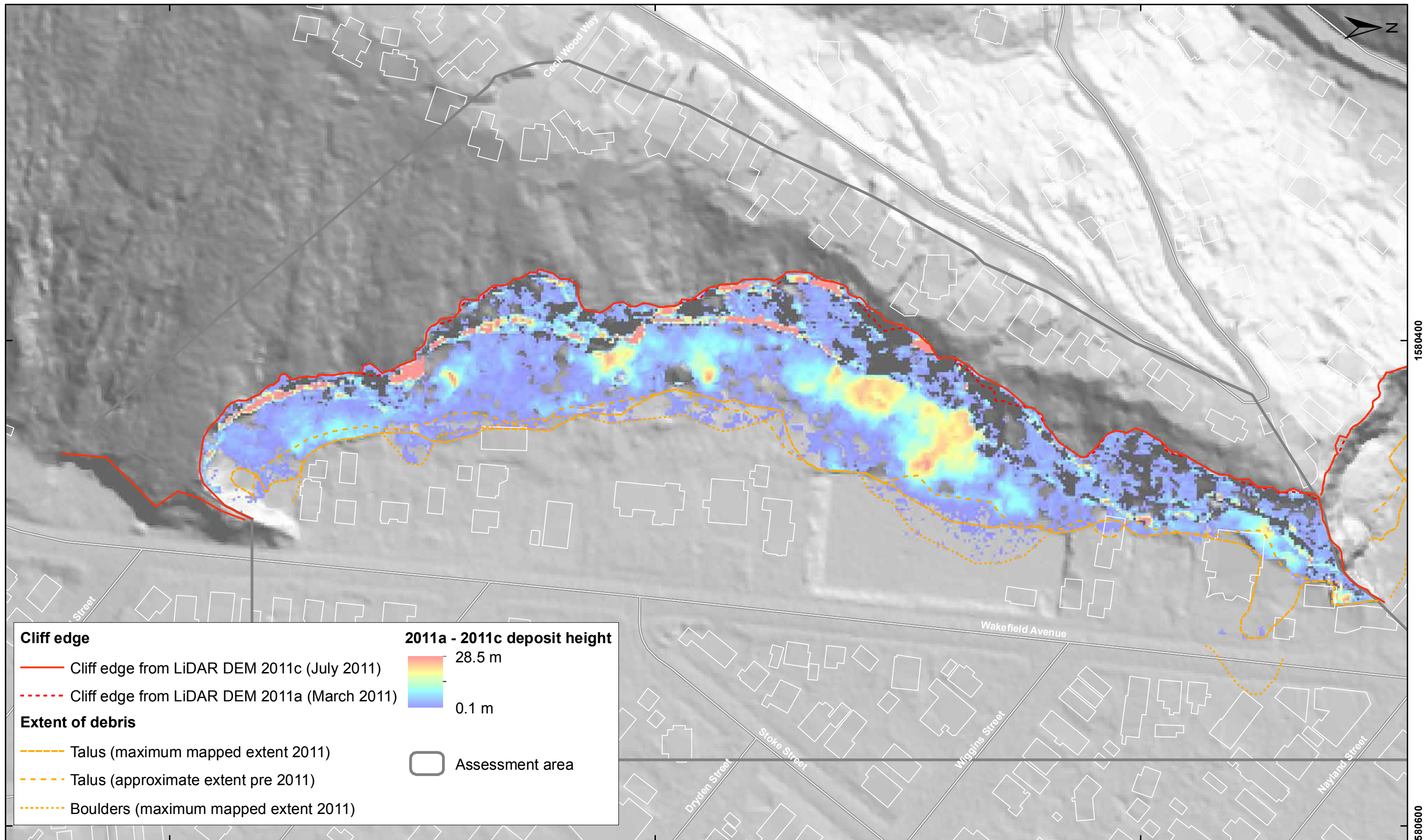
**Richmond Hill Road
 Christchurch**

APPENDIX 2

Map 2

FINAL

REPORT: CR2014/34	DATE: June 2014
----------------------	--------------------



Cliff edge	2011a - 2011c deposit height 28.5 m 0.1 m
———— Cliff edge from LiDAR DEM 2011c (July 2011) - - - - - Cliff edge from LiDAR DEM 2011a (March 2011)	
Extent of debris	Assessment area
- - - - - Talus (maximum mapped extent 2011) - - - - - Talus (approximate extent pre 2011) Boulders (maximum mapped extent 2011)	



EXPLANATION:
 Background shade model derived from NZAM post earthquake 2011c (July 2011) LiDAR survey resampled to a 1 m ground resolution.
 Roads and building footprints provided by Christchurch City Council (20/02/2012).
 PROJECTION: New Zealand Transverse Mercator 2000

DRW:
BL
 CHK:
CM



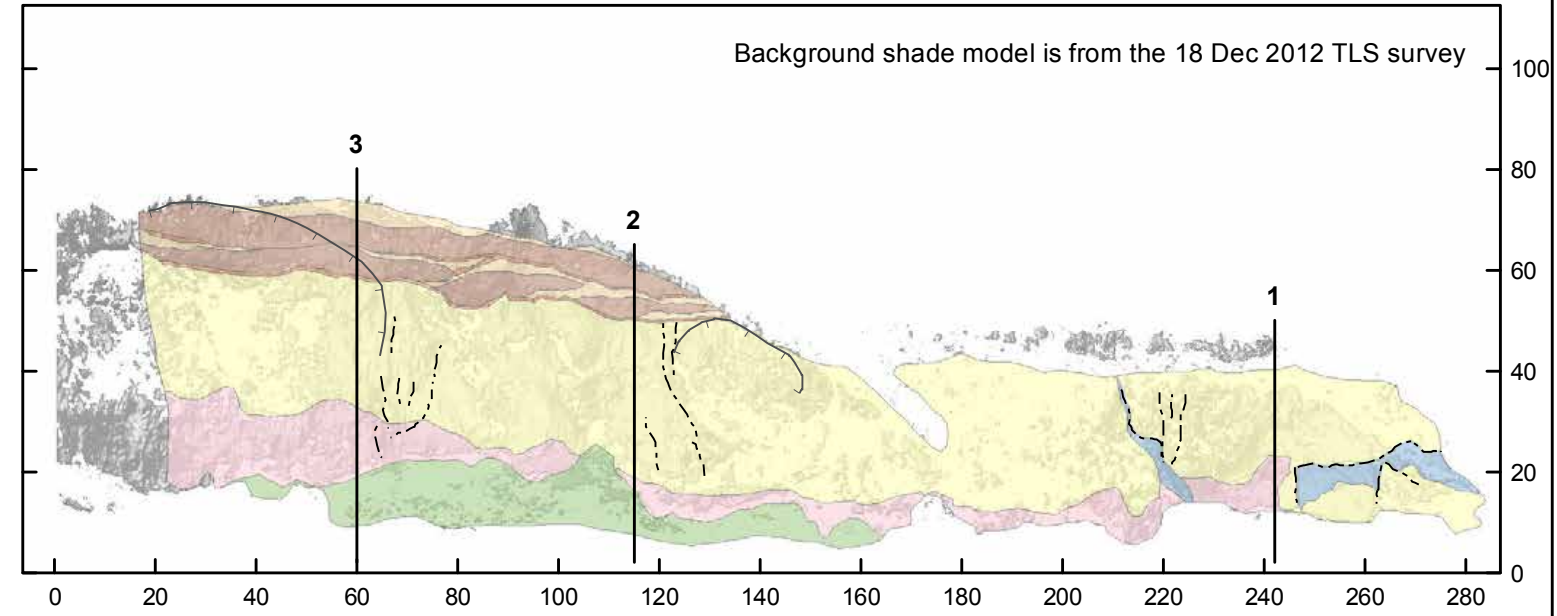
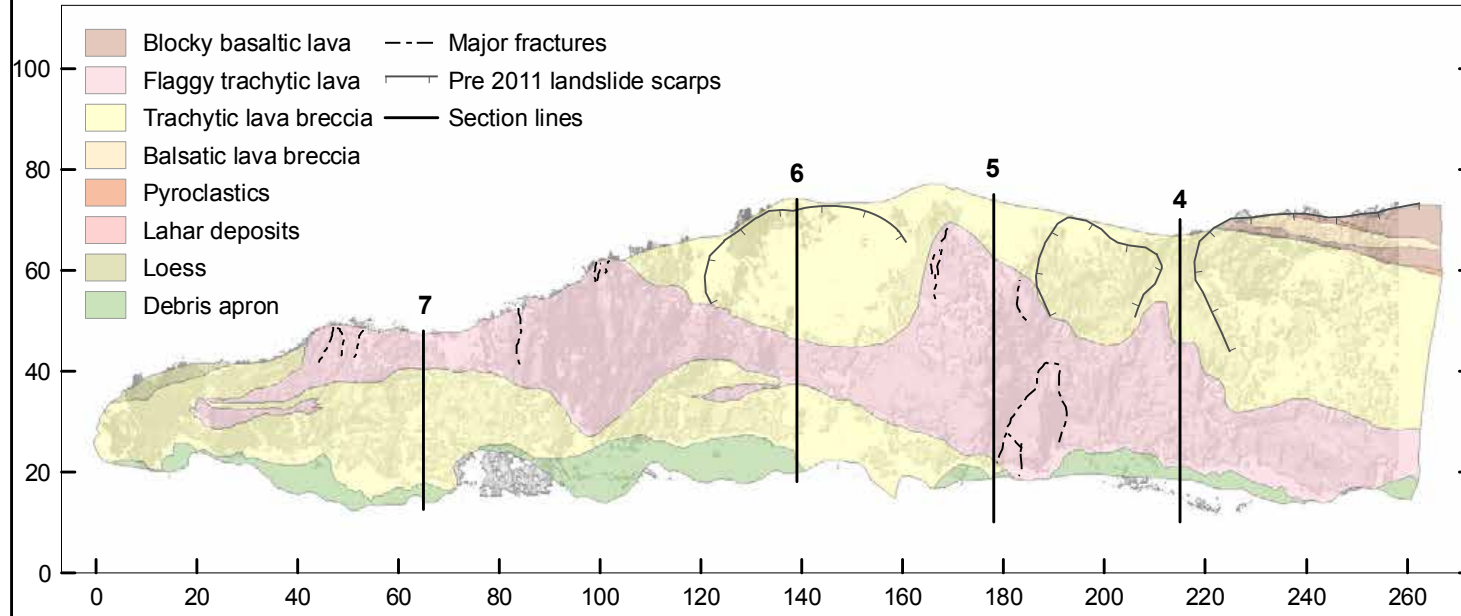
**RESULTS FROM AIRBORNE LiDAR SURVEYS
 ESTIMATED TALUS DEPOSITS
 March 2011 - July 2011**

**Richmond Hill Road
 Christchurch**

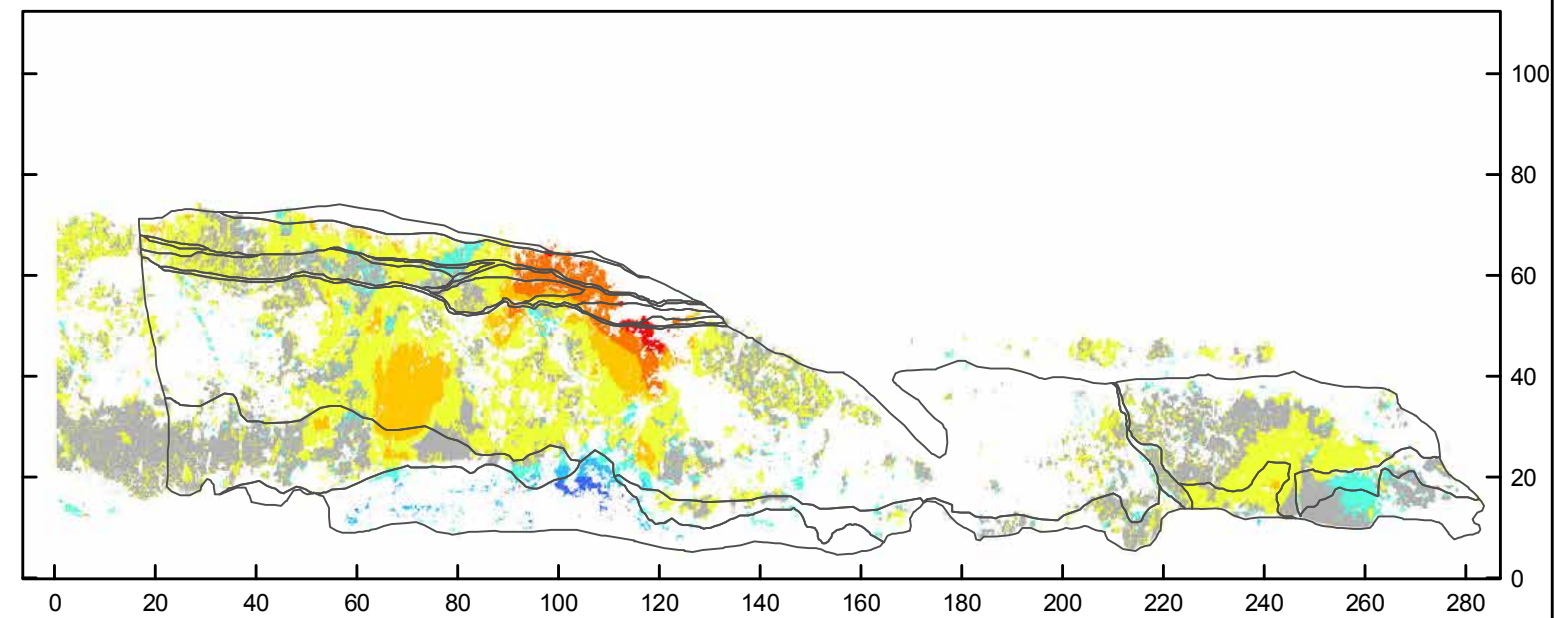
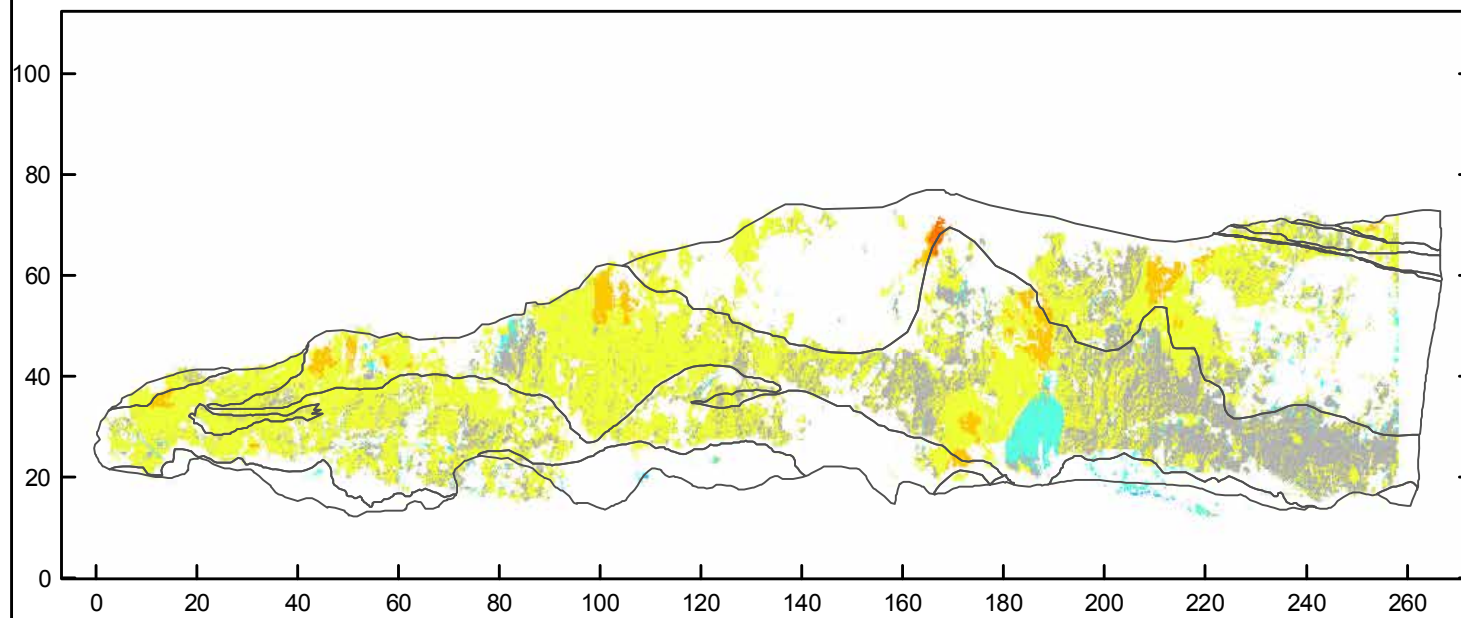
APPENDIX 2	
Map 3	
FINAL	
REPORT: CR2014/34	DATE: June 2014

A3 APPENDIX 3: RESULTS FROM THE TERRESTRIAL LASER SCAN SURVEYS

Geology

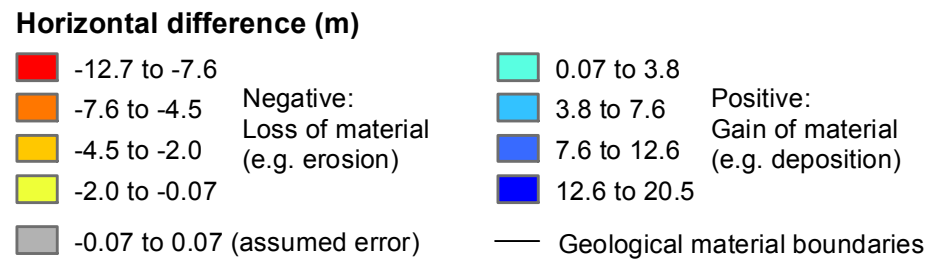


Surface change model 1 March 2011 - 18 December 2012



Wakefield South

Wakefield North



EXPLANATION:

Surface change models show horizontal changes of the cliff-face surface between given survey dates. Changes in the order of +/- 0.07 m are assumed to be error. The surveys were carried out using RIEGL LMSZ420i terrestrial laser scanner (TLS) in 2011 and 2012. The views are all frontal elevation i.e. as if standing at the bottom of the cliff looking towards it, with the data projected onto the chainage.

DRW:
BL
CHK:
CM



**RESULTS FROM TERRESTRIAL LASER SCAN SURVEYS
CLIFF FRONTAL ELEVATION, GEOLOGY MAP
AND SURFACE CHANGE MODELS**

**Richmond Hill Road
Christchurch**

APPENDIX 3

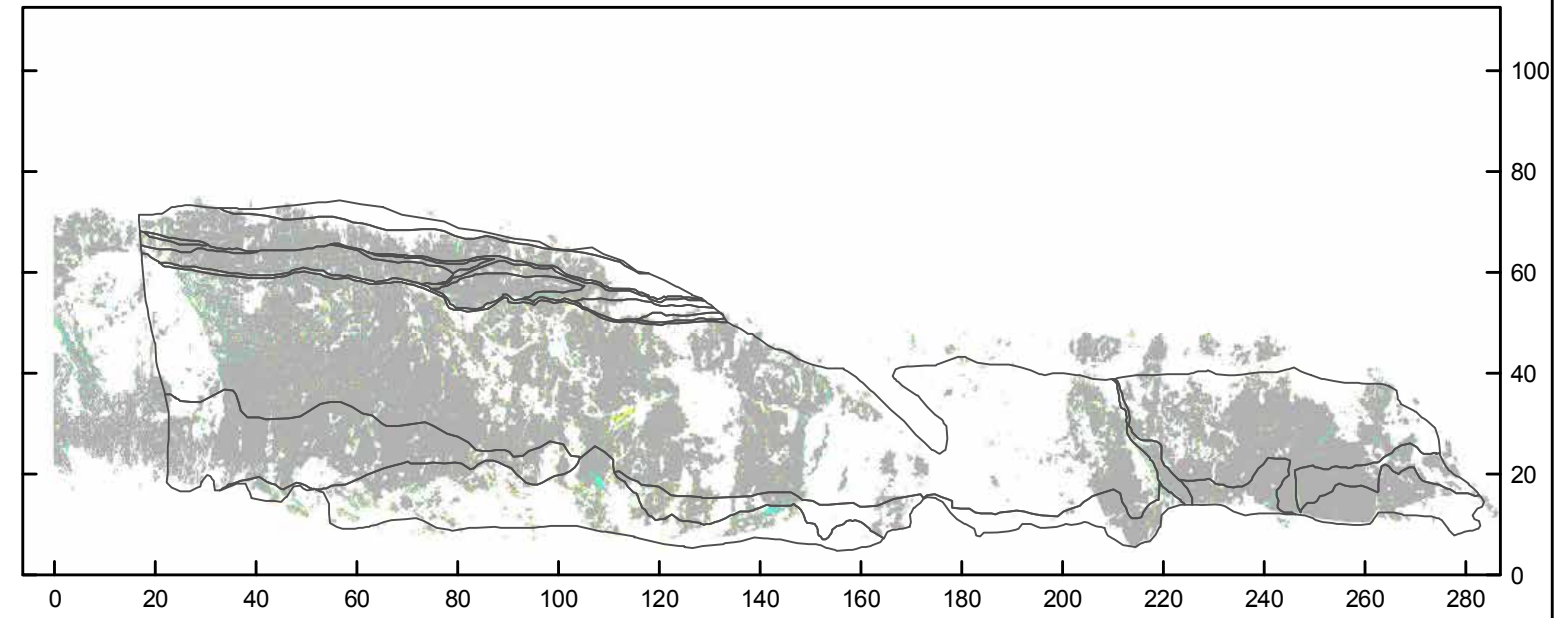
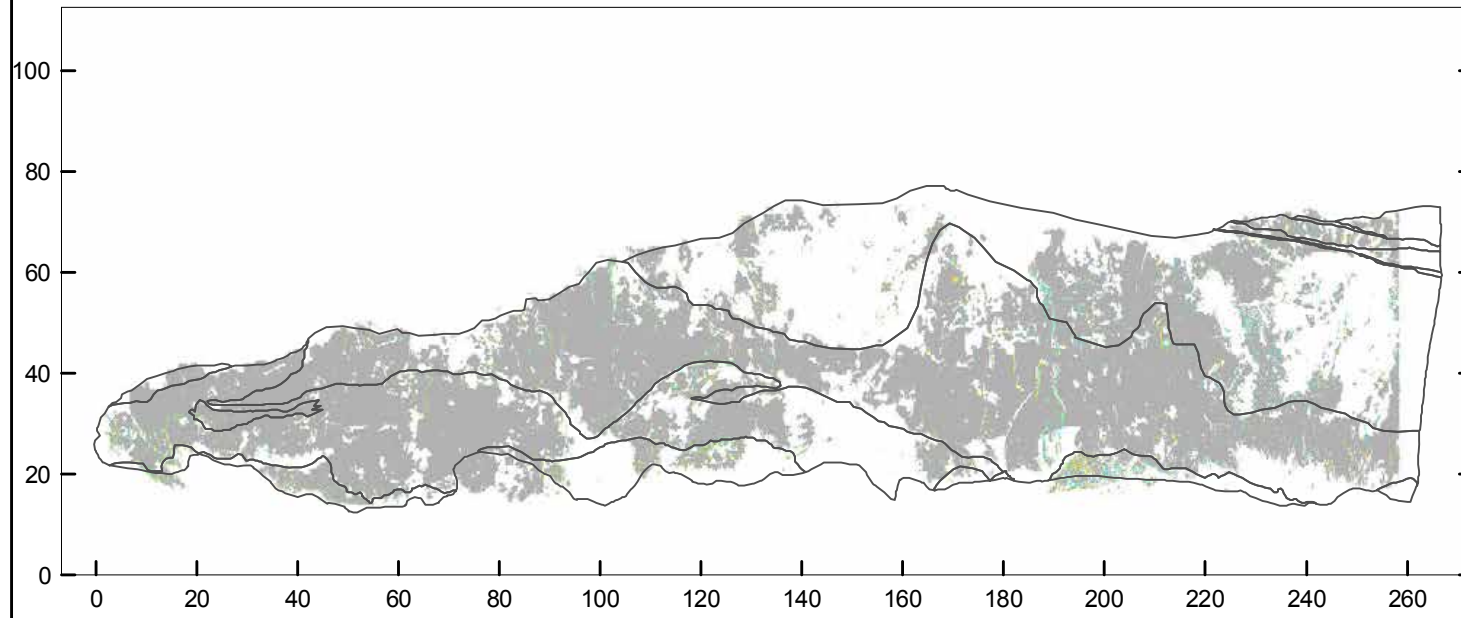
Map 1

FINAL

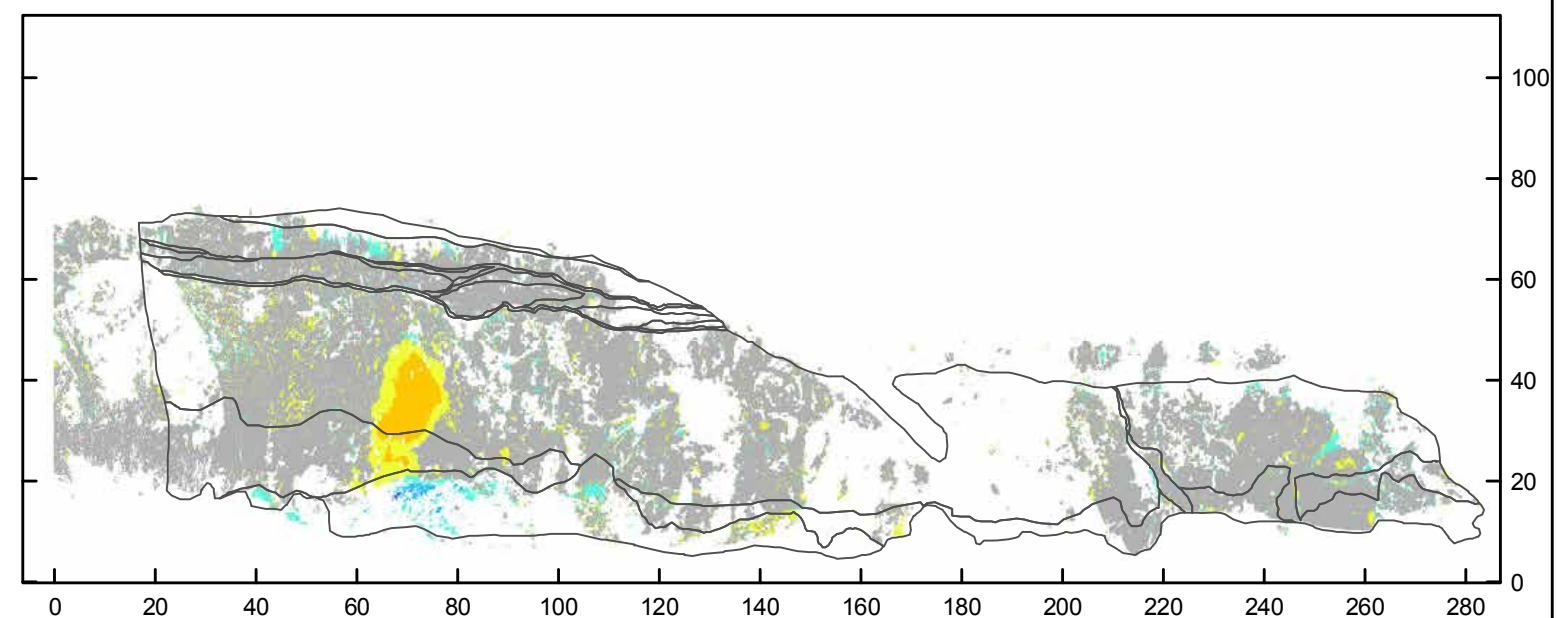
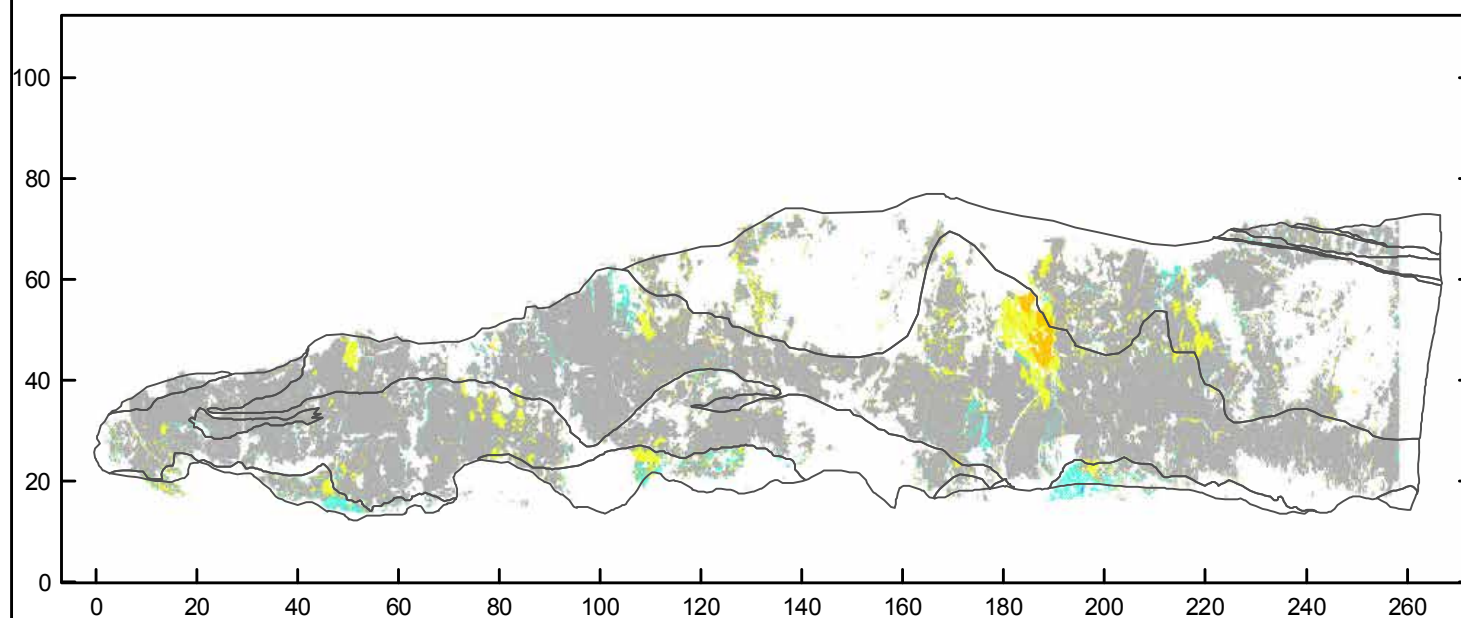
REPORT:
CR2014/34

DATE:
June 2014

Surface change model 1 March 2011 - 8 March 2011

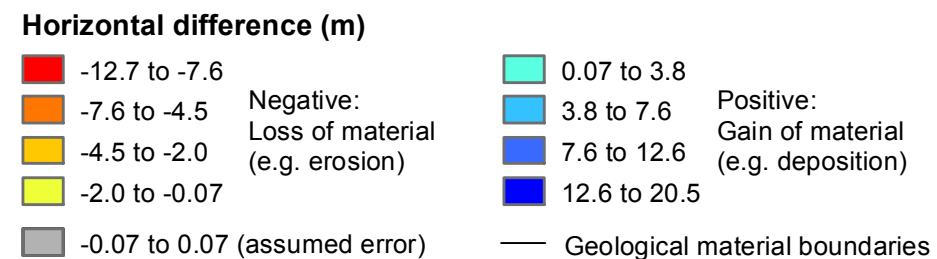


Surface change model 8 March 2011 - 3 May 2011



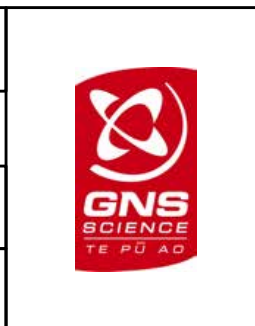
Wakefield South

Wakefield North



EXPLANATION:
Surface change models show horizontal changes of the cliff-face surface between given survey dates. Changes in the order of +/- 0.07 m are assumed to be error. The surveys were carried out using RIEGL LMSZ420i terrestrial laser scanner (TLS) in 2011 and 2012. The views are all frontal elevation i.e. as if standing at the bottom of the cliff looking towards it, with the data projected onto the chainage.

DRW:
BL
CHK:
CM



**RESULTS FROM TERRESTRIAL LASER SCAN SURVEYS
CLIFF FRONTAL ELEVATION, GEOLOGY MAP
AND SURFACE CHANGE MODELS**

**Richmond Hill Road
Christchurch**

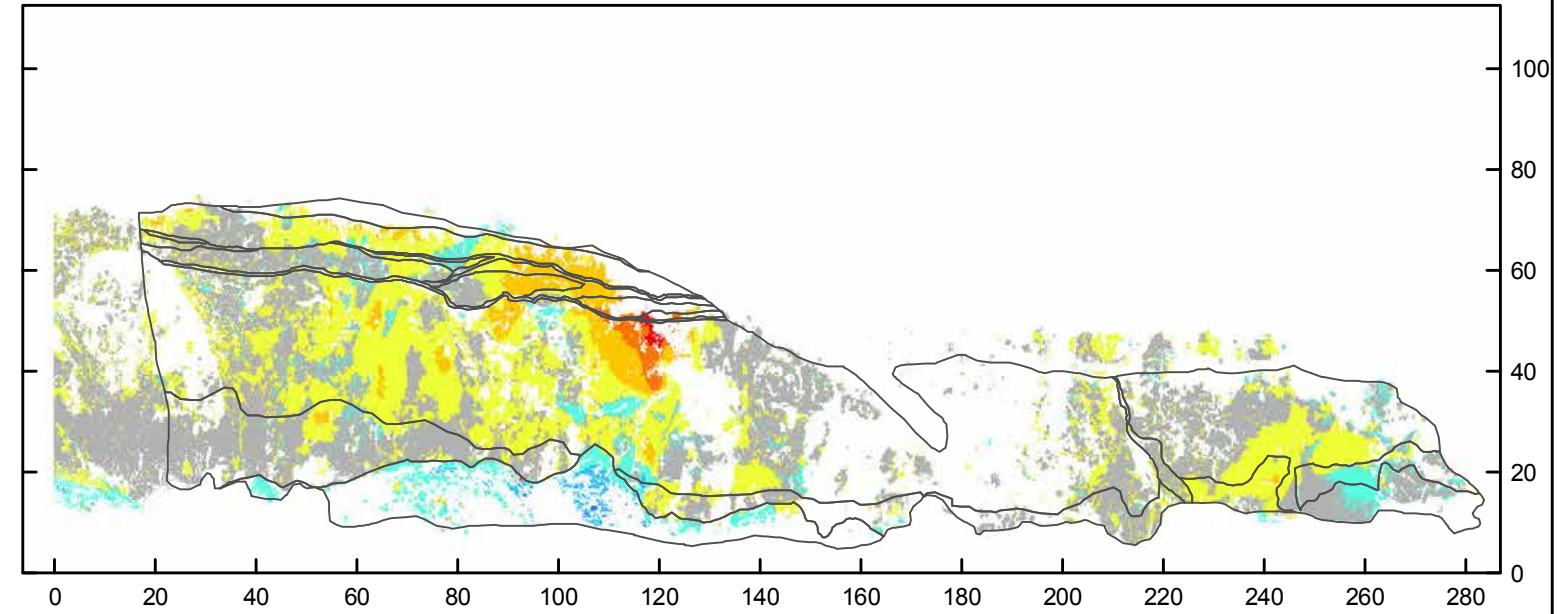
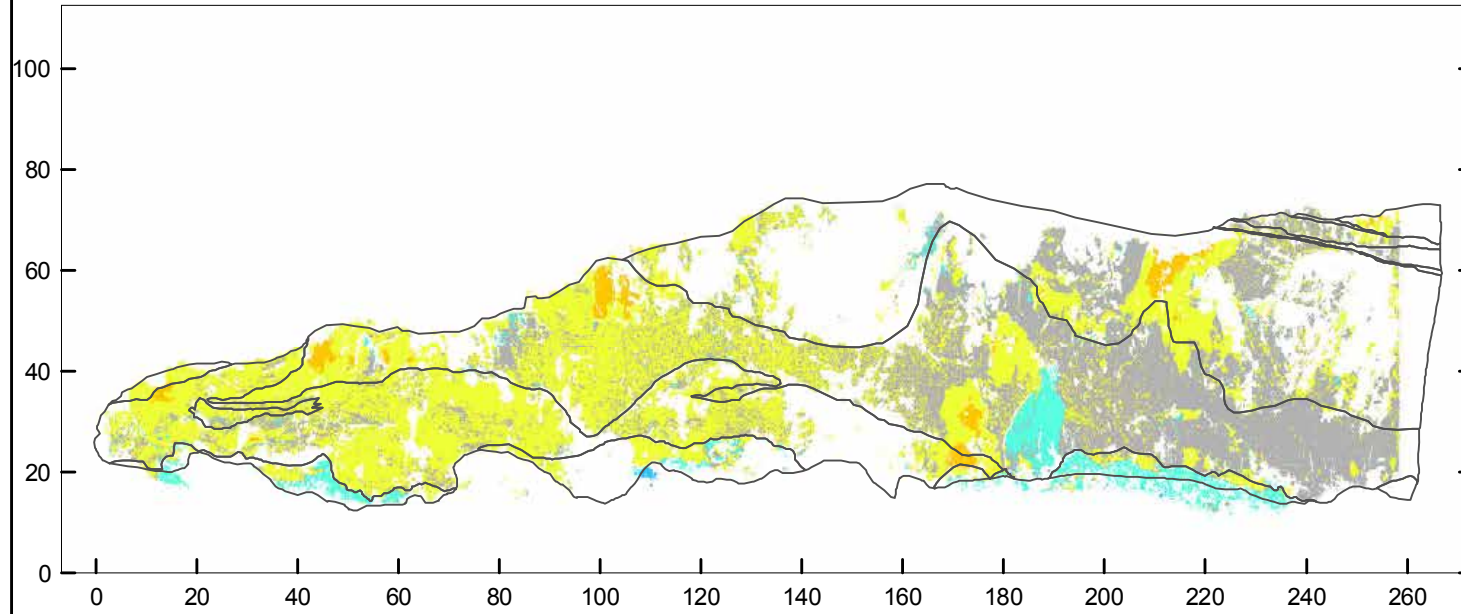
APPENDIX 3

Map 2

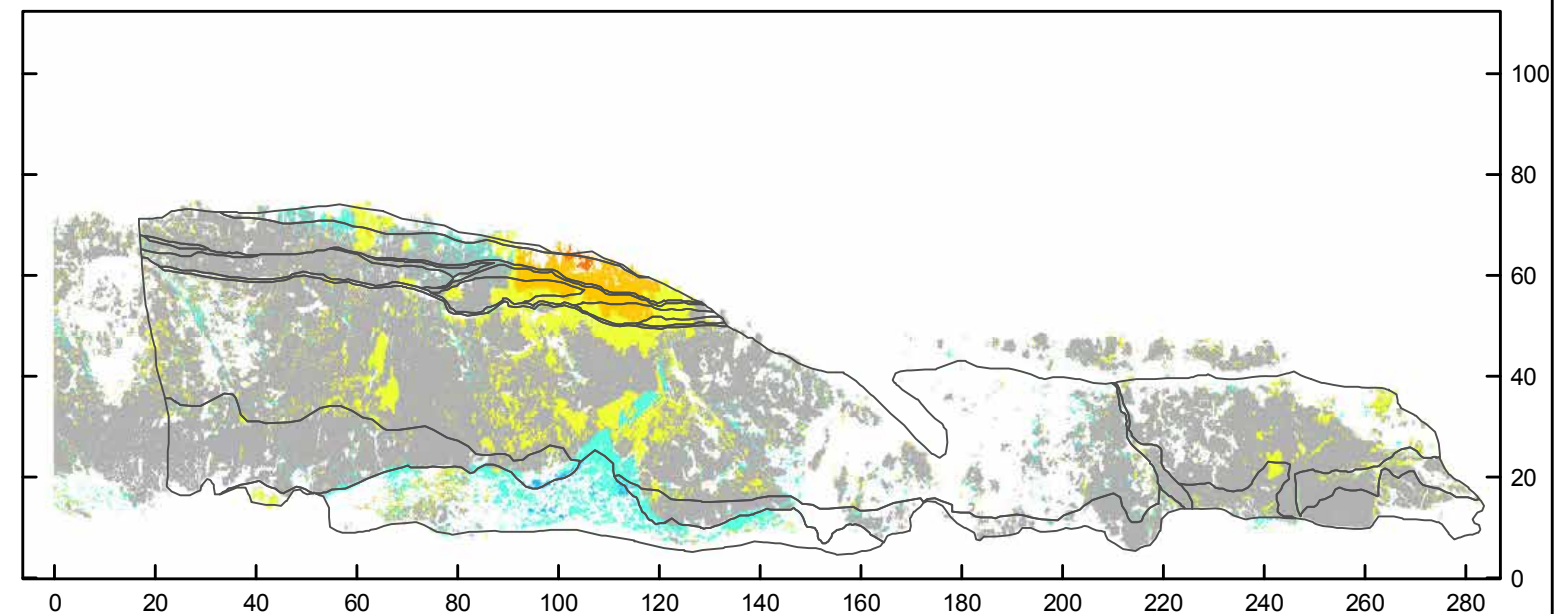
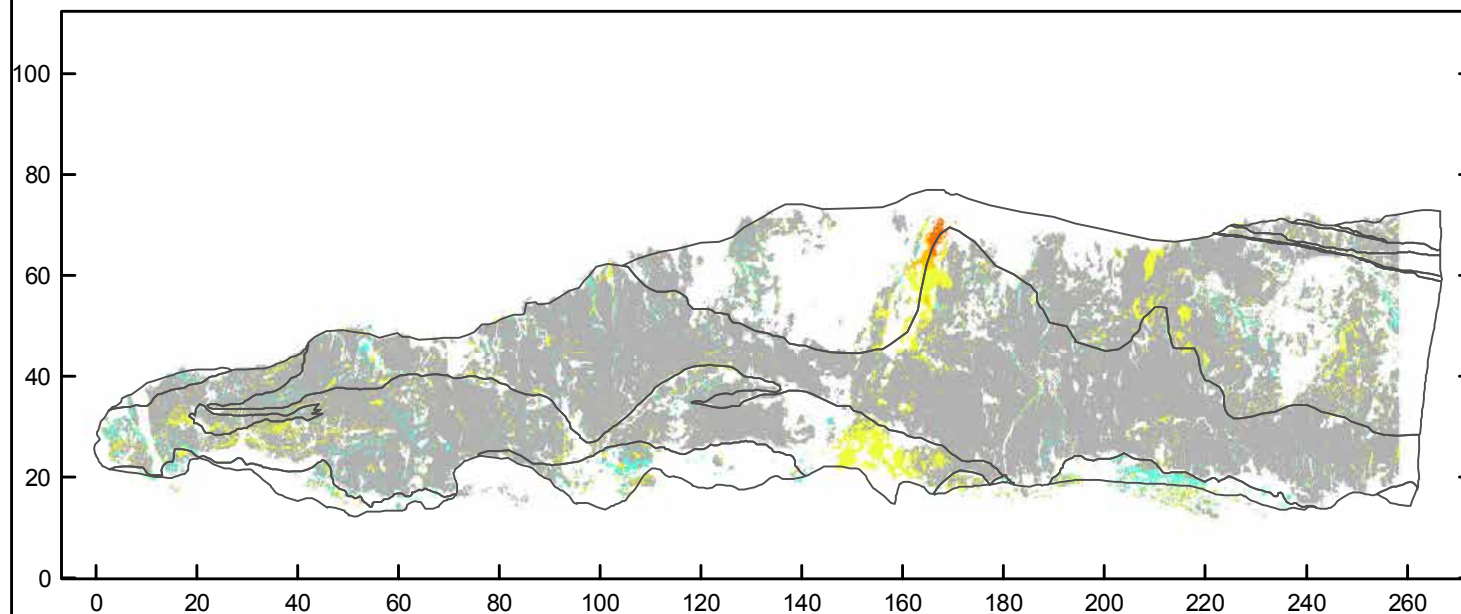
FINAL

REPORT: CR2014/34	DATE: June 2014
----------------------	--------------------

Surface change model 3 May 2011 -16 June 2011

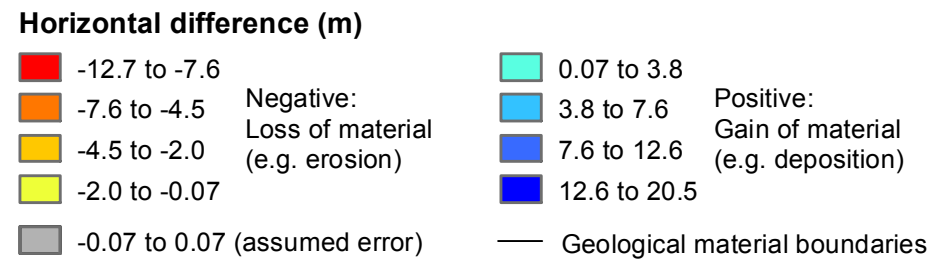


Surface change model 16 June 2011 - 16 January 2012



Wakefield South

Wakefield North



EXPLANATION:

Surface change models show horizontal changes of the cliff-face surface between given survey dates. Changes in the order of +/- 0.07 m are assumed to be error. The surveys were carried out using RIEGL LMSZ420i terrestrial laser scanner (TLS) in 2011 and 2012. The views are all frontal elevation i.e. as if standing at the bottom of the cliff looking towards it, with the data projected onto the chainage.

DRW:
BL
CHK:
CM



RESULTS FROM TERRESTRIAL LASER SCAN SURVEYS
CLIFF FRONTAL ELEVATION, GEOLOGY MAP
AND SURFACE CHANGE MODELS

Richmond Hill Road
Christchurch

APPENDIX 3

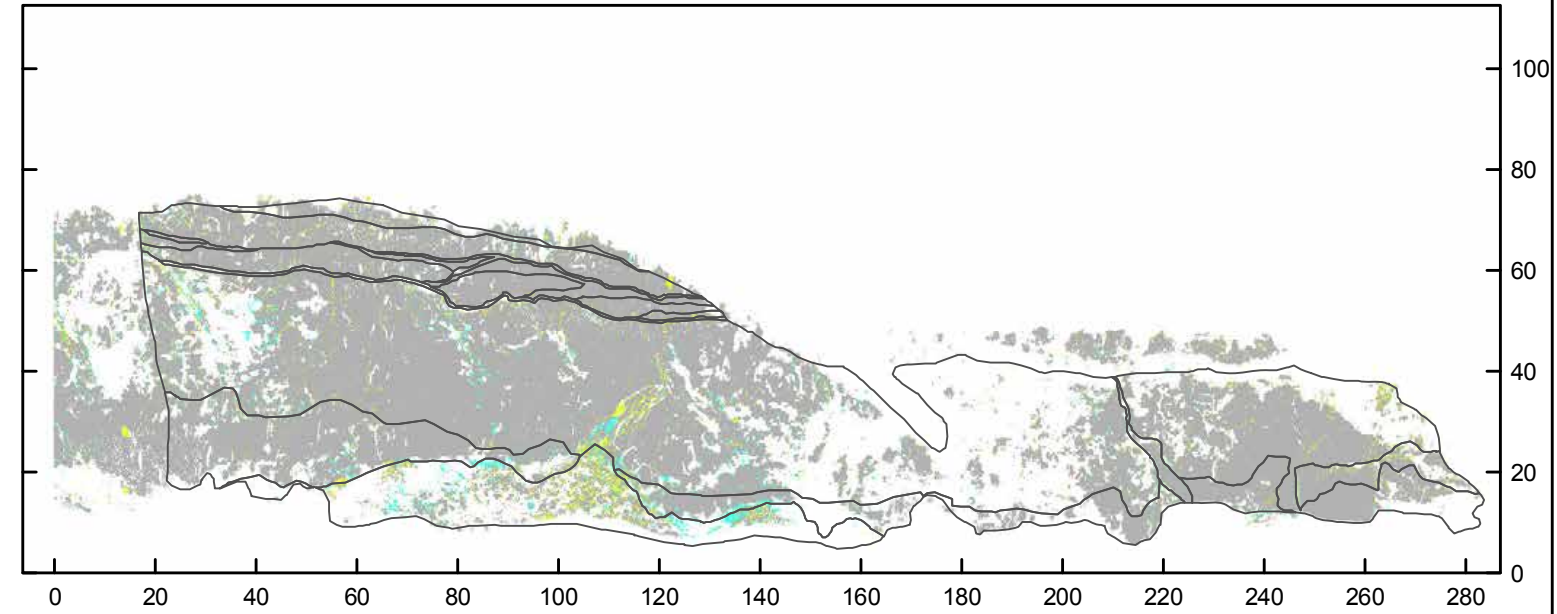
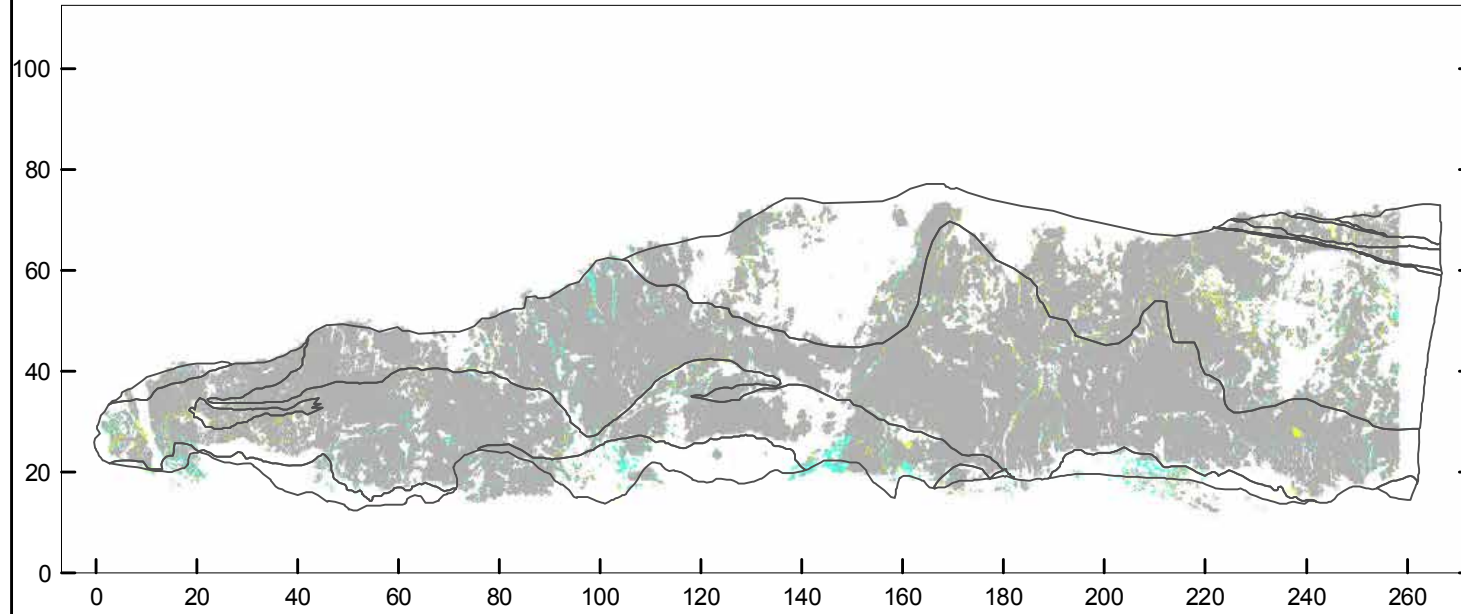
Map 3

FINAL

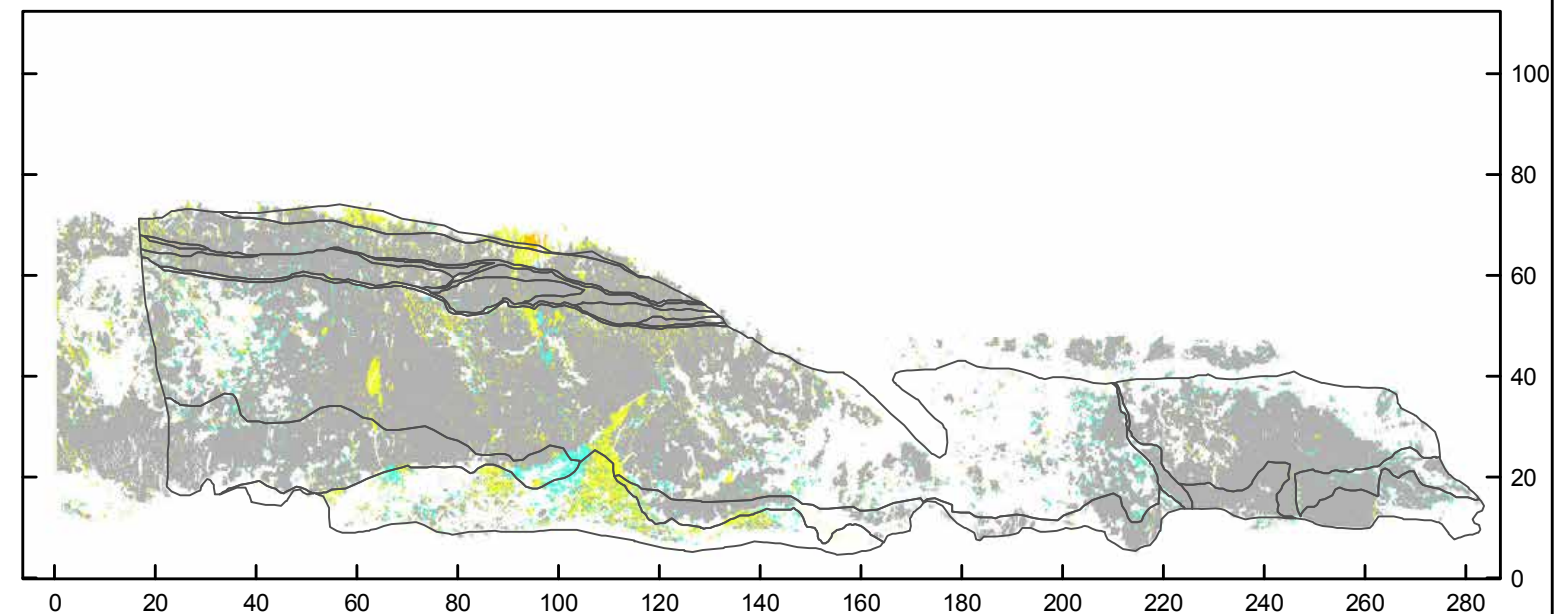
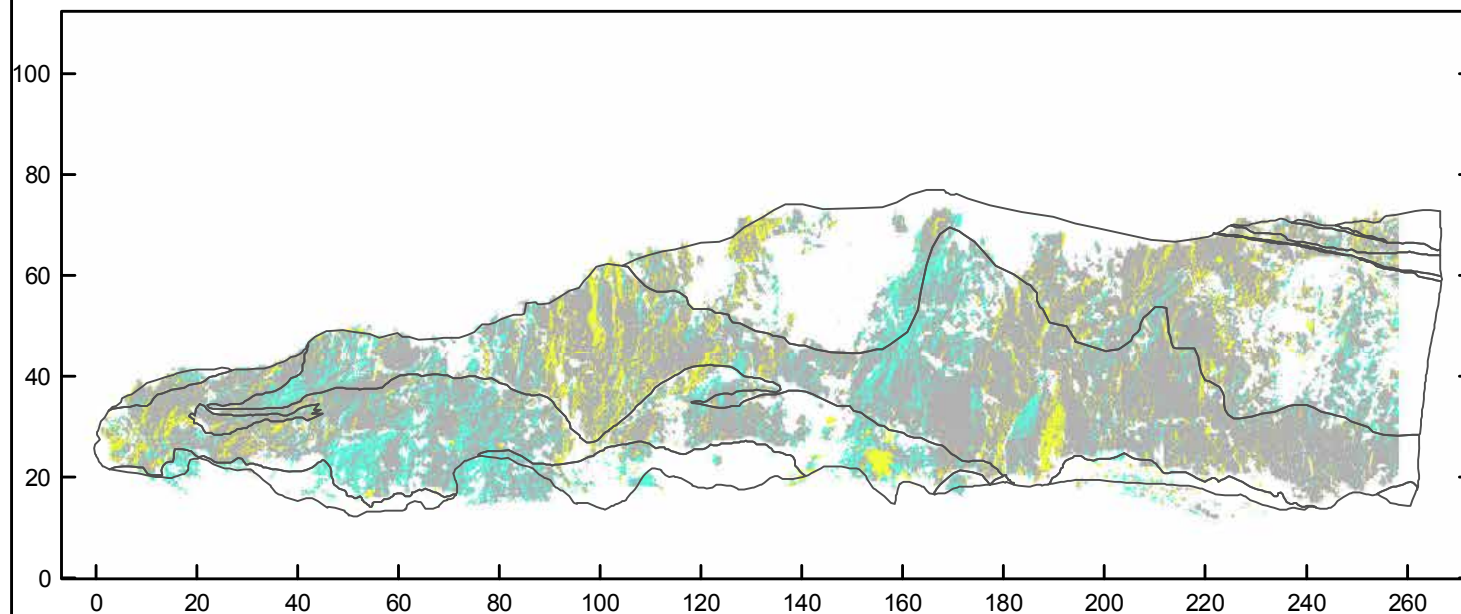
REPORT:
CR2014/34

DATE:
June 2014

Surface change model 16 January 2012 - 2 May 2012

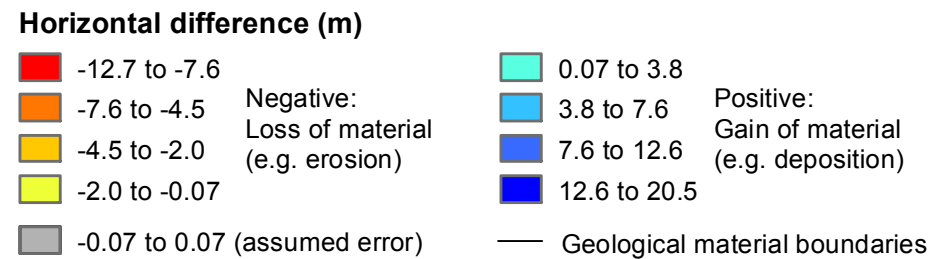


Surface change model 2 May 2012 - 13 September 2012



Wakefield South

Wakefield North



EXPLANATION:

Surface change models show horizontal changes of the cliff-face surface between given survey dates. Changes in the order of +/- 0.07 m are assumed to be error. The surveys were carried out using RIEGL LMSZ420i terrestrial laser scanner (TLS) in 2011 and 2012. The views are all frontal elevation i.e. as if standing at the bottom of the cliff looking towards it, with the data projected onto the chainage.

DRW:
BL

CHK:
CM



**RESULTS FROM TERRESTRIAL LASER SCAN SURVEYS
CLIFF FRONTAL ELEVATION, GEOLOGY MAP
AND SURFACE CHANGE MODELS**

**Richmond Hill Road
Christchurch**

APPENDIX 3

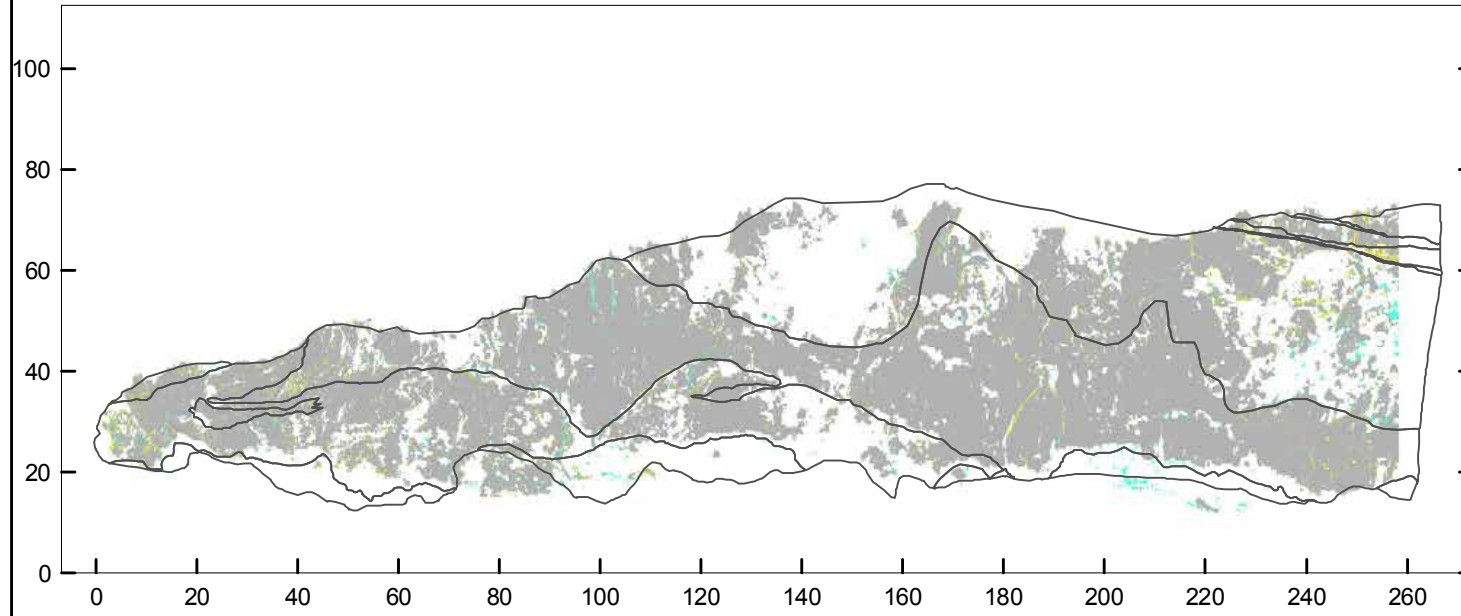
Map 4

FINAL

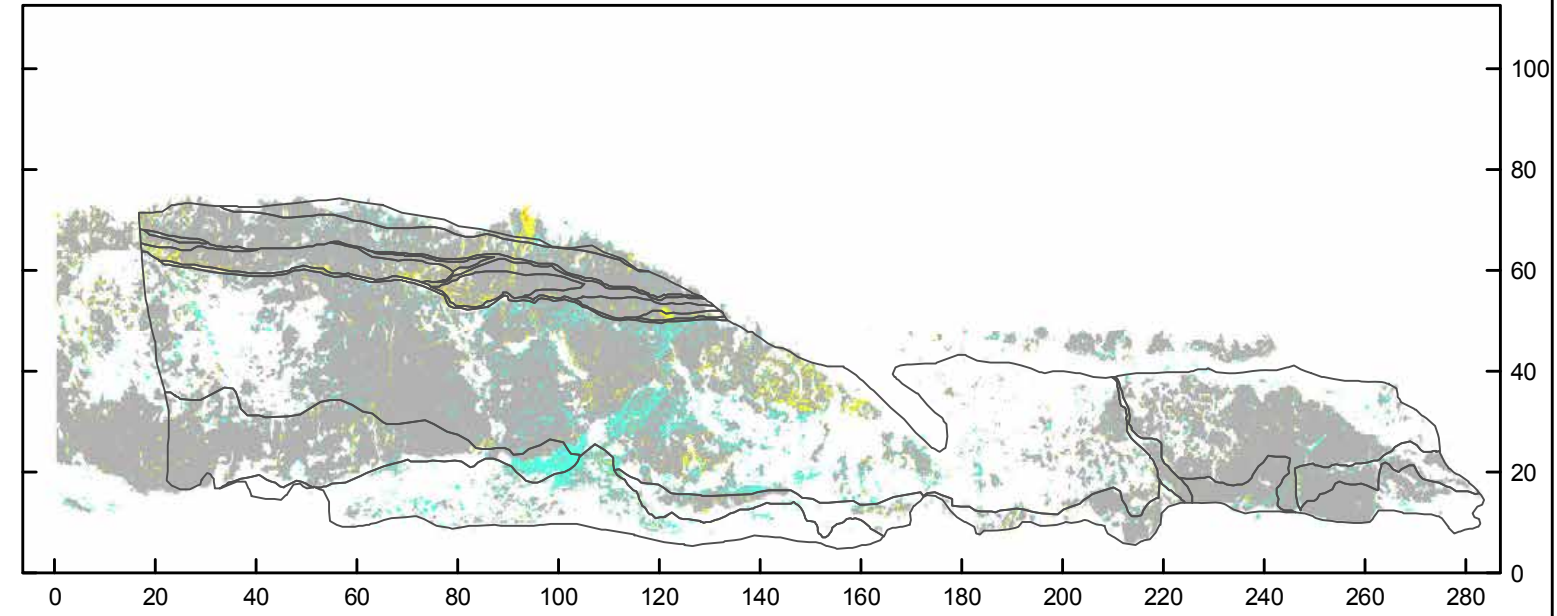
REPORT:
CR2014/34

DATE:
June 2014

Surface change model 13 September 2012 - 18 December 2012

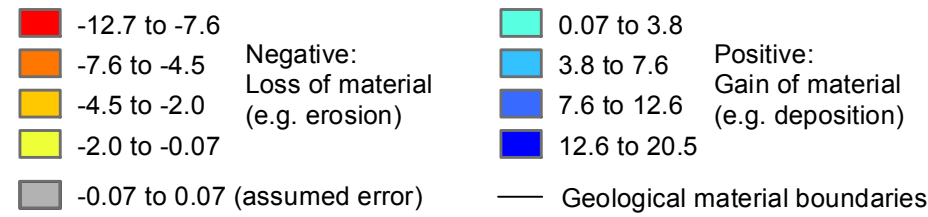


Wakefield South



Wakefield North

Horizontal difference (m)



EXPLANATION:

Surface change models show horizontal changes of the cliff-face surface between given survey dates. Changes in the order of +/- 0.07 m are assumed to be error. The surveys were carried out using RIEGL LMSZ420i terrestrial laser scanner (TLS) in 2011 and 2012. The views are all frontal elevation i.e. as if standing at the bottom of the cliff looking towards it, with the data projected onto the chainage.

DRW:
BL
CHK:
CM



RESULTS FROM TERRESTRIAL LASER SCAN SURVEYS
CLIFF FRONTAL ELEVATION, GEOLOGY MAP
AND SURFACE CHANGE MODELS

Richmond Hill Road
Christchurch

APPENDIX 3

Map 5

FINAL

REPORT:
CR2014/34

DATE:
June 2014

A4 APPENDIX 4: RESULTS FROM THE SURVEY OF CADASTRAL SURVEY MARKS

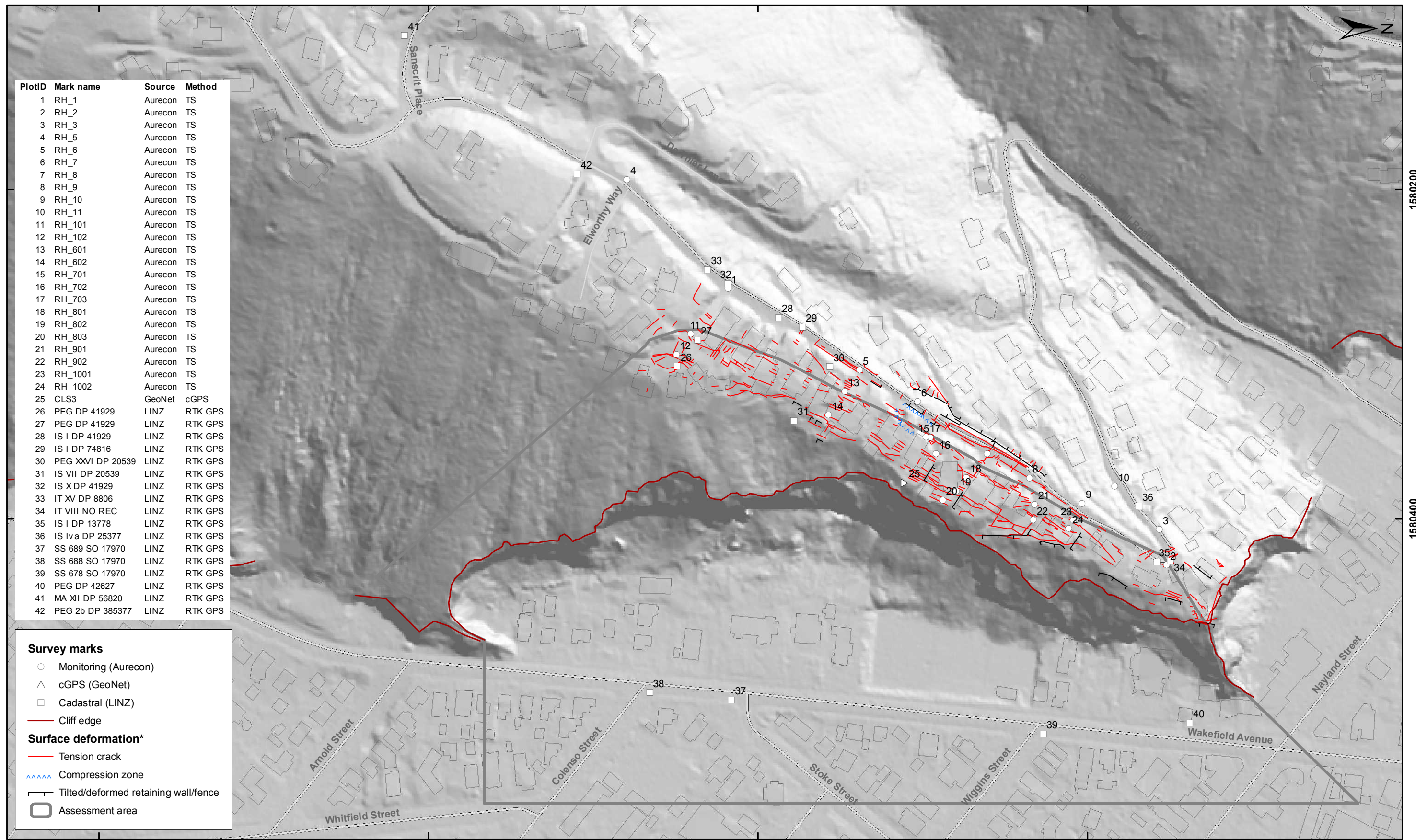
PlotID	Mark name	Source	Method
1	RH_1	Aurecon	TS
2	RH_2	Aurecon	TS
3	RH_3	Aurecon	TS
4	RH_5	Aurecon	TS
5	RH_6	Aurecon	TS
6	RH_7	Aurecon	TS
7	RH_8	Aurecon	TS
8	RH_9	Aurecon	TS
9	RH_10	Aurecon	TS
10	RH_11	Aurecon	TS
11	RH_101	Aurecon	TS
12	RH_102	Aurecon	TS
13	RH_601	Aurecon	TS
14	RH_602	Aurecon	TS
15	RH_701	Aurecon	TS
16	RH_702	Aurecon	TS
17	RH_703	Aurecon	TS
18	RH_801	Aurecon	TS
19	RH_802	Aurecon	TS
20	RH_803	Aurecon	TS
21	RH_901	Aurecon	TS
22	RH_902	Aurecon	TS
23	RH_1001	Aurecon	TS
24	RH_1002	Aurecon	TS
25	CLS3	GeoNet	cGPS
26	PEG DP 41929	LINZ	RTK GPS
27	PEG DP 41929	LINZ	RTK GPS
28	IS I DP 41929	LINZ	RTK GPS
29	IS I DP 74816	LINZ	RTK GPS
30	PEG XXVI DP 20539	LINZ	RTK GPS
31	IS VII DP 20539	LINZ	RTK GPS
32	IS X DP 41929	LINZ	RTK GPS
33	IT XV DP 8806	LINZ	RTK GPS
34	IT VIII NO REC	LINZ	RTK GPS
35	IS I DP 13778	LINZ	RTK GPS
36	IS Iva DP 25377	LINZ	RTK GPS
37	SS 689 SO 17970	LINZ	RTK GPS
38	SS 688 SO 17970	LINZ	RTK GPS
39	SS 678 SO 17970	LINZ	RTK GPS
40	PEG DP 42627	LINZ	RTK GPS
41	MA XII DP 56820	LINZ	RTK GPS
42	PEG 2b DP 385377	LINZ	RTK GPS

Survey marks

- Monitoring (Aurecon)
- △ cGPS (GeoNet)
- Cadastral (LINZ)
- Cliff edge

Surface deformation*

- Tension crack
- ~~~~~ Compression zone
- Tilted/deformed retaining wall/fence
- Assessment area



5175200

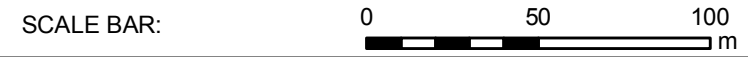
5175400

5175600

5175800

1580200

1580400



EXPLANATION:
 * Taken from report CR2012/317
 Background shade model derived from NZAM post earthquake 2011c (July 2011) LiDAR survey resampled to a 1 m ground resolution.
 Roads and building footprints provided by Christchurch City Council (20/02/2012).
 PROJECTION: New Zealand Transverse Mercator 2000

DRW:
BL
 CHK:
CM, GA



**SURVEY MARKS
Index Map**

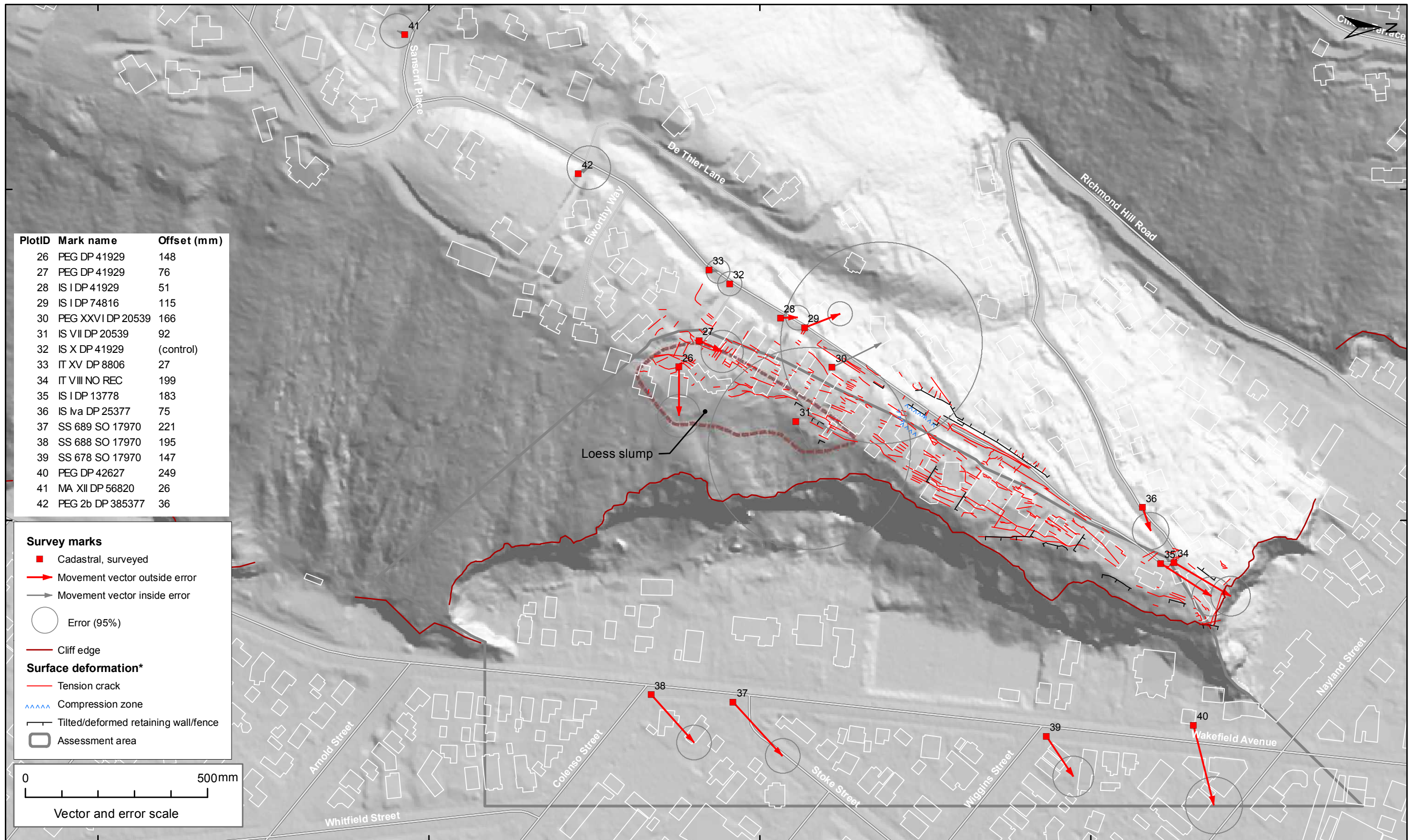
**Richmond Hill Road
Christchurch**

APPENDIX 4

Map 1

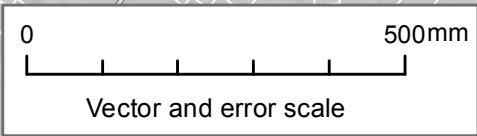
FINAL

REPORT:
CR2014/34 DATE:
June 2014



PlotID	Mark name	Offset (mm)
26	PEG DP 41929	148
27	PEG DP 41929	76
28	IS I DP 41929	51
29	IS I DP 74816	115
30	PEG XXVI DP 20539	166
31	IS VII DP 20539	92
32	IS X DP 41929	(control)
33	IT XV DP 8806	27
34	IT VIII NO REC	199
35	IS I DP 13778	183
36	IS Iva DP 25377	75
37	SS 689 SO 17970	221
38	SS 688 SO 17970	195
39	SS 678 SO 17970	147
40	PEG DP 42627	249
41	MA XII DP 56820	26
42	PEG 2b DP 385377	36

- Survey marks**
- Cadastral, surveyed
 - Movement vector outside error
 - Movement vector inside error
 - Error (95%)
 - Cliff edge
- Surface deformation***
- Tension crack
 - AAAAA Compression zone
 - Tilted/deformed retaining wall/fence
 - Assessment area



5175200

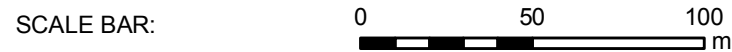
5175400

5175600

5175800

1580200

1580400



EXPLANATION:

* Taken from report CR2012/317

Background shade model derived from NZAM post earthquake 2011c (July 2011) LiDAR survey resampled to a 1 m ground resolution.
 Roads and building footprints provided by Christchurch City Council (20/02/2012).
 PROJECTION: New Zealand Transverse Mercator 2000

DRW:
BL
CHK:
CM, GA



MOVEMENT VECTORS
Cadastral Marks (Source: LINZ)
Total Movement - Pre 22-02-2011 to 30-10-2012

Richmond Hill Road
Christchurch

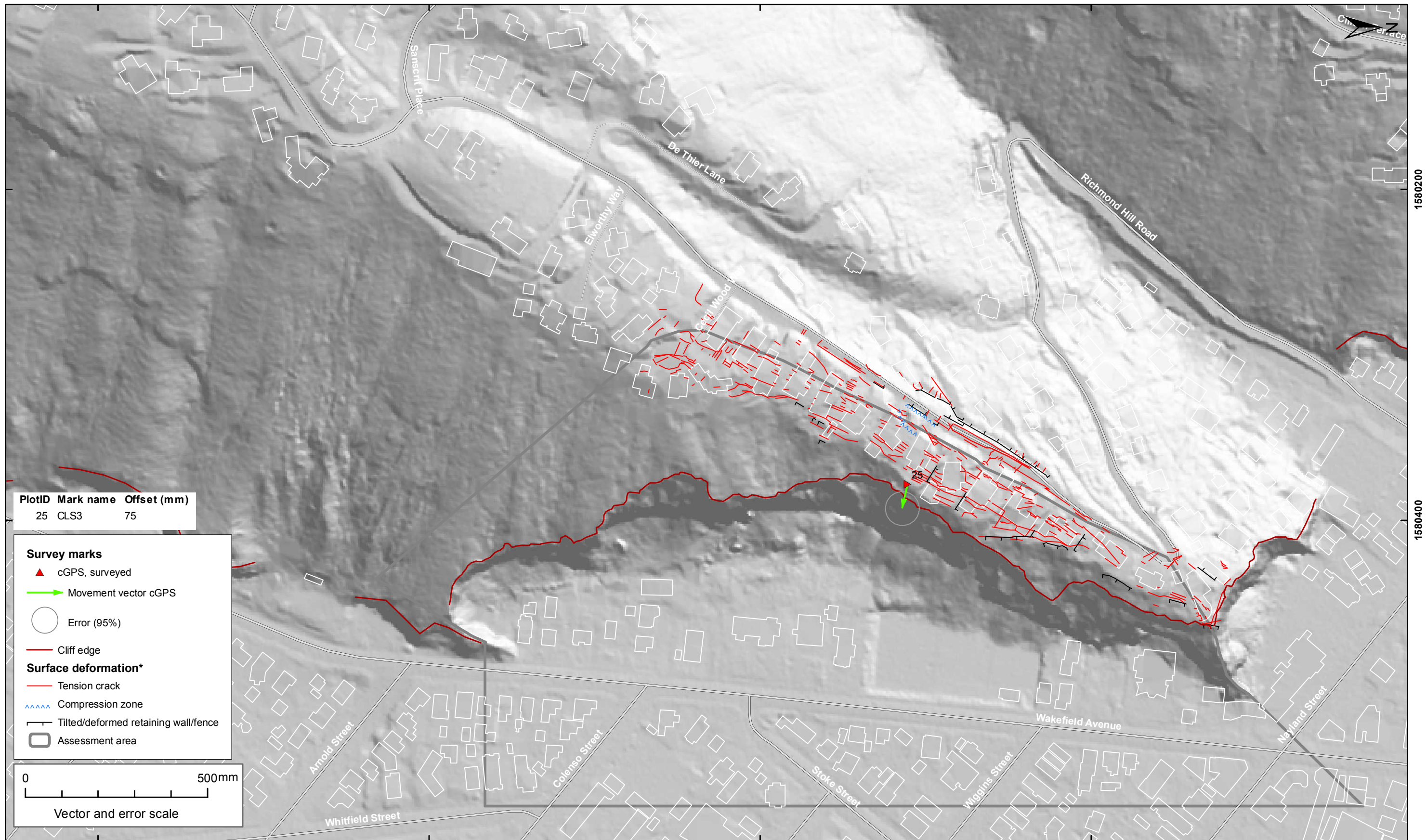
APPENDIX 4

Map 2

FINAL

REPORT:
CR2014/34

DATE:
June 2014



SCALE BAR: 0 50 100 m

EXPLANATION:

* Taken from the report CR2012/317

Background shade model derived from NZAM post earthquake 2011c (July 2011) LiDAR survey resampled to a 1 m ground resolution.

Roads and building footprints provided by Christchurch City Council (20/02/2012).

PROJECTION: New Zealand Transverse Mercator 2000

DRW:
BL

CHK:
CM, GA



MOVEMENT VECTORS
cGPS Marks (Source: GeoNet)
Earthquake Related Movement - 23 Dec 2011 (M 5.9)

Richmond Hill Road
Christchurch

APPENDIX 4

Map 3

FINAL

REPORT:
CR2014/34

DATE:
June 2014

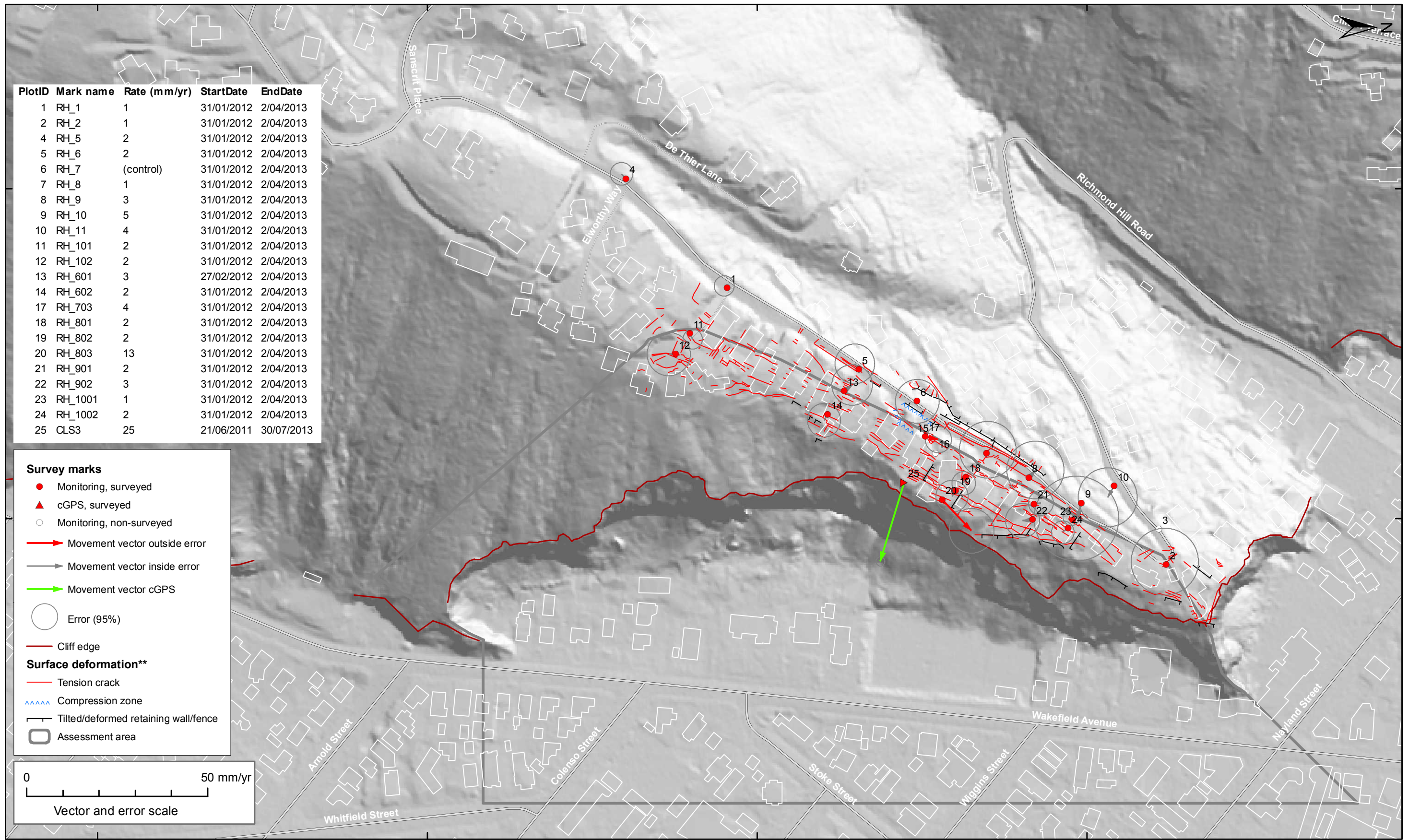
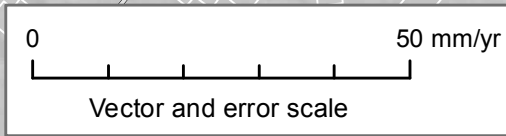
PlotID	Mark name	Rate (mm/yr)	StartDate	EndDate
1	RH_1	1	31/01/2012	2/04/2013
2	RH_2	1	31/01/2012	2/04/2013
4	RH_5	2	31/01/2012	2/04/2013
5	RH_6	2	31/01/2012	2/04/2013
6	RH_7	(control)	31/01/2012	2/04/2013
7	RH_8	1	31/01/2012	2/04/2013
8	RH_9	3	31/01/2012	2/04/2013
9	RH_10	5	31/01/2012	2/04/2013
10	RH_11	4	31/01/2012	2/04/2013
11	RH_101	2	31/01/2012	2/04/2013
12	RH_102	2	31/01/2012	2/04/2013
13	RH_601	3	27/02/2012	2/04/2013
14	RH_602	2	31/01/2012	2/04/2013
17	RH_703	4	31/01/2012	2/04/2013
18	RH_801	2	31/01/2012	2/04/2013
19	RH_802	2	31/01/2012	2/04/2013
20	RH_803	13	31/01/2012	2/04/2013
21	RH_901	2	31/01/2012	2/04/2013
22	RH_902	3	31/01/2012	2/04/2013
23	RH_1001	1	31/01/2012	2/04/2013
24	RH_1002	2	31/01/2012	2/04/2013
25	CLS3	25	21/06/2011	30/07/2013

Survey marks

- Monitoring, surveyed
- ▲ cGPS, surveyed
- Monitoring, non-surveyed
- Movement vector outside error
- Movement vector inside error
- Movement vector cGPS
- Error (95%)
- Cliff edge

Surface deformation**

- Tension crack
- ~~~~~ Compression zone
- Tilted/deformed retaining wall/fence
- Assessment area



5175200

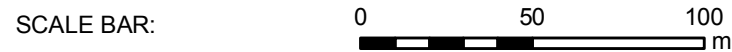
5175400

5175600

5175800

1580200

1580400



EXPLANATION:
 * Movement with assumed earthquake induced landslide movement and tectonic (earthquake) movement removed. Movement estimated from least squares adjustment (assuming a linear trend).
 ** Taken from report CR2012/317
 Background shade model derived from NZAM post earthquake 2011c (July 2011) LiDAR survey resampled to a 1 m ground resolution.
 Roads and building footprints provided by Christchurch City Council (20/02/2012).
 PROJECTION: New Zealand Transverse Mercator 2000

DRW:
BL
 CHK:
CM, GA



MOVEMENT VECTORS
Monitoring and cGPS Marks (Source: Aurecon, GeoNet)
Filtered Linear Movement*

Richmond Hill Road
Christchurch

APPENDIX 4

Map 4

FINAL

REPORT: CR2014/34 DATE: June 2014

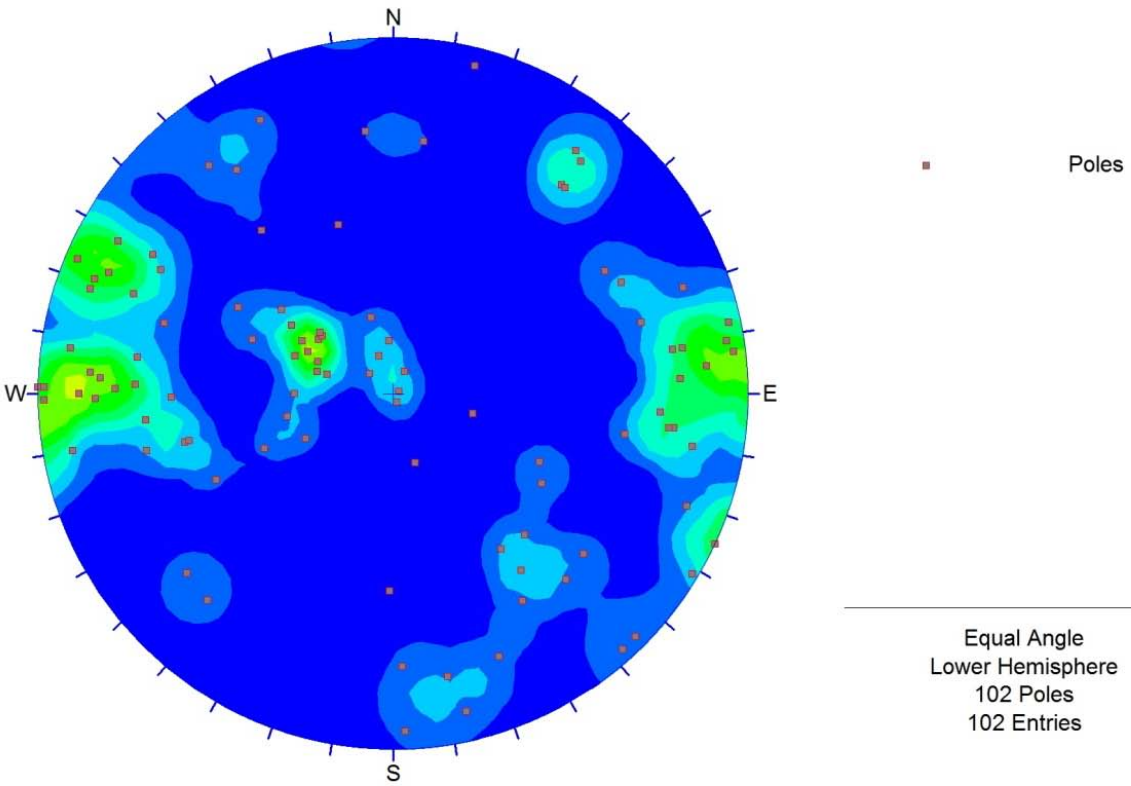
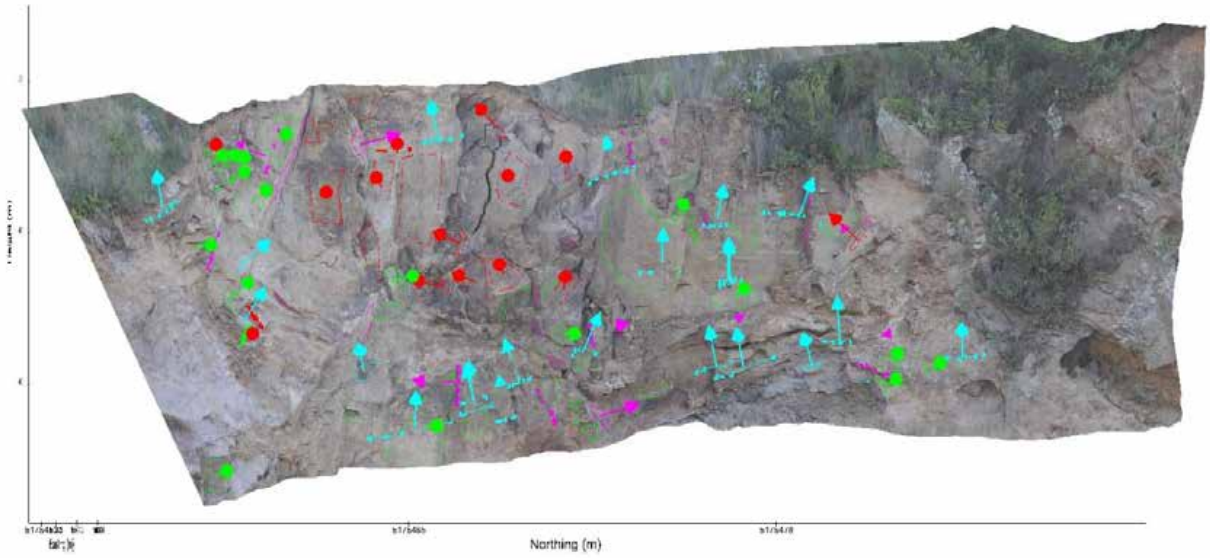
A5 APPENDIX 5: STEREONET KINEMATIC ANALYSIS OF RICHMOND HILL DISCONTINUITY DATA

The methods adopted to derive the results in Appendix 5 are described in:

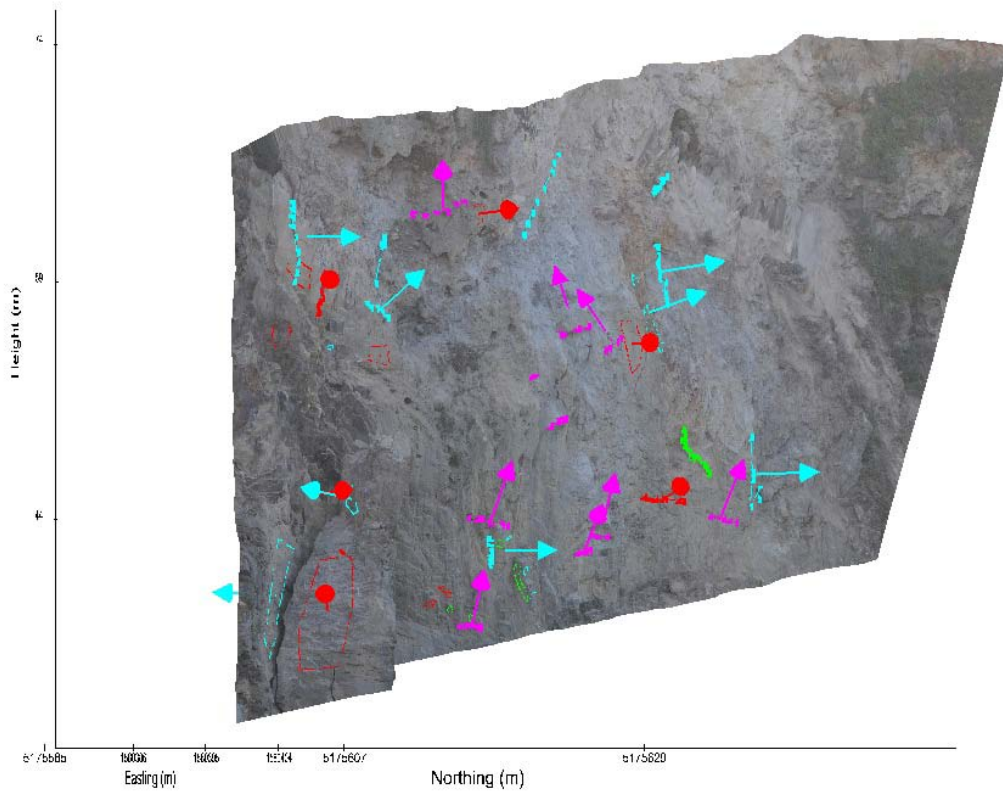
Brideau, M-A., Massey, C.I., Archibald, G.C., Jaboyedoff, M. 2012 Terrestrial photogrammetry and LiDAR investigation of the cliffs associated with the seismically triggered rockfalls during the February and June 2011 Christchurch earthquakes. p. 1179–1185 In: Eberhardt, E.B., Froese, C., Turner, K., Leroueil, S., Landslides and engineered slopes: protecting society through improved understanding: proceedings of the 11th International and 2nd North American Symposium on Landslides and Engineered Slopes, Banff, Canada, 3–8 June 2012. CRC Press.

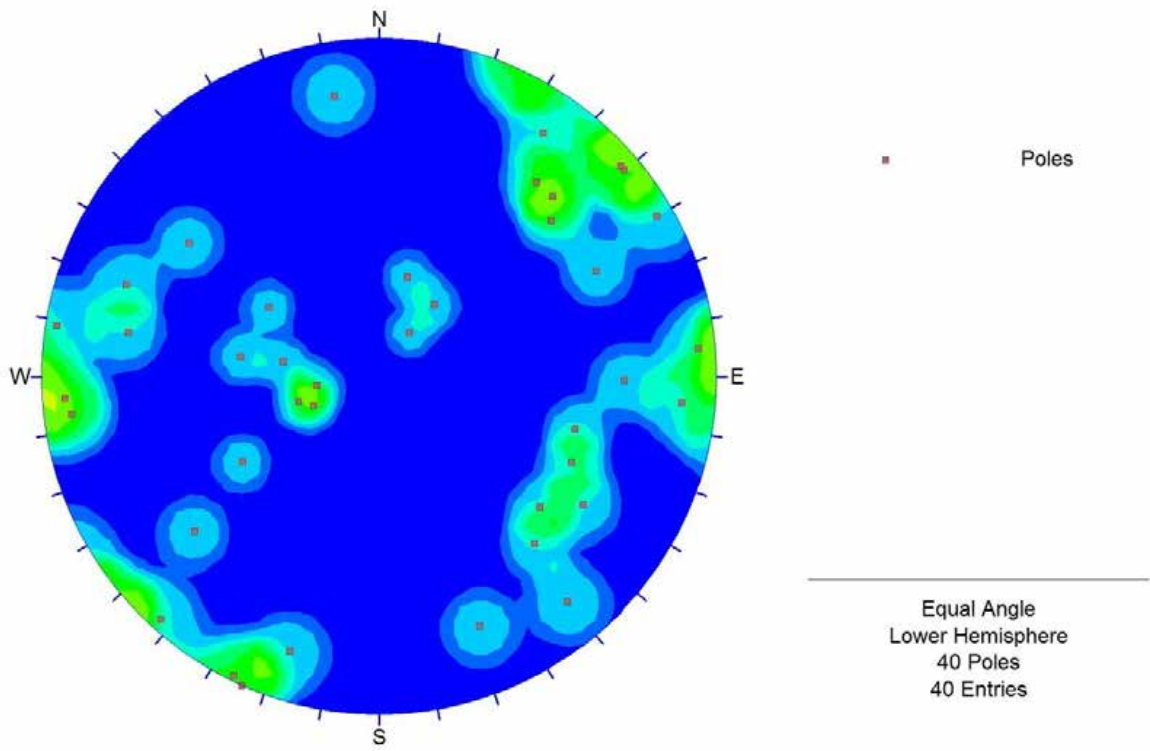
Wakefield pair 1, discontinuity orientation, July 20, 2011





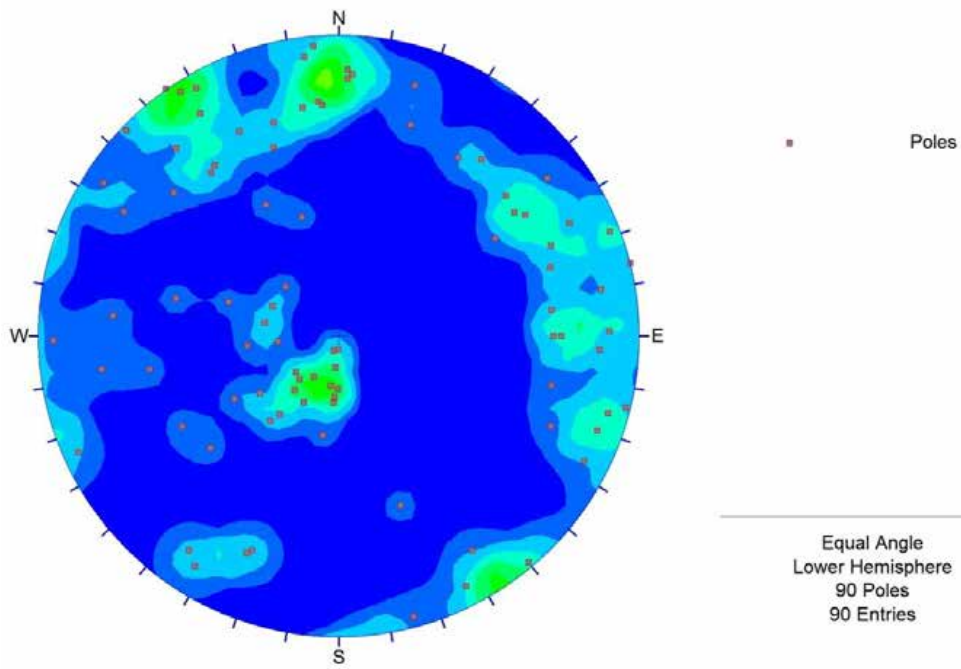
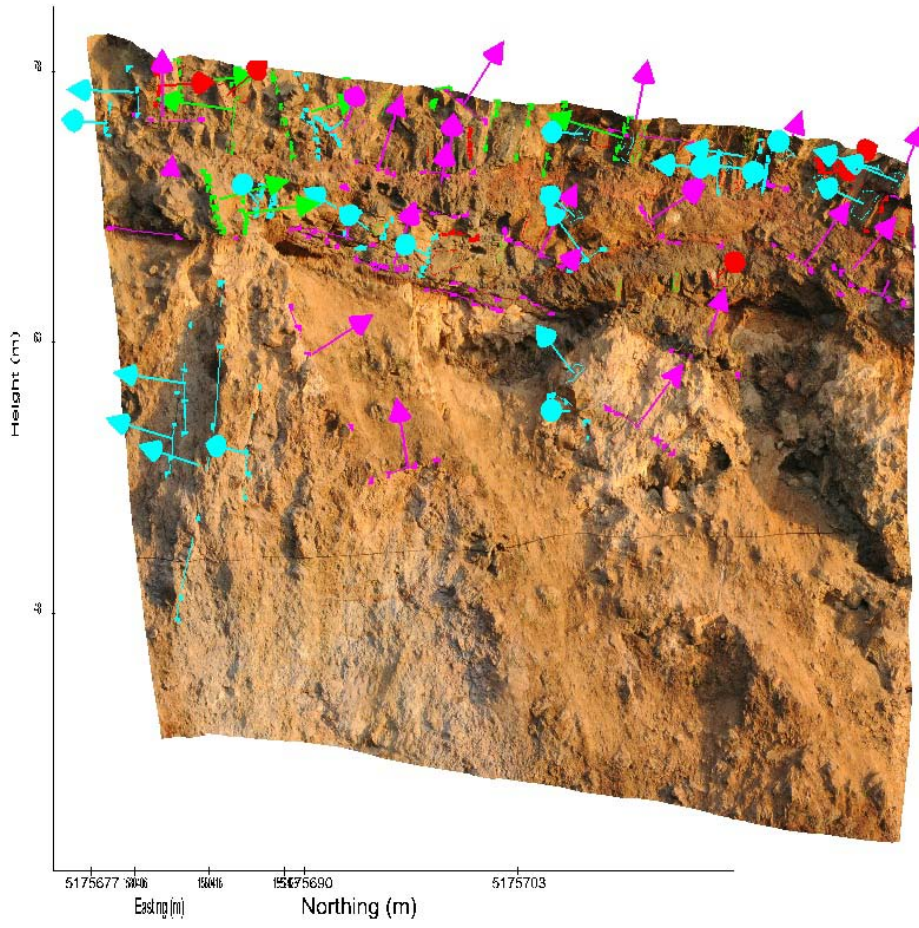
Wakefield pair 2, discontinuity orientation, July 20, 2011



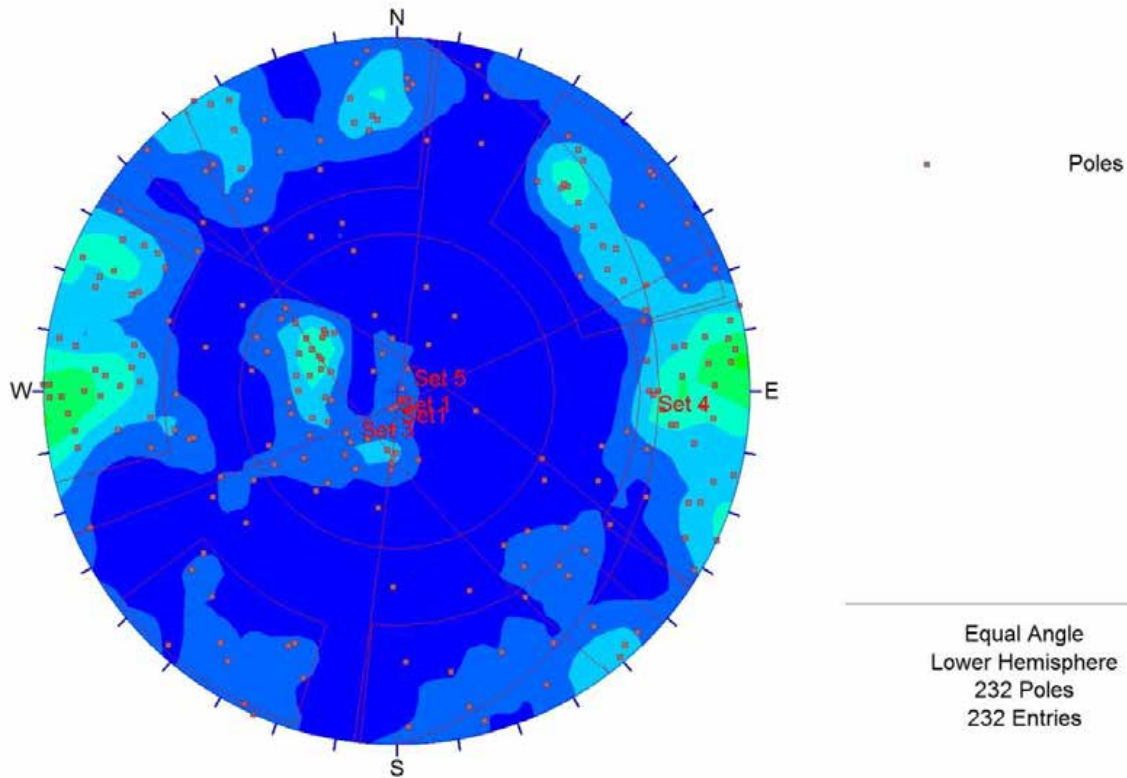


Wakefield pair 3, discontinuity orientation, July 20, 2011





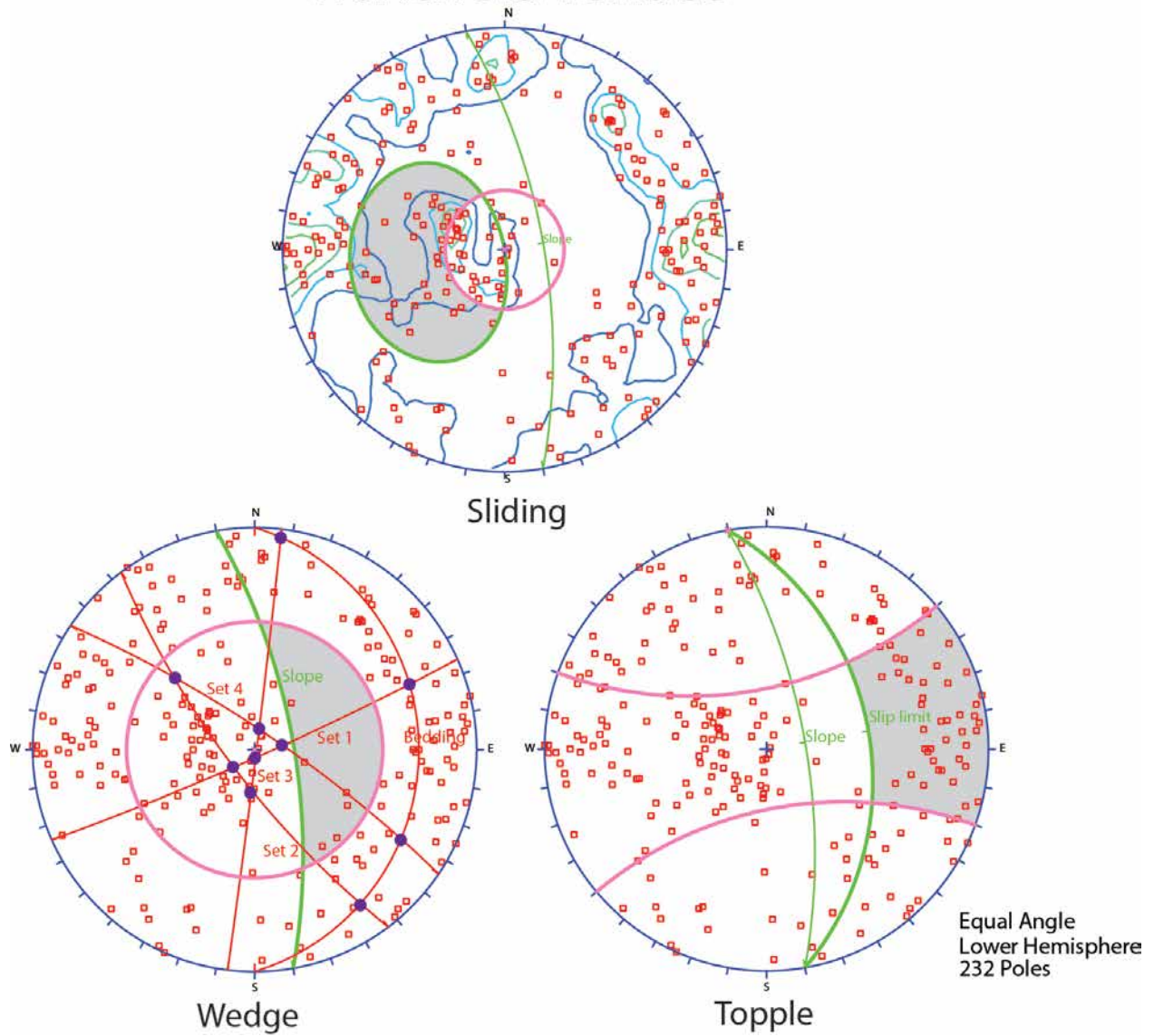
Wakefield all 3 pairs combined, discontinuity orientation, July 20, 2011



Set	Dip	Direction
1	89	097
2	86	156
3	76	233
4	17	090
5	80	034

Preliminary kinematic analysis of the Wakefield Terrace. Assumed slope 70°/080° (dip/dip direction) and friction angle of 30°.

Wakefield Terrace



A6 APPENDIX 6: RESULTS FROM THE TWO-DIMENSIONAL SITE RESPONSE ASSESSMENT FOR CROSS-SECTION 2

A6.1 DYNAMIC CONDITIONS –GROUND RESPONSE

The results from the two-dimensional site response modelling are shown for cross-section 2. The maximum acceleration (A_{MAX}) at the slope crest derived from the modelling of each synthetic earthquake time history has been plotted in Figure A6.1. The slope crest is defined as the convex break in slope between the lower steeper slope and the upper less steep slope. Each point on the graph represents the response of this location to a given synthetic free field rock outcrop earthquake input motion (Table A6.1).

The fundamental frequency of the slope varies from 3.3 to 6 Hz based on the equation in Bray and Travasarou (2007), where frequency = $1/(4 \times H/V_s)$, and H = slope height of 65 m, and V_s = shear wave velocity of between 850 and 1500 m/s. The dominant frequency of the input motions is 3.6 Hz and then 5.7 Hz. The “tuning ratio” defined as the ratio between the dominant frequency of the input motion and the fundamental frequency of the slope is about 1.1 and 1.0 (Wartman et al., 2013).

Results from the seismic response assessment suggest that the PGA amplification factors (S_T) for Richmond Hill vary between 1.7 and 3.4 times for horizontal motions, with a mean of 2.8, and 2.3 and 3.6 for vertical motions with a mean of 2.7 (Figure A6.2 and A6.3).

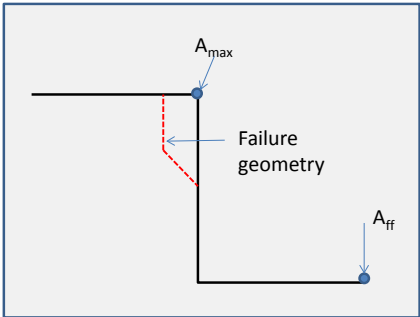
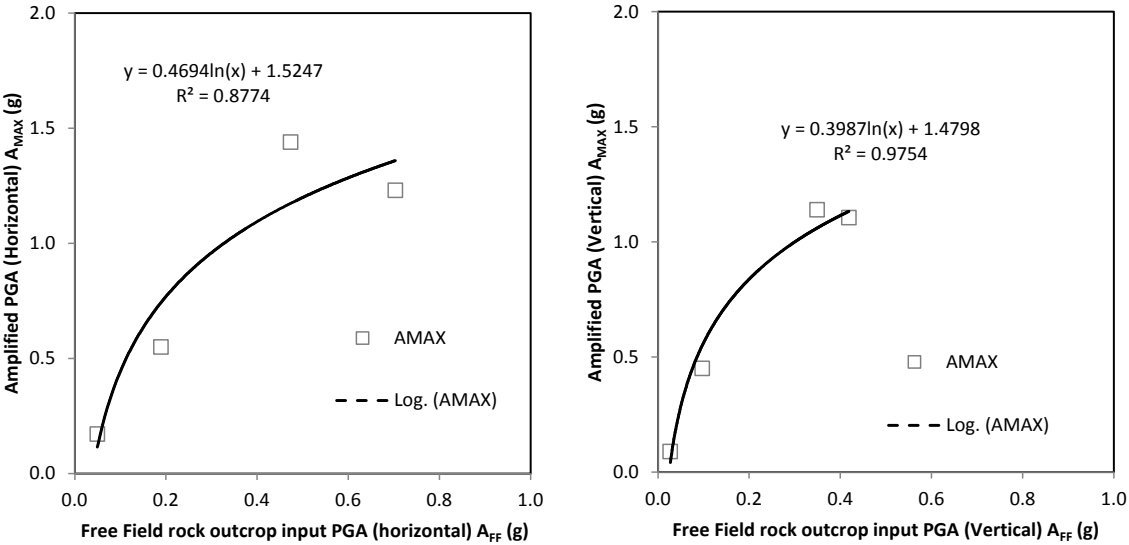


Figure A6.1 Amplification relationship between the synthetic free field rock outcrop input motions (A_{FF}) and the modelled cliff edge maximum accelerations (A_{MAX}) for cross-section 2. A schematic diagram showing the locations of the various recorded accelerations is shown.

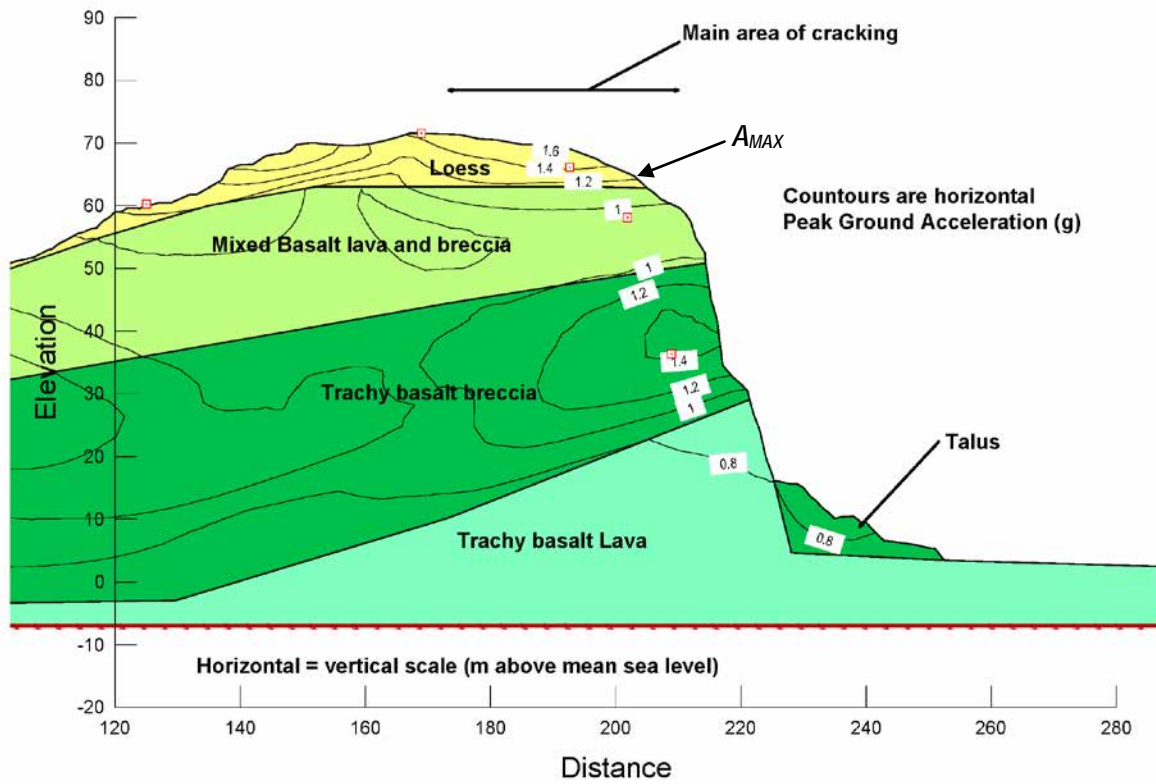


Figure A6.2 Modelled peak horizontal ground acceleration contours for the 22 February 2011 earthquake at Richmond Hill, cross-section 2, adopting the 2003 airborne LiDAR slope surface geometry. Contours are peak horizontal ground accelerations (g).

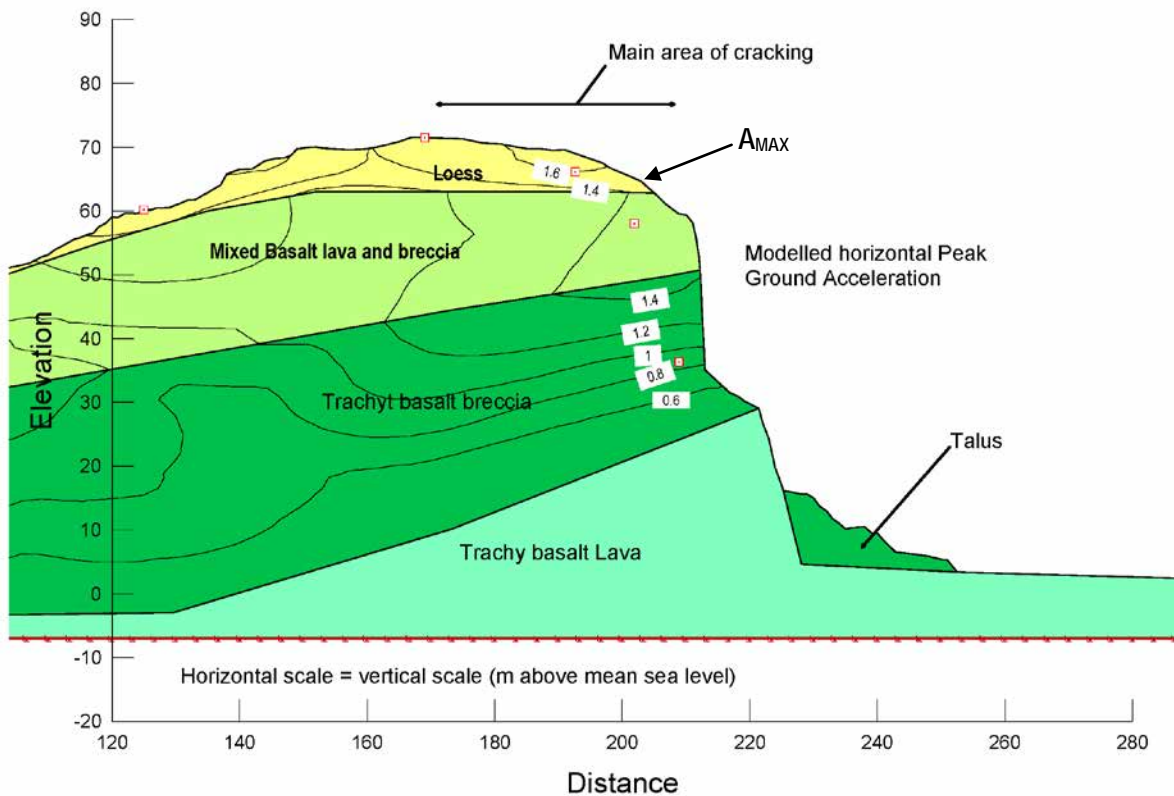


Figure A6.3 Modelled peak horizontal ground acceleration contours for the 13 June 2011 earthquake at Richmond Hill, cross-section 2, adopting the 2003 airborne LiDAR slope surface geometry. Contours are peak horizontal ground accelerations (g).

Results from this assessment have shown that the relationship between the peak ground acceleration of the free field input motion and the corresponding modelled peak acceleration at the cliff edge (A_{MAX}), is linear up to an input peak acceleration of about 0.4 g. In this range of peak accelerations the amplification factor is typically in the order of about 3.0 times the input free field peak acceleration. Above peak ground accelerations of 0.4 g the relationship becomes non-linear, where the amplification factor reduces to about 1.5 times the input free field peak acceleration.

Table A6.1 Results from the two-dimensional site response assessment for cross-section 2 using the synthetic free field rock outcrop motions for the Richmond Hill site by Holden et al. (2014) as inputs to the assessment.

Earthquake (2011)	Free field input PGA (horizontal) – A_{FF} (g)	Free field input PGA (vertical) – A_{FF} (g)	Maximum PGA (horizontal) at cliff edge – A_{MAX} (g)	Maximum PGA (vertical) at cliff edge – A_{MAX} (g)
22 February	0.70	0.42	1.23	1.11
16 April	0.05	0.03	0.17	0.09
13 June	0.47	0.35	1.44	1.14
23 December	0.19	0.10	0.55	0.45

The relationship between the modelled vertical and horizontal peak ground accelerations recorded at the cliff edge (A_{MAX}) is shown in Figure A6.4. The gradient of the linear fit is 0.64 (± 0.05) – errors at one standard deviation (STD), with a gradient of 0.7 being the mean plus two standard deviations. The relationship between horizontal and vertical peak ground accelerations appears linear to a horizontal peak ground acceleration of 1.4 g, but then appears to become non-linear at higher horizontal peak ground accelerations.

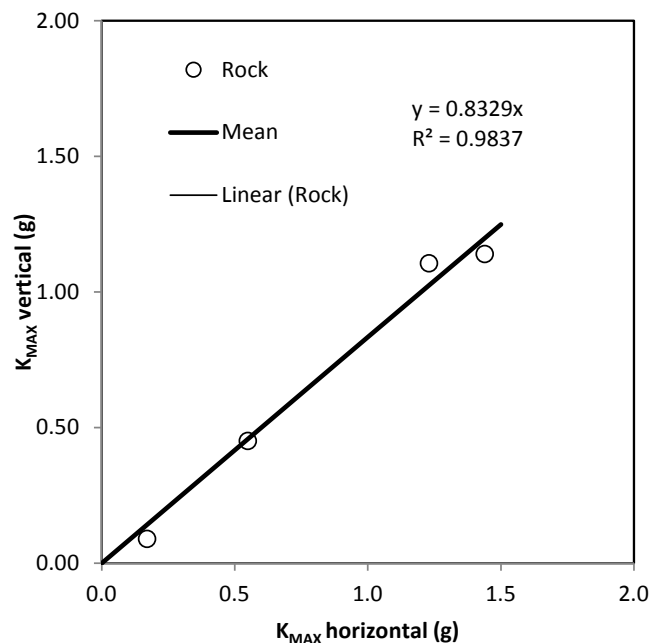


Figure A6.4 Relationship between the modelled horizontal and vertical maximum accelerations modelled at the cliff edge (A_{MAX}) for cross-section 2, using the synthetic free field rock outcrop motions for the Richmond Hill site by Holden et al. (2014) as inputs to the assessment. The mean trend line is fitted for A_{MAX} all data.

Eurocode 8, Part 5, Annex A, gives some simplified amplification factors for the seismic action used in the verification of the stability of slopes. Such factors, denoted S_T , are to a first approximation considered independent of the fundamental period of vibration and, hence, multiply as a constant scaling factor.

Eurocode 8, Part 5, Annex A recommends:

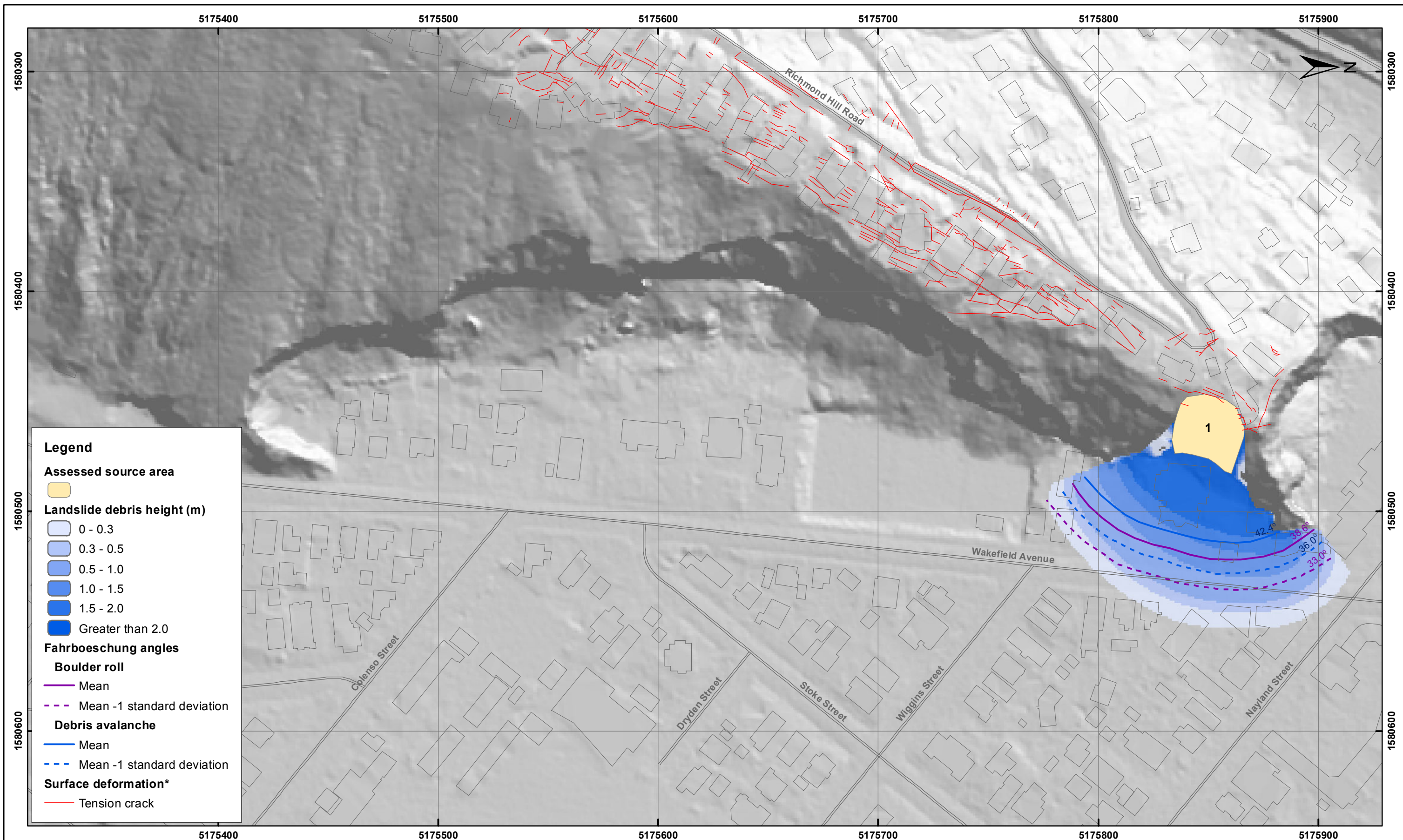
1. Isolated cliffs and slopes. A value $S_T \geq 1.2$ should be used for sites near the top edge;
2. Ridges with crest width significantly less than the base width. A value $S_T \geq 1.4$ should be used near the top of the slopes for average slope angles greater than 30° and a value $S_T > 1.2$ should be used for smaller slope angles;
3. Presence of a loose surface layer. In the presence of a loose surface layer, the smallest S_T value given in a) and b) should be increased by at least 20%;
4. Spatial variation of amplification factor. The value of S_T may be assumed to decrease as a linear function of the height above the base of the cliff or ridge, and to be unity at the base.

These amplification factors should in preference be applied when the slopes belong to two-dimensional topographic irregularities, such as long ridges and cliffs of height greater than about 30 m.

Ashford and Sitar (2002) recommend an S_T of 1.5 be applied to the maximum free field acceleration behind the crest based on their assessment of slopes typically $>60^\circ$ to near vertical and of heights (toe to crest) of typically >30 m. This factor is based on the assessment of slopes that failed during the 1989 Loma Prieta M_W 6.9 earthquake.

However, the results from this assessment also show that the relationship between the peak free field acceleration and peak ground acceleration at the cliff edge is non-linear, i.e., amplified at low rock input peak accelerations but less so at high rock input accelerations. These results are similar to those reported by others, e.g., Bray and Rathje, (1998) and Kramer (1996), indicating that the choice of amplification factor used, should vary with the magnitude of the peak acceleration of the input motion.

**A7 APPENDIX 7: RAMMS MODELLING RESULTS FOR SOURCE AREAS
1–10 ADOPTING THE MIDDLE ESTIMATES OF SOURCE VOLUME;
DEBRIS HEIGHT**

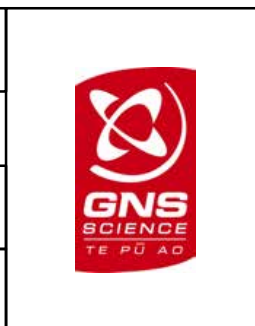


SCALE BAR: 0 50 100 m

EXPLANATION:
 * Taken from report CR2012/317
 Background shade model derived from NZAM post earthquake 2011c (July 2011) LiDAR survey resampled to a 1 m ground resolution. Roads and building footprints and types provided by Christchurch City Council (20/02/2012).
 PROJECTION: New Zealand Transverse Mercator 2000

DRW:
BL, WR

CHK:
CM



ESTIMATED LANDSLIDE RUNOUT HEIGHT
Source 1 - Middle Volume (7,800 m³)

Richmond Hill Road - Port Hills
Christchurch

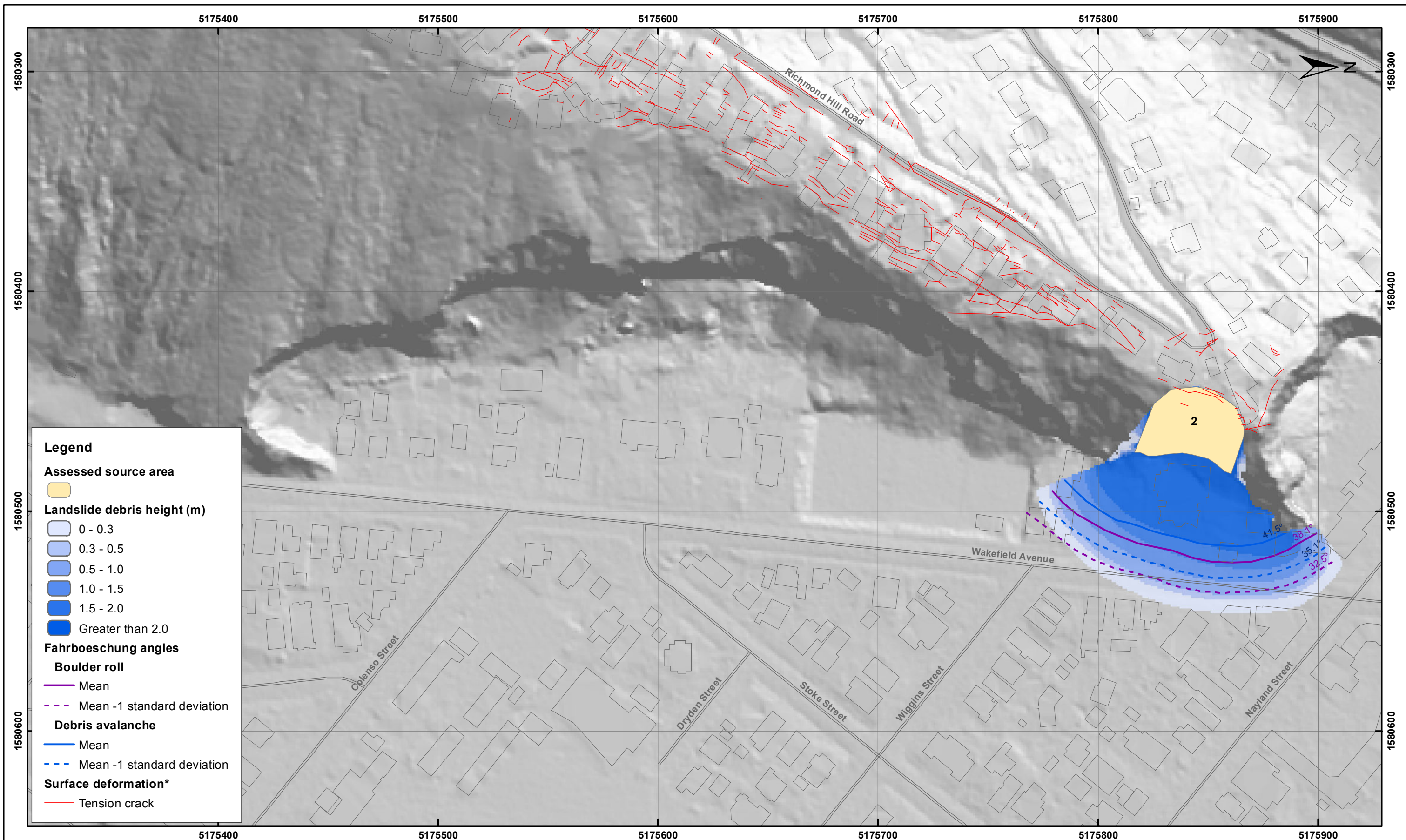
APPENDIX 7

Map 1

FINAL

REPORT:
CR2014/34

DATE:
June 2014

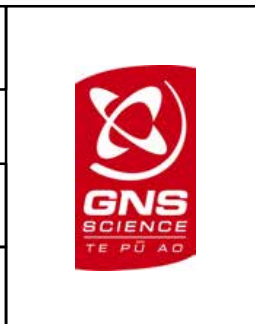


SCALE BAR: 0 50 100 m

EXPLANATION:
 * Taken from report CR2012/317
 Background shade model derived from NZAM post earthquake 2011c (July 2011) LiDAR survey resampled to a 1 m ground resolution. Roads and building footprints and types provided by Christchurch City Council (20/02/2012).
 PROJECTION: New Zealand Transverse Mercator 2000

DRW:
BL, WR

CHK:
CM



ESTIMATED LANDSLIDE RUNOUT HEIGHT
Source 2 - Middle Volume (12,000 m³)

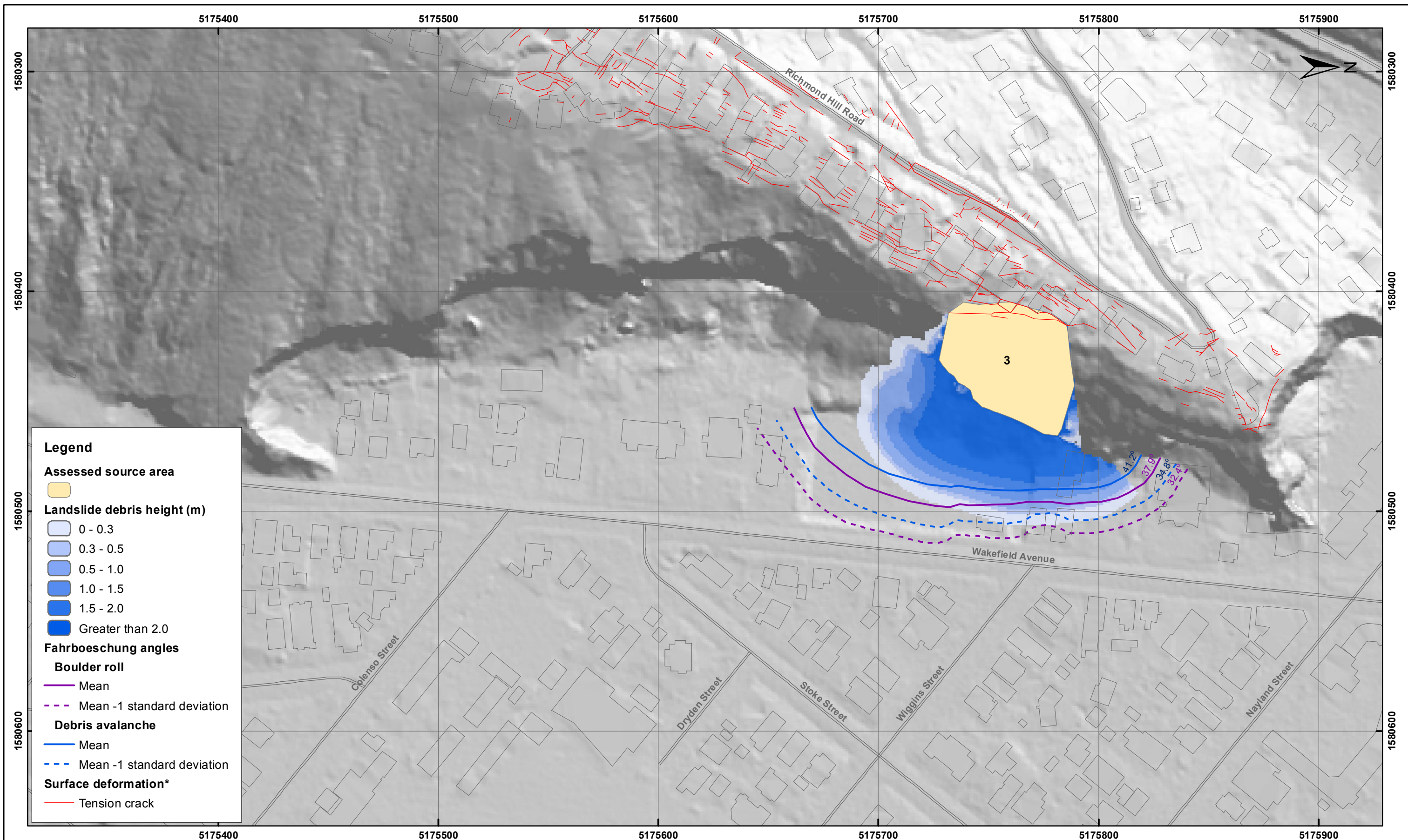
Richmond Hill Road - Port Hills
Christchurch

APPENDIX 7


Map 2







FINAL

REPORT: CR2014/34 DATE: June 2014







Legend


Assessed source area


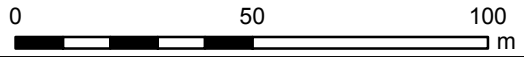
Landslide debris height (m)
 0 - 0.3
 0.3 - 0.5
 0.5 - 1.0
 1.0 - 1.5
 1.5 - 2.0
 Greater than 2.0

Fahrboeschung angles

Boulder roll
 Mean
 Mean -1 standard deviation

Debris avalanche
 Mean
 Mean -1 standard deviation

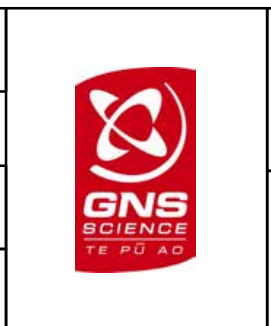
Surface deformation*
 Tension crack

SCALE BAR: 

EXPLANATION:
 * Taken from report CR2012/317
 Background shade model derived from NZAM post earthquake 2011c (July 2011) LiDAR survey resampled to a 1 m ground resolution. Roads and building footprints and types provided by Christchurch City Council (20/02/2012).
 PROJECTION: New Zealand Transverse Mercator 2000

DRW:
BL, WR

CHK:
CM



ESTIMATED LANDSLIDE RUNOUT HEIGHT
Source 3 - Middle Volume (13,600 m³)

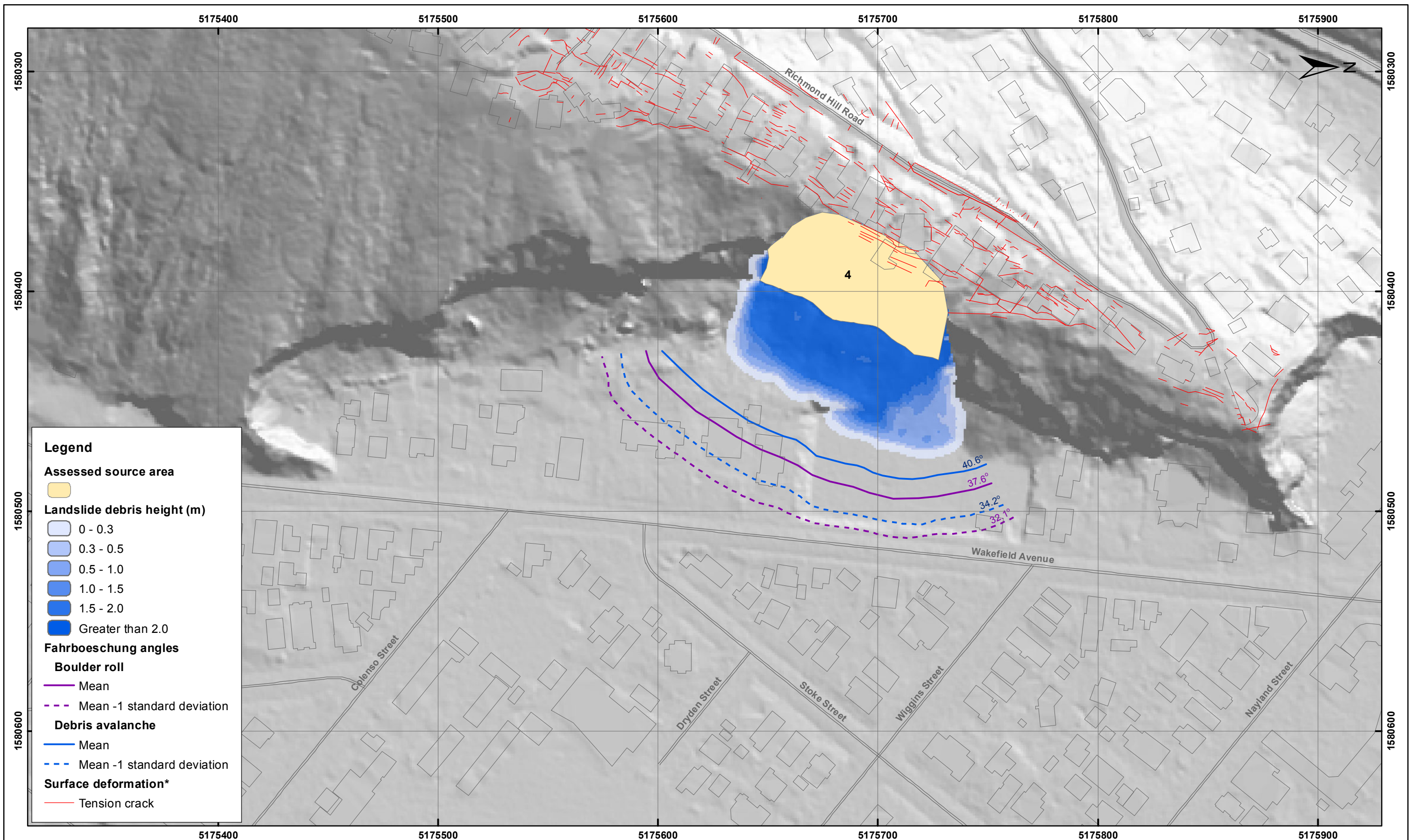
Richmond Hill Road - Port Hills
Christchurch

APPENDIX 7

Map 3

FINAL

REPORT: CR2014/34 DATE: June 2014



Legend

Assessed source area
 Yellow

Landslide debris height (m)

- 0 - 0.3
- 0.3 - 0.5
- 0.5 - 1.0
- 1.0 - 1.5
- 1.5 - 2.0
- Greater than 2.0

Fahrboeschung angles

Boulder roll

- Mean
- Mean -1 standard deviation

Debris avalanche

- Mean
- Mean -1 standard deviation

Surface deformation*

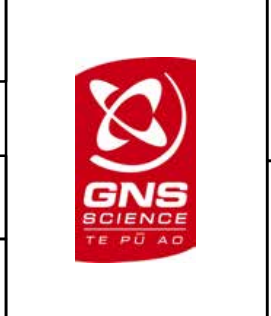
- Tension crack

SCALE BAR: 0 50 100 m

EXPLANATION:
 * Taken from report CR2012/317
 Background shade model derived from NZAM post earthquake 2011c (July 2011) LiDAR survey resampled to a 1 m ground resolution. Roads and building footprints and types provided by Christchurch City Council (20/02/2012).
 PROJECTION: New Zealand Transverse Mercator 2000

DRW:
BL, WR

CHK:
CM



ESTIMATED LANDSLIDE RUNOUT HEIGHT
Source 4 - Middle Volume (18,100 m³)

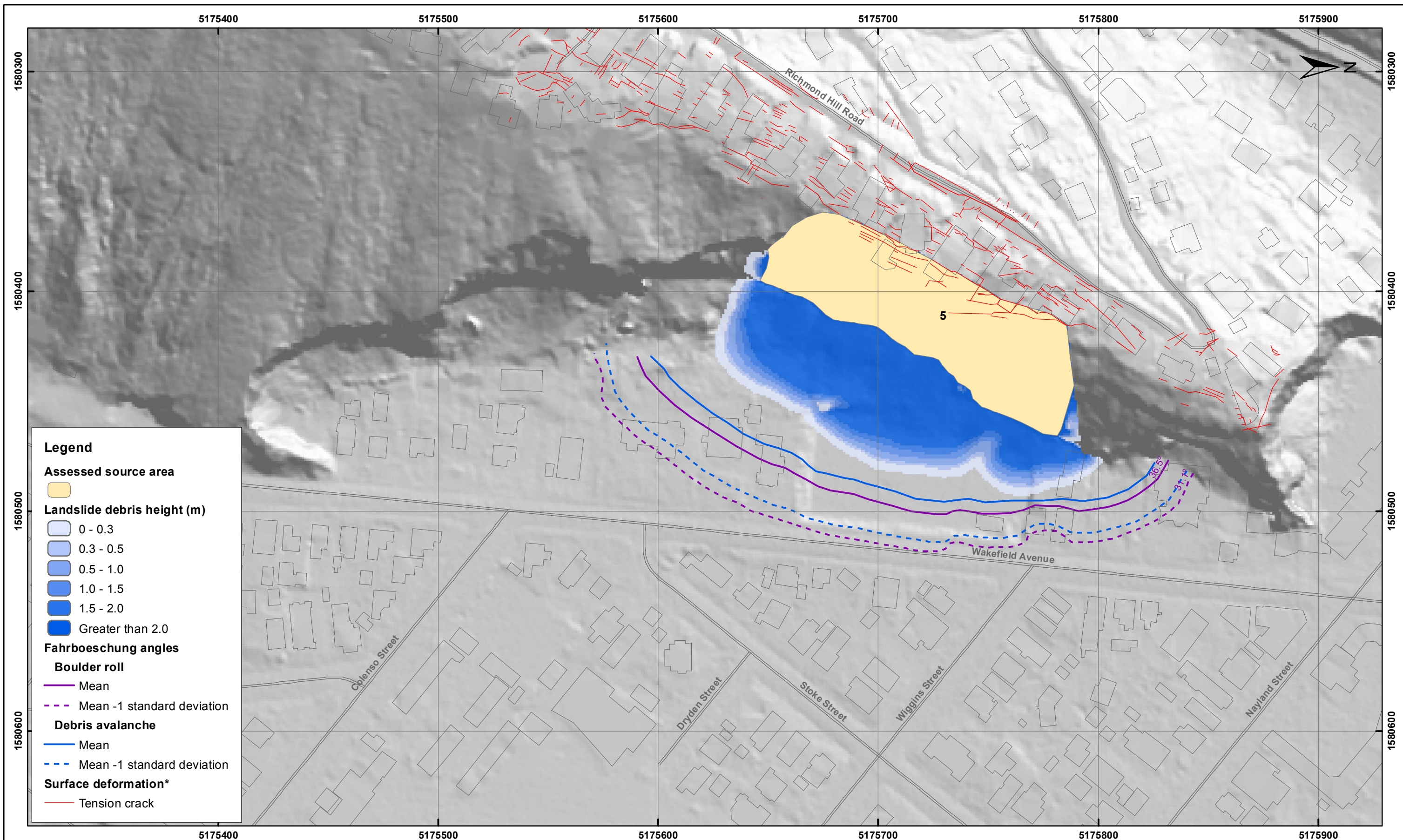
Richmond Hill Road - Port Hills
Christchurch

APPENDIX 7

Map 4

FINAL

REPORT: CR2014/34 DATE: June 2014

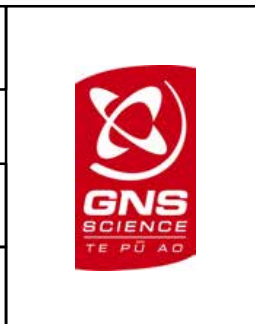


SCALE BAR: 0 50 100 m

EXPLANATION:
 * Taken from report CR2012/317
 Background shade model derived from NZAM post earthquake 2011c (July 2011) LiDAR survey resampled to a 1 m ground resolution. Roads and building footprints and types provided by Christchurch City Council (20/02/2012).
 PROJECTION: New Zealand Transverse Mercator 2000

DRW:
BL, WR

CHK:
CM



ESTIMATED LANDSLIDE RUNOUT HEIGHT
Source 5 - Middle Volume (45,200 m³)

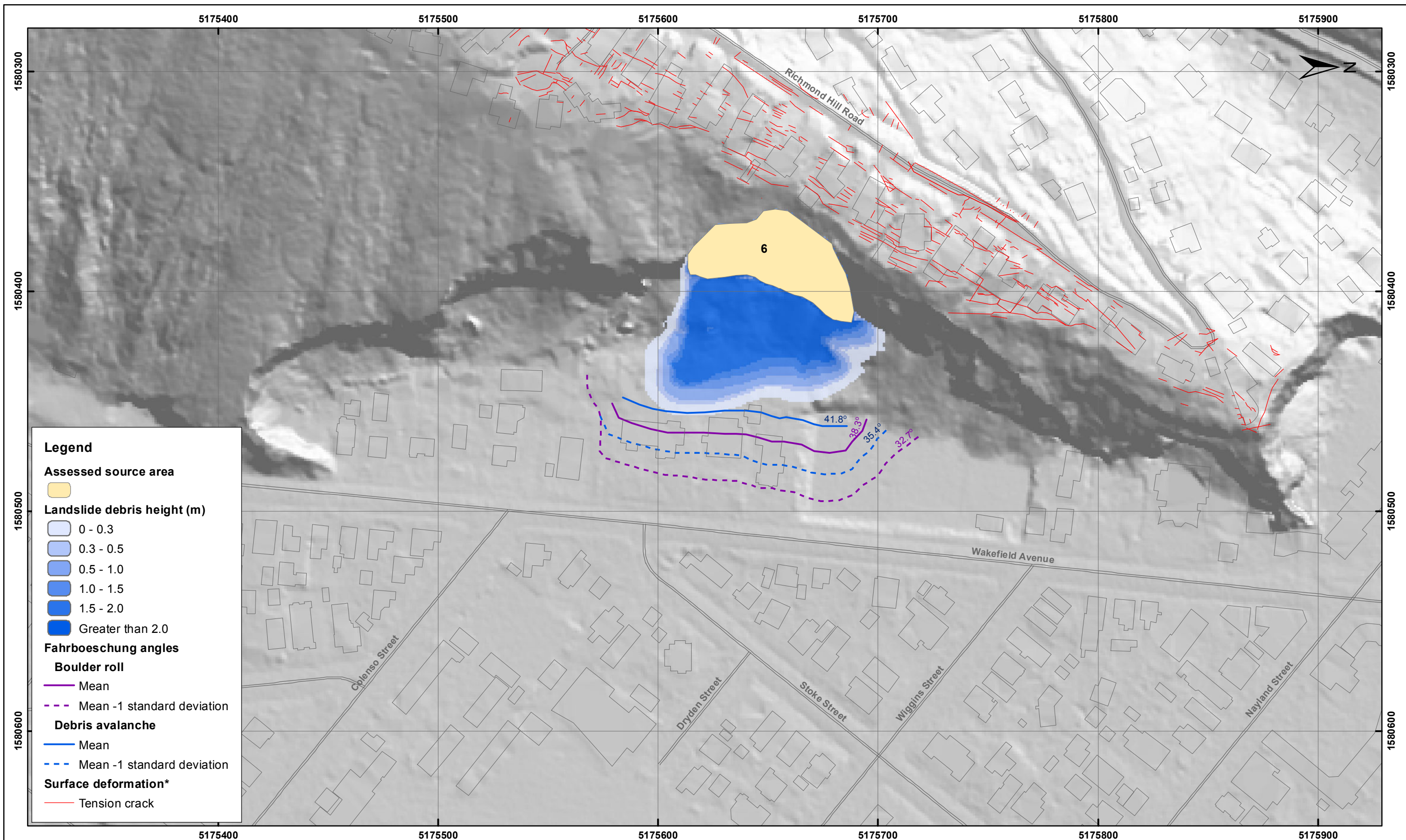
Richmond Hill Road - Port Hills
Christchurch

APPENDIX 7

Map 5

FINAL

REPORT: CR2014/34 DATE: June 2014

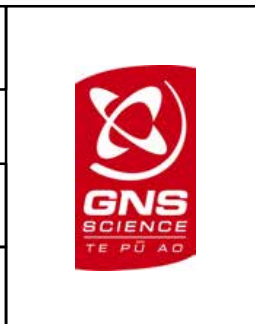


SCALE BAR: 0 50 100 m

EXPLANATION:
 * Taken from report CR2012/317
 Background shade model derived from NZAM post earthquake 2011c (July 2011) LiDAR survey resampled to a 1 m ground resolution. Roads and building footprints and types provided by Christchurch City Council (20/02/2012).
 PROJECTION: New Zealand Transverse Mercator 2000

DRW:
BL, WR

CHK:
CM



ESTIMATED LANDSLIDE RUNOUT HEIGHT
Source 6 - Middle Volume (10,100 m³)

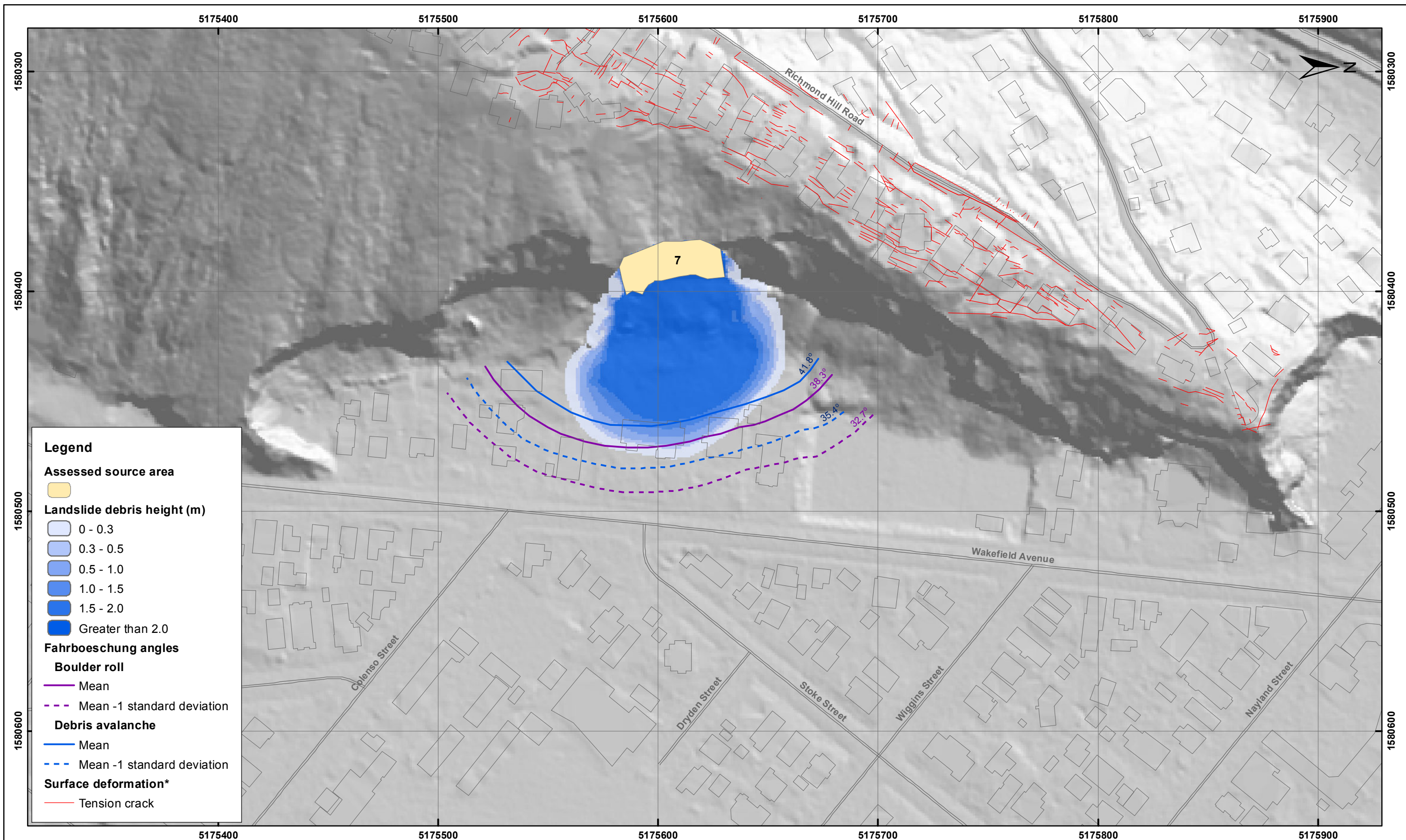
Richmond Hill Road - Port Hills
Christchurch

APPENDIX 7

Map 6

FINAL

REPORT: CR2014/34 DATE: June 2014



Legend

Assessed source area

Landslide debris height (m)

- 0 - 0.3
- 0.3 - 0.5
- 0.5 - 1.0
- 1.0 - 1.5
- 1.5 - 2.0
- Greater than 2.0

Fahrboeschung angles

Boulder roll

- Mean
- Mean -1 standard deviation

Debris avalanche

- Mean
- Mean -1 standard deviation

Surface deformation*

- Tension crack

SCALE BAR:

EXPLANATION:
 * Taken from report CR2012/317
 Background shade model derived from NZAM post earthquake 2011c (July 2011) LiDAR survey resampled to a 1 m ground resolution.
 Roads and building footprints and types provided by Christchurch City Council (20/02/2012).
 PROJECTION: New Zealand Transverse Mercator 2000

DRW:
BL, WR

CHK:
CM



ESTIMATED LANDSLIDE RUNOUT HEIGHT
Source 7 - Middle Volume (10,100 m³)

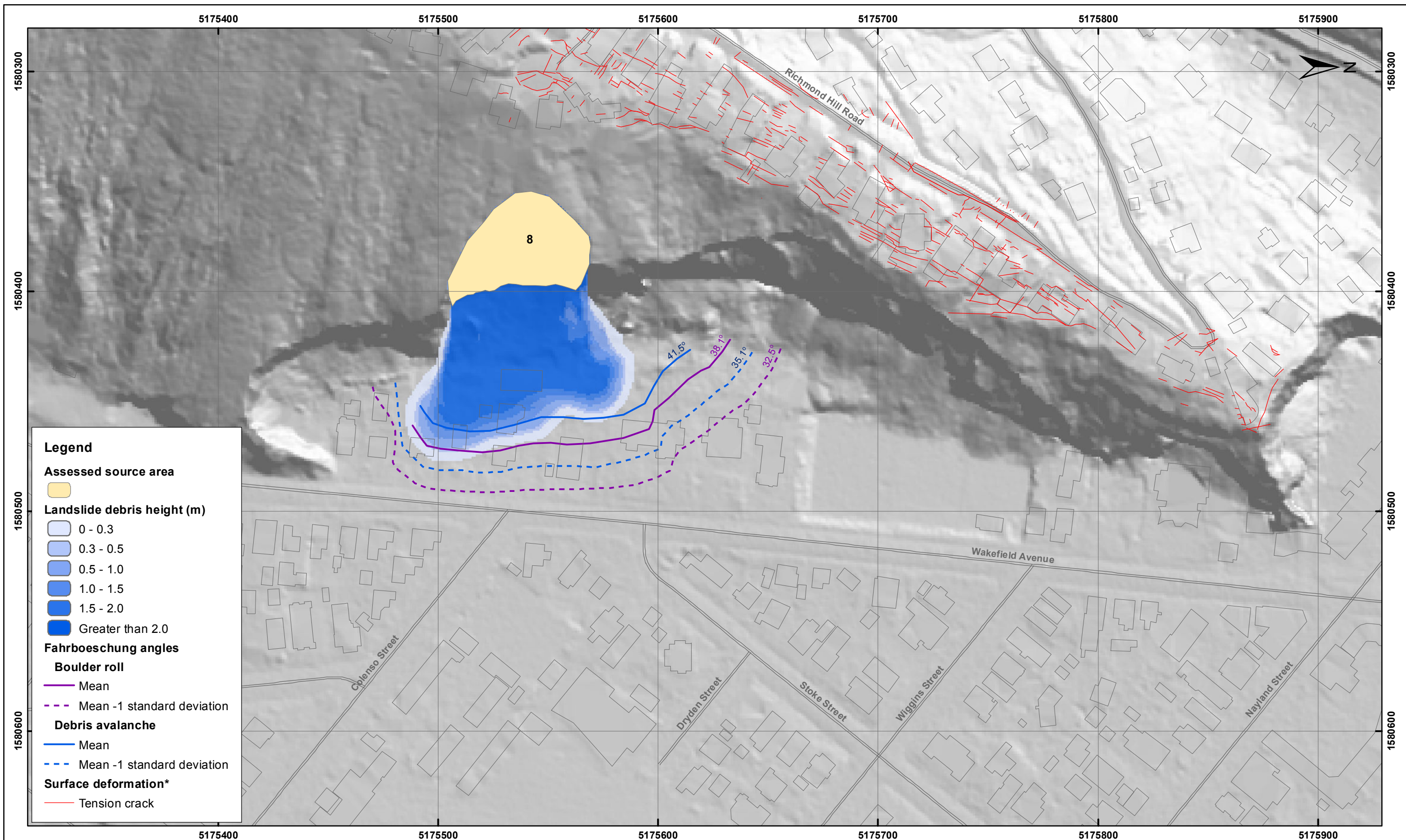
Richmond Hill Road - Port Hills
Christchurch

APPENDIX 7

Map 7

FINAL

REPORT: CR2014/34 DATE: June 2014



- Legend**
- Assessed source area**
 - Yellow
 - Landslide debris height (m)**
 - 0 - 0.3
 - 0.3 - 0.5
 - 0.5 - 1.0
 - 1.0 - 1.5
 - 1.5 - 2.0
 - Greater than 2.0
 - Fahrboeschung angles**
 - Boulder roll**
 - Mean
 - Mean -1 standard deviation
 - Debris avalanche**
 - Mean
 - Mean -1 standard deviation
 - Surface deformation***
 - Tension crack



EXPLANATION:
 * Taken from report CR2012/317
 Background shade model derived from NZAM post earthquake 2011c (July 2011) LiDAR survey resampled to a 1 m ground resolution. Roads and building footprints and types provided by Christchurch City Council (20/02/2012).
 PROJECTION: New Zealand Transverse Mercator 2000

DRW:
BL, WR
 CHK:
CM



ESTIMATED LANDSLIDE RUNOUT HEIGHT
Source 8 - Middle Volume (11,700 m³)

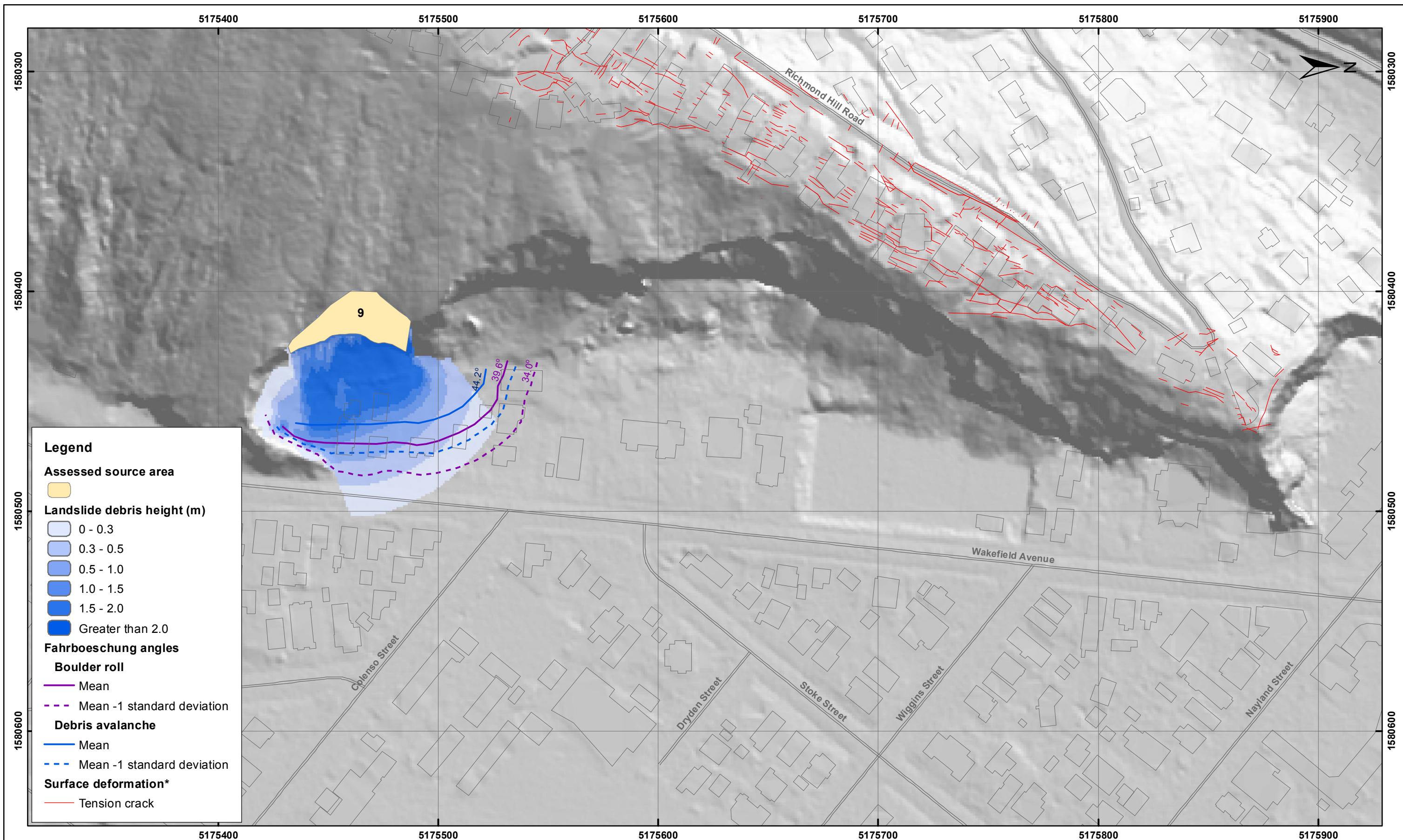
Richmond Hill Road - Port Hills
Christchurch

APPENDIX 7

Map 8

FINAL

REPORT: CR2014/34 DATE: June 2014



Legend

Assessed source area

Yellow polygon

Landslide debris height (m)

- 0 - 0.3
- 0.3 - 0.5
- 0.5 - 1.0
- 1.0 - 1.5
- 1.5 - 2.0
- Greater than 2.0

Fahrboeschung angles

Boulder roll

- Mean (solid purple line)
- Mean -1 standard deviation (dashed purple line)

Debris avalanche

- Mean (solid blue line)
- Mean -1 standard deviation (dashed blue line)

Surface deformation*

- Tension crack (red dashed line)

SCALE BAR: 0 50 100 m

EXPLANATION:

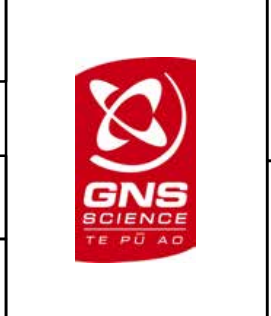
* Taken from report CR2012/317

Background shade model derived from NZAM post earthquake 2011c (July 2011) LiDAR survey resampled to a 1 m ground resolution. Roads and building footprints and types provided by Christchurch City Council (20/02/2012).

PROJECTION: New Zealand Transverse Mercator 2000

DRW:
BL, WR

CHK:
CM



ESTIMATED LANDSLIDE RUNOUT HEIGHT
Source 9 - Middle Volume (3,400 m³)

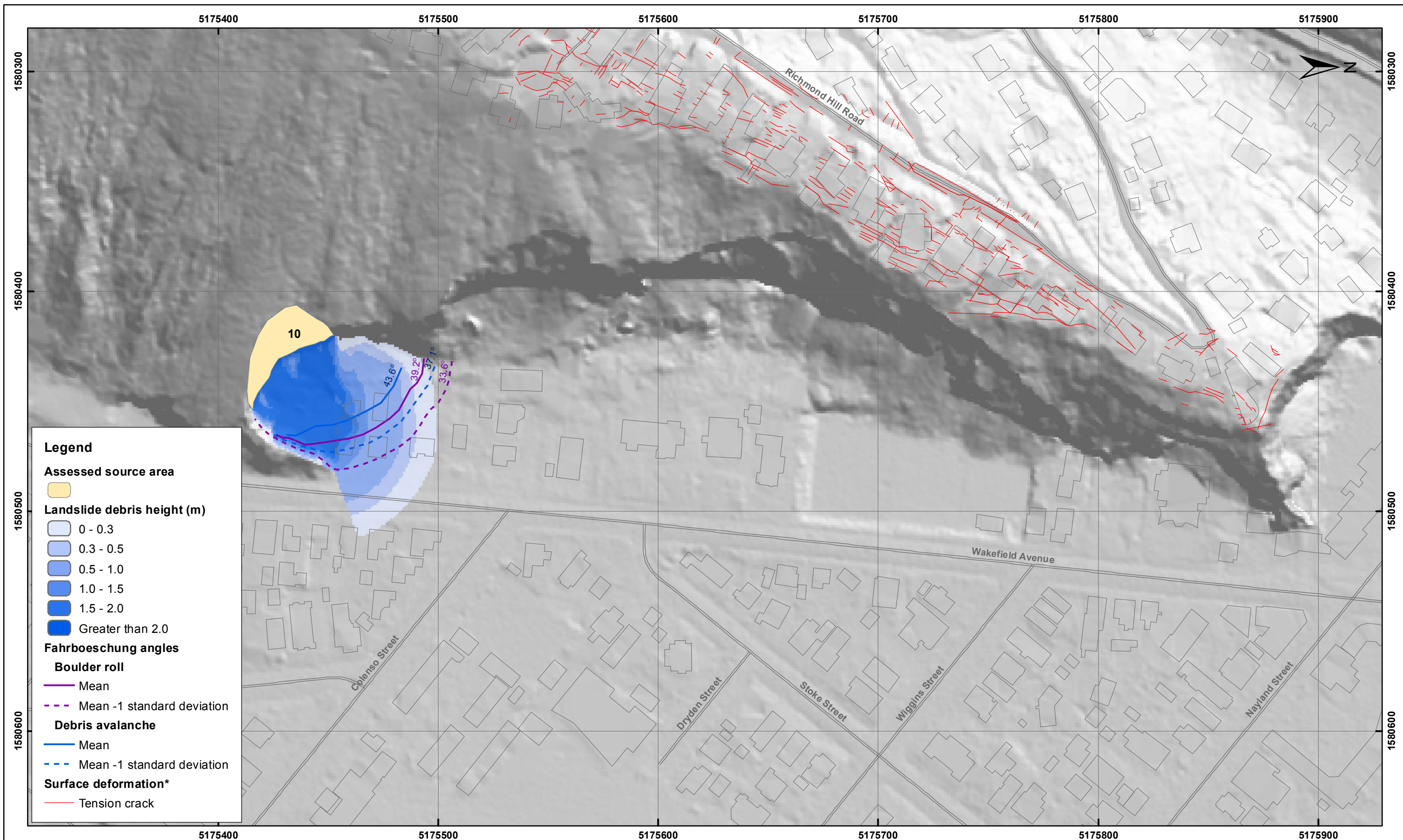
Richmond Hill Road - Port Hills
Christchurch

APPENDIX 7

Map 9

FINAL

REPORT: CR2014/34 DATE: June 2014

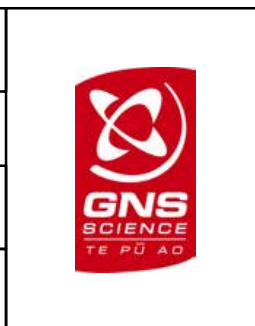


SCALE BAR: 0 50 100 m

EXPLANATION:
 * Taken from report CR2012/317
 Background shade model derived from NZAM post earthquake 2011c (July 2011) LiDAR survey resampled to a 1 m ground resolution. Roads and building footprints and types provided by Christchurch City Council (20/02/2012).
 PROJECTION: New Zealand Transverse Mercator 2000

DRW:
BL, WR

CHK:
CM



ESTIMATED LANDSLIDE RUNOUT HEIGHT
Source 10 - Middle Volume (4,500 m³)

Richmond Hill Road - Port Hills
Christchurch

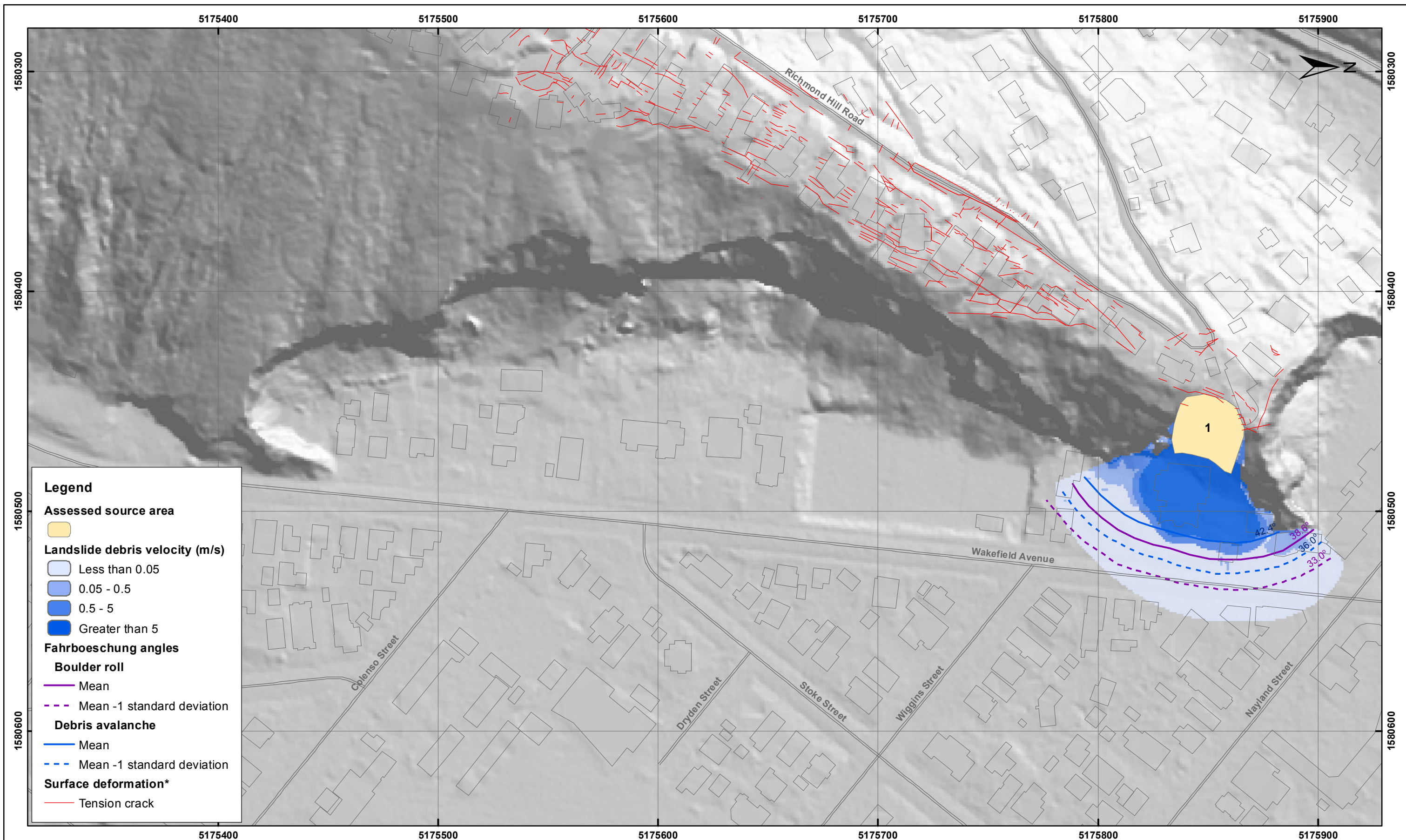
APPENDIX 7

Map 10

FINAL

REPORT: CR2014/34 DATE: June 2014

**A8 APPENDIX 8: RAMMS MODELLING RESULTS FOR SOURCE AREAS
1–10 ADOPTING THE MIDDLE ESTIMATES OF SOURCE VOLUME;
DEBRIS VELOCITY**

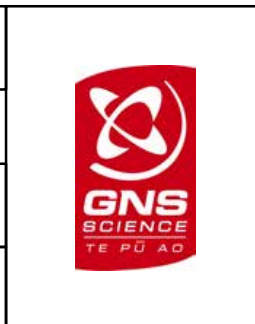


SCALE BAR: 0 50 100 m

EXPLANATION:
 * Taken from report CR2012/317
 Background shade model derived from NZAM post earthquake 2011c (July 2011) LiDAR survey resampled to a 1 m ground resolution. Roads and building footprints and types provided by Christchurch City Council (20/02/2012).
 PROJECTION: New Zealand Transverse Mercator 2000

DRW:
BL, WR

CHK:
CM



ESTIMATED LANDSLIDE RUNOUT VELOCITY
Source 1 - Middle Volume (7,800 m³)

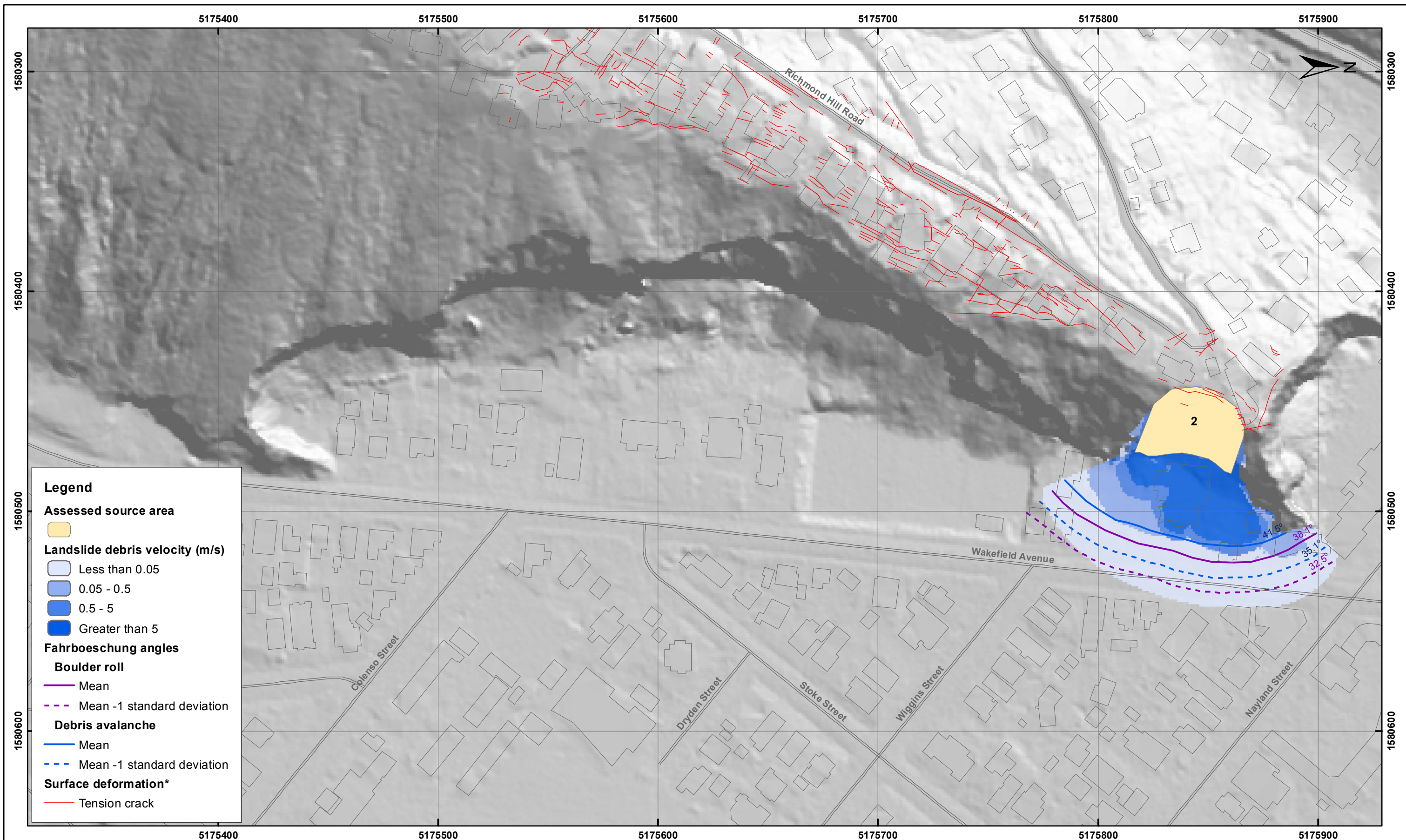
Richmond Hill Road - Port Hills
Christchurch

APPENDIX 8

Map 1

FINAL

REPORT: CR2014/34 DATE: June 2014

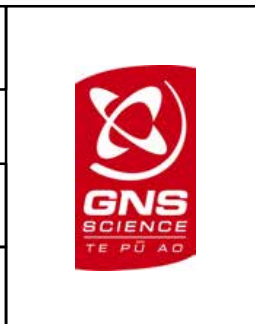


SCALE BAR: 0 50 100 m

EXPLANATION:
 * Taken from report CR2012/317
 Background shade model derived from NZAM post earthquake 2011c (July 2011) LiDAR survey resampled to a 1 m ground resolution. Roads and building footprints and types provided by Christchurch City Council (20/02/2012).
 PROJECTION: New Zealand Transverse Mercator 2000

DRW:
BL, WR

CHK:
CM



ESTIMATED LANDSLIDE RUNOUT VELOCITY
Source 2 - Middle Volume (12,000 m³)

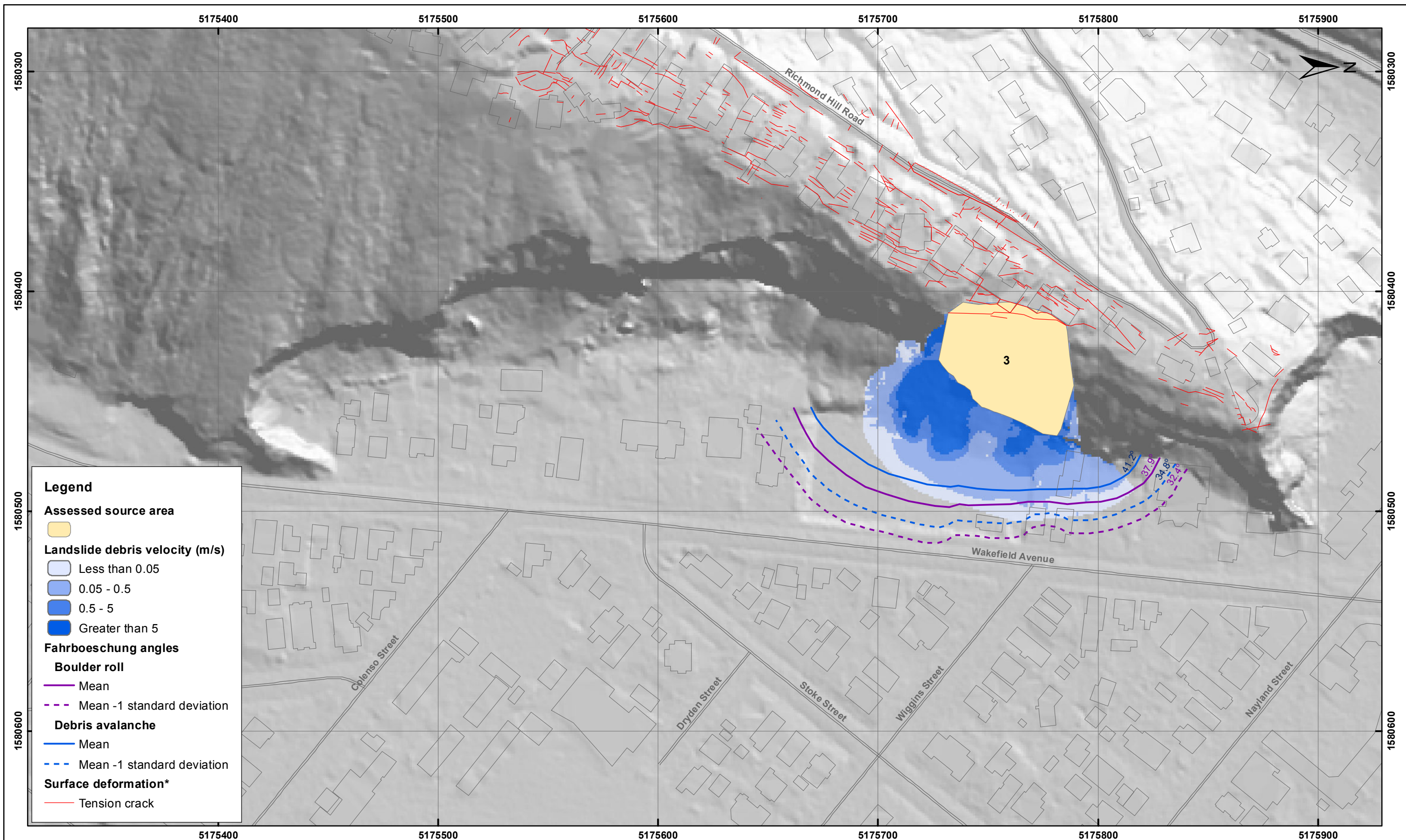
Richmond Hill Road - Port Hills
Christchurch

APPENDIX 8

Map 2

FINAL

REPORT: CR2014/34 DATE: June 2014

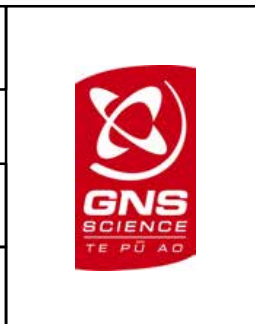


SCALE BAR: 0 50 100 m

EXPLANATION:
 * Taken from report CR2012/317
 Background shade model derived from NZAM post earthquake 2011c (July 2011) LiDAR survey resampled to a 1 m ground resolution. Roads and building footprints and types provided by Christchurch City Council (20/02/2012).
 PROJECTION: New Zealand Transverse Mercator 2000

DRW:
BL, WR

CHK:
CM



ESTIMATED LANDSLIDE RUNOUT VELOCITY
Source 3 - Middle Volume (13,600 m³)

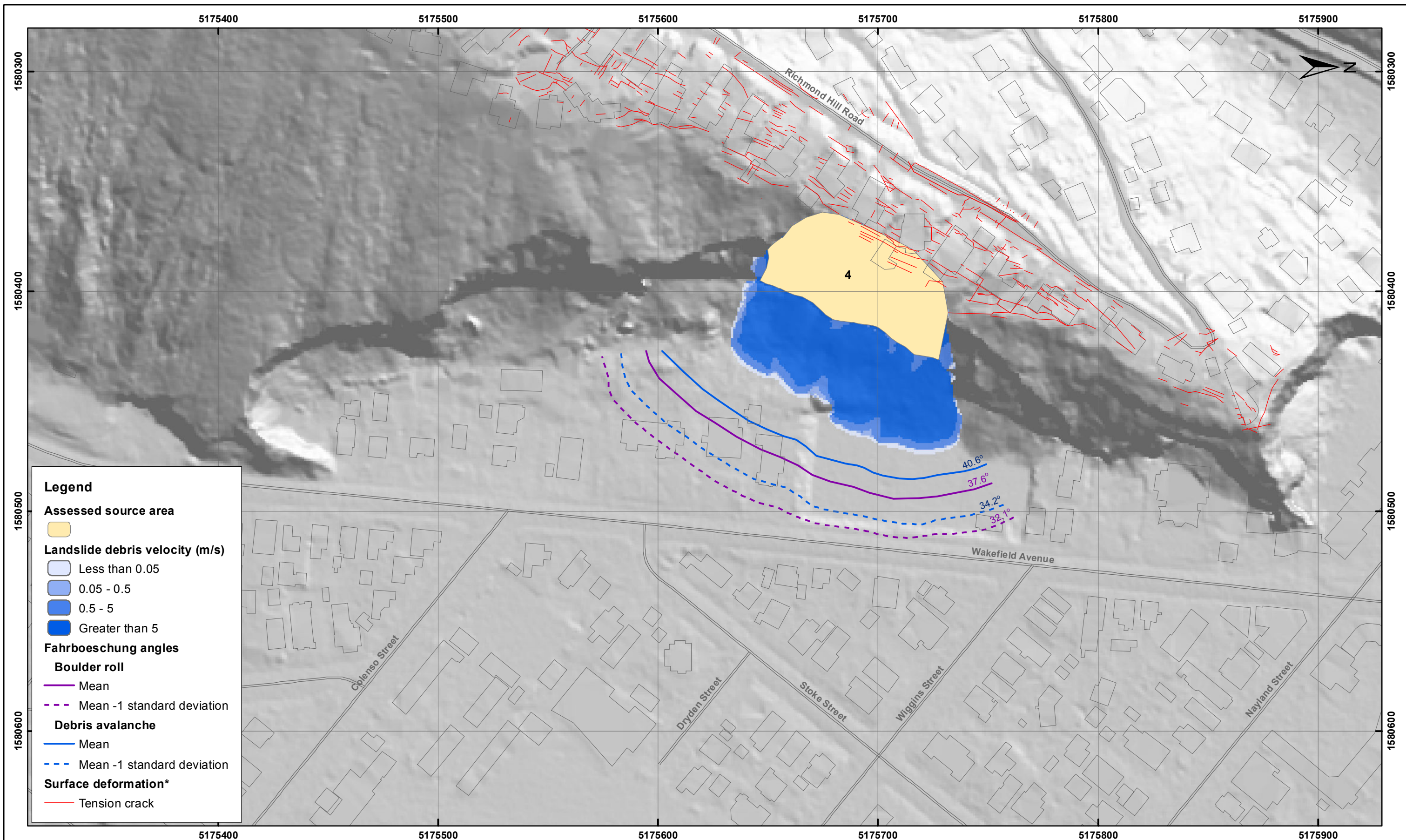
Richmond Hill Road - Port Hills
Christchurch

APPENDIX 8

Map 3

FINAL

REPORT: CR2014/34 DATE: June 2014

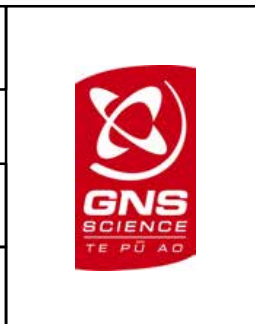


SCALE BAR: 0 50 100 m

EXPLANATION:
 * Taken from report CR2012/317
 Background shade model derived from NZAM post earthquake 2011c (July 2011) LiDAR survey resampled to a 1 m ground resolution. Roads and building footprints and types provided by Christchurch City Council (20/02/2012).
 PROJECTION: New Zealand Transverse Mercator 2000

DRW:
BL, WR

CHK:
CM



ESTIMATED LANDSLIDE RUNOUT VELOCITY
Source 4 - Middle Volume (18,100 m³)

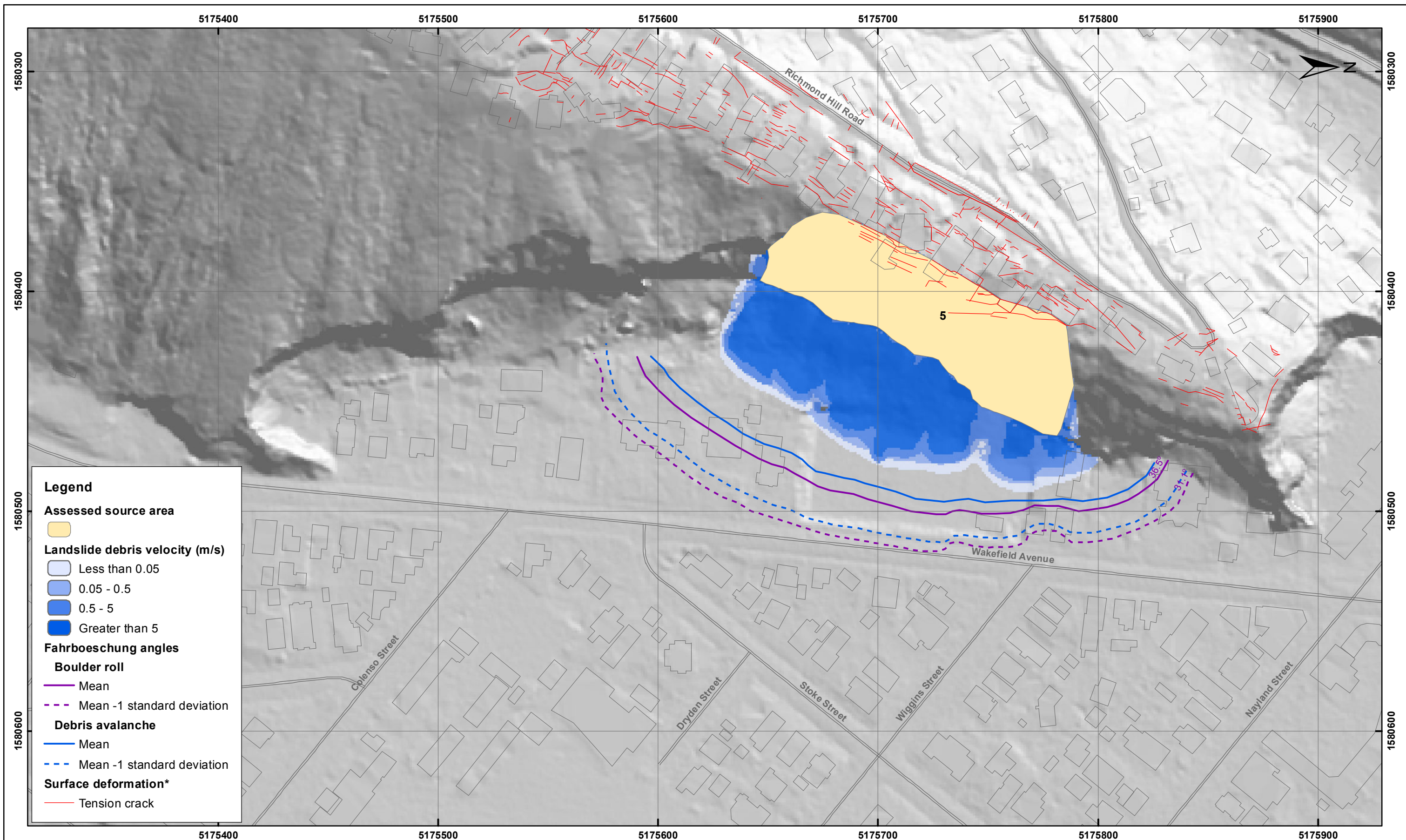
Richmond Hill Road - Port Hills
Christchurch

APPENDIX 8

Map 4

FINAL

REPORT: CR2014/34 DATE: June 2014

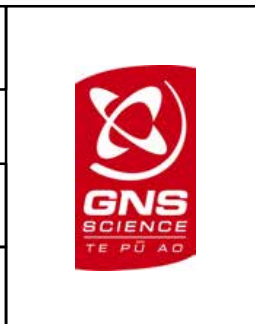


SCALE BAR: 0 50 100 m

EXPLANATION:
 * Taken from report CR2012/317
 Background shade model derived from NZAM post earthquake 2011c (July 2011) LiDAR survey resampled to a 1 m ground resolution. Roads and building footprints and types provided by Christchurch City Council (20/02/2012).
 PROJECTION: New Zealand Transverse Mercator 2000

DRW:
BL, WR

CHK:
CM



ESTIMATED LANDSLIDE RUNOUT VELOCITY
Source 5 - Middle Volume (45,200 m³)

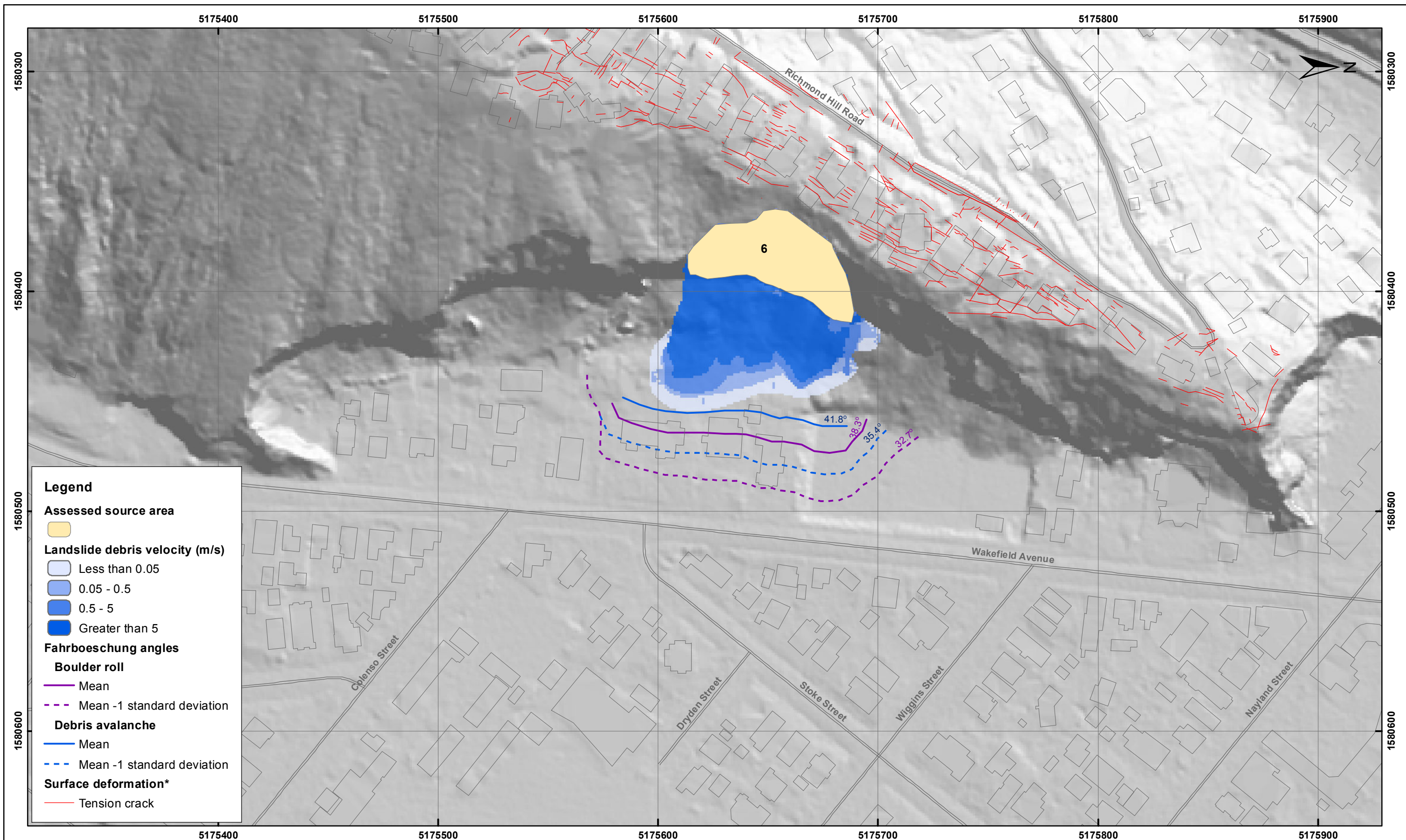
Richmond Hill Road - Port Hills
Christchurch

APPENDIX 8

Map 5

FINAL

REPORT: CR2014/34 DATE: June 2014

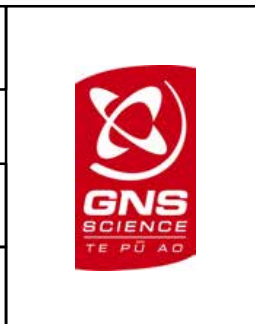


SCALE BAR: 0 50 100 m

EXPLANATION:
 * Taken from report CR2012/317
 Background shade model derived from NZAM post earthquake 2011c (July 2011) LiDAR survey resampled to a 1 m ground resolution. Roads and building footprints and types provided by Christchurch City Council (20/02/2012).
 PROJECTION: New Zealand Transverse Mercator 2000

DRW:
BL, WR

CHK:
CM



ESTIMATED LANDSLIDE RUNOUT VELOCITY
Source 6 - Middle Volume (10,100 m³)

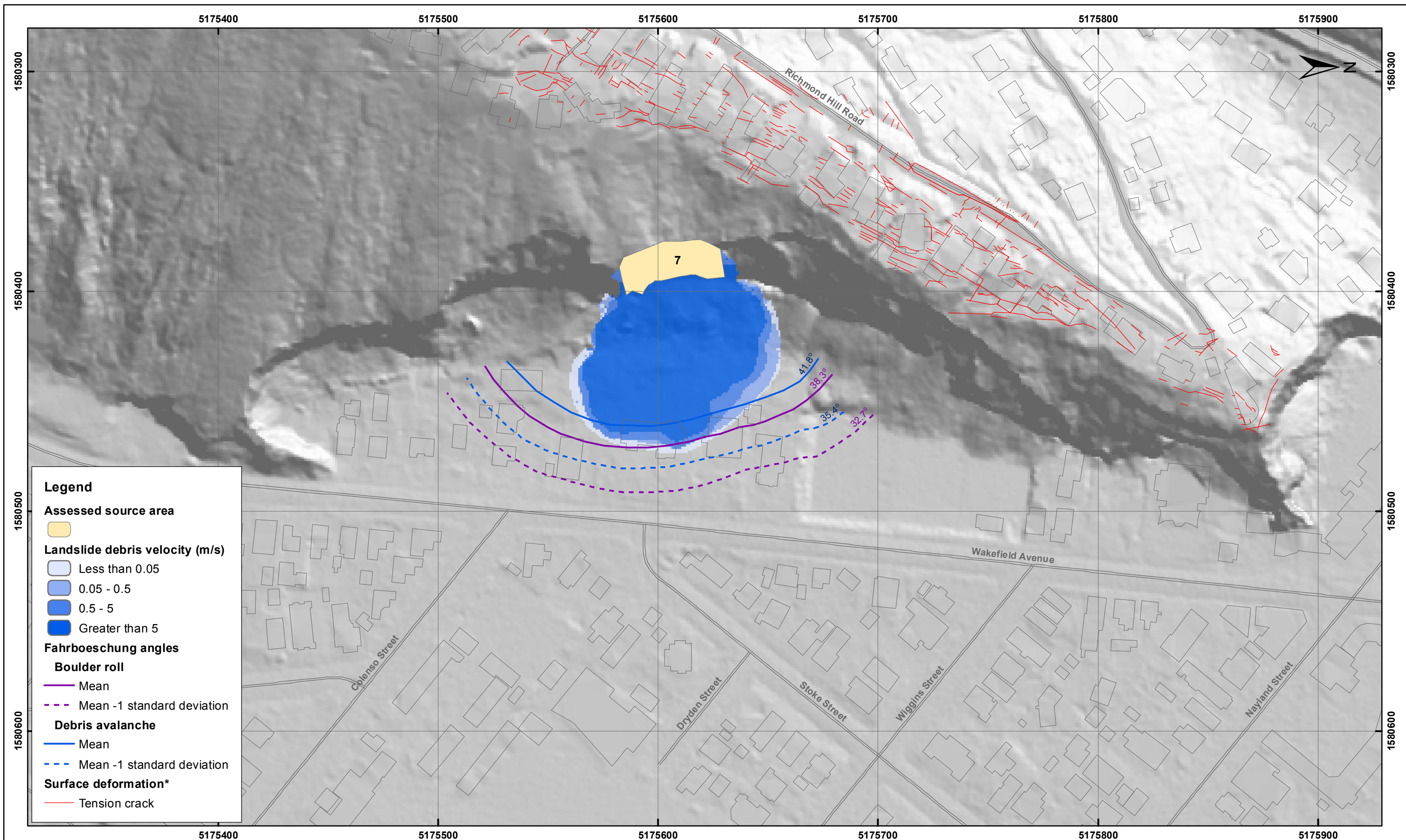
Richmond Hill Road - Port Hills
Christchurch

APPENDIX 8

Map 6

FINAL

REPORT: CR2014/34 DATE: June 2014

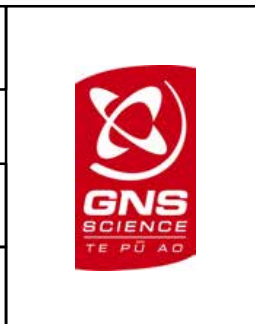


SCALE BAR: 0 50 100 m

EXPLANATION:
 * Taken from report CR2012/317
 Background shade model derived from NZAM post earthquake 2011c (July 2011) LiDAR survey resampled to a 1 m ground resolution. Roads and building footprints and types provided by Christchurch City Council (20/02/2012).
 PROJECTION: New Zealand Transverse Mercator 2000

DRW:
BL, WR

CHK:
CM



ESTIMATED LANDSLIDE RUNOUT VELOCITY
Source 7 - Middle Volume (10,100 m³)

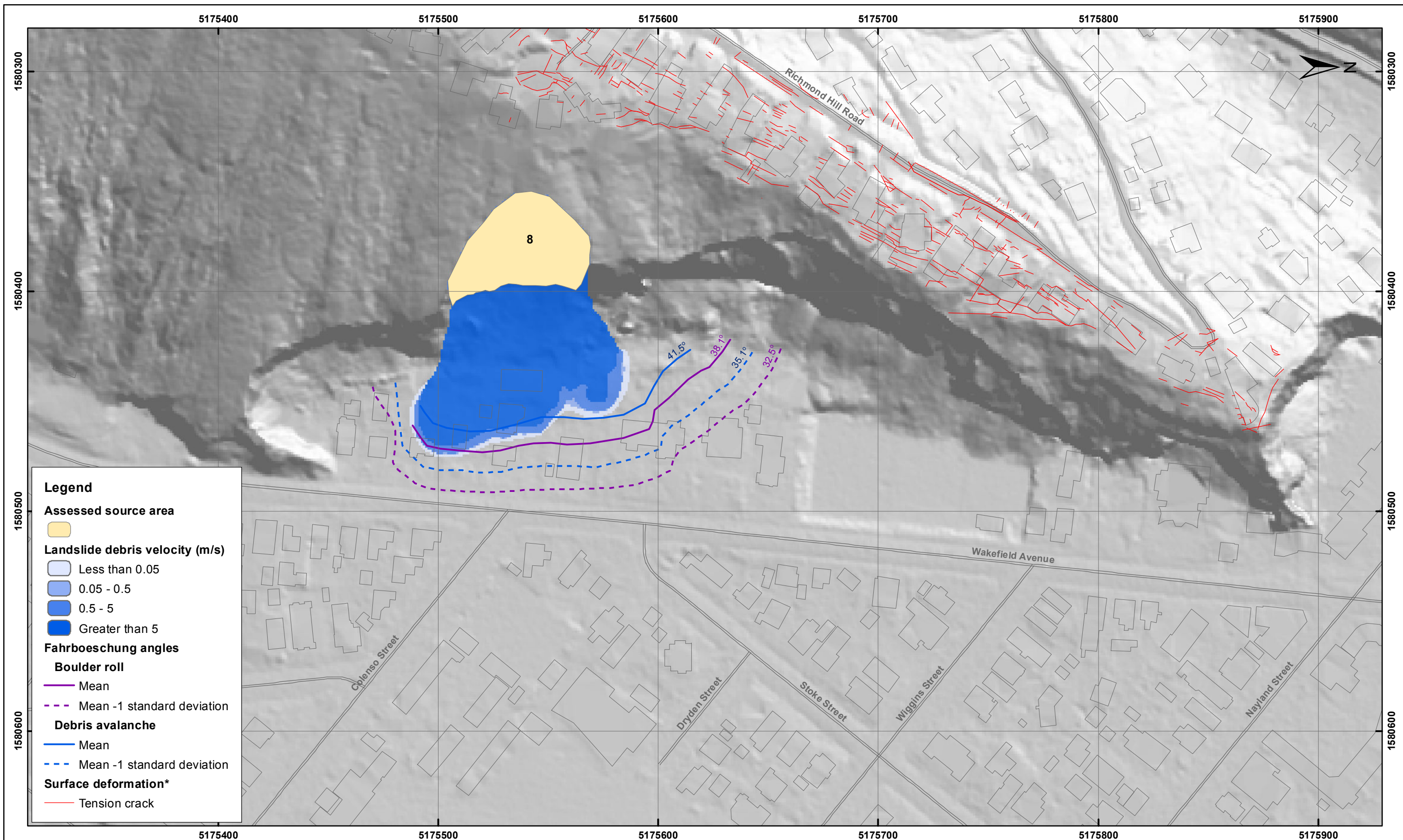
Richmond Hill Road - Port Hills
Christchurch

APPENDIX 8

Map 7

FINAL

REPORT: CR2014/34 DATE: June 2014



Legend

Assessed source area

Landslide debris velocity (m/s)
 Less than 0.05
 0.05 - 0.5
 0.5 - 5
 Greater than 5

Fahrboeschung angles
Boulder roll
 Mean
 Mean -1 standard deviation

Debris avalanche
 Mean
 Mean -1 standard deviation

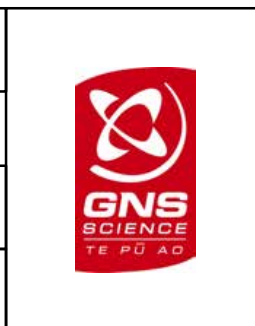
Surface deformation*
 Tension crack

SCALE BAR:

EXPLANATION:
 * Taken from report CR2012/317
 Background shade model derived from NZAM post earthquake 2011c (July 2011) LiDAR survey resampled to a 1 m ground resolution. Roads and building footprints and types provided by Christchurch City Council (20/02/2012).
 PROJECTION: New Zealand Transverse Mercator 2000

DRW:
BL, WR

CHK:
CM



ESTIMATED LANDSLIDE RUNOUT VELOCITY
Source 8 - Middle Volume (11,700 m³)

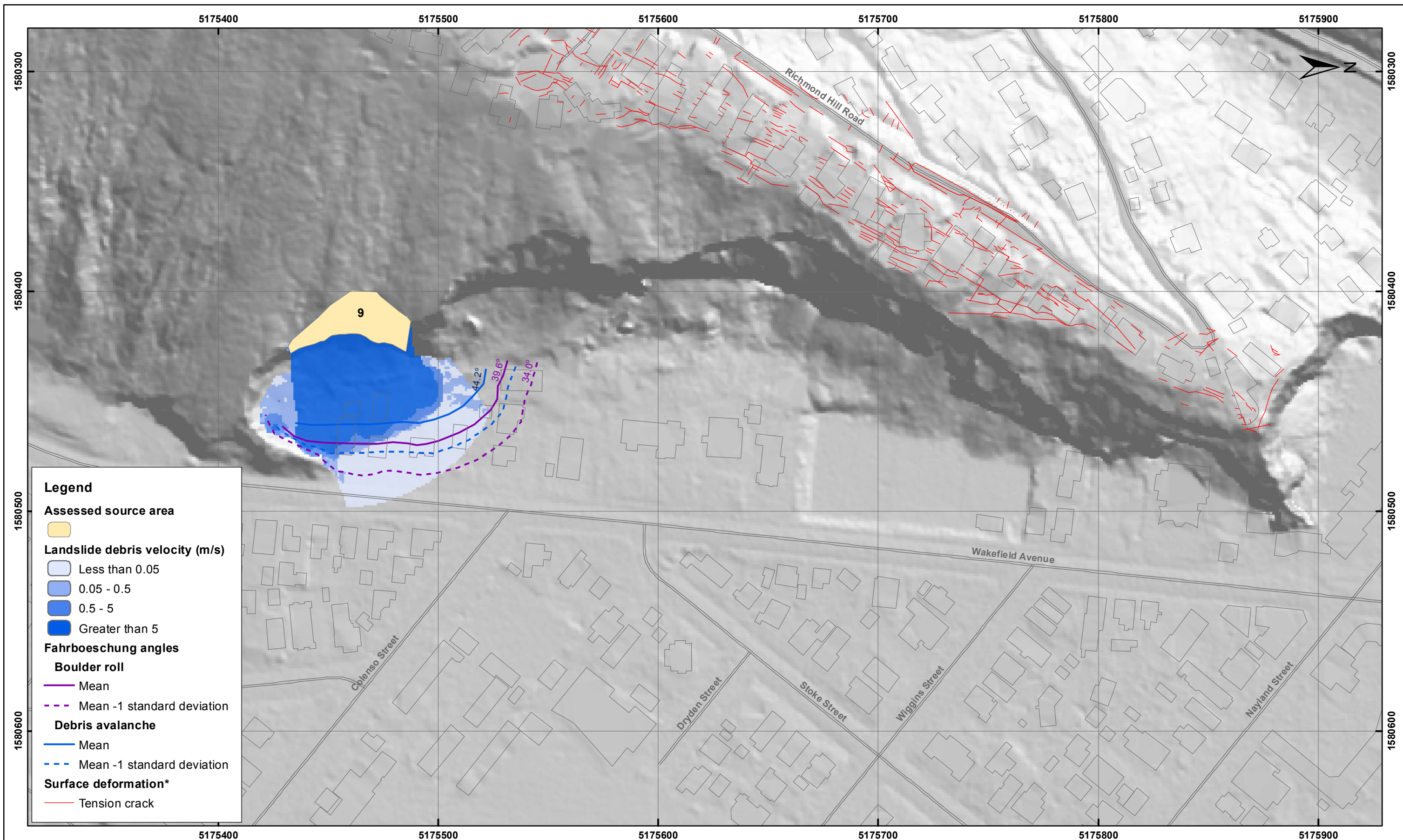
Richmond Hill Road - Port Hills
Christchurch

APPENDIX 8
 Map 8

FINAL

REPORT:
CR2014/34

DATE:
June 2014



Legend

Assessed source area

Landslide debris velocity (m/s)
 Less than 0.05
 0.05 - 0.5
 0.5 - 5
 Greater than 5

Fahrboeschung angles
Boulder roll
 Mean
 Mean -1 standard deviation

Debris avalanche
 Mean
 Mean -1 standard deviation

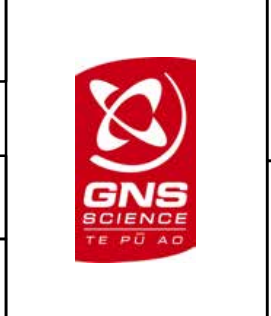
Surface deformation*
 Tension crack

SCALE BAR:

EXPLANATION:
 * Taken from report CR2012/317
 Background shade model derived from NZAM post earthquake 2011c (July 2011) LiDAR survey resampled to a 1 m ground resolution. Roads and building footprints and types provided by Christchurch City Council (20/02/2012).
 PROJECTION: New Zealand Transverse Mercator 2000

DRW:
BL, WR

CHK:
CM



ESTIMATED LANDSLIDE RUNOUT VELOCITY
Source 9 - Middle Volume (3,400 m³)

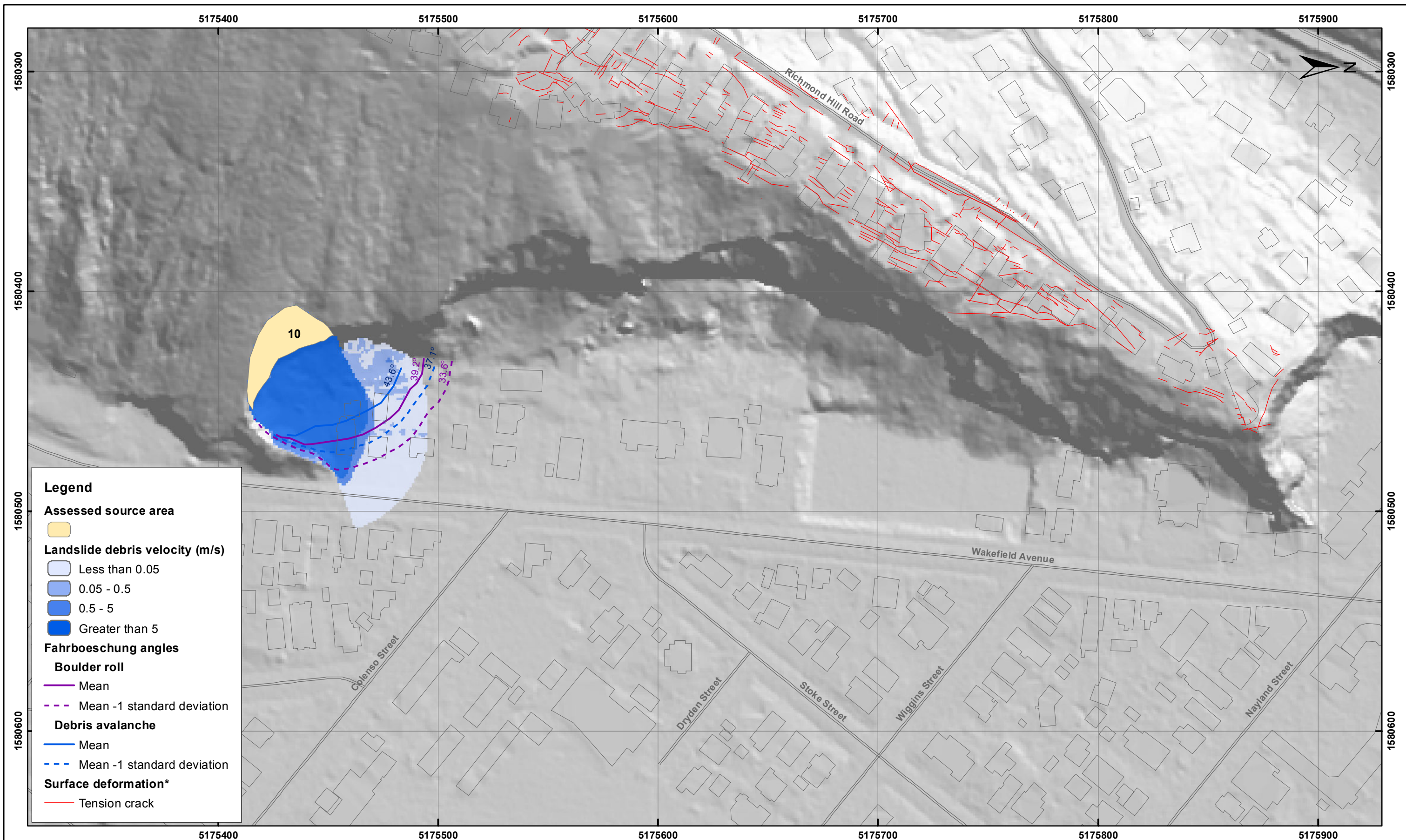
Richmond Hill Road - Port Hills
Christchurch

APPENDIX 8

Map 9

FINAL

REPORT: CR2014/34 DATE: June 2014

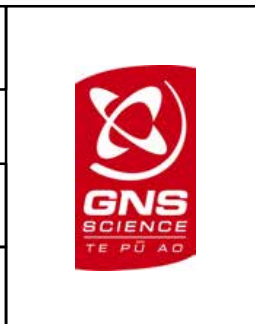


SCALE BAR: 0 50 100 m

EXPLANATION:
 * Taken from report CR2012/317
 Background shade model derived from NZAM post earthquake 2011c (July 2011) LiDAR survey resampled to a 1 m ground resolution. Roads and building footprints and types provided by Christchurch City Council (20/02/2012).
 PROJECTION: New Zealand Transverse Mercator 2000

DRW:
BL, WR

CHK:
CM



ESTIMATED LANDSLIDE RUNOUT VELOCITY
Source 10 - Middle Volume (4,500 m³)

Richmond Hill Road - Port Hills
Christchurch

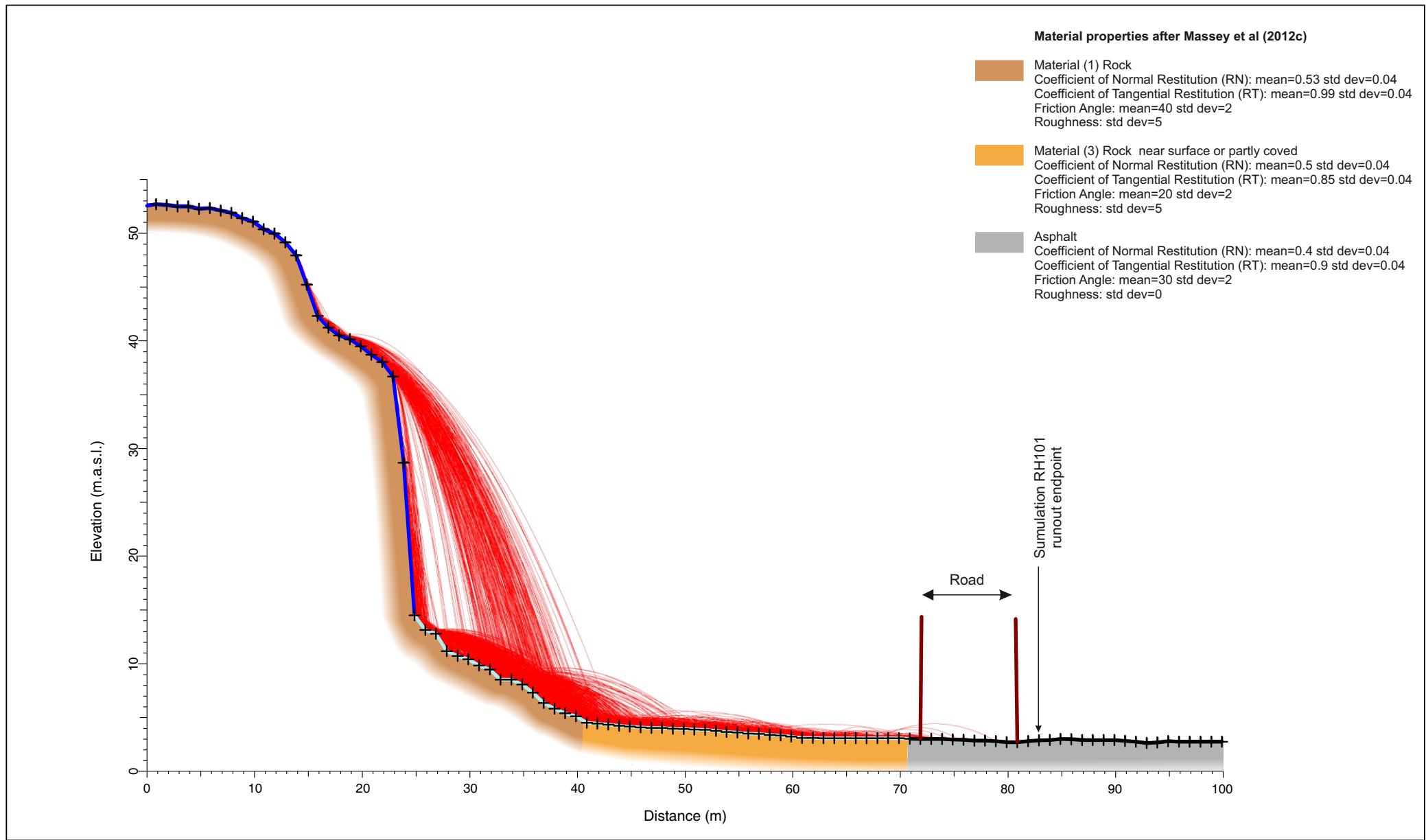
APPENDIX 8

Map 10

FINAL

REPORT: CR2014/34 DATE: June 2014

A9 APPENDIX 9: ROCKFALL MODELLING RESULTS FOR CROSS-SECTIONS 1 AND 7



Input material parameters from Massey et al 2012c
 Number of rocks = 2000
 Unit weight 27 KN/m³
 Cut of velocity 0.1m/sec
 Simulated rock mass 1,000kg (~0.3m³)

DRW:
PC
 CHK:
CM/FDP



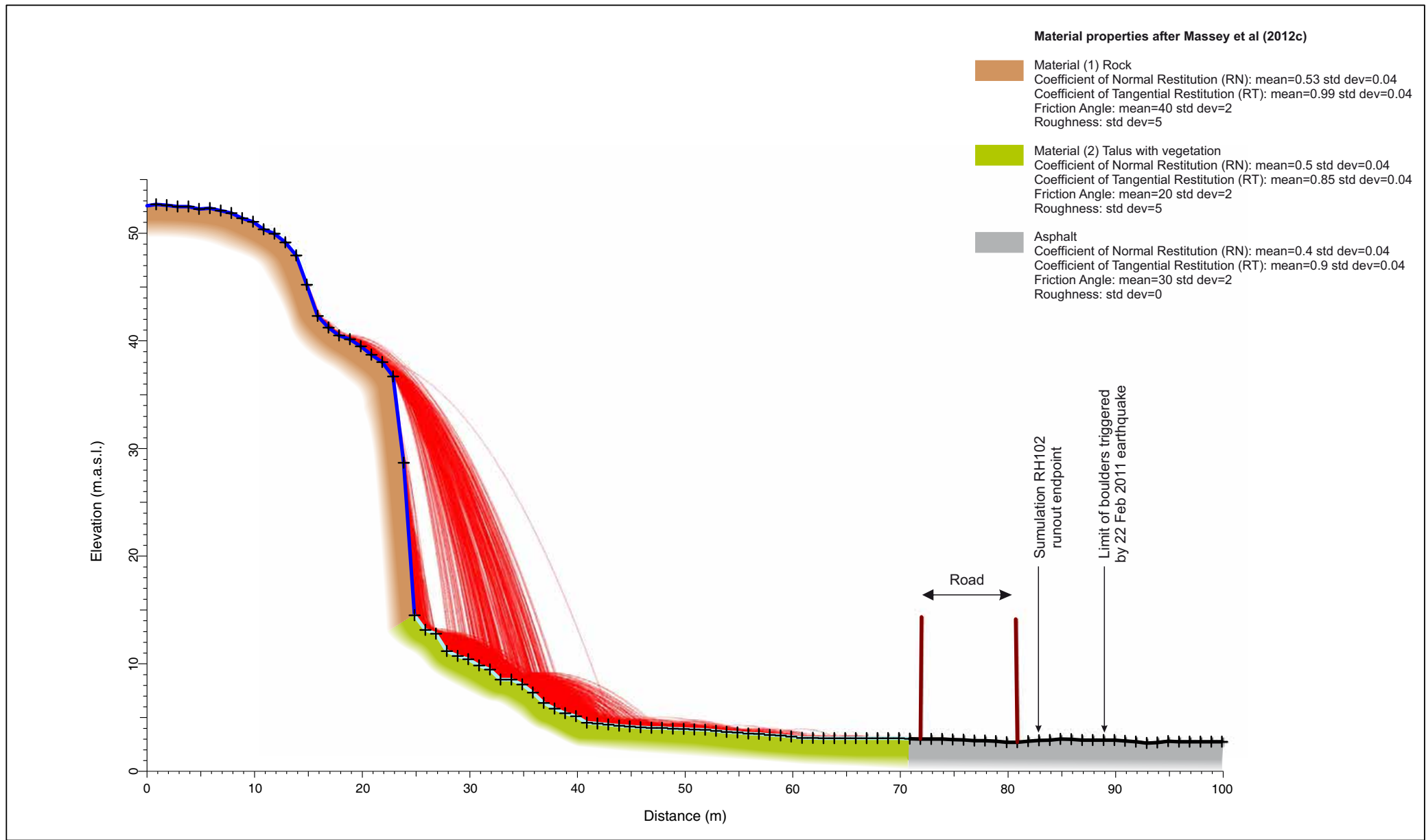
SECTION 1
RocFall® simulation RH101


Richmond Hill Road
Christchurch

APPENDIX 9

FINAL

REPORT: CR2014/34 DATE: June 2014

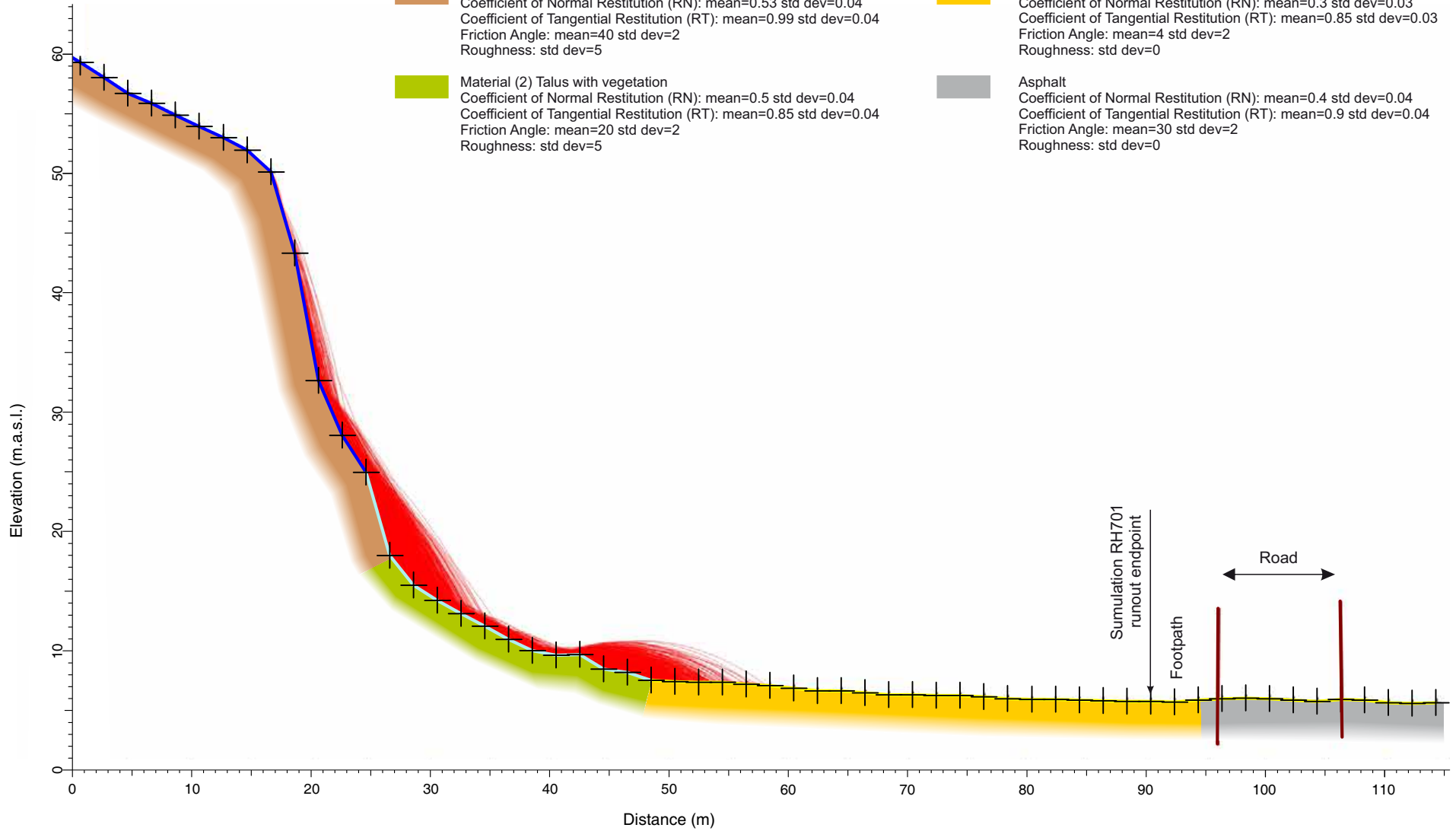


Input material parameters from Massey et al 2012c Number of rocks = 2000 Unit weight 27 KN/m ³ Cut of velocity 0.1m/sec Simulated rock mass 1,000kg (~0.3m ³)	DRW: PC		SECTION 1 RocFall® simulation RH102		APPENDIX 9	
	CHK: CM/FDP		Richmond Hill Road Christchurch		FINAL	
				REPORT: CR2014/34	DATE: June 2014	

Material properties after Massey et al (2012c)

- Material (1) Rock
Coefficient of Normal Restitution (RN): mean=0.53 std dev=0.04
Coefficient of Tangential Restitution (RT): mean=0.99 std dev=0.04
Friction Angle: mean=40 std dev=2
Roughness: std dev=5
- Material (2) Talus with vegetation
Coefficient of Normal Restitution (RN): mean=0.5 std dev=0.04
Coefficient of Tangential Restitution (RT): mean=0.85 std dev=0.04
Friction Angle: mean=20 std dev=2
Roughness: std dev=5

- Material (5) Colluvium with vegetation - smooth
Coefficient of Normal Restitution (RN): mean=0.3 std dev=0.03
Coefficient of Tangential Restitution (RT): mean=0.85 std dev=0.03
Friction Angle: mean=4 std dev=2
Roughness: std dev=0
- Asphalt
Coefficient of Normal Restitution (RN): mean=0.4 std dev=0.04
Coefficient of Tangential Restitution (RT): mean=0.9 std dev=0.04
Friction Angle: mean=30 std dev=2
Roughness: std dev=0



Input material parameters from Massey et al 2012c
 Number of rocks = 2000
 Unit weight 27 KN/m³
 Cut of velocity 0.1m/sec
 Simulated rock mass 1,000kg (~0.3m³)

DRW:
PC
 CHK:
CM/FDP



SECTION 7
RocFall® simulation RH 701

Richmond Hill Road
Christchurch

APPENDIX 9

FINAL

REPORT:
CR2014/34

DATE:
June 2014



www.gns.cri.nz

Principal Location

1 Fairway Drive
Avalon
PO Box 30368
Lower Hutt
New Zealand
T +64-4-570 1444
F +64-4-570 4600

Other Locations

Dunedin Research Centre
764 Cumberland Street
Private Bag 1930
Dunedin
New Zealand
T +64-3-477 4050
F +64-3-477 5232

Wairakei Research Centre
114 Karetoto Road
Wairakei
Private Bag 2000, Taupo
New Zealand
T +64-7-374 8211
F +64-7-374 8199

National Isotope Centre
30 Gracefield Road
PO Box 31312
Lower Hutt
New Zealand
T +64-4-570 1444
F +64-4-570 4657